

REPORT DOCUMENTATION PAGE			Form Approved OMB No. 0704-0188	
Public reporting burden for this collection of information is estimated to average 1 hour per response, including the time for reviewing instructions, searching existing data sources, gathering and maintaining the data needed, and completing and reviewing the collection of information. Send comments regarding this burden estimate or any other aspect of this collection of information, including suggestions for reducing this burden, to Washington Headquarters Services, Directorate for Information Operations and Reports, 1215 Jefferson Davis Highway, Suite 1204, Arlington, VA 22202-4302, and to the Office of Management and Budget, Paperwork Reduction Project (0704-0188), Washington, DC 20503.				
1. AGENCY USE ONLY (Leave blank)		2. REPORT DATE 14 Oct 97		3. REPORT TYPE AND DATES COVERED
4. TITLE AND SUBTITLE ENVIRONMENTAL DURABILITY OF ADHESIVELY BONDED JOINTS				5. FUNDING NUMBERS
6. AUTHOR(S) Lawrence M. Butkus				
7. PERFORMING ORGANIZATION NAME(S) AND ADDRESS(ES) The Georgia Institute of Technology				8. PERFORMING ORGANIZATION REPORT NUMBER 97-028D
9. SPONSORING/MONITORING AGENCY NAME(S) AND ADDRESS(ES) THE DEPARTMENT OF THE AIR FORCE AFIT/CIA 2950 P STREET, BLDG 125 WPAFB OH 45433				10. SPONSORING/MONITORING AGENCY REPORT NUMBER
11. SUPPLEMENTARY NOTES				
12a. DISTRIBUTION AVAILABILITY STATEMENT <div style="border: 1px solid black; padding: 5px; text-align: center;"> DISTRIBUTION STATEMENT A Approved for public release Distribution Unlimited </div>				12b. DISTRIBUTION CODE
13. ABSTRACT (Maximum 200 words) <div style="font-size: 2em; font-weight: bold; text-align: center;">19971021 154</div> <div style="text-align: right; font-weight: bold; transform: rotate(-10deg);"> DISTRIBUTION INSPECTED 4 </div>				
14. SUBJECT TERMS				15. NUMBER OF PAGES 343
				16. PRICE CODE
17. SECURITY CLASSIFICATION OF REPORT		18. SECURITY CLASSIFICATION OF THIS PAGE		19. SECURITY CLASSIFICATION OF ABSTRACT
				20. LIMITATION OF ABSTRACT

ENVIRONMENTAL DURABILITY OF ADHESIVELY BONDED JOINTS

Lawrence M. Butkus, Major, USAF

1997

343 pages

Ph.D., Mechanical Engineering

The Georgia Institute of Technology

The goal of this project was to evaluate the environmental durability of adhesively bonded aircraft joints using fracture mechanics and the strain energy release rate concept. Three bonded aerospace material systems, two epoxies and one polyimide, were investigated. Adhesive specimens were tested for tensile and toughness behavior. Bonded joint specimens were subject to Mode I, Mode II, and mixed mode fracture tests and to Mode I fatigue tests. Prior to testing, selected specimens were exposed for up to 10,000 hours to isothermal and thermally cyclic conditions simulating aircraft service environments. Analysis was accomplished using finite element programs and closed-form solutions. Environmental exposure caused reductions in the failure strain, strength, and toughness, of the adhesive specimens and in the toughness and fatigue threshold of the bonded joint specimens. Specimens exposed to high temperature and humidity prior to testing and those tested at low temperatures indicative of high altitude operations experienced the most significant toughness losses. The fatigue crack growth rate sensitivity appeared to be unaffected by environmental exposure. Results are discussed in terms of their relationship to bonded joint design and should prove valuable to efforts aimed at extending the lives of aging aircraft using bonded repairs as well as to efforts focused on using adhesive bonding for future aerospace structures.

Key Sources

Baker, A.A., "Bonded Composite Repair of Metallic Aircraft Structures," in Composite Repair of Military Aircraft Structures: Proceedings of the 79th Meeting of the AGARD (Advisory Group for Aerospace Research & Development) Structures and Materials Panel, Seville, Spain, 1994, pp. 1-1 to 1-14.

Belason, E.B., "Fatigue and Static Ultimate Tests of Boron/Epoxy Doublers Bonded to 7075-T6 Aluminum with a Simulated Crack," in Proceedings of the 18th Symposium of the International Conference on Aeronautical Fatigue, Melbourne, Australia, May 1995.

Brussat, T.R., Chiu, S.T., and Mostovoy, S., *Fracture Mechanics for Structural Adhesive Bonds - Final Report*, Lockheed Co., Burbank, CA, for the USAF Materials Laboratory, AFML-TR-77-163, July 1987.

Butkus, L.M., Mathern, P.D., and Johnson, W.S., "Tensile Properties and Plane-Stress Fracture Toughness of Thin Film Aerospace Adhesives," *The Journal of Adhesion*, submitted: June 1997.

Carlsson, L.A., Gillespie, J.W., and Pipes, R.B., "On The Analysis and Design of the End Notched Flexure (ENF) Specimen for Mode II Testing," *Journal of Composite Materials*, Vol. 20, Nov. 1986, pp. 594-605.

Goland, M. and Reissner, E., "The Stresses in Cemented Joints," *Journal of Applied Mechanics*, American Society of Mechanical Engineers, New York, NY, Vol. 11, Mar. 1944.

Hart-Smith, L.J. and Thrall, E.W., "Structural Analysis of Adhesive-Bonded Joints," in Adhesive Bonding of Aluminum Alloys, E.W. Thrall and R.W. Shannon, eds., Marcel Dekker, Inc., New York, NY, 1985.

Hashemi, S., Kinloch, A.J., and Williams, J.G., "Corrections Needed in Double-Cantilever Beam Tests for Assessing the Interlaminar Failure of Fibre-Composites," *Journal of Materials Science Letters*, Vol. 8, 1989.

Irwin, G.R. and Kies, J.A., "Critical Energy Rate Analysis of Fracture Strength," *Welding Journal Research Supplement*, Apr. 1954, pp. 193S-198S.

Johnson, W.S. and Butkus, L.M., "Considering Environmental Conditions in the Design of Bonded Structures: A Fracture Mechanics Approach," *International Journal of Fatigue and Fracture of Engineering Materials and Structures*, accepted: July 1997.

Johnson, W.S. and Mall, S., "A Fracture Mechanics Approach for Designing Adhesively Bonded Joints," in Delamination and Debonding of Materials, ASTM STP 876, W.S. Johnson, ed., American Society for Testing and Materials, Philadelphia, PA, 1985.

Johnson, W.S. and Mangalgi, P.D., "Influence of the Resin on Interlaminar Mixed-Mode Fracture," Toughened Composites, ASTM STP 937, N.J. Johnston, ed., American Society for Testing and Materials, Philadelphia, PA, 1987.

Johnson, W.S., "Stress Analysis of the Cracked Lap-Shear Specimen: An ASTM Round Robin," *Journal of Testing and Evaluation*, Vol. 15, No. 6, American Society for Testing and Materials, Philadelphia, PA, Nov 1987, pp. 303-324.

Kinloch, A.J., "Interfacial Fracture Mechanical Aspects of Adhesive Bonded Joints - A Review," *Journal of Adhesion*, Vol. 10, 1979, pp. 193-219.

Klemann, B.M. and DeVilbiss, T., "The Fracture Toughness of Thin Polymeric Films," *Polymer Engineering and Science*, Vol. 36, No. 1, Jan 1996, 126-134.

Mall, S., Johnson, W.S. and Everett, R.A., Jr., "Cyclic Debonding of Adhesively Bonded Composites," in Adhesive Joints: Formation, Characteristics and Testing, K.L. Mittal, ed., Plenum Press, New York, NY, 1982, pp. 639-656.

Potter, D.L., *Primarily Adhesive Bonded Structure Technology (PABST), Design Handbook for Adhesive Bonding*, Douglas Aircraft Co., Long Beach, CA, for the USAF Flight Dynamics Laboratory, AFFDL-TR-79-3129, Jan 1979.

Ripling, E.J., Mostovoy, S., and Patrick, R.L., "Application of Fracture Mechanics to Adhesive Joints." in Adhesion, ASTM STP 360, American Society for Testing and Materials, Philadelphia, PA, 1963.

Roderick, G.L., Everett, R.A., and Crews, J.H., Jr., "Cyclic Debonding of Unidirectional Composites Bonded to Aluminum Sheet For Constant Amplitude Loading," Fatigue of Composite Materials, ASTM STP 569, American Society for Testing and Materials, Philadelphia, PA, 1975, pp. 295-306.

Rybicki, E. F., and Kanninen, M. F., "A Finite Element Calculation Of Stress Intensity Factor by a Modified Crack Closure Integral," *Engineering Fracture Mechanics*, Vol. 9, 1977, pp. 931-938.

Schliekelmann, R.J., "Past, Presence, and Future of Structural Adhesive Bonding in Aero-Space Applications," *Transactions of the Japanese Society of Composite Materials*, Vol. 5, No. 1/2, Dec. 1979, pp. 1-12.

Shaw, S.J., "Adhesive Joint Failure - A Fracture Mechanics Approach," in Adhesion 7: Proceedings of the 20th Annual Conference on Adhesion and Adhesives, K.W. Allen, ed., Elsevier Applied Science Publishers, London, UK, 1983.

Valentin, R.V., *Finite Element Analysis of Adhesively Bonded Joints*, Masters Thesis, Georgia Institute of Technology, Atlanta, GA, July 1997.

Williams, J.G., "Fracture Mechanics of Polymers and Adhesives," in Fracture of Non-Metallic Materials, K.P.herrmann and L.H. Larsson, eds., ECSC, EEC, EAEC, Brussels, 1987, pp. 227-255.

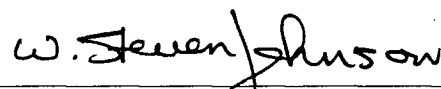
ENVIRONMENTAL DURABILITY OF ADHESIVELY BONDED JOINTS

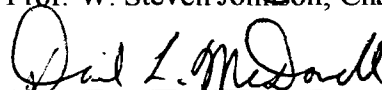
A Thesis
Presented to
The Academic Faculty
by


Lawrence M. Butkus

In Partial Fulfillment
of the Requirements for the Degree
Doctor of Philosophy of Mechanical Engineering

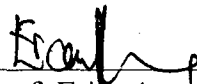
Georgia Institute of Technology
September 1997

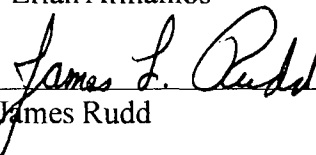
ENVIRONMENTAL DURABILITY OF ADHESIVELY BONDED JOINTS

Prof. W. Steven Johnson, Chairman

Prof. David McDowell

Prof. Richard Neu

Prof. Jianmin Qu

Prof. Erian Armanios

Mr. James Rudd

Date Approved 19 September 1997

ACKNOWLEDGMENTS

First and foremost, all credit for the successful completion of this project must be given to the Lord, Our God, who makes all things possible. I also wish to express my deepest love and appreciation to my wife, Kathy, my daughters, Claire and Grace, and my family for their unwavering support and inspiration. And no academic endeavor would be complete without a mentor; I had a great one in Prof. Steve Johnson whom I am glad to have had as an advisor and honored to count as a friend and colleague.

Reflected in this thesis are the efforts, suggestions, thoughts, and ideas of many people who assisted in this research including (but certainly not limited to):

Committee Members: Prof. Dave McDowell, Prof. Rick Neu, Prof. Jianmin Qu, Prof. Erian Armanios, all from the Georgia Institute of Technology, and Mr. Jim Rudd from Wright-Patterson AFB, OH

Technical Assistants: Rick Brown and John Graham from the Georgia Institute of Technology; Richard Simms, Jerry Rowell, and Duane Kelly from Robins AFB, GA

Industry Contacts: Bob Bell, Carol Burke, Scott Reeve, and Dave Schneider from Lockheed Martin; Kevin Pate and Tuan Cao from The Boeing Company; Rich Mayhew from CYTEC Engineered Materials; Don Oplinger from the FAA Technical Center

Colleagues: Rodolfo Valentin, Peter Mathern Scott Fawaz, Tom Lacy, Mark Horstemeyer, Jeff Calcalterra, Ed Li, Col. "Row" Rogacki, Maj. Rob Fredell, ...

TABLE OF CONTENTS

ACKNOWLEDGMENTS.....	iii
TABLE OF CONTENTS.....	iv
LIST OF TABLES.....	xiv
LIST OF FIGURES.....	xv
LIST OF SYMBOLS AND ABBREVIATIONS.....	xxii
SUMMARY.....	xxix
I. INTRODUCTION.....	33
II. BACKGROUND.....	38
2.1. Adhesive Bonding in Aerospace Applications.....	40
2.1.1 Adhesively Bonded Aircraft Structures.....	41
2.1.1.1. Control Surfaces on the F-22.....	42
2.1.1.2. Wing and Fuselage Structures on the High Speed Civil Transport.....	43
2.1.2. Adhesively Bonded Repairs.....	44
2.1.2.1. Repairs Using Bonded Boron-Epoxy Patches.....	45
2.1.2.2. Repairs Using Other Bonded Materials.....	46
2.2. Design and Analysis Approaches.....	48
2.2.1. Stress Based Approaches.....	48

2.2.2. Fracture Mechanics Analyses.....	50
2.3. Analytical Methods	58
2.4. Environmental Issues	61
2.5. A Fracture Mechanics Approach to the Durability of Bonded Joints	64
III. MATERIALS AND SPECIMENS	70
3.1. Description of Materials.....	71
3.1.1. Adhesives.....	71
3.1.1.1. FM-73.....	71
3.1.1.2 AF-191.....	73
3.1.1.3. FM-x5	74
3.1.2. Bonded Joint Systems.....	75
3.1.2.1. Aluminum/FM [®] 73M (Al/FM [®] 73M/Al).....	75
3.1.2.2. Aluminum/FM [®] 73M/Boron-Epoxy (Al/FM [®] 73M/B-Ep).....	76
3.1.2.3. Graphite-Bismaleimide/AF-191M (Gr-BMI/AF-191M/Gr-BMI)	77
3.1.2.4. Titanium/FM [®] x5 (Ti/FM [®] x5/Ti).....	78
3.2. Specimen Geometry	78
3.2.1. Geometry of Adhesive Specimens.....	78
3.2.1.1. Adhesive Tensile Test and Fracture Toughness Specimens	79
3.2.1.2. Adhesive Specimens Used for Chemical and Physical Analysis	81
3.2.2. Geometry of Bonded Joint Specimens.....	81

3.2.2.1. The Double Cantilever Beam (DCB) Geometry	85
3.2.2.2. The End-Notched Flexure (ENF) Geometry	87
3.2.2.3. The Cracked Lap Shear (CLS) Geometry	89
3.3. Specimen Fabrication	91
3.3.1. Adhesive Specimen Fabrication	91
3.3.1.1. Curing of Adhesive Sheets	92
3.3.1.2. Die Cutting of Adhesive Specimens	92
3.3.2. Bonded Joint Specimen Fabrication	93
3.3.2.1 Fabrication of Al/FM [®] 73M/Al Specimens	94
3.3.2.2. Fabrication of Al/FM [®] 73M/B-Ep Specimens	94
3.3.2.3. Fabrication of Gr-BMI/AF-191M/Gr-BMI Specimens	95
3.3.2.4. Fabrication of Ti/FM [®] x5/Ti Specimens	95
IV. ENVIRONMENTAL EXPOSURE	97
4.1. Long-term Isothermal Exposure	98
4.1.1. Isothermal Conditions	98
4.1.2. Equipment	101
4.2. Cyclic Thermal Exposure	103
4.2.1. Cyclic Thermal Conditions	103
4.2.2. Equipment	106
4.3. Storage	107

4.3.1. Storage Conditions	108
4.3.2. Equipment.....	108
4.4. Testing.....	108
4.4.1. Testing Conditions.....	109
4.4.2. Equipment.....	109
V. MECHANICAL TESTING PROCEDURES.....	112
5.1. Mechanical Testing of Adhesive Specimens.....	112
5.1.1. Tensile Testing of Adhesive Specimens.....	113
5.1.2. Fracture Toughness Testing of Adhesive Specimens.....	116
5.2. Mechanical Testing of Bonded Joint Specimens.....	116
5.2.1. Monotonic Fracture Toughness Testing of Bonded Joint Specimens	120
5.2.1.1. Monotonic Fracture Toughness Testing of DCB Specimens	121
5.2.1.2. Monotonic Fracture Toughness Testing of ENF Specimens.....	125
5.2.1.3. Monotonic Fracture Toughness Testing of CLS Specimens.....	128
5.2.2. Fatigue Testing of Bonded Joint Specimens	131
5.2.2.1. Fatigue Testing of the DCB Geometry	132
5.2.2.2. Fatigue Testing of the CLS Geometry	133
VI. ANALYSIS OF MECHANICAL TESTS.....	135
6.1. Analysis of the Adhesive Tensile Tests	136
6.2. Analysis of the Adhesive Fracture Toughness Tests	137

6.3. Analysis of the Double Cantilever Beam Specimens.....	139
6.3.1. Closed-Form Solution for the Mode I Strain Energy Release Rate (G_I).....	140
6.3.2. Analysis of Double Cantilever Beam Specimens Subjected to Fatigue.....	142
6.4. Analysis of the End-Notched Flexure Specimens.....	144
6.5. Analysis of the Cracked Lap Shear Specimens.....	147
6.6. Finite Element Analyses	148
6.6.1. Programs.....	149
6.6.2. Assumptions and Model Details	149
6.6.3. Determination of Strain Energy Release Rate	151
6.6.4. Verification of Analysis	152
6.6.5. Analysis of the Curved Al/FM [®] 73M/B-Ep Specimens	153
6.7. Statistical Analysis of Multiple Data Points.....	156
VII. CHEMICAL AND PHYSICAL TESTING PROCEDURES.....	159
7.1. Fourier Transform Infrared Spectroscopy (FTIR).....	159
7.2. Differential Scanning Calorimetry (DSC).....	162
7.3. Thermogravimetric Analysis (TGA).....	165
VIII. RESULTS AND DISCUSSION.....	169
8.1. Adhesives.....	169
8.1.1. FM [®] 73	171
8.1.1.1. FTIR Spectroscopy	172

8.1.1.2. Differential Scanning Calorimetry (DSC).....	178
8.1.1.3. Thermogravimetric Analysis (TGA).....	179
8.1.1.4 Mechanical Test Results.....	180
8.1.1.5. Summary of Test Results for the FM [®] 73 Adhesive.....	187
8.1.2. AF-191.....	188
8.1.2.1. FTIR Spectroscopy	189
8.1.2.2. Differential Scanning Calorimetry (DSC).....	193
8.1.2.3. Thermogravimetric Analysis (TGA).....	194
8.1.2.4. Mechanical Test Results.....	195
8.1.2.5. Summary of Test Results for the AF-191 Adhesive	201
8.1.3. FM [®] x5.....	202
8.1.3.1. FTIR Spectroscopy	203
8.1.3.2. Differential Scanning Calorimetry (DSC).....	207
8.1.3.3. Thermogravimetric Analysis (TGA).....	208
8.1.3.4. Mechanical Test Results.....	209
8.1.3.5. Summary of Test Results for the FM [®] x5 Adhesive.....	213
8.2. Bonded Joints.....	214
8.2.1. Al/FM [®] 73M/Al	214
8.2.1.1. Mode I (DCB).....	218
8.2.1.2. Mode II (ENF).....	224

8.2.1.3. Mixed Mode (CLS).....	225
8.2.1.4. Summary of Test Results for the Al/FM [®] 73M/Al System.....	227
8.2.2. Al/FM [®] 73M/B-Ep.....	229
8.2.2.1. Mode I (DCB).....	231
8.2.2.2. Mixed Mode (CLS).....	236
8.2.2.3. Summary of Test Results for the Al/FM [®] 73M/B-Ep System.....	239
8.2.3. Gr-BMI/AF-191M/Gr-BMI.....	241
8.2.3.1. Mode I (DCB).....	243
8.2.3.2. Mode II (ENF).....	249
8.2.3.3. Mixed Mode (CLS).....	250
8.2.3.4. Summary of Test Results for the Gr-BMI/AF-191M System.....	252
8.2.4. Ti/FM [®] x5/Ti.....	256
8.2.4.1. Mode I (DCB).....	257
8.2.4.2. Mode II (ENF).....	262
8.2.4.3. Mixed Mode (CLS).....	264
8.2.4.4. Summary of Test Results for the Ti/FM [®] x5/Ti System.....	265
8.3. Discussion of Results.....	267
8.3.1. Exposure and Test Environments	267
8.3.2. Chemical and Physical Analysis Methods.....	270
8.3.3. Material Properties	270

IX. CASE STUDIES.....	274
9.1. Case Study 1: The Boeing/Textron Bonded Doubler Program.....	274
9.1.1. Materials and Specimens.....	275
9.1.2. Boeing/Textron Testing Procedures	277
9.1.3. Finite Element Analysis.....	278
9.1.4. Comparison of the Experimental Data and Finite Element Analysis.....	281
9.2. Case Study 2: Bonded Patches on C-141 Transport Aircraft.....	283
X. SUMMARY AND CONCLUSIONS	285
XI. LESSONS LEARNED AND RECOMMENDATIONS.....	293
11.1. Lessons Learned.....	293
11.1.1. Specimen Design	293
11.1.2. Specimen Fabrication	293
11.1.3. Crack Length Determination	294
11.2. Recommendations for Future Work.....	295
11.2.1. Materials and Environments	295
11.2.1.1. Evaluate Other Surface Preparations.....	295
11.2.1.2. Conduct Additional Chemical and Physical Analyses of Adhesives ..	296
11.2.1.3. Investigate “True” Service Environments	297
11.2.2. Test Procedures.....	298
11.2.2.1. Conduct Additional Tests at Various Mode I/II Ratios.....	298

11.2.2.2. Duplicate Loading Conditions for Specific Applications	299
11.2.3. Analysis	300
11.2.3.1. Improve Current Models of the Adhesive Layer.....	300
11.2.3.2. Conduct Parametric Studies on Bonded Joint Applications.....	301
11.2.3.3. Expand Current Finite Element Models.....	301
11.2.4. Additional Topics for Further Research	302
APPENDIX A. SPECIMEN FABRICATION PROCEDURES.....	304
A.1. Adhesive Sheets Used for Tensile and Fracture Toughness Tests	304
A.1.2. Curing of FM [®] 73 and AF-191 Sheets.....	304
A.1.2. Curing of FM [®] x5 Sheets	305
A.2. Aluminum/FM [®] 73M/Aluminum (Al/FM [®] 73M/Al) Specimens	306
A.2.1. Surface Preparation of 7075-T651 Bare Aluminum Plates.....	306
A.2.2 Assembly of Al/FM [®] 73M/Al Panels	307
A.2.3 Bonding of Al/FM [®] 73M/Al Panels	308
A.2.4 Cutting of Al/FM [®] 73M/Al Panels to Form Individual Specimens.....	308
A.3. Aluminum/FM [®] 73M/Boron-Epoxy (Al/FM [®] 73M/B-Ep) Specimens.....	308
A.3.1. Aluminum/Boron-Epoxy Combinations for Various Specimen Geometries.....	309
A.3.2. Curing of Boron-Epoxy Laminates	309
A.3.3. Surface Preparation of Cured Boron-Epoxy Laminates.....	310
A.3.4. Assembly and Curing of Al/FM [®] 73M/B-Ep Panels	310

A.3.5. Bonding of Hinges to Double Cantilever Beam Specimen Panels.....	310
A.3.6. Cutting of Al/FM [®] 73M/B-Ep Panels to Form Individual Specimens.....	311
A.4. Graphite-Bismaleimide/AF-191M (Gr-BMI/AF-191M/Gr-BMI) Specimens ..	311
A.4.1. Gr-BMI Composite Adherend Lay-Ups.....	311
A.4.2. Curing of Gr-BMI Laminates.....	312
A.4.3. Surface Preparation of Cured Gr-BMI Laminates	312
A.4.4. Assembly of Gr/BMI/AF-191M/Gr-BMI Panels.....	313
A.4.5. Bonding of Gr-BMI/AF-191M/Gr-BMI Panels.....	313
A.4.6. Bonding of Hinges to Double Cantilever Beam Specimen Panels.....	314
A.4.7. Cutting Gr-BMI/AF-191M Panels to Form Individual Specimens.....	315
A.5. Titanium/FM [®] x5/Titanium (Ti/FM [®] x5/Ti) Specimens	315
A.5.1. Surface Preparation of Ti-6Al-4V Titanium Plates.....	316
A.5.2. Assembly of Ti/FM [®] x5/Ti Panels	316
A.5.3. Bonding of Ti/FM [®] x5/Ti Panels	317
A.5.4. Cutting Ti/FM [®] x5/Ti Panels to Form Individual Specimens.....	317
APPENDIX B. CONFIDENCE INTERVAL ANALYSIS OF SELECTED BONDED	
SYSTEMS.....	318
ENDNOTES.....	325
VITA.....	340

LIST OF TABLES

Table 1. Summary of Current Operational Bonded Boron-Epoxy Repairs.....	47
Table 2. Summary of Environmental Exposure Conditions.....	99
Table 3. Summary Table for Tests and Analyses of Adhesive Specimens.....	171
Table 4. In-Plane Properties of FM [®] 73U (unsupported) and FM [®] 73M (supported) ..	182
Table 5. Properties of FM [®] 73U Following Exposure to Various Environments	185
Table 6. In-Plane Properties of AF-191U (unsupported) and AF-191M (supported) ..	197
Table 7. Properties of AF-191U Following Exposure to Various Environments	200
Table 8. Properties of FM [®] x5 Following Exposure to Various Environments.....	211
Table 9. Summary of Tests Conducted on Bonded Joint Specimens	216
Table 10. Material Properties Used for the Model of the Boeing/Textron Specimen	278

LIST OF FIGURES

Figure 1. Mixed mode fracture toughness of several matrix and adhesive systems	53
Figure 2. Relation between total strain energy release rate and bond line crack growth rate for bonded composite joints using FM [®] 300 and EC-3445 adhesives	55
Figure 3. Effect of taper angle on joint performance for bonded composite joints	57
Figure 4. Possible environmental effects on the a) fracture toughness and b) fatigue crack growth behavior of adhesively bonded joints	66
Figure 5. Exposure effects may require design changes to meet operating requirements ..	68
Figure 6. Scrim cloths contained in a) FM [®] 73M, b) AF-191M, and c) FM [®] x5	75
Figure 7. Specimen geometry for (a) the ASTM D 638M Type M-III “dogbone” specimen used for tensile testing, and (b) the “straight-sided” specimen used for fracture toughness testing	80
Figure 8. Bond lines of the a) Al/FM [®] 73M/Al, b) Al/FM [®] 73M/B-Ep, c) Gr-BMI/AF- 191M/Gr-BMI, and d) Ti/FM [®] x5/Ti bonded systems	84
Figure 9. Double cantilever beam (DCB) specimen geometries	86
Figure 10. End-notched flexure (ENF) specimen geometries	88
Figure 11. Cracked lap shear (CLS) specimen geometries	90
Figure 12. Shim and gripping details for CLS specimens	91

Figure 13. One of the ovens used for isothermal exposure	101
Figure 14. Humidity chamber used to maintain a “hot/wet” environment.....	102
Figure 15. Thermal cycle profiles.....	105
Figure 16. Thermal cycling unit.....	106
Figure 17. Specimens loaded onto the automatic trolley tray	107
Figure 18. CLS specimen instrumented for temperature validation.....	111
Figure 19. Adhesive film specimen test apparatus showing (a) Questar Microscope (partially hidden behind laser unit), (b) laser extensometer, (c) mechanical test frame, (d) pneumatic grips, and (e) PC for test control and data acquisition..	114
Figure 20. Use of laser extensometer to measure adhesive test specimen gage length	115
Figure 21. Typical test frame arrangement.....	117
Figure 22. Ink stamp used to apply 0.5 mm graduated scales to specimen edges	119
Figure 23. Testing an Al/FM [®] 73M/Al DCB specimen using pins-and-clevises	122
Figure 24. Testing a Gr-BMI/AF-191M/Gr-BMI DCB specimen using hinges	122
Figure 25. Typical load vs. displacement data from a single DCB specimen	124
Figure 26. Typical end-notched flexure specimen test set-up	127
Figure 27. A Gr-BMI/AF-191M/Gr-BMI ENF specimen being tested.....	127
Figure 28. Placement of an extensometer on the cracked lap shear specimens	130
Figure 29. Typical cracked lap shear test set-up	131
Figure 30. Obtaining the Intercept Yield Strength.....	137

Figure 31. Determination of the end correction term, Δ	142
Figure 32. The modified crack closure technique (model is of unit width)	152
Figure 33. A comparison of load vs. displacement data obtained experimentally and computed using the ABAQUS finite element program.....	154
Figure 34. Computed Mode I, Mode II and total applied strain energy release rates for an Al/FM [®] 73M/B-Ep DCB specimen as a function of load for a single crack length	155
Figure 35. Typical FTIR spectroscopy results	161
Figure 36. Typical Differential Scanning Calorimetry results.....	165
Figure 37. The Perkin Elmer TGA 7 Thermogravimetric Analyzer.....	166
Figure 38. Typical Thermogravimetric Analysis results.....	168
Figure 39. Weight changes in FM [®] 73U adhesive due to long-term exposure	172
Figure 40. Full FTIR transmittance spectra for FM [®] 73U adhesives.....	173
Figure 41. Expanded FTIR transmittance spectra for FM [®] 73U adhesives	174
Figure 42. General epoxy curing and crosslinking process.....	176
Figure 43. Results from the DSC analysis of the FM [®] 73U adhesive.....	179
Figure 44. Results from the thermogravimetric analysis of the FM [®] 73U adhesive.....	180
Figure 45. Tensile behavior of the FM [®] 73U and FM [®] 73M adhesives	182
Figure 46. Tensile behavior of FM [®] 73U adhesive exposed to various environments	184
Figure 47. Process zone in FM [®] 73U during a plane stress fracture toughness test	186

Figure 48. Weight changes in AF-191U adhesive due to long-term exposure.....	189
Figure 49. Full FTIR transmittance spectra for AF-191U adhesives	190
Figure 50. Expanded FTIR transmittance spectra for AF-191U adhesives.....	191
Figure 51. Results from the DSC analysis of the AF-191U adhesive.....	194
Figure 52. Results from the thermogravimetric analysis of the AF-191U adhesive	195
Figure 53. Tensile behavior of the AF-191U and AF-191M adhesives.....	196
Figure 54. Tensile behavior of AF-191U adhesive exposed to various environments....	199
Figure 55. Process zone in AF-191U during a plane stress fracture toughness test.....	200
Figure 56. Weight changes in FM [®] x5 adhesive due to long-term exposure.....	203
Figure 57. Full FTIR transmittance spectra for FM [®] x5 adhesives.....	204
Figure 58. Expanded FTIR transmittance spectra for FM [®] x5 adhesives.....	205
Figure 59. Typical polyimide structure	206
Figure 60. Results from the DSC analysis of the FM [®] x5 adhesive	207
Figure 61. Results from the thermogravimetric analysis of the FM [®] x5 adhesive.....	209
Figure 62. Tensile behavior of FM [®] x5 adhesive exposed to various environments.....	210
Figure 63. Weight changes in Al/FM [®] 73/Al bonded joint specimens due to exposure...217	
Figure 64. Mode I fracture toughness of the Al/FM [®] 73/Al bonded system	219
Figure 65. Fracture surfaces of the Al/FM [®] 73M/Al bonded system	220
Figure 66. Mode I fatigue behavior of the Al/FM [®] 73/Al bonded system	223
Figure 67. Summary of toughness data for the Al/FM [®] 73M/Al bonded system.....	227

Figure 68. Weight changes in Al/FM [®] 73M/B-Ep bonded specimens due to exposure ..	231
Figure 69. Fracture toughness of the Al/FM [®] 73/B-Ep DCB specimens.....	232
Figure 70. Fracture surfaces of the Al/FM [®] 73M/B-Ep bonded system.....	233
Figure 71. Fatigue behavior of the Al/FM [®] 73/B-Ep bonded system.....	235
Figure 72. Mixed mode fracture toughness of Al/FM [®] 73M/B-Ep CLS specimens with boron-epoxy straps	238
Figure 73. Summary of toughness data for the Al/FM [®] 73M/B-Ep bonded system	239
Figure 74. Weight changes in Gr-BMI/AF-191M/Gr-BMI bonded joint specimens due to exposure.....	243
Figure 75. Effect of environmental exposure on the Mode I fracture toughness of the Gr-BMI/AF-191/Gr-BMI bonded system.....	244
Figure 76. Effect of test temperature on the Mode I fracture toughness of the Gr- BMI/AF-191/Gr-BMI bonded system	245
Figure 77. Fracture surfaces of the Gr-BMI/AF-191/Gr-BMI bonded systems.....	246
Figure 78. Mode I fatigue behavior of the Gr-BMI/AF-191M/Gr-BMI system	248
Figure 79. Mode II fracture toughness of the Gr-BMI/AF-191/Gr-BMI system.....	249
Figure 80. Mixed Mode fracture toughness of the Gr-BMI/AF-191/Gr-BMI bonded system with unidirectional adherends	251
Figure 81. Mixed mode fracture toughness of the Gr-BMI/AF-191/Gr-BMI bonded system with quasi-isotropic adherends.....	252

Figure 82. Summary of fracture toughness data for the Gr-BMI/AF-191M/Gr-BMI bonded system with unidirectional adherends.....	253
Figure 83. Summary of fracture toughness data for the Gr-BMI/AF-191M/Gr-BMI bonded system with quasi-isotropic adherends	254
Figure 84. Weight changes in Ti/FM [®] x5/Ti bonded joint specimens due to exposure....	257
Figure 85. Mode I fracture toughness of the Ti/FM [®] x5/Ti bonded system	259
Figure 86. Fracture surfaces of the Ti/FM [®] x5/Ti bonded system	260
Figure 87. Mode I fatigue behavior of the Ti/FM [®] x5/Ti bonded system	261
Figure 88. Mode II fracture toughness of the Ti/FM [®] x5/Ti bonded system.....	262
Figure 89. Mixed mode fracture toughness of the Ti/FM [®] x5/Ti bonded system	264
Figure 90. Summary of fracture toughness data for the Ti/FM [®] x5/Ti bonded system....	266
Figure 91. Geometry of the Boeing/Textron patched panel.....	277
Figure 92. Model of the Boeing/Textron patched panel fatigue test specimen.....	279
Figure 93. Mode I fracture toughness of the Al/FM [®] 73/Al bonded system (with estimated confidence intervals).....	319
Figure 94. Fracture toughness of the Al/FM [®] 73/B-Ep DCB specimens (with estimated confidence intervals).....	320
Figure 95. Effect of environmental exposure on the Mode I fracture toughness of the Gr-BMI/AF-191/Gr-BMI system (with estimated confidence intervals).....	321

Figure 96. Effect of test temperature on the Mode I fracture toughness of the Gr-BMI/AF-191/Gr-BMI bonded system	322
Figure 97. Mode II fracture toughness of the Gr-BMI/AF-191/Gr-BMI bonded system (with estimated confidence intervals).....	323
Figure 98. Mode I fracture toughness of the Ti/FM [®] x5/Ti bonded system (with estimated confidence intervals).....	324

LIST OF SYMBOLS AND ABBREVIATIONS

α	coefficient of thermal expansion
a	crack length
a_i or a_0	initial crack length
AF-191	toughened epoxy adhesive manufactured by 3 M
Al/FM [®] 73M/Al	designation for bonded joint specimens fabricated with two aluminum adherends joined with FM [®] 73M toughened epoxy adhesive
Al/FM [®] 73M/B-Ep	designation for bonded joint specimens fabricated with one aluminum adherend and one boron-epoxy composite adherend joined with FM [®] 73M toughened epoxy adhesive
ASTM	American Society for Testing & Materials
b	width of a bonded joint specimen
C	compliance (δ/P)
CLS	cracked lap shear bonded joint specimen geometry
C-141	USAF four-engined heavy transport aircraft, <i>Starlifter</i>
δ	displacement, crack mouth opening, or center point deflection

Δ	intercept of the a-axis obtained from a linear relationship between $C^{1/3}$ and a (crack length)
da/dN	crack growth rate per cycle
DCB	double cantilever beam bonded specimen geometry
DSC	differential scanning calorimetry
ΔG	strain energy release rate range
ΔG_I	Mode I strain energy release rate range
$\Delta G_{I,th}$	Mode I threshold strain energy release rate range
ΔG_T	total strain energy release rate range
$\Delta G_{T,th}$	total threshold strain energy release rate range
ΔK	stress intensity range
δ_y	nodal separation distance for the modified crack closure integral
E	elastic modulus
E_l	elastic modulus of the lap in a CLS specimen
ENF	end-notched flexure bonded specimen geometry
E_s	elastic modulus of the strap in a CLS specimen
ϵ_f	failure strain
$f(a/W)$	geometric factor for single-edge notched specimens = $1.12\sqrt{\pi}$
F-22	USAF newest twin-engined fighter aircraft, <i>Raptor</i>

F4/5521	designation for Textron's boron-epoxy pre-preg material
FAA	Federal Aviation Administration
FM [®] 73	toughened epoxy adhesive manufactured by CYTEC
FM [®] x5	polyimide adhesive manufactured by CYTEC
FPL	Forest Products Lab
FTIR	Fourier Transform Infrared
G	strain energy release rate
G _I	Mode I strain energy release rate
G _{IC}	Mode I critical strain energy release rate
G _{II}	Mode II strain energy release rate
G _{IIC}	Mode II critical strain energy release rate
GLARE [™]	laminated material consisting of aluminum and fiberglass layers
Gr-BMI/AF-191M/Gr-BMI	designation for bonded joint specimens fabricated with two graphite fiber-reinforced bismaleimide composite adherends joined with AF-191M toughened epoxy adhesive
G _T	total strain energy release rate
G _{TC}	total critical strain energy release rate
η	bond line thickness
hr.	hour
HSCT	High Speed Civil Transport

Hz	Hertz (1/sec.)
IM7/5250-4	designation for BASF's graphite fiber-reinforced bismaleimide pre-preg
in.	inch
K	stress intensity
kip	kilo-pounds (100 pounds)
km	kilometer
kN	kilonewton
kPa	kilopascal
L	distance from center loading point to outer roller in ENF testing
lb.	pound
LVDT	linear variable differential transformer (displacement measuring device)
m	meter
m	slope of a line describing the relationship between compliance and crack length with an equation of $C = C_o + ma^3$
μ	true mean of a property
mi.	mile
mm	millimeter
Mpa	Megapascal

N	number of cycles
ν	Poisson's ratio
n	fatigue crack growth sensitivity exponent, as in: $da/dN = C(\Delta G_T)^n$
n	sample size (for confidence interval calculations)
NASA	National Aeronautics and Space Administration
P	load
PABST	Primary Aircraft Bonded Structures Technology
P_n	nodal force for the modified crack closure integral
psi	pounds per square inch
R-ratio	ratio of P_{min}/P_{max} or $\delta_{min}/\delta_{max}$
R^2	correlation coefficient for curve-fitting (perfect correlation between data and an equation give an R^2 value of 1)
RAAF	Royal Australian Air Force
RAF	Royal Air Force
RCAF	Royal Canadian Air Force
RT	room temperature, approximately 22°C (72°F)
s	standard deviation
sec.	second
SLVC	super linear variable capacitor (displacement measuring device)

σ_f	applied far-field stress at fracture instability
σ_{iys}	intercept yield strength
σ_{uts}	ultimate tensile strength
σ_{ys}	yield strength
$\sigma_{ys(0.2)}$	0.2% offset yield strength
t	thickness of one adherend
$t_{\alpha/2}$	Student t-distribution value (for confidence interval calculations)
TGA	thermogravimetric analysis
Ti-6Al-4V	a titanium alloy
Ti/FM [®] x5/Ti	designation for bonded joint specimens fabricated with two titanium adherends joined with FM [®] x5 polyimide adhesive
t_l	thickness of the lap adherend in a CLS specimen
t_s	thickness of the strap adherend in a CLS specimen
USAF	United States Air Force
W	specimen width for adhesive tensile and fracture toughness specimens
W/g	watts per gram
\bar{x}	average value
°C	degrees Centigrade (Celsius)

°F	degrees Fahrenheit
7075-T651	an aluminum alloy used for wing and fuselage construction
$(1-\alpha)$	degree of certainty for computing a confidence interval ($\alpha = 0.05$ for a 95% confidence interval)

SUMMARY

Adhesive bonding is being investigated for a number of aerospace applications. Among these are the joining of composites and metals for various assemblies and the bonding of composite patches to cracked metallic structures for repair purposes. Understanding the environmental durability of adhesively bonded joints is crucial to ensuring the safety and structural integrity of these components.

The goal of the research reported in this thesis was to investigate, quantify, and improve the understanding of how environmental exposure affects the fracture and fatigue behavior of bonded joints intended for aerospace use.

Four bonded aerospace material systems were investigated: 1) aluminum bonded to aluminum using a toughened epoxy adhesive, 2) aluminum bonded to a boron-epoxy composite using a toughened epoxy adhesive, 3) graphite fiber-reinforced bismaleimide aluminum bonded to graphite fiber-reinforced bismaleimide using a toughened epoxy adhesive, and 4) titanium bonded to titanium using a polyimide adhesive.

Adhesives film specimens were tested in parallel with bonded joint specimens. This approach was taken to determine if changes in bonded joint performance could be linked directly to changes in the behavior of the adhesives.

Bonded joint specimens and adhesive samples were exposed to various environments for up to 10,000 hours prior to being mechanically tested. These environments were based on aircraft service conditions and included isothermal exposure to high temperature low humidity (hot/dry), and high temperature high humidity (hot/wet) conditions, and well as thermal cycling between low and high service temperature extremes.

The chemical and physical characteristics of the adhesives were analyzed using spectroscopy, differential scanning calorimetry, and thermogravimetric analysis. Tensile and plane stress fracture toughness tests were also performed on the adhesive specimens.

Bonded joint specimens were fabricated in double cantilever beam, end-notched flexure, and cracked lap shear geometries to examine the Mode I, II, and mixed mode fracture and fatigue characteristics of the bonded material systems. Monotonic fracture toughness and fatigue crack growth tests were performed on these specimens.

Test results were analyzed using closed-form and finite element solutions using linear elastic fracture mechanics assumptions. Bonded joint specimens with dissimilar adherends required a detailed finite element analysis to determine the magnitude of thermal residual stresses in the bond line and the effect of mismatched adherend flexural stiffnesses.

Results showed that environmental exposure is detrimental in varying degrees. Hot/wet conditions (high temperature plus high humidity) appeared to be most severe.

Long term exposure to these conditions significantly reduced the strength and toughness of the epoxy adhesives, resulted in lower fracture toughness in bonded joint specimens, and reduced the fatigue threshold for the aluminum/aluminum and aluminum/boron-epoxy systems. In addition, significantly lower toughness values were observed in bonded joint specimens tested -54°C (-65°F), a temperature encountered during high altitude, sub-sonic flight. Reductions in toughness occurred under all modes of loading.

The fracture path in the bonded joint specimens depended upon the nature of the adherends and specimen geometry. For bonded joint specimens having metal adherends, fracture was, in most cases, cohesive suggesting that surface preparation of the adherends was adequately resistant to the exposure conditions. Fracture in the aluminum/boron-epoxy system followed a path within the composite matrix resulting in very low toughness values relative to the other systems tested. Fracture in the bonded graphite-bismaleimide specimens employing quasi-isotropic adherends was interlaminar within the off-axis plies near the bond line.

In fatigue, the bonded joints exhibited very low threshold levels compared to monotonic fracture toughness. In addition, large differences in the crack growth rate were observed to occur with small changes in the applied strain energy release rate. These extremely high crack growth rate sensitivities were manifested in the form of very steep slopes in da/dN vs. ΔG_T curves.

The results of the experimental program were compared with an independent study of the fatigue behavior of bonded composite patches and also with design load levels from a specific aircraft application.

The findings of this research emphasize the necessity of accounting for environmental effects in the design of adhesively bonded joints, highlight trends in the characteristics of adhesives and adhesively bonded joints exposed to various service conditions, and provide data on the fracture and fatigue performance of specific bonded aerospace materials.

CHAPTER I

INTRODUCTION

Adhesive bonding has been advocated for decades as a method of aircraft structural fabrication. Proponents cite the advantages bonding offers in terms of weight savings, fatigue resistance, improved aerodynamic qualities, and possible long-term cost reductions. Several studies have confirmed the benefits of using adhesives for structural joining. However, despite the recommendations of many research and development efforts, the vast majority of adhesive bonding in aerospace components remains in non-structural or secondary applications. Adhesive bonding is still not accepted on par with traditional riveted construction.

The reason for this reluctance on the part of the aircraft industry depends on several factors. First, mechanical fastening is a deeply entrenched production method, and, in today's highly competitive market, redesigning, retooling, and retraining to incorporate adhesive bonding is often cost prohibitive. The fear of the catastrophic failure of a primary structural bond caused by poor surface preparation has also prevented wider implementation of adhesive bonding. In addition, even with adequate surface preparation, the long-term environmental durability of adhesively bonded joints is

not fully understood. The research conducted for this thesis was aimed at increasing this understanding by using fracture mechanics to examine various bonded material systems.

With the increased number of bonded composite aircraft components and bonded repairs made to cracked metallic structures, knowledge of adhesive bonding is becoming crucial to aircraft design and life extension. Design and analysis of bonded joints has traditionally been performed using a variety of stress-based approaches. However, fracture mechanics, which has become an accepted method for the study of metallic structures, has also been shown to be a viable tool for bonded joint analysis. Durability and damage tolerance guidelines, already in existence for metallic aircraft structures, need to be developed for bonded structures, and fracture mechanics provides one method for doing so.

The goal of this research was to investigate, quantify, and improve the understanding of how environmental exposure affects the fracture and fatigue behavior of bonded joints intended for aerospace use. To attain the goal of this program, several objectives were identified. These included: 1) characterizing the mechanical behavior of several aerospace adhesives and adhesively bonded material systems, 2) quantifying the degradation in the fracture and fatigue properties of bonded joints due to environmental exposure, and 3) relating experimental data obtained during analyses performed for this research with specific issues of bonded joint design. These objectives served to guide the research described in the following thesis.

Motivation for this project came from several directions with the primary focus being on bonded structures for aerospace use. First, a desire exists to supplement current stress-based approaches to bonded joint design. Although stress-based methods have proven their worth over the last several decades, fracture mechanics can more accurately address the problems of bond line defects and fatigue of bonded components. Impetus for this research also came from a need to link knowledge of environmental effects with the fracture and fatigue characteristics of bonded joints. As bonding becomes more prevalent and aircraft design lives lengthen, understanding, in general terms, the interaction of the operating environment with material properties becomes increasingly important. In addition, several organizations including the Federal Aviation Administration, the U.S. Air Force, and major airframe manufacturers have concerns about the performance of specific adhesively bonded systems. Finally, this research was undertaken to respond to the recent increased emphasis for life extension of aging aircraft. This trend has highlighted the need to address the durability of bonded composite repairs to cracked metallic components and the projected lifetimes of bonded structures for future aircraft designs. Understanding the behavior of adhesive joints subjected to various environmental conditions serves as the basic motivating factor for this research and for the eventual development and refinement of durability and damage tolerance guidelines for bonded aerospace structures.

In pursuing the major goal, satisfying the objectives, and responding to the motivations behind this research, the overall intent was to provide a general assessment of the basic problem of bonded joint durability. To do so, a broad experimental and computational effort was undertaken to examine the behavior of a variety of bonded material systems exposed to a number of operating environments, and assessed using a collection of techniques. Fracture mechanics analyses were emphasized not with the intent of supplanting well-established stress-based approaches but, rather, to best analyze the specimens used and to demonstrate an alternate analytical technique.

The remainder of this thesis is divided into ten additional chapters. Chapter II provides historical and background information on bonded joint applications for aerospace, analytical techniques, and environmental issues. This section also includes a discussion of a design philosophy related to bonded joints,¹ Chapter III describes the three adhesive systems and four bonded joint systems investigated for this research. This section also discusses fabrication and specimen geometry. Chapter IV addresses several environmental issues. These include long-term isothermal and thermal cycling exposure, specimen storage, and testing environments. Chapter V reviews mechanical testing procedures which included tensile and fracture toughness tests on adhesive film specimens,² as well as fracture and fatigue experiments conducted on bonded joint specimens. Chapter VI discusses the various closed-form and finite element analyses used throughout the project to analyze the results of the test programs. Chapter VII

outlines the chemical and physical analyses performed on adhesive film specimens. These included spectroscopy, differential scanning calorimetry, and thermogravimetry. Chapter VIII summarizes and discusses results of the chemical and physical analyses of the adhesive film specimens, the tensile and fracture toughness testing of the adhesive film specimens and the fracture and fatigue tests conducted on bonded joint specimens. Chapter IX includes the results of two case studies³ which related experimental results obtained from this research to specific aerospace applications. Chapter X provides a brief summary and discussion of the major conclusions of this work. Chapter XI lists lessons learned and recommendations for additional research. Finally, Appendix A provides detailed fabrication procedures used in the production of test specimens, and Appendix B includes additional charts not included in the text which include confidence intervals obtained from multiple fracture toughness values.

CHAPTER II

BACKGROUND

It may be argued that adhesive bonding has existed since man first used crude animal- or plant-based resins in the construction of small laminated boxes and other household items. Today's aerospace structural bonding techniques are much more sophisticated and are designed to exploit the advantages offered by adhesives.

These advantages are particularly attractive to engineers considering the use of adhesives for airframe production and structural repair. Bonded structures can be lighter, often by as much as 14%,⁴ than those that are mechanically fastened. Because of the lack of rivet holes which act as stress raisers, bonded structures are also more fatigue resistant and may withstand 50% more cycles at the design limit load than mechanically-fastened structures.⁵ The lack of a need for rivet holes is particularly attractive when joining composite structures where those holes would cut a significant number of load bearing fibers. In addition, bonded aircraft structures permit smoother contours which reduce drag, reduce susceptibility to galvanic corrosion, and may offer potential long-term cost savings due to smaller part counts and fewer required machining operations. Furthermore, when used for the repair of cracked structures, adhesively bonded composite patches can

reduce ΔK values by up to 80% and curtail further crack growth in the repaired structure.^{6,7,8}

Despite these attractive advantages, adhesives are currently widely used only on secondary aircraft structures such as bonding honeycomb core to aluminum or composite facesheets, or as a redundant means of fastening such as on so-called "bolted-bonded" lap joints commonly used on commercial aircraft. Aircraft manufacturers are reluctant to use bonding on primary structures for a number of reasons. First, the process demands adequate surface preparation following stringent procedures⁹ which, if neglected, may lead to catastrophic joint failure. Past experiences with bonded joint failures due to poor surface preparation are perhaps the primary reason behind the lack of support for adhesive bonding in the aerospace industry. In addition, frequent and sophisticated inspection is also cited as a drawback of adhesive bonds.¹⁰ Indeed, the presence of low-strength, yet physically intact, bond area is undetectable with current non-destructive evaluation techniques. Finally, many production facilities require re-tooling and personnel would require re-training if adhesive bonding were to be implemented on a large scale to replace traditional riveted fabrication methods. In today's highly competitive market, such costly changes often outweigh the benefits offered by adhesive joints.

However, adhesively bonded joints continue to receive attention in the aerospace industry where the quest for reduced weight and increased fatigue resistance have accompanied the drive for structural improvements. As bonded joints are specified for an

expanding number of aerospace applications the need for knowledge about their strength, toughness, fatigue resistance, and durability also increases. This need has been recognized by many. Kutscha & Hofer recommended in 1969 that materials and analytical techniques be investigated to aid in bonded joint design.¹¹ In 1984, a National Materials Advisory Board committee recommended that the chemistry and mechanics of adhesive bonds and interphase regions be studied to enable joints to be used under severe environments.¹² Most recently, an increased emphasis on extending the lives of aging and cracked metallic aircraft structures using bonded repairs has sparked a renewed interest in adhesive bonding.

This chapter reviews a representative number of these studies of adhesively bonded joints. Key sections describe current aerospace applications of adhesives, discuss popular analysis methods, identify key environmental concerns, and review design philosophies pertinent to the application of adhesive joints for aircraft structural applications.

2.1. Adhesive Bonding in Aerospace Applications

Adhesive bonding of aerospace components is a fabrication technique which, though over 70 years old, has increased markedly in popularity during the last two decades. It has been a focal point in many studies concerning the fabrication of primary aircraft structures and the repair of aging aircraft.

Many of the successes of adhesive bonding may be attributed to military applications which began in the early days of flight and during the First World War. Significant breakthroughs such as the use of phenolic resins in wood and wood-to-metal joints¹⁰ occurred during the World War II era on aircraft such as the RAF's *Mosquito*. Building upon these advances in military aircraft, engineers at Fokker began bonding structural metal components on the successful F-27 and F-28 commercial airliners in the late 1940's and early 1950's.^{13,14,15} Military use of bonded metal structures occurred almost simultaneously on aircraft like the USAF's B-58 *Hustler*.¹⁰

Continued work in this field has led to the development of several bonded systems, some of which have been investigated for the research reviewed in this thesis. These systems and their applications are described in the following sections.

2.1.1 Adhesively Bonded Aircraft Structures

Engineers and designers have long sought to exploit the advantages offered by adhesive bonding in the construction of new aircraft structures. Perhaps the earliest (and certainly the most cited) comprehensive study was the Primary Adhesively Bonded Structures Technology (PABST) program sponsored by the USAF and performed by the Douglas Aircraft Co. in the mid-1970's.^{9,16} This effort examined the performance of adhesively bonded aluminum for a transport aircraft fuselage. It included some investigations of the effects of environmental exposure, but these were aimed at determining an aging protocol to simulate service conditions and were deemed

inconclusive. The basic conclusion of the study was that that construction of a 15% lighter structure with a cost savings of 20% was feasible. In a testament to the fatigue resistance of adhesive bonds, the mainly bonded test structure withstood 68,000 pressure cycles (approximately 3.5 lifetimes) with only 7 cracks observed in bonded areas, all of which initiated at nearby rivet holes.¹⁷ Unfortunately, the successes of the PABST program were never fully incorporated in transport aircraft design. The previously mentioned reluctance of the aircraft industry to employ adhesive bonding on a large scale resulted in the next military transport, the C-17, being manufactured using primarily traditional, riveted designs.

However, the advantages of adhesive bonding highlighted by the PABST program and the advent of the use of composite materials have fostered additional programs investigating bonding for aircraft structural applications. Many of these programs have examined adhesives for use in high performance aircraft such as the F-16,⁴ F-5,¹⁸ and A-7⁵ where minimizing weight is a major design goal. More recently, two major aerospace vehicle programs have incorporated adhesive bonding into the design of structural components. These programs include the U.S. Air Force's new F-22 fighter and NASA's High Speed Civil Transport.

2.1.1.1. Control Surfaces on the F-22

The U.S. Air Force and its contractors have chosen adhesive bonding for use on newer aircraft such as the F-22 fighter which employ large amounts of composite

materials. Specific bonded applications on the F-22 include control surfaces fabricated from composite laminates¹⁹ that transfer pressure-induced and inertial loads to internal structures. Though the F-22 is a costly venture,^{20,21} these bonded assemblies augment the aircraft's performance by reducing weight and aerodynamic drag. These joints must also possess environmental durability for they may be exposed to temperatures of 104°C (220°F) during high performance, "edge-of-the-envelope" maneuvers. The F-22's manufacturers chose graphite fiber-reinforced bismaleimide composites bonded with 3M's AF-191M toughened epoxy adhesive as the material system for these control surfaces. This bonded material system was also investigated for the research project covered in the present report.

2.1.1.2. Wing and Fuselage Structures on the High Speed Civil Transport

A future application of adhesive bonding exists on the wings and fuselage of NASA's High Speed Civil Transport supersonic aerospace vehicle. Here, engineers plan to use a recently developed advanced polyimide adhesive to manufacture structural joints²² and also to bond facesheets to honeycomb core.²³ The HSCT is designed to carry 250 passengers for 9250 km (5750 mi.) at a target speed of Mach 2.4, so these wing and fuselage structures will be subject to temperatures in the 149-177°C (300-350°F) range,²⁴ requiring the use of titanium adherends and severely testing the durability of the bond line. Yet, adhesives are crucial to economical operations of this commercial venture because of the weight and cost savings afforded by bonded construction. The HSCT's

polyimide/titanium system was also investigated for the research project covered in the this thesis.

2.1.2. Adhesively Bonded Repairs

Advances in repair technology using composite patches and an increased emphasis on extending the lifetimes of aging aircraft, have generated a great deal of interest in the use of adhesives for repairs. Adhesively bonded composite repairs to metal structures may currently be the subject of more research and development than are bonded primary structural composites. As with the initial development of structural bonding, most bonded repairs have been made to military aircraft, but adhesively bonded patches are slowly being adopted by commercial carriers as well..

To understand why the number of bonded repairs is so large and continuing to increase, consider the case of the USAF inventory. In 1995, it was reported that 41% of the active duty fleet was over 24 years old.²⁵ In 1996, the average age of USAF aircraft was nearly 18 years.²⁶ In 1997, the average age of the C-141, B-52, and C/KC-135 fleets exceeded 30 years.²⁷ By the year 2005, when the F-22 is expected to be fully operational, the average age of fighter aircraft will exceed 20 years.²⁶ The aging of the fleet, combined with missions that often stress airframes beyond original design limits,²⁷ and the current emphasis on extending aircraft lives well into the next century^{28,29} have combined with corrosion and fatigue to make quick, effective, fatigue resistant bonded composite repairs extremely attractive.

2.1.2.1. Repairs Using Bonded Boron-Epoxy Patches

Pioneering work in Australia⁸ and the U.S.³⁰ has resulted in widespread usage of boron-epoxy composite laminates to repair cracked metallic structures. The primary advantage offered by this type of bonded repair is a significant reduction in crack growth in the underlying metallic structure due to the use of a much stiffer patch material. The stiff patches direct more of the load into the repair than is transferred through the cracked primary structure. This problem has been studied extensively³¹⁻³⁴ with the reduction in stress levels and ΔK at the crack tip and the increase in patched component life being well-documented.

The majority of these patches have been applied to military aircraft with the most prevalent use of the technique being the repair of nearly 500 fatigue cracks emanating from wing skin fuel transfer holes ("weep-holes") on the USAF C-141 fleet.³⁵ However, commercial aircraft are also slowly transitioning to the use of bonded boron-epoxy repairs. One example is a large quasi-isotropic patch applied to the rear passenger door of an L-1011 airliner designed to increase the life of this fatigue critical region. After an extensive study of materials, installation, and performance,^{36,37} the patch received FAA certification³⁸ and has seen several months of transatlantic service with no detectable debonds.³⁹

Though no exhaustive survey exists of all bonded aircraft repairs, an estimated 6500 boron-epoxy patches are in worldwide use on military aircraft and over 200 have

been applied to commercial aircraft.⁴⁰ Table 1 shows a brief synopsis of some of the many bonded boron-epoxy repairs in use.

2.1.2.2. Repairs Using Other Bonded Materials

Although the bonded boron-epoxy system has dominated the bonded repair arena, other materials are being investigated as substitutes.

Carbon fiber reinforced composites have been successfully used by the RAF for repairs to the Tornado GR1 fighter⁴¹ and have been studied by the Australian Aeronautical Research Laboratories.⁴² This material has the advantage of being less expensive than boron-epoxy and of having superior flexibility which permits it to be used on repairs having small radii. However, some risk of galvanic corrosion exists when using this material if the carbon fibers are not adequately separated from the underlying aluminum structure by the adhesive layer.

GLARE™ laminates,⁴³ comprised of alternating aluminum and fiberglass layers, have also been employed in a limited number of repairs. Currently in use on a USAF C-5 fuselage crown region,⁴⁴ this material matches the thermal properties and formability of aluminum but offers the crack suppression qualities of composites.

Table 1. Summary of Current Operational Bonded Boron-Epoxy Repairs^{6,8,45}

OWNER	AIRCRAFT	COMPONENT	NUMBER OF AIRCRAFT	NUMBER OF PATCHES	DATE
MILITARY					
USAF	C-141	Wing Skin	~150	~1500	1993-94
	F-111	Wing Pivot	411	~800	1973-83
	B-1	Dorsal Longeron	96	~190	1991-96
	C-5	Fuselage	1	2	1996
	C-130	Gear Door	1	1	1992
	T-38	Access Door	3	4	1994
RAAF	F-111	Wing Pivot, Skin	~1500	total	1975-96
	C-130	Wing Stiffener			
	Mirage III	Wing & Tail Skin			
	Macchi	Wheel			
RAF	Hawk	Wing Skin	1	1	1993
	Harrier	Fuselage	1	1	1993
RCAF	F-5	Wing Skin	~25	~50	1992-99
Dutch Air Force	F-16	Wing Skin	~3	~3	1996
COMMERCIAL					
Air Inter (France)	Mercure	Door Frames	11	~100	1973-78
Ansett (Australia)	Boeing 767	Keel Beam	1	2	1989
	BAE 146	Engine Cowl	1	6	1992
Qantas	Boeing 747	Various "decals" [†]	1	9	1990
Australian Airlines	Boeing 727	Fuselage "decals" [†]	1	9	1989
Boeing	Boeing 747	Various	1*	11	~1989
	Boeing 747	Various	1*	13	1990
Air Wisconsin	BAE 146	Engine Cowl	1	6	1992
Federal Express	Boeing 747	Various "decals" [†]	2	25	1993

* indicates static test airframe

[†] "decals" are patches applied to uncracked structure to test durability

2.2. Design and Analysis Approaches

The analysis of bonded joints has been the subject of a vast amount of research during the last half century. The intent of this section is to give the reader a brief overview of the two major types of bonded joint analysis: stress-based approaches, and fracture mechanics.

2.2.1. Stress Based Approaches

The stress-based approach focuses on determining the distribution of shear and normal (or “peel”) stresses within the adhesive bond line under static loading conditions.

In their seminal work in this field, Goland & Reissner⁴⁶ investigated single lap shear joints with thin (“inflexible”) and thick (“flexible”) adhesive layers. They based their work on the theory of cylindrically bent plates and assumed plane stress. Their results indicated that both shear and normal stresses approach maxima at the free edge of the joint regardless of bond line thickness.

Harrison & Harrison⁴⁷ also investigated the stresses in the adhesive layer basing their work on the assumption of isotropic linear elasticity of the adhesive layer. They confirmed Goland & Reissner’s earlier results concerning stress concentrations at the ends of lap joints and determined that a state of uniform stress existed within the joint at a distance of several bond line thicknesses from each edge. Furthermore, they applied a probabilistic flaw effect to explain the reduction in joint strength with adhesive thickness.

Further refinements of Goland & Reissner's work were performed by Vinson¹⁷ and Carpenter & Patton.⁴⁸ Both of these analytical efforts determined that the shear stress concentration reached a maximum near, not at, the free edge of a single lap joint.

The focus on single lap joints for the evaluation of adhesives continued with the development of a standardized single lap shear test procedure, ASTM D 1002-72.⁴⁹ This test was designed to compare the shear strengths of adhesives, but ASTM practice does not recommend that it be used to develop design allowables. Though simple in form, this ASTM lap shear geometry sparked a great deal of criticism. Guess, *et al.*⁵⁰ maintained that the test was simple and economical. However, they also stated that the test underestimated an adhesive's shear strength compared to thick adherend lap shear tests because failure of the adhesive was driven by the normal "peel" stress concentrations at the edges of the joint. Adams⁵¹ agreed and, using a finite element analysis demonstrated that failure of the adhesive layer occurs in tension, due to high peel stresses, rather than in shear, as suggested by the lap shear joint's name. Furthermore, Adams also showed that the presence and shape of a fillet at the edge of the adhesive bond line determines the location of the peak peel stress.

Hart-Smith rigorously attacked the problem of stress-based bonded joint analysis. As one of the principal engineers assigned to the PABST program, he focused on the analysis and design of adhesively bonded joints for practical use in aircraft structures. Beginning his work on the classical single lap joint geometry, Hart-Smith observed that

the average adhesive shear stress was an inadequate design criteria due to the previously identified peel stress concentrations.⁵² Realizing that adhesives exhibit elasto-plastic behavior, he incorporated a simpler bi-linear elastic adhesive model into his work on double-lap joints.⁵³ Hart-Smith re-confirmed that improperly designed joints fail due to excessive peel stresses at the edges, and maintained that properly designed joints fail only when the shear strain energy per unit bonded area in the adhesive layer exceeds a critical value.⁵³ He extended these concepts into the design of stepped, scarf, and other joint geometries.^{54,55} Hart-Smith's basic design tenets of increasing joint overlap and tapering adherend edges to minimize peel stresses and of ensuring that the adhesive bond strength exceeds that of the adherends have become widely accepted.^{9,56,57} To date, the stress-based approach to bonded joint design has functioned well and has been incorporated into computerized design programs used in the aerospace industry.

2.2.2. Fracture Mechanics Analyses

The stress-based approach, though rigorous and useful, is primarily based on considerations of static strength and does not fully address the behavior of bonded joints in the presence of flaws. Fracture mechanics has emerged as a method to more accurately evaluate these effects of bond line flaws and fatigue in the presence of cracks.

Founded upon the basic theories developed by Griffith and Irwin, the use of fracture mechanics for bond analysis was first proposed by Ripling, Mostovoy, & Patrick.⁵⁸ At the time of their research, the stress intensity factor, K , had become

accepted for describing fracture in metals. However, K solutions are based upon homogeneous materials, the verification of a stress field singularity in the form $(1/r)^{1/2}$, and require difficult stress analyses to determine the appropriate geometric scaling factor if they are to be extended to heterogeneous systems such as bonded joints. Ripling, *et al.*, recognized the inhomogeneity of bonded systems and proposed the use of the more fundamental (and, some would argue, more practical) strain energy release rate, G, to replace K in describing fracture of adhesive joints. In further work, the authors used the strain energy release rate in a detailed analysis of a Mode I, double cantilever beam specimen.⁵⁹

The use of established or easily-obtained K solutions also depends upon the full development of a plastic zone ahead of the crack tip. In adhesive joints, the plastic zone in the adhesive layer is often restricted by the adherends. Shaw⁶⁰ and Williams⁶¹ investigated this phenomenon and used it to further support the choice of an energy (G) approach rather than a stress intensity (K) approach for describing the fracture behavior of bonded joints.

As with stress intensity, the strain energy release rate may consist of one or more modes, and a number of specimens have been developed to investigate Mode I, II, III, and mixed mode fracture and fatigue behavior of adhesively bonded joints. The most common is the double cantilever beam (DCB) which tests resistance to Mode I cracking. Mode II or shear type fracture may be investigated using the end-notched flexure (ENF) specimen

first suggested by Russell & Street⁶² and subsequently analyzed by Carlsson, *et al.*⁶³ Although DCB and ENF specimens may be analyzed in a straightforward manner, often using established closed-form solutions, mixed-mode loading (particularly Modes I and II) is most prevalent in bonded components. The mode mixity occurring in service has been addressed using specimens such as the cracked lap shear (CLS) specimen developed by Brussat *et al.*,⁶⁴ and the mixed mode bending (MMB) test designed by Reeder & Crews.⁶⁵ These specimens, though more realistic, also require more complicated analyses. In an effort to understand mixed mode behavior from more easily obtained single mode results, relationships between the Mode I, Mode II and mixed mode toughness of adhesive materials have been proposed. One such relationship will be outlined in the following sections.

Using the concept of fracture mechanics and the specimen geometries just described, Johnson, Mall, and Mangalgi addressed the specific problems of fatigue and fracture in bonded composite materials in a series of articles.⁶⁶⁻⁶⁹ Some of their conclusions are summarized in the following paragraphs.

In an effort to assess the fracture behavior of common bonded composite systems, Johnson & Mangalgi²⁴ surveyed a variety of sources and collected static toughness values of seven adhesive and polymer matrix resins used in fiber reinforced composites. Results from their summary are shown in Figure 1 and illustrate a wide distribution of fracture toughness values ranging from those of relatively brittle systems such as the

Hercules 3501-6 and Narmco 5208 epoxy matrix resins to that of Hexcel's F-185 rubber-modified epoxy adhesive. Figure 1 indicates a type of performance envelope for the

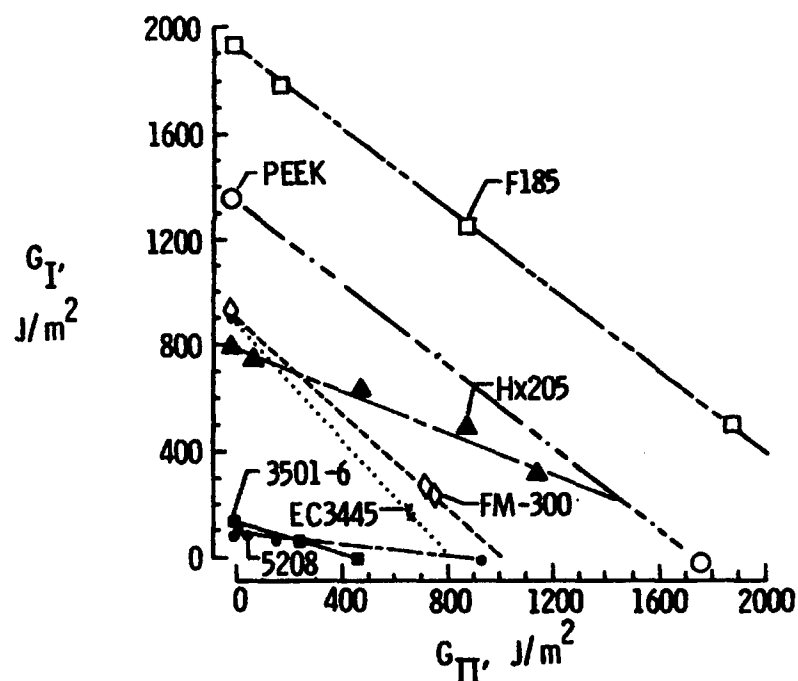


Figure 1. Mixed mode fracture toughness of several matrix and adhesive systems²⁴

Mode I, Mode II, and mixed-mode failure of the polymer systems examined. Note that toughness or energy required to cause fracture under Mode II shear conditions (G_{IIC}) is typically higher than that required under Mode I peel conditions (G_{IC}). The authors proposed that this inequality was based upon the structure of the polymers and suggested that the relatively lower Mode I toughness values may be due to a high degree

of cross-linking in the polymers resulting in an inability to sufficiently deform plastically or to increase in volume. Since such dilatation is not necessary under shear deformation, higher Mode II toughness values are expected, especially for the more brittle systems. Furthermore, the authors suggested that environmental exposure to heat and/or moisture may affect one mode of toughness to a greater extent than another mode depending upon the effect that the exposure has on the polymer structure.

To investigate the fatigue crack growth characteristics of bonded composite joints, Johnson & Mall²⁵ employed the CLS specimen geometry. In fatigue tests on Narmco T300/5208 graphite reinforced composites bonded with FM[®]300 (American Cyanamid) and EC-3445 (3M Corp.) rubber-modified epoxies, the authors developed da/dN vs. G_{total} (G_T) curves similar to the da/dN vs. ΔK relationships used to describe fatigue in metals (Fig. 2). Correlation between da/dN and G_T was good despite the use of different adherend thicknesses as denoted by the thick and thin strap data in Figure 2. With the selection of a threshold crack growth rate of 10^{-6} mm/cycle (3.94×10^{-8} in./cycle), their work also confirmed earlier findings indicating that static fracture toughness values far exceeded the threshold strain energy release rates ($G_{T,th}$) required for bond line crack growth in bonded composites.²⁷ In comparing Figures 1 and 2, it can be seen that $G_{T,th}$ values are approximately 10% of the static toughness values for the two adhesives examined. Finally, the fatigue studies also revealed that the slopes of the crack growth

curves (indicated in Figure 2 by "n") for adhesive bonds are much higher than those for metals. This implies that adhesive bonds have a greater sensitivity to small changes in

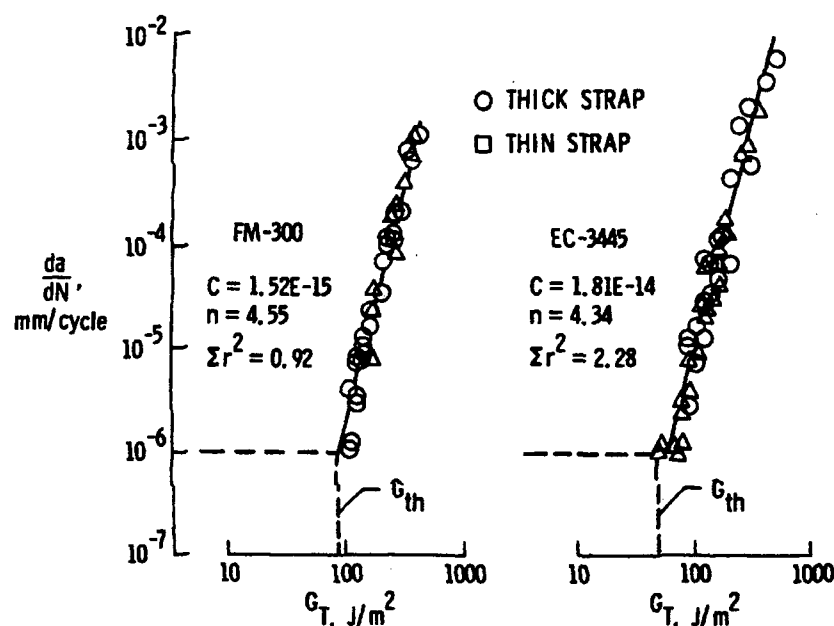


Figure 2. Relation between total strain energy release rate and bond line crack growth rate for bonded composite joints using FM[®]300 and EC-3445 adhesives²⁵

the applied strain energy release rate making bond line crack growth rates far less predictable under conditions of variable loading. This fatigue characteristic is of great concern to the aircraft industry since a major emphasis in aircraft design has been placed on the ability to accurately predict crack growth and, thereby, service life, based upon applied loads and experimentally-determined crack growth rates.

For the same report,²⁵ Johnson & Mall also examined the effect of tapered adherends on the fatigue crack growth behavior of the CLS specimens. Tapering was shown by Hart-Smith to drastically reduce the peel stresses present at the joint ends and thereby enhance the strength of bonded structures. A 5° taper (not impractical with current manufacturing methods and often used for bonded composite fabrication) was believed to reduce peel stresses to such an extent that bond line cracking would be eliminated. However, though Johnson & Mall found that tapering improved the fatigue resistance of bonded joints, there was no guarantee against bond line cracking even with a taper angle as shallow as the recommended 5°. A summary of their results is given in Figure 3 which includes experimental data and finite element predictions. By reducing the taper angle from 90° (no taper) to 5°, it was found that the stress required to reach the threshold strain energy release rate level ($G_{T,th}$) was increased by approximately 50% and that most of the improvement came with taper angles below 10°. Such a change to the geometry of the bonded joint can, therefore, permit tapered adherends to carry more load than untapered adherends or permit adhesives with lower $G_{T,th}$ values to be substituted for those with greater $G_{T,th}$ values for a given joint loading. Changes in the taper angle may also serve to offset the effects of environmental exposure.

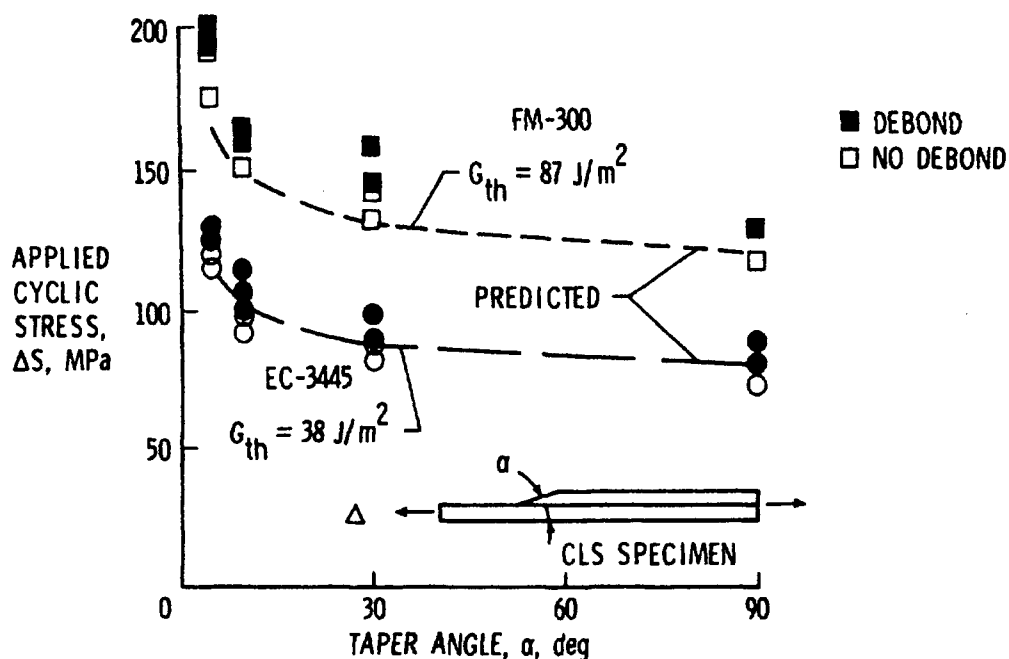


Figure 3. Effect of taper angle on joint performance for bonded composite joints²⁵

Although an in-depth discussion about the merits and drawbacks of the stress-based and fracture mechanics approaches is not the focus of this research, the numerous studies previously described illustrate that the use of fracture mechanics has definite merit in assessing the behavior of bonded joints. Fracture mechanics supplements and complements stress-based analyses by adequately describing static toughness and fatigue crack growth characteristics. In addition, fracture mechanics permits bond lines with defects to be examined using a quantifiable toughness parameter. In similar cases, stress-based approaches employ a number of less physically-based concepts such as the point stress, average stress, or strength of a singularity. DeVries, *et al.*⁷⁰ conducted a study

which directly compared stress-based and fracture mechanics approaches for the analysis of a single lap joint. They concluded that the fracture mechanics approach was more versatile because stress-based approaches were unable to provide a joint shear strength independent of lap length, adherend thickness, and adhesive thickness. However, the fracture mechanics approach was able to analyze the joint independent of its geometric characteristics. Thus, the fracture mechanics analysis is easily adaptable to joints of several different geometries.

As static, yield, fatigue, and fracture analyses are integrated in the evaluation and design of metallic components, so should stress-based and fracture mechanics approaches be combined for the analyses of adhesively bonded joints. However, based upon the desire to obtain information regarding the monotonic and fatigue behavior of bonded joints containing known flaws, and upon previous studies which demonstrated its applicability, fracture mechanics was chosen as the prime analytical tool for the research presented in this thesis.

2.3. Analytical Methods

The analysis of bonded joints may be carried out either through closed-form solutions or using finite element methods. Some of these methods will be described in a later portion of this thesis covering the analysis of the experimental specimens. However, a brief review of some of the more widely used finite element and numerical analyses are provided here for the benefit of those who may wish to further investigate bonded joint

analysis and to demonstrate the range of analytical techniques and programs available to the designer.

A number of stress-based programs were developed by Hart-Smith⁵²⁻⁵⁵ in conjunction with his analysis of various joint geometries. The aircraft industry has used these programs extensively for bonded joint design. Hart-Smith's programs use FORTRAN IV and account for thermal mismatch of the adherends and the elastic-plastic behavior of the adhesive. The programs include A4EA (for the shear strength of single-lap joints), A4EB (for the shear strength of double-lap joints), A4EC (for the elastic strength of scarf joints), A4ED (for the lower bound elastic-plastic strength of scarf joints), A4EE (for the elastic strength of stepped lap joints), and A4EF (for the elastic-plastic strength of stepped lap joints).

TJOINTL and TJOINTNL, developed by Oplinger,⁷¹ are also stress-based. These programs are designed to provide the shear and peel stresses in double-lap joints manufactured with adhesives that are either linearly elastic (TJOINTL) or nonlinear (TJOINTNL). An advantage of this pair of programs is that they may easily be run on a PC.

Two of the most widely used finite element programs used for bonded joint analysis are GAMNAS and ABAQUS.⁷² The GAMNAS (Geometric And Nonlinear Analysis of Structures) program was developed by Dattaguru, *et al.*⁷³ specifically for bonded joint analysis. It employs four-noded quadrilateral elements and can

accommodate nonlinear material behavior, adherend bending, and crack tip rotations. GAMNAS provides a direct output of the bond line strain energy release rate based upon the modified crack closure technique. This technique, first proposed by Rybicki & Kanninen,⁷⁴ determines the nodal forces and displacements required to close the crack to its original position. The nodal force multiplied by the nodal displacement is the work or energy required to close the crack and, thus, is equivalent to the strain energy "released" as the crack tip propagates.

ABAQUS is a commercially available finite element code able to perform mechanical, thermal, and other analyses. It employs a number of element types and, like GAMNAS, is capable of geometric and material nonlinear analyses. Unlike GAMNAS, ABAQUS does not use the modified crack closure technique. However, this technique may be easily performed using nodal forces and displacements furnished by ABAQUS. This is the procedure that was used for the ABAQUS work conducted in support of this thesis.

Despite their versatility, these finite element programs may often have more capability, and thus more complexity, than needed. The recent increase in the use of adhesives for repairs to aircraft structures has fostered a growing number of simpler and more specialized computer programs. Notable among these are CALCUREP⁷⁵ and PCRep.⁷⁶ Both are menu-driven, PC-based programs designed to provide rapid solutions

for adhesively bonded patch design including size, material, and adhesive shear stress information.

2.4. Environmental Issues

Regardless of the type of analysis used to investigate the behavior of adhesively bonded joints, it is imperative that environmental effects be considered. In many cases, environmental attack most severely affects the interphase regions, however, adhesive properties may also be affected. In theory, it may not be necessary for all such effects to be considered detrimental, however. For example, increased plasticization, caused by moisture absorption or by elevated temperatures, may increase the toughness of a bond line by permitting the adhesive to dissipate a greater amount of stored energy through plastic deformation. However, the vast majority of studies performed on the environmental durability of adhesively bonded joints suggest that heat and moisture are detrimental to bond performance.

In the early 1970's, a rash of failures in bonded honeycomb construction in U.S. Navy aircraft prompted a study by Walton & Nash.⁷⁷ They examined the durability of bonded aluminum single lap joints and found that 12 days of exposure to salt fog reduced strengths up to 19% even with an "optimum" surface preparation.

Brockmann⁷⁸ examined the behavior of exposed steel and aluminum lap joints which used epoxy, polyurethane, and polyimide adhesives. These were exposed to 30°C (86°F), 92% relative humidity (rh) conditions and also cycled between this environment

and -20°C (-4°F) for up to 12 months. The polyimides performed well, but the other adhesives exhibited increased adhesive fracture with exposure times. The author suggested that swelling and chemical changes within the adhesive and structural changes in the interphase region caused by moisture absorption caused this degradation.

Environmental tests on several modified epoxy and phenolic adhesives were reviewed by DeLollis.⁷⁹ Environmental conditions included laboratory storage for 11 years, atmospheric exposure in Florida and Panama for up to 3 years, and some attempts at accelerated testing including water immersion and salt water spray. These studies concluded that although long-term ambient storage was not detrimental, significant strength losses were caused by extended periods of atmospheric exposure primarily due to moisture absorption. The correlation between results from accelerated aging and real-time exposure tests were poor.

Marceau, *et al.*⁸⁰ conducted fatigue tests of single lap and double cantilever beam aluminum/epoxy specimens in several environments. The fatigue threshold decreased and the crack growth rate sensitivity increased for specimens tested at 60°C (140°F) regardless of the humidity levels. It was suggested that the elevated temperature appeared to have a dominant effect because the relatively short times the specimens were exposed to high humidity levels during the tests did not permit significant moisture absorption.

The fatigue behavior of aluminum joints bonded with epoxy was also studied by Hufferd, *et al.*⁸¹ Pre-fatigue moisturization of aluminum cracked lap shear joints resulted in increased crack growth rates and growth rate sensitivities for tests conducted at room temperature.

Investigating the fracture mechanics of interfacial failure in epoxy bonded steel and aluminum, Kinloch⁸² also examined the roles of humidity and moisture absorption. He suggested that a critical moisture concentration must exist in the adhesive for environmental attack to be significant. Once this level is reached, failure of the bond could occur through rupture of secondary bonds, structural changes in the oxide layer, corrosion, or adhesive failure in the primer. Kinloch also proposed that some of the detrimental effects of moisture absorption could be offset by increased plasticization of the adhesive.

The concept of a moisturization threshold was also explored by Brewis.⁸³ In tests on aluminum bonded with an epoxy adhesive, he observed that exposure to relative humidity levels in excess of 80% reduces strength while joints can withstand long periods of exposure to 50% rh with no effects.

Askins & Konopinski⁸⁴ examined the effects of moisture absorption and thermal spikes on the behavior of adhesively bonded aluminum honeycomb sandwich specimens. Moisture reduced the tensile strength of the neat epoxy adhesive by 50% and the flat-

wise strength of the honeycomb specimens by 30%. Thermal spikes combined with moisturization reduced the flat-wise strength of the honeycomb specimens by up to 75%

2.5. A Fracture Mechanics Approach to the Durability of Bonded Joints

Design of metal aerospace components has successfully integrated static and yield strength analyses with fracture mechanics to accommodate various philosophies including safe-life, fail-safe, durability, and damage tolerance. The design of adhesively bonded composite structures and bonded composite repairs to existing metallic structures can also benefit from the use of both stress-based and fracture mechanics approaches. However, to fully understand the durability of bonded joints, the effect of operating environments on the fatigue and fracture properties of the adhesive must also be known. Groundwork has been laid by the investigators previously mentioned and by studies of the effects of various environments on some adhesive properties, but needs still exist to address the performance of specific adherend-adhesive combinations and to combine environmental, fatigue, and fracture studies of bonded systems.

For example, it has been shown that moisture absorption results in varying degrees of plasticization, strength loss, and increased ductility of some epoxy adhesives. However, the effect of moisture on the fatigue and fracture properties of bonded joints employing these adhesives is still not fully understood. In addition, since adhesive joints are systems comprised of adherends, adhesives, and inter-phase regions, the performance of each of these components may strongly affect the performance of the joint. Thus,

general knowledge of the behavior of adhesives exposed to various environments must be supplemented by knowledge of the behavior of specific bonded systems.

In reviewing some of the trends observed by Johnson, Mall, and Mangalgiri²⁴⁻²⁷ for room temperature behavior of as-received bonded composite specimens, it appears that environmental exposure (i.e. exposure to heat and/or moisture) may affect the behavior of bonded joints in several ways that can be highlighted using a fracture mechanics approach. Some of the possible effects of environmental exposure on the performance of bonded composite joints will be discussed in the following paragraphs using schematic diagrams which parallel those shown in Figures 1-3.

Figure 4 illustrates some possible effects properties of adhesive joints under monotonic and cyclic loading. As shown (Fig. 4a.), environmental exposure may affect the static fracture behavior of bonded joints by changing the fracture toughness in general or by preferentially altering the fracture toughness in one mode compared to another. These possible effects were suggested by Johnson and Mangalgiri²⁴ in their discourse on the relationship between polymer structure and toughness under various modes of fracture.

Such changes in the structure of the polymer and in its fracture toughness may translate into effects on fatigue behavior, in the form of the shift in the locus of da/dN vs. G_T data shown in Fig. 4b., which indicates a change in the threshold level and rate of crack growth for a given level of applied load or strain energy release rate. Alternatively, the

effect on fatigue behavior may be manifested only by a change in the slope of the da/dN vs. G_T data, indicating a change in the sensitivity of the crack growth rate to changes in applied load or strain energy release rate.

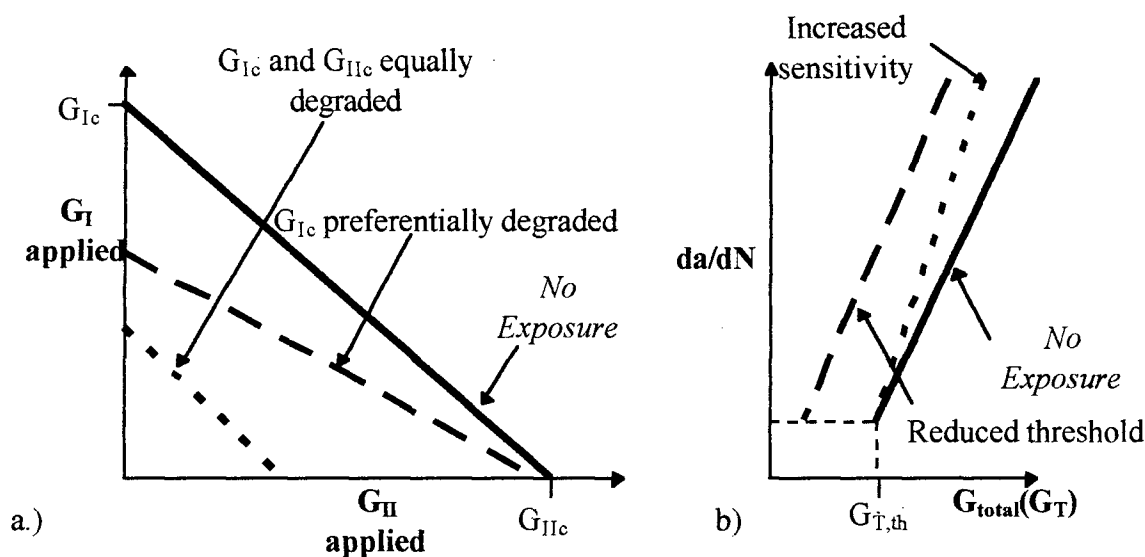


Figure 4. Possible environmental effects on the a) fracture toughness and b) fatigue crack growth behavior of adhesively bonded joints

Although Figure 4 shows the changes as detrimental, there is no reason to doubt that exposure to some environments may enhance bonded joint performance. For example, moisture absorption by an epoxy adhesive may plasticize it to an extent that it is able to withstand increased dilatation during Mode I loading, thereby increasing its Mode I fracture toughness (G_{Ic}) while maintaining its level of Mode II fracture toughness (G_{IIc}) at the level present prior to exposure. In addition, the changes due to

environmental exposure need not be changes in the adhesive, but may, instead, be changes in the inter-phase which control the strength of the adhesive/adherend bonds. In this case, the adhesive may not be directly affected by the environment at all, but the inter-phase region may be weakened to an extent that it becomes the strength- or fatigue-limiting constituent of the joint. The importance of these possible trends in fracture toughness and crack growth behavior is crucial to designers for it is their task to ensure a bonded joint's integrity of over the life of the structure. Knowledge of these trends may result in so called "knockdown" factors to limit the loads applied to affected joints or alterations in the geometric designs of the joints.

Environmentally-induced changes in the toughness and fatigue crack growth behavior of several bonded joint systems have been examined for this research. Data contained later in this thesis will be provided in a format similar to that of Figures 4.

In order to compensate or design for changes in the fatigue and fracture performance of a composite joint due to environmental exposure, measures might be taken such as those shown in Figure 5.

Figure 5 illustrates, for a case where exposure has shifted the crack growth threshold, that environmental effects may also force geometric modifications to be made in order to achieve a desired design lifetime for a given cyclic stress level. Such modifications may reduce the total applied strain energy release rate, G_T , perhaps through changes in the adherend taper angle. For the case where one mode of toughness is

preferentially attacked, other design changes may permit a bonded joint to be loaded in a manner that better exploits its less-degraded properties. In any case, knowledge of the way in which the environment affects a joint's fatigue and fracture properties will lead to improved designs.

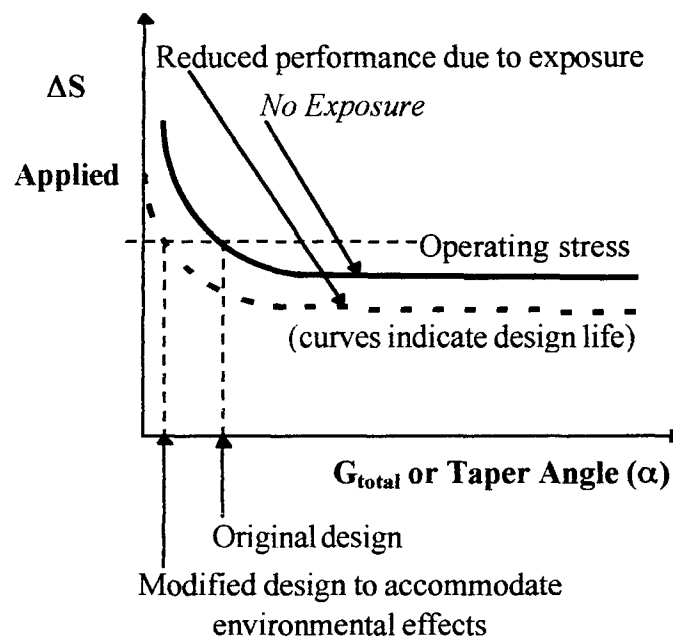


Figure 5. Exposure effects may require design changes to meet operating requirements

Thus, to design efficient, effective, and durable bonded composite joints, it is necessary to determine the effect of service environments on the adhesive properties examined by stress-based and fracture mechanics approaches. Changes in strength,

preferred mode of fracture, and crack growth behavior during long-term exposures will all affect the design of bonded joints used for structural and repair purposes. Through the use of stress analyses to ensure adequate static strength, fracture mechanics and fatigue analyses to ensure adequate damage tolerance, and environmental studies to ensure adequate long-term durability, adhesively bonded aircraft joints and repairs can be designed and fabricated to meet the increasingly stringent requirements for extended aircraft lifetimes.

CHAPTER III

MATERIALS AND SPECIMENS

This research project examined a number of different adhesives and adhesively bonded joint systems. The adhesives and adherends were chosen because of their current or future use in aerospace applications.

Examination of the adhesives themselves used specimens fabricated from thin cured sheets of three adhesives (two toughened epoxies: AF-191 and FM[®]73, and one polyimide: FM[®]x5). These specimens were mechanically tested to determine tensile and fracture toughness properties. Portions of the cured sheets were also subjected to chemical and physical analyses using differential scanning calorimetry (DSC), thermogravimetric analysis (TGA), and FTIR spectroscopy. The purposes this battery of tests were: 1) to identify environmentally-induced changes occurring solely in the adhesives to assist in understanding the behavior of bonded joints which might be affected by these changes as well as by changes in the properties of the inter-phase regions or adherends, and 2) to determine the mechanical properties of the adhesive for subsequent incorporation into finite element models.

The same three adhesives were also used to fabricate bonded joint specimens featuring metal and/or composite adherends. The bonded joint specimens were tested

under Mode I, Mode II and mixed mode (I/II) loading conditions to determine their fracture toughness and fatigue properties.

This chapter provides further information about the adhesive and adherend materials and about specimen fabrication. A detailed description of specimen manufacturing may be found in Appendix A.

3.1. Description of Materials

This section provides a general description of the three types of adhesives and four bonded joint material systems which were investigated.

3.1.1. Adhesives

Two epoxy-based adhesives, FM[®]73 and AF-191, and one polyimide-based adhesive, FM[®]x5, were examined for this project. As specimens cut from cured sheets, these adhesives were subject to tensile and fracture toughness testing and to various chemical and physical analyses. As bonding agents, they were also used in the fabrication of bonded joint specimens using metal and/or composite adherends.

3.1.1.1. FM-73

FM[®]73 is a toughened epoxy adhesive manufactured by CYTEC Engineered Materials, Inc. (Havre de Grace, MD). It has an advertised use temperature of 82°C (180°F).⁸⁵ This adhesive was used in the U.S. Air Force's successful Primary Adhesively Bonded Structures Technology (PABST) program.¹⁶ It is currently being used to bond

composite patches to cracked metallic aerospace structures on military and commercial aircraft where conditions may approach 71°C (160°F) and high (>90%) relative humidity.

Two varieties of FM[®]73 were tested: FM[®]73M containing a non-woven polyester scrim cloth (Figure 6a); and FM[®]73U, an unsupported “neat” resin.

FM[®]73M was tested because the scrim-containing version of the adhesive was used in the fabrication of bonded joint specimens investigated for this research. The volume fraction of the scrim cloth was approximately 2%. This scrim cloth is used, apparently, to improve the handling qualities of the adhesive film and to control bondline thickness. Tensile and fracture toughness tests did not show that the scrim cloth acted as a significant reinforcement material for the adhesive film.

The purpose for testing the unsupported “neat” resin, FM[®]73U, was to determine the effects of environmental exposure on the adhesive polymer itself (i.e. without the presence of a scrim cloth).

Specimens cut from cured sheets of the supported and unsupported varieties were tested for tensile and fracture toughness properties. Only the supported FM[®]73M was used as an adhesive in the bonded joint specimens.

Cured sheets of both varieties of FM[®]73 had a nominal weight of 290 g/m² (0.06 lb./ft.²) and an approximate thickness of 0.25 mm (10 mils). The cured FM[®]73M is yellow-orange in color and, as a single layer, is translucent.

3.1.1.2 AF-191

AF-191 is a modified epoxy adhesive manufactured by 3M Corporation (St. Paul, MN). It has an advertised use temperature of 177°C (350°F).⁸⁶ This adhesive is used on the F-22 fighter aircraft in areas where temperatures could reach 104°C (220°F).

Two varieties of AF-191 were tested: AF-191M containing a non-woven nylon scrim cloth (Figure 6b); and AF-191U, an unsupported "neat" resin.

As with the testing of the FM[®]73 adhesive films, the AF-191M was tested because this version of the adhesive was used to fabricate bonded joint specimens investigated for this research. The volume fraction of the scrim cloth was approximately 4%. Again, as with the FM[®]73M, this scrim cloth is used to improve the handling qualities and to control bondline thickness rather than to impart any reinforcement to the adhesive film.

The purpose for testing the unsupported "neat" resin, AF-191U, was to determine the effects of environmental exposure on the adhesive polymer itself (i.e. without the presence of a scrim cloth).

Specimens cut from cured sheets of the supported and unsupported varieties were tested for tensile and fracture toughness properties. Only the supported AF-191M was used as an adhesive for bonded joint specimens.

Cured sheets of both varieties of AF-191 had a nominal weight of 260 g/m^2 (0.05 lb./ft.^2) and an approximate thickness of 0.25 mm (10 mils). The cured AF-191 film is pale yellow in color and, as a single layer, is translucent.

3.1.1.3. FM-x5

FM[®]x5 is a semi-crystalline amorphous polyimide blend of PETI-5 and other thermoplastic resins manufactured by CYTEC Engineered Materials, Inc. (Havre de Grace, MD). This adhesive is being considered for wing and fuselage structures on the High Speed Civil Transport where temperatures may approach 177°C (350°F), the adhesive's advertised maximum use temperature.^{87,88}

Currently, FM[®]x5 is only available as a film containing a woven glass scrim cloth (Figure 6c). This scrim cloth has a volume fraction of approximately 40% and imparts physical integrity to the adhesive. Without the scrim cloth, the FM[®]x5 is extremely fragile and friable as a dry, uncured film (the form used for bonding) or as a cured sheet.⁸⁹

Specimens cut from cured sheets of FM[®]x5 were provided by the manufacturer and were tested for tensile and fracture toughness properties. The same form of FM[®]x5 was also used to produce bonded joint specimens.

The nominal weight of the cured FM[®]x5 was 515 g/m^2 (0.10 lb./ft.^2), and it had an approximate thickness of 0.34 mm (13 mils). The FM[®]x5 film is dark brown in color and, as a single layer, is nearly opaque.

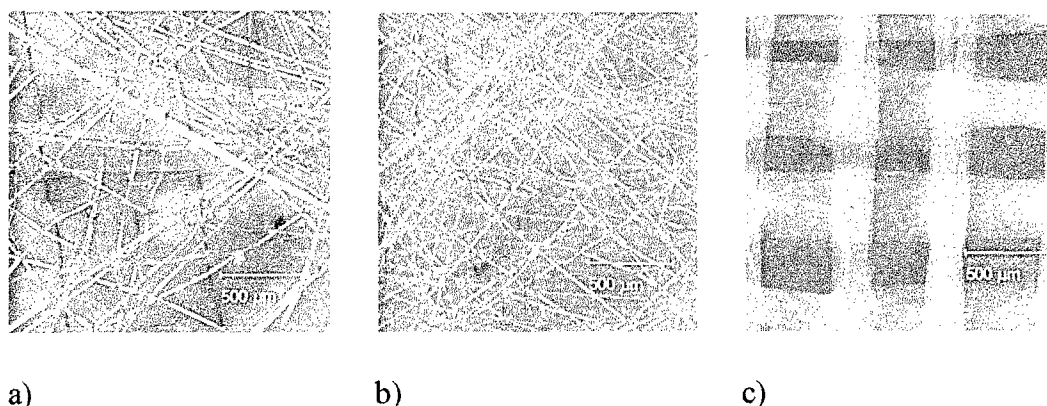


Figure 6. Scrim cloths contained in a) FM®73M, b) AF-191 M, and c) FM®x5

3.1.2. Bonded Joint Systems

Four bonded joint systems were examined for this project. The choice of these systems was governed by their current or future use on the USAF's C-141 *Starlifter* transport and F-22 *Raptor* fighter and on NASA's High Speed Civil Transport commercial aerospace vehicle. This collection of applications provided a variety of bonded material systems which operate or are intended to operate over a wide range of environmental conditions. The following sections provide further descriptions of these material systems.

3.1.2.1. Aluminum/FM®73M (Al/FM®73M/Al)

In support of the C-141, Lockheed Martin Aeronautical Systems Co. (Marietta, GA) provided specimens made from 7075-T651 bare aluminum bonded with FM®73M modified epoxy adhesive. The 7075-T651 alloy is used for wing skins and structures

which contain the repaired "weep-holes" mentioned earlier in this thesis. Although there are no aluminum-to-aluminum bonded structures on the C-141, it was decided to investigate the durability of this bonded system to better understand the behavior of the FM[®]73M adhesive and to evaluate the bonded system which formed the backbone of the PABST program. Because it used the same adhesive, the Al/FM[®]73M/Al system provided a good counterpart to the Al/FM[®]73M/B-Ep system described in the following section.

3.1.2.2. Aluminum/FM[®]73M/Boron-Epoxy (Al/FM[®]73M/B-Ep)

Due to the advanced age of the C-141 airframe and mission changes which have resulted in unexpectedly severe loading conditions, fatigue cracking of metal skins and components is becoming more prevalent. Use of bonded boron-epoxy patches, as previously discussed, is a popular repair method. Therefore, a second group of test specimens was fabricated by Lockheed Martin to reflect the materials used in these repairs: bare 7075-T651 aluminum and F4/5521 boron-epoxy pre-preg (supplier: Textron Specialty Materials, Inc., Lowell, MA) composite laminates bonded with FM[®]73M film adhesive.

Various lay-ups were used for the boron-epoxy composite laminates which served as the adherends. In all cases, 90° plies were used simply to provide support and prevent longitudinal splitting of the laminates. The number of 0° plies was adjusted for each specimen geometry to give the composite laminate adequate strength or stiffness. For all

specimen geometries, the ply lay-up was determined by engineers at Lockheed Martin (the manufacturer of the specimens) using their standard practices for calculating the strength and stiffness of boron-epoxy laminates.

For the double cantilever beam (DCB) Mode I specimen geometry, trial tests on practice specimens were used to determine that a 20 ply lay-up $[0_4/90/0_3/90/0]_s$ was adequate to withstand loads attained during testing.

For the end-notched flexure (ENF) Mode II specimens, a 28 ply lay-up $[0_4/90/0_3/90/0_3/90/0]_s$ was chosen to match the bending stiffness of the aluminum. For the cracked lap shear (CLS) mixed Mode I/II specimen which used boron-epoxy as the lap, a 19 ply $[0_2/90/0_2/90/0_2/90/\bar{0}]_s$ was chosen to match the extensional stiffness of the aluminum. Finally, for the cracked lap shear (CLS) mixed Mode I/II specimen which used boron-epoxy as the strap, a 13 ply $[0_{13}]$ lay-up was chosen to match the extensional stiffness of the aluminum.

3.1.2.3. *Graphite-Bismaleimide/AF-191M (Gr-BMI/AF-191M/Gr-BMI)*

Lockheed Martin also provided specimens fabricated from materials used for bonded composite control surfaces on the new F-22 fighter. Adherends consisted of IM7/5250-4 graphite-bismaleimide laminates (pre-preg supplier: BASF Materials, Inc., Anaheim, CA). This composite was chosen for its high temperature resistance. Specimens contained composite adherends that were either predominantly unidirectional

$[0_4/90]_s$ or quasi-isotropic $[\pm 45/0_2/\pm 45/90]_s$. The quasi-isotropic adherends matched the lay-up used for specific F-22 components. AF-191M was used as the adhesive.

3.1.2.4. Titanium FM[®]x5 (Ti/FM[®]x5/Ti)

Plans for NASA's High Speed Civil Transport call for an extensive use of adhesive bonding on wing and fuselage structures. Bonding may be used for structural joints or to attach honeycomb reinforcement to metallic or composite face sheets. Materials used for these applications are required to withstand the high temperatures expected to be experienced by the Mach 2+ HSCT airframe. Therefore, specimens provided by the Boeing Defense & Space Group (Seattle, WA) were constructed of Ti-6Al-4V titanium adherends bonded with and CYTEC's FM[®]x5 polyimide adhesive.

3.2. Specimen Geometry

The following sections describe the geometries of the two main families of test specimens: the adhesive test specimens fabricated from cured sheets of the adhesives previously described, and the bonded joint specimens consisting of the bonded material systems outlined in the preceding section.

3.2.1. Geometry of Adhesive Specimens

This section describes the geometry of adhesive specimens used for mechanical testing and for chemical and physical analyses.

3.2.1.1. Adhesive Tensile Test and Fracture Toughness Specimens

Mechanical testing of the adhesive specimens utilized two specimen geometries (Fig. 7) for evaluations of tensile and fracture toughness properties. The approximate thickness of the adhesive specimens ranged from 0.25 mm (10 mils) for the FM[®]73 and AF-191 adhesives to 0.34 mm (13 mils) for the FM[®]x5.

Tensile tests of the cured adhesive film employed specimens with a “dogbone” shape conforming to ASTM D 638M, Type M-III.⁹⁰

Fracture toughness testing of the adhesive sheets used a single edge-notched geometry with the same gross dimensions as the “dogbone” tensile test specimens. A 3 mm (0.12 in.) long notch was placed at the specimen midpoint along one edge of each specimen. A razor blade was carefully used to “saw” the starter notch. During this procedure, specimens were supported in a simple jig fabricated from two pieces of polyethylene cut to the dimensions of the single-edge notched specimen and containing slots to guide the razor blade. The jig prevented out-of-plane buckling and aided in locating and forming the starter notches. This geometry, though not standardized, was chosen because of its similarity to the tensile test specimen and because it was easily fabricated from the available cured adhesive sheets.

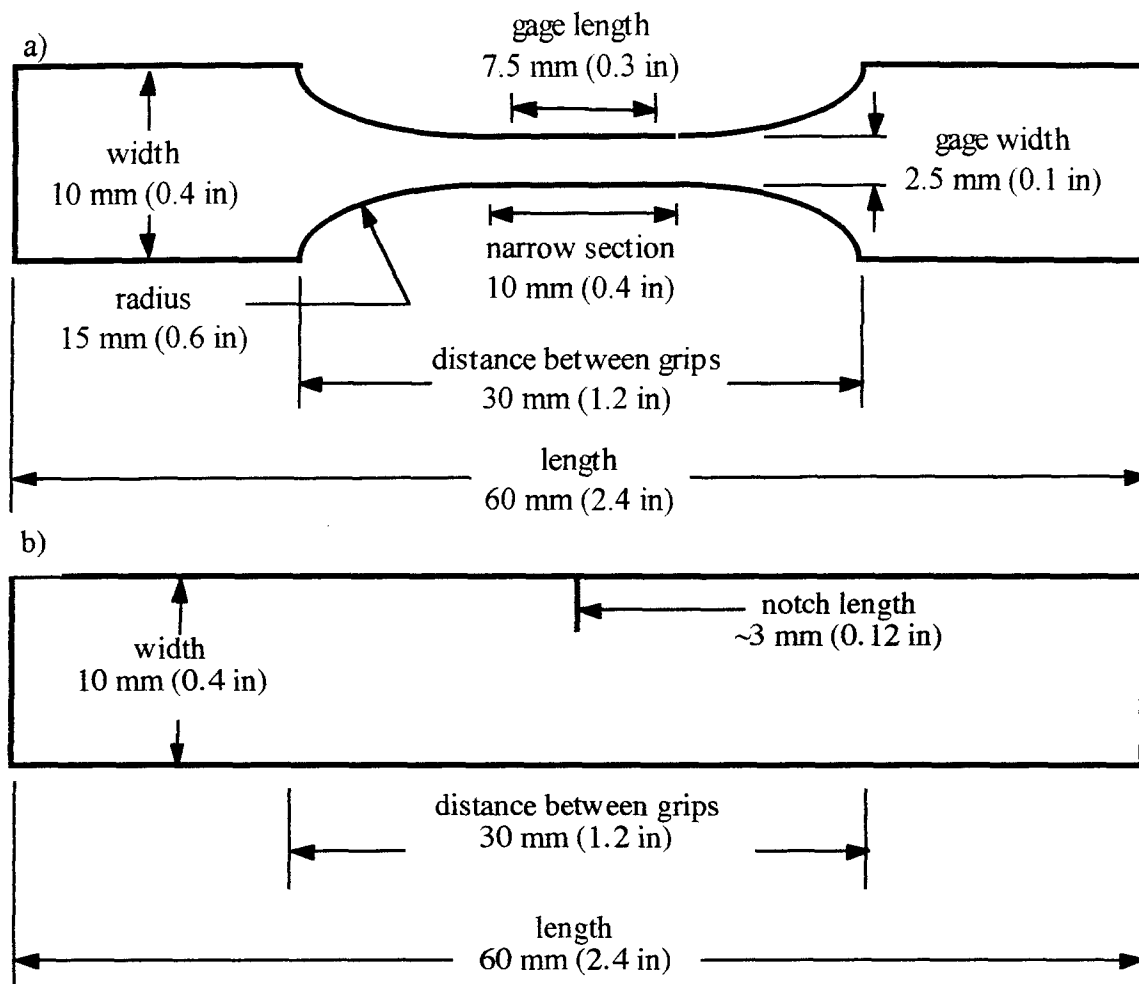


Figure 7. Specimen geometry for (a) the ASTM D 638M Type M-III "dogbone" specimen used for tensile testing, and (b) the "straight-sided" specimen used for fracture toughness testing

3.2.1.2. Adhesive Specimens Used for Chemical and Physical Analysis

No specific geometry was required for the adhesive specimens examined using differential scanning calorimetry (DSC), thermogravimetric analysis (TGA), or FTIR spectroscopy. However, some general guidelines were followed in creating the adhesive specimens that were analyzed with these techniques. All specimens analyzed by DSC, TGA, and FTIR spectroscopy were obtained from the same cured adhesive sheets used for the tensile and fracture toughness test specimens.

For the DSC tests, several small (> 4 mm [> 0.16 in.] in diameter) pieces of each adhesive film were used. These pieces had a total weight of approximately 20-25 mg and were cut to fit into the aluminum specimen holder for the DSC device.

For the TGA tests, a single piece of each adhesive film similar in size to the DSC specimens was used. Each piece weighed approximately 10 mg.

The only requirement for the FTIR spectroscopy specimens were that they were thin enough to permit the transmission of infrared radiation. This requirement was easily satisfied by the thin nature of the cured adhesive sheets. Since spectroscopy is a non-destructive method, specimens used for this analysis were the same as those used for tensile and fracture toughness testing.

3.2.2. Geometry of Bonded Joint Specimens

Fracture toughness and fatigue testing of the bonded joint systems employed three specimen geometries: 1) the double cantilever beam (DCB), 2) the end-notched flexure

(ENF), and 3) the cracked lap shear (CLS). These geometries were chosen for their ability to measure fracture and fatigue properties under Mode I (DCB), Mode II (ENF), and mixed Mode I/II (CLS) loading.

Adherend thicknesses were chosen based upon the consideration of a number of factors. These included: 1) the dimensions of the material to be bonded for specific applications on the C-141, F-22, and HSCT, 2) the adherend thickness estimated to permit bond line failure rather than adherend failure or yielding based upon rough preliminary estimates of the critical strain energy release rate of the adhesive, and 3) the availability of materials from the specimen manufacturers (Lockheed Martin and Boeing).

The width of all bonded joint specimens was nominally 25.4 mm (1.0 in.). This dimension was chosen based upon prior investigations of bonded joint fracture behavior reviewed in Chapter 2 and upon the ease with which these specimens could be tested. Wider specimens could have required loads that the current test laboratory machines would have been incapable of producing. Narrower specimens would have accentuated edge effects on the crack front. The 25.4 mm (1.0 in.) width used resulted in fairly straight crack fronts and permitted modest loads to be used for testing. It is recognized, however, that this specimen width is relatively narrow compared with bonded joints in service. Thus, because of the small distance between the edges of the bonded specimens and their centers, environmental exposure may have affected the performance of the bonded specimens to a greater degree than it would have affected bonded joints in service.

where the edge-to-center distance is much larger. The smaller edge-to-center distance on the specimens permitted a greater percentage of their bond line to be affected (compared to that of a bonded joint in service) and may have accentuated any environmentally-induced changes in their fracture and fatigue behavior.

The approximate bond line thickness (η) for these specimens ranged from 125 μm (4.9 mils) for the Al/FM[®]73M/Al system, to 225 μm (8.9 mils) for the Al/FM[®]73M/B-Ep system, to 250 μm (9.8 mils) for the Gr-BMI/AF-191M/Gr-BMI systems, to 340 μm (13.4 mils) for the Ti/FM[®]x5/Ti system. (Fig. 8).

Special attention should be paid to the geometry of the Al/FM[®]73M/B-Ep specimens. Because of the coefficient of thermal expansion mismatch between the aluminum ($\alpha_{\text{Al}} = 22.1 \times 10^{-6}/^{\circ}\text{C}$ [$12.3 \times 10^{-6}/^{\circ}\text{F}$]) and the boron-epoxy ($\alpha_{\text{B-Ep}} = 4.5 \times 10^{-6}/^{\circ}\text{C}$ [$2.5 \times 10^{-6}/^{\circ}\text{F}$]), these specimens were distinctly curved with the aluminum on the concave side. The extent of this curvature was measured at various temperatures. As expected, the stress-free temperature at which the specimen curvature vanished was found to be the processing temperature of the specimens (approx. 116 $^{\circ}\text{C}$ [240 $^{\circ}\text{F}$]).

Although this curvature was manifest in the specimens tested for this project, such gross deformations of repaired aircraft structures do not occur due to the amount of stiffening provided by supporting members. Nevertheless, the curvature exhibited by the Al/FM[®]73M/B-Ep system does indicate the formation of a significant amount of residual stress in the bond line. These thermal stresses produced a residual state of Mode II strain

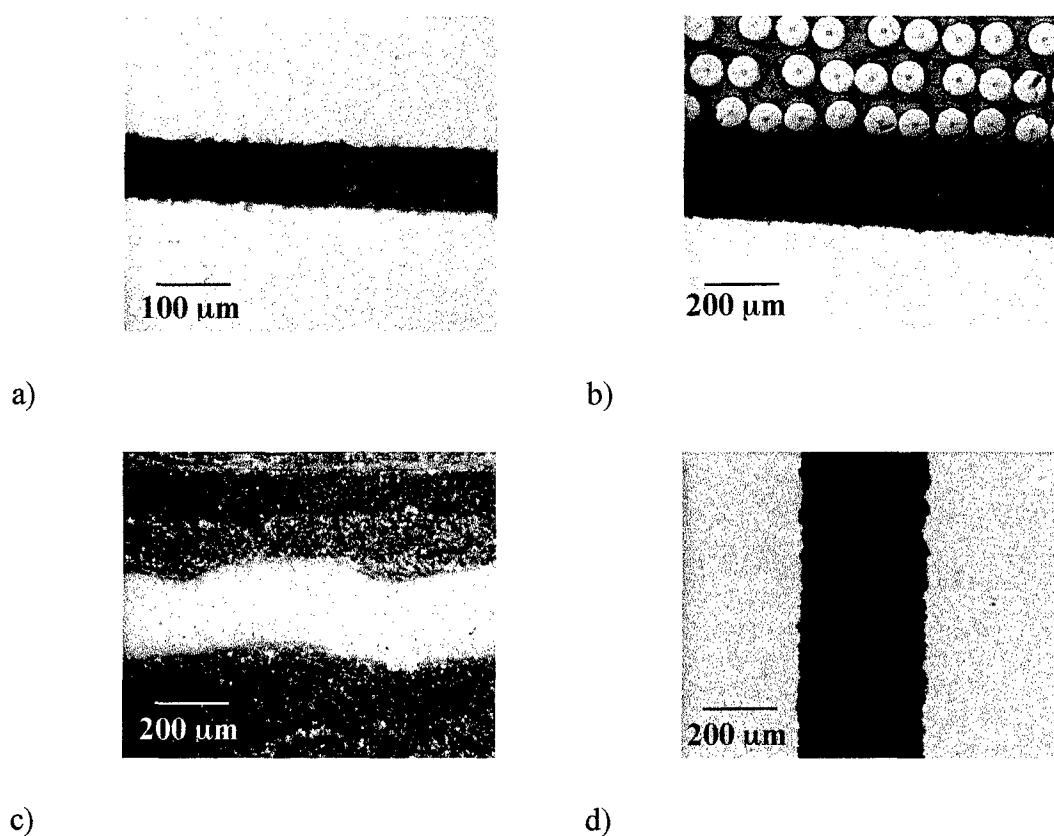


Figure 8. Bond lines of the a) Al/FM[®]73M/Al, b) Al/FM[®]73M/B-Ep, c) Gr-BMI/AF-191M/Gr-BMI, and d) Ti/FM[®]x5/Ti bonded systems

energy release rate within the bond line following curing. When the Al/FM[®]73M/B-Ep specimens were tested, applied loads combined with this residual stress state and to produce a mixture of Modes I and II at the crack tip. This was the case even in the double cantilever beam specimens which are normally used to examine only Mode I crack growth.⁷² The presence of adherends with different flexural moduli in these specimens also added to the mode mixity. This issue was examined extensively by Valentin⁷² and will be discussed further during the course of this thesis.

3.2.2.1. *The Double Cantilever Beam (DCB) Geometry*

Figure 9 shows the various versions of DCB specimens tested. The DCB specimen was used to subject specimens to primarily Mode I loading. However, because of dissimilar adherends, the Al/FM[®]73M/B-Ep specimens also experienced considerable Mode II as previously discussed.

The basic shape consisted of two adherends approximately 305 mm (12 in.) long and 25.4 mm (1 in.) wide. The length of DCB specimens tested at elevated or reduced temperatures was reduced to approximately 190 mm (7.5 in.) to permit them to fit into the environmental chamber mounted on the test frame.

An insert of Teflon[™] or Kapton[™] film was used to prevent bonding of a 57 mm (2.25 in.) region on each specimen. This film served as an initial, artificial "crack" between the two adherends and its tip provided an easily identifiable location from which this crack could be extended into the bond line region.

Load transfer was performed using either pin joints (for the Al/FM[®]73M/Al and Ti/FM[®]x5/Ti systems) or hinges (for the Al/FM[®]73M/B-Ep and Gr-BMI/AF-191M/Gr-BMI systems) affixed to one end of each specimen. The initial crack length, a_i , depended upon the method of load transfer because the loading line was slightly different for the pin and hinge load transfer mechanisms.

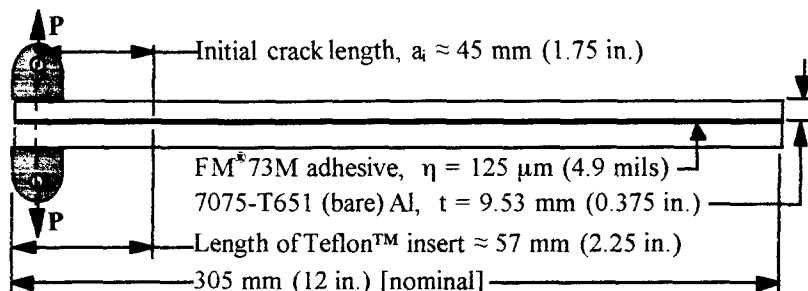
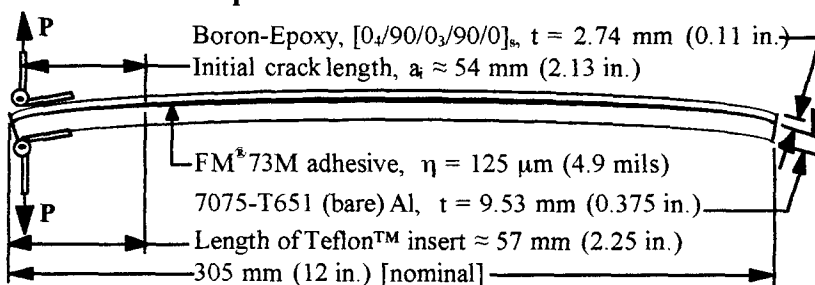
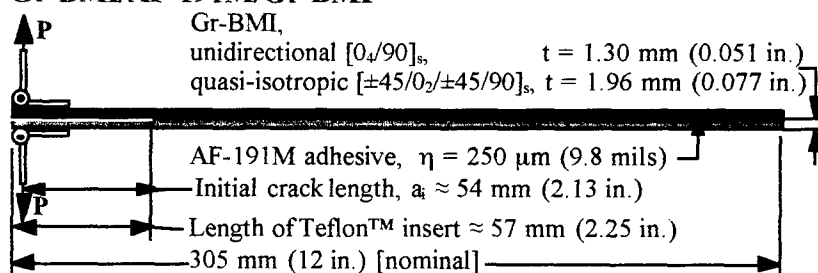
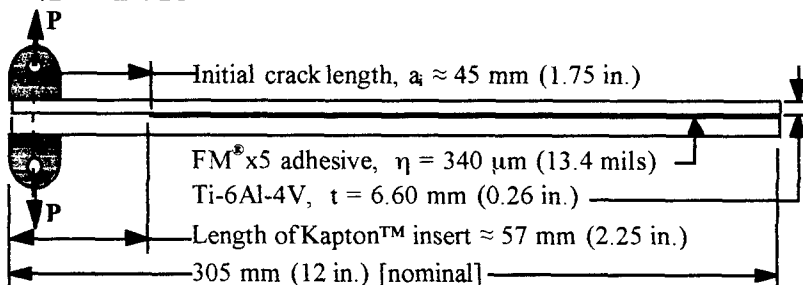
Al/FM[®]73M/Al**Al/FM[®]73M/B-Ep****Gr-BMI/AF-191M/Gr-BMI****Ti/FM[®]x5/Ti**

Figure 9. Double cantilever beam (DCB) specimen geometries

3.2.2.2. *The End-Notched Flexure (ENF) Geometry*

Figure 10 shows the various versions of ENF specimens tested. The ENF geometry was used to subject specimens to Mode II loading.

The basic shape was similar to that of the DCB specimens and consisted of two adherends approximately 305 mm (12 in.) long and 25.4 mm (1 in.) wide. An insert of Teflon™ or Kapton™ film was used to prevent bonding of a 57 mm (2.25 in.) region on each specimen. As with the DCB specimens, this film provided a location from which a crack could be extended into the bond line region.

A three-point bending fixture was used to apply loads to the specimens. This fixture had a 101 mm (4 in.) span between the two outermost loading points. The crack tip was positioned halfway between an outer loading point and the middle loading point. Thus, the initial crack length, a_i , for these specimens was always 25.4 mm (1 in.).

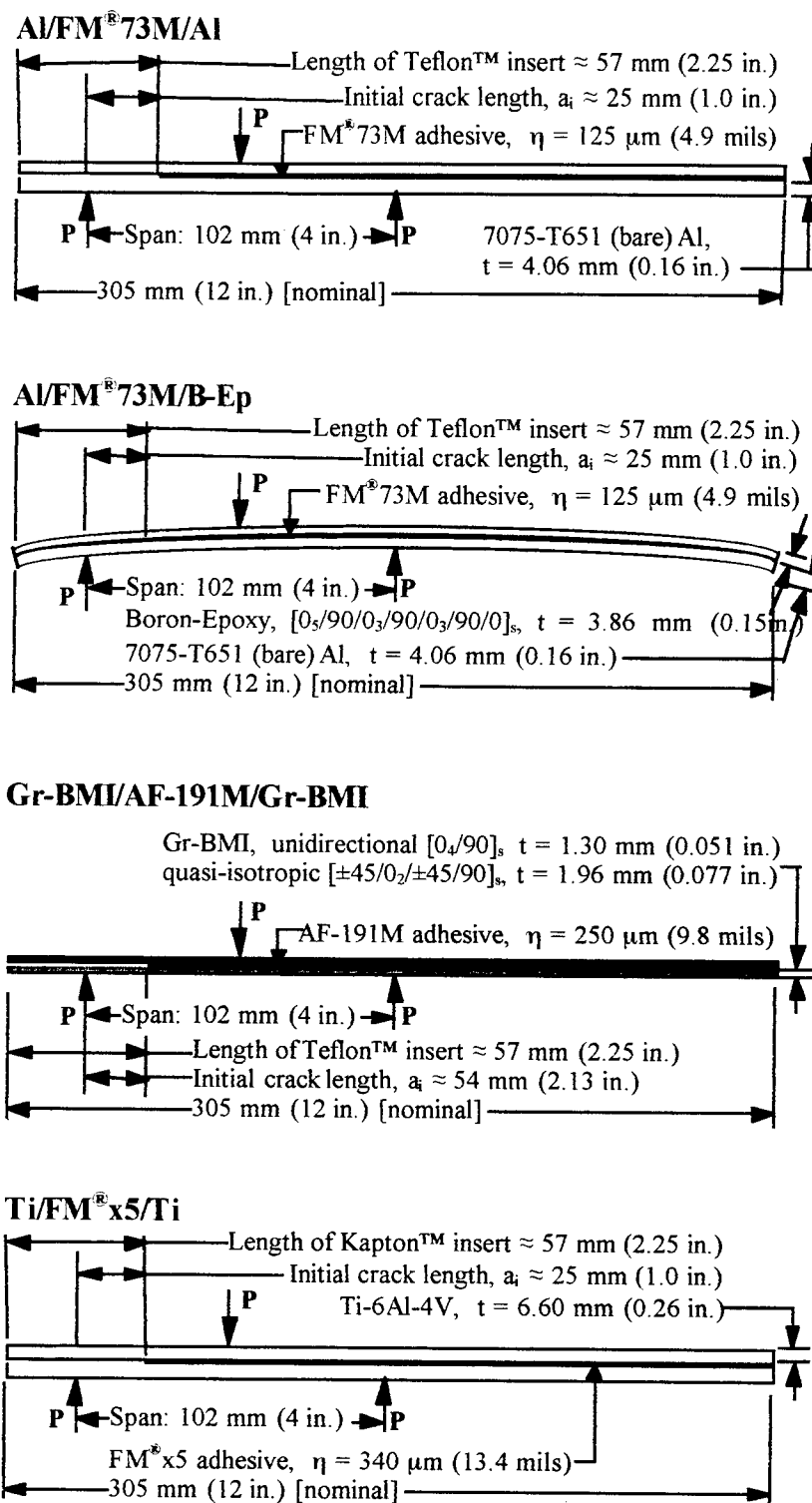


Figure 10. End-notched flexure (ENF) specimen geometries

3.2.2.3. *The Cracked Lap Shear (CLS) Geometry*

Figure 11 shows the various versions of the CLS geometry used to subject specimens to mixed Mode I/II loading. This type of specimen most closely duplicates the type of loading found in aerospace structures.

Like the DCB and ENF specimens, the CLS specimens consisted of two adherends approximately 25.4 mm (1 in.) wide. The length of the CLS specimens was only 190 mm (7.5 in.) to permit them to fit into the test frame. Two versions of the Al/FM[®]73M/B-Ep CLS specimen were tested; one had a boron-epoxy lap (shorter adherend) and an aluminum strap (longer adherend), and one had the opposite configuration. An insert of Teflon[™] or Kapton[™] film was used to prevent bonding of the first 6.4 mm (0.25 in.) of each specimen. This film provided a location from which a crack could be extended into the bond line region:

Because the CLS specimens were tested between fixed grips (i.e. no flexible members were contained in the load train), shims were adhesively bonded to the strap prior to testing. (Fig. 12) This allowed the long axis of the specimens to be aligned with the loading axis. One exception to this procedure occurred during the testing of the Gr-BMI/AF-191M/Gr-BMI specimens at elevated temperatures. During these tests, the adhesively shims debonded from the strap during loading at temperature. Therefore, these CLS specimens were tested without shims at elevated temperatures. A finite

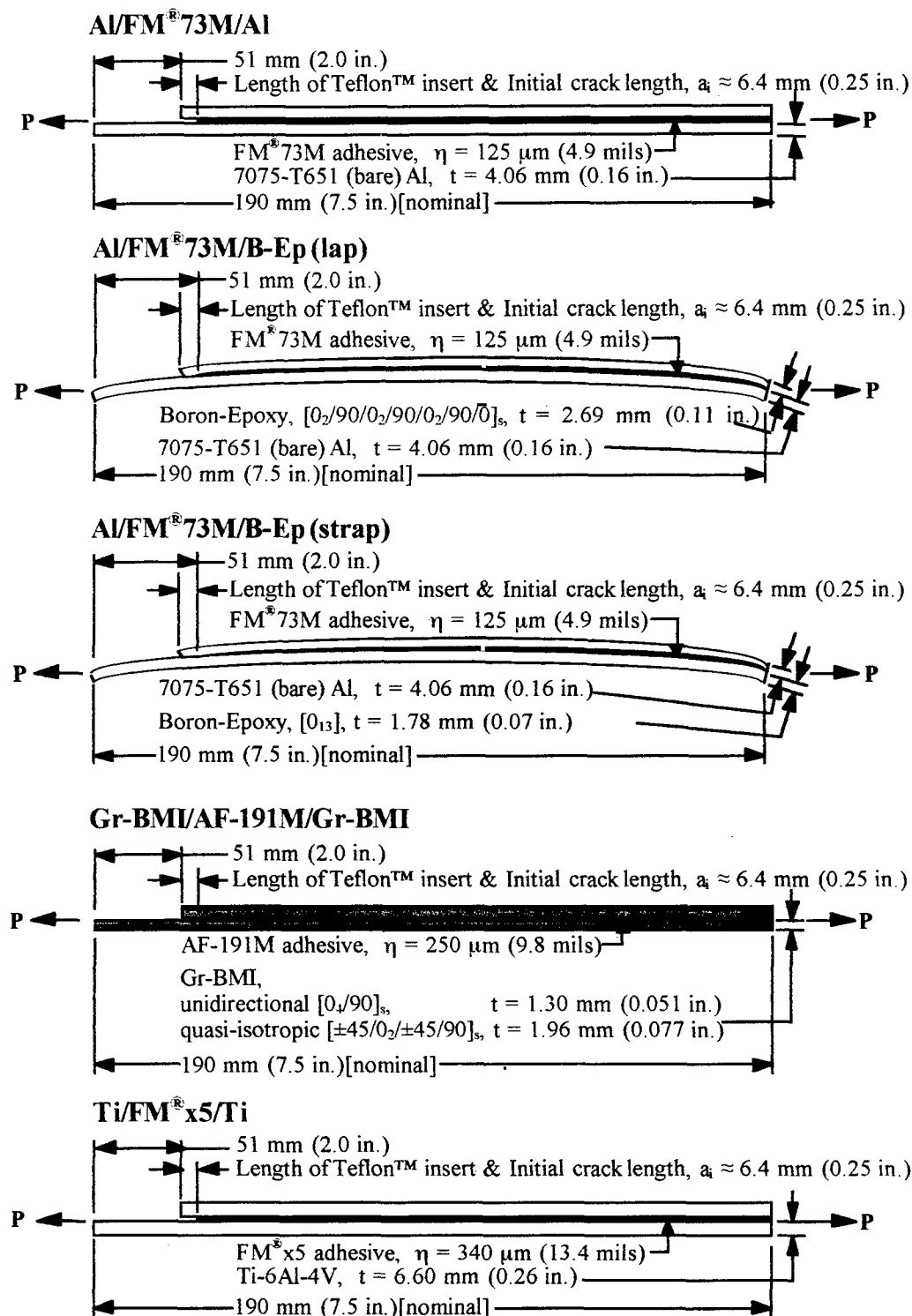


Figure 11. Cracked lap shear (CLS) specimen geometries

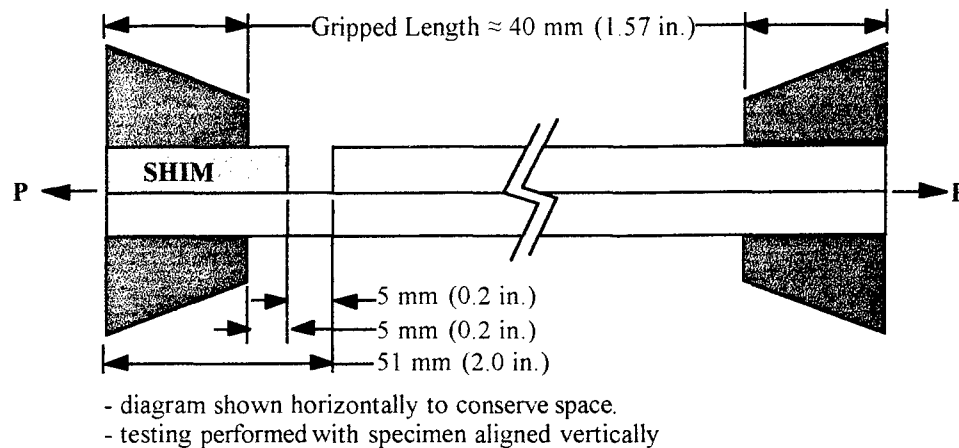


Figure 12. Shim and gripping details for CLS specimens

element analysis of these specimens found that the level of strain energy release rate in the bond line was independent of the presence or absence of a shim.

3.3. Specimen Fabrication

The following sections describe the procedures used to manufacture the adhesive and bonded joint specimens used in this research. For all specimens, care was taken to ensure that curing and bonding procedures closely matched those recommended by the adhesive manufacturers or those currently in use by the aerospace industry. Detailed curing and bonding procedures may be found in Appendix A.

3.3.1. Adhesive Specimen Fabrication

Fabrication of the adhesive specimens used for tensile and fracture toughness testing consisted of two main steps: curing the adhesive, and cutting individual specimens.

3.3.1.1. Curing of Adhesive Sheets

Sheets of the modified epoxy adhesive films, AF-191 and FM[®]73, were cured at the Georgia Institute of Technology. Curing profiles were tailored to approximate the time-temperature histories used by the manufacturers' of the bonded joint specimens investigated for this study.

Essentially void-free sheets (approximately 250 mm × 250 mm [10 in. × 10 in.]) of the AF-191 and FM[®]73 adhesives were cured in a Precision "Thelco" circulating air oven. Cure temperatures were 115°C (240°F) for the FM[®]73 adhesive and 177°C (350°F) for the AF-191 adhesive film. Single layers of these adhesive films were cured without pressure on an aluminum plate which was covered with a porous Teflon[™] cloth to prevent the adhesives from adhering to the plate. Trial runs made using a vacuum bag or autoclave and attempts at curing multiple film layers resulted in cured sheets with unacceptably high levels of voids. Therefore, only single layers of the FM[®]73 and AF-191 films were cured without pressure or vacuum.

FM[®]x5 sheets (approximately 150 mm × 150 mm [6 in. × 6 in.]) were cured in an autoclave and provided by CYTEC Engineered Materials, Inc. The cure temperature used for the FM[®]x5 adhesive was 350°C (662°F).

3.3.1.2. Die Cutting of Adhesive Specimens

Adhesive test specimens were cut from the cured adhesive sheets using steel rule dies. These dies were manufactured from hardened and sharpened thin steel stock by

Dienetics, Inc. (Jenison, MI). The steel stock was bent to match the desired specimen shape and retained this shape by having its unsharpened edge pressed into a hardwood block. The resulting die resembled a cookie cutter.

To cut the specimens, a die was placed on a flat surface with the cutting edge facing up, a piece of cured adhesive film was placed on top of the die, and a small, rigid sheet of polyethylene was placed on top of the adhesive film. The top surface of the polyethylene sheet was struck firmly with a rubber or dead weight mallet. This produced specimens with clean edges and consistent dimensions.

3.3.2. Bonded Joint Specimen Fabrication

All bonded joint specimens were fabricated by major airframe manufacturers according to their current industrial practices for adhesive bonding. Lockheed Martin Aeronautical Systems Co. (Marietta, GA) manufactured the Al/FM[®]73M/Al, Al/FM[®]73M/B-Ep, and Gr-BMI/AF-191M/Gr-BMI specimens. Boeing Defense & Space Group (Seattle, WA) manufactured the Ti/FM[®]x5/Ti specimens.

The basic procedure used to fabricate the bonded joint specimens was to first bond together large sheets of adherend materials which had had their surfaces appropriately prepared. If composites were used in a particular bonded system, laminates were cured first and then secondarily bonded. Individual specimens were then cut from the large bonded panels.

Following the fabrication of the bonded panels but prior to cutting the individual specimens, all bonded panels were ultrasonically C-scanned. Poorly bonded panels and specimens from poorly bonded regions were discarded.

3.3.2.1 Fabrication of Al/FM[®]73M/Al Specimens

Prior to bonding, the surfaces of 7075-T651 bare aluminum sheets were prepared to permit adequate adhesion between the FM[®]73M and the metal. Surface preparation of the aluminum included an Al₂O₃ grit blast, followed by a sodium dichromate (Forest Products Lab, "FPL") etch, and the application of CYTEC's protective BR[®]127 primer. The purpose of the primer was to protect the delicate oxide film on the aluminum which is crucial to achieving a high quality bond.

Bonding of the prepared aluminum sheets was performed at 116°C (240°F) under full vacuum for 150 minutes. The resulting bond line thickness was approximately 125 μm (4.9 mils).

3.3.2.2 Fabrication of Al/FM[®]73M/B-Ep Specimens

The boron-epoxy composite adherends for these specimens were cured prior to bonding. Surface preparation of the pre-cured boron-epoxy laminates consisted of hand sanding with 280 grit abrasive paper followed by a methanol wipe.

Surface preparation of the aluminum was as described in the previous section.

As with Al/FM[®]73M/Al system, bonding of the Al/FM[®]73M/B-Ep system was carried out at 116°C (240°F) using full vacuum for 150 minutes. The resulting bond line thickness was approximately 225 μm (8.9 mils).

Using F M[®]73M adhesive, hinges were bonded on to the Al/FM[®]73M/B-Ep DCB specimens at 110°C (230°F) using full vacuum for 150 minutes.

3.3.2.3. Fabrication of Gr-BMI/AF-191M/Gr-BMI Specimens

As with the boron-epoxy adherend material, the graphite-bismaleimide adherends were cured prior to bonding. Pre-bond surface preparation of the cured composite laminates consisted of removal of the protective peel ply, hand sanding with 180 grit abrasive paper, and a methanol wipe.

Secondary bonding of the Gr-BMI adherends with AF-191M adhesive was carried out in an autoclave at 177°C (350°F) and 310 kPa (45 psi) for 60 minutes. The resulting bond line thickness was approximately 250 μm (9.8 mils).

Using F M[®]73M adhesive, hinges were bonded on to the Gr-BMI/AF-191M/Gr-BMI DCB specimens at 121°C (250°F) using full vacuum for 60 minutes.

3.3.2.4. Fabrication of Ti/FM[®]x5 Ti Specimens

Prior to bonding, the surfaces of Ti-6Al-4V titanium sheets were prepared to permit adequate adhesion between the F M[®]x5 and the metal. Surface preparation was carried out using Boeing's standard chromic acid etch and the application of CYTEC's

protective BR[®]x5 primer. This primer, essentially a diluted form of the FM[®]x5 adhesive, served the same purpose as the BR[®]127 primer used on the aluminum - protection of the delicate anodized surface of the titanium necessary for bonding.

Bonding of the titanium sheets was performed in an autoclave at 350°C (662°F) and 345 kPa (50 psi) for 90 minutes. The resulting bond line thickness was approximately 340 µm (13 mils).

CHAPTER IV

ENVIRONMENTAL EXPOSURE

The major thrust of this research was to investigate the durability of bonded joints exposed to typical service environments. Specific exposure environments were chosen based upon the particular application in which an adhesive or bonded system is used or will be used, upon previous research in this area, and upon discussions with the bonded joint specimen manufacturers. Two main versions of environmental exposure were performed for this research: long-term isothermal exposure for up to 10,000 hours, and cyclic thermal exposure for up to 500 cycles. In all cases, specimens were not loaded during these exposures. Table 2 provides a summary of the various isothermal conditions to which selected adhesive and bonded joint test specimens were exposed prior to testing.

A concerted effort was made to make the environmental exposure as realistic as possible. Temperature and humidity levels were chosen only after extensive discussions with the bonded joint specimen manufacturers. The exposure environments were based upon specific aircraft environments in which the bonded joint systems are or will be operated. No attempt was made to alter these operating conditions to accelerate the effects of the environments on the adhesive or bonded joint specimens. Obviously, constraints placed upon this research project in terms of time and equipment usage

precluded exposure times and numbers of thermal cycles from exactly matching aircraft lifetimes or numbers of flights. Thus, although the exposure environments are realistic, the times for which specimens have been exposed are somewhat arbitrary. Nevertheless, such compromises were deemed necessary in order to evaluate the characteristics of specific adhesives given the constraints of performing the research.

This chapter will outline the specific exposure conditions used for the adhesive and bonded joint test specimens. The environments in which the specimens were stored and tested will also be identified. In addition, the equipment used to perform the various types of exposures will be described.

4.1. Long-term Isothermal Exposure

Long-term isothermal exposure conditions were subdivided into two main varieties, "hot/wet" during which specimens were simultaneously exposed to high temperature and high humidity conditions, and "hot/dry" during which specimens were exposed only to high temperature. In addition, a small number of specimens were exposed to room temperature, high humidity ("RT/wet") conditions.

4.1.1. Isothermal Conditions

Several different isothermal exposure conditions were used. These were based upon the types of environments experienced by or projected for the bonded systems on the C-141 transport, the F-22 fighter, and the HSCT aerospace vehicle.

Table 2. Summary of Environmental Exposure Conditions

APPLICATION	ADHESIVE OR BONDED SYSTEM	PRE-TEST EXPOSURE ENVIRONMENTS
C-141 <i>bonded repairs</i>	FM[®]73U adhesive	<ul style="list-style-type: none"> • None (as-received) • Hot/Dry: 71°C [160°F] 0% rh, 5000 hrs. • RT/Wet: 22°C [72°F] >90% rh, 5000 hrs. • Hot/Wet: 71°C [160°F] >90% rh, 5000 hrs.
	FM[®]73M adhesive	<ul style="list-style-type: none"> • None (as-received)
	Al/FM[®]73M/Al bonded system	<ul style="list-style-type: none"> • None (as-received) • Hot/Dry: 71°C [160°F] 0% rh, 5000 hrs. • RT/Wet: 22°C [72°F] >90% rh, 5000 hrs. • Hot/Wet: 71°C [160°F] >90% rh, 5000 hrs. • Hot/Wet: 71°C [160°F] >90% rh, 5000 hrs. then stored in desiccant for 5000 hrs. • Hot/Wet: 71°C [160°F] >90% rh, 10000 hrs. • Cycled: -54°C [-65°F] to 71°C [160°F], 100 Cycles
	Al/FM[®]73M/B-Ep bonded system	<ul style="list-style-type: none"> • None (as-received) • Hot/Wet: 71°C [160°F] >90% rh, 5000 hrs. • Hot/Wet: 71°C [160°F] >90% rh, 5000 hrs. then stored in desiccant for 5000 hrs. • Cycled: -54°C [-65°F] to 71°C [160°F], 100 Cycles
F-22 <i>control surfaces</i>	AF-191U adhesive	<ul style="list-style-type: none"> • None (as-received) • Hot/Dry: 104°C [220°F] 0% rh, 5000 hrs. • Hot/Wet: 71°C [160°F] >90% rh, 5000 hrs. • Cycled: -54°C [-65°F] to 104°C [220°F], 100 Cycles
	AF-191M adhesive	<ul style="list-style-type: none"> • None (as-received)
	Gr-BMI/AF-191M/Gr-BMI bonded system	<ul style="list-style-type: none"> • None (as-received) • Hot/Dry 104°C [220°F] 0% rh, 5000 hrs. • Hot/Dry 104°C [220°F] 0% rh, 10000 hrs. • Cycled: -54°C [-65°F] to 104°C [220°F], 100 Cycles
HSCT <i>wing or fuselage components</i>	FM[®]x5 adhesive	<ul style="list-style-type: none"> • None (as-received) • Hot/Dry 177°C [350°F] 0% rh, 5000 hrs. • Hot/Wet 71°C [160°F] >90% rh, 5000 hrs. • Cycled: -54°C [-65°F] to 163°C [325°F], 500 Cycles
	Ti/FM[®]x5/Ti bonded system	<ul style="list-style-type: none"> • None (as-received) • Hot/Dry 177°C [350°F] 0% rh, 5000 hrs. • Hot/Dry 177°C [350°F] 0% rh, 10000 hrs. • Hot/Wet 71°C [160°F] >90% rh, 5000 hrs. • Hot/Wet 71°C [160°F] >90% rh, 10000 hrs. • Cycled: -54°C [-65°F] to 163°C [325°F], 500 Cycles

Because of its worldwide airlift capability, the C-141 is exposed to a wide range of environments including high temperature and high humidity levels. During extended ground operations at tropical airfields, operating conditions for this aircraft can approach so-called hot/wet conditions of 71°C (160°F) with high (>90%) relative humidity (rh). Some adhesive and bonded joint specimens from the C-141 program were also exposed to hot/dry (71°C [160°F], 0% rh) and RT/wet (22°C [72°F], >90% rh) conditions. To determine if the effects of exposure to high humidity levels were reversible, some of the specimens exposed to hot/wet conditions for 5,000 hours were, in turn, placed in a desiccator at room temperature in an attempt to remove any moisture absorbed during exposure.

During future service, the F-22 will also be exposed to a wide range of environments including similar "hot/wet" conditions as the C-141. Selected AF-191U adhesive specimens were exposed to the hot/wet (71°C [160°F], >90% rh) environment for 5,000 hours. However, it was determined by Lockheed Martin engineers that the most severe environment for the AF-191 adhesive and Gr-BMI/AF-191M/Gr-BMI bonded system will occur during maximum performance, "edge-of-the-envelope" operations of the aircraft. Thus, a hot/dry condition of 104°C (220°F) with 0% rh was chosen as the primary exposure condition.

The greatest range of conditions to which the bonded systems examined for this research will be exposed will undoubtedly be those of the High Speed Civil Transport.

Because of its intended use as a worldwide commercial air vehicle, the HSCT may operate under a variety of conditions. These include hot/wet (71°C [160°F], $>90\%$ rh) ground conditions and extended time at supersonic speeds where frictional heating may create a hot/dry (177°C [350°F], $>90\%$ rh) for bonded components.

4.1.2. Equipment

Long-term isothermal exposures were performed using Thermotron (Holland, MI) model OV-12 circulating air ovens. (Fig. 13) Humidity was monitored by a humidistat placed in each oven or chamber.

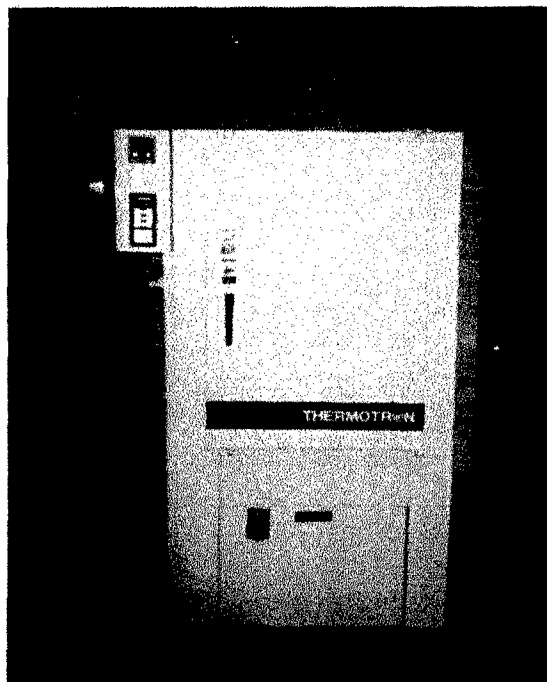


Figure 13. One of the ovens used for isothermal exposure

Hot/wet exposure of selected adhesive specimens and of selected Al/FM[®]73M/Al, Al/FM[®]73M/B-Ep, and Ti/FM[®]x5/Ti bonded joint specimens was also performed using a Thermotron model OV-12 oven. However, specimens were first sealed in a humidity chamber (Fig. 14) which was placed in an oven held at 71°C (160°F). The humidity chamber was constructed using a 9.5 liter (2.5 gal.) glass jar laid sideways and cradled in a wooden support. Specimens were not immersed but, instead, were supported over a pool

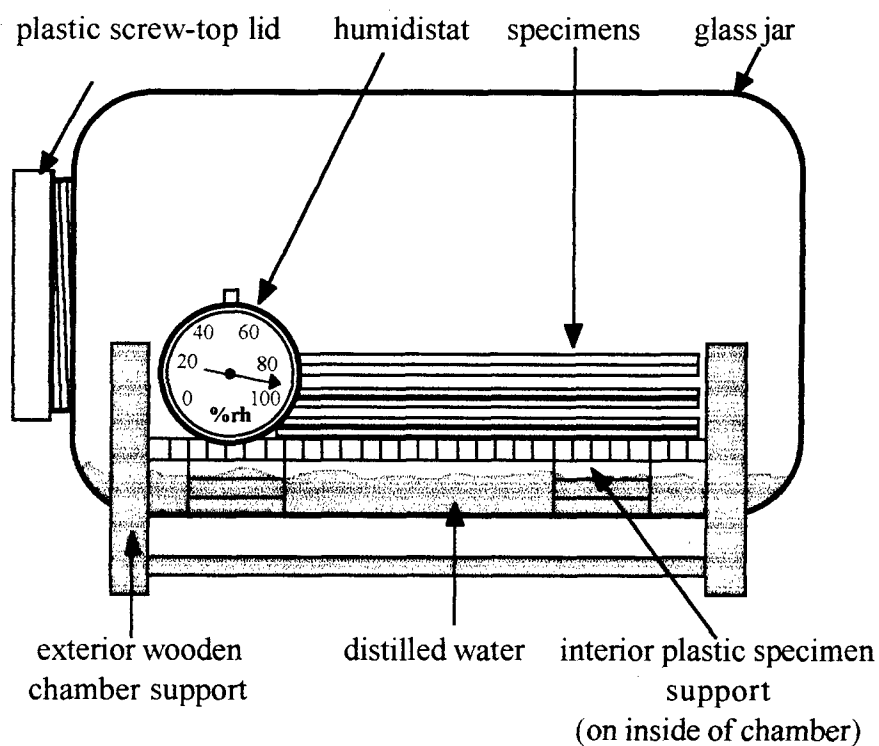


Figure 14. Humidity chamber used to maintain a "hot/wet" environment

of distilled water by a plastic grate. A humidistat was placed inside the chamber, and the chamber was sealed tightly before being placed in the exposure oven. Constant humidity levels of 92-98% rh were obtained using this apparatus.

RT/wet exposure of selected FM[®]73U specimens was performed using the same humidity chamber apparatus that was used for hot/wet exposure with the obvious difference of not having the chamber placed in an oven.

4.2. Cyclic Thermal Exposure

In addition to being subjected to isothermal exposure, selected specimens were also thermally cycled prior to testing. This cyclic thermal exposure was performed to simulate temperature excursions encountered during flight operations and to assist in determining whether the properties of adhesives and bonded joints could be affected by specific time-temperature histories.

4.2.1. Cyclic Thermal Conditions

Cyclic thermal conditions were determined by the maximum and minimum temperatures experienced by or expected for the C-141, F-22, and HSCT air vehicles.

Prior to thermal cycling, the bonded joint specimens from the C-141 and F-22 programs which were selected for exposure to the cyclic environment were first exposed for 300 hours to hot/wet conditions. This procedure was carried out to introduce

moisture into the bond line. Such a procedure, it was believed, would better simulate service conditions for the C-141 and F-22.

The common low temperature extreme used for all thermal cycling was -54°C (-65°F). This temperature corresponded to conditions typically encountered during high altitude ($>10,000\text{ m}$ [$>33,000\text{ ft.}$]), subsonic flight, a condition routinely experienced by many military aircraft and commercial airliners, particularly those on transcontinental or transoceanic routes.

The maximum temperature used during thermal cycling varied according to the particular adhesively bonded system being examined. Thus, the maximum cyclic temperature for the C-141-related adhesive and bonded joint specimens was 71°C (160°F), and the maximum cyclic temperature for the F-22-related adhesive and bonded joint specimens was 104°C (220°F). The maximum cyclic temperature for the HSCT-related materials was reduced by Boeing engineers from the hot/dry isothermal exposure level of 177°C (350°F) to a lower 163°C (325°F).

Due to the nature of the equipment used to perform the thermal cycling, it was impossible to control the humidity present in the cycling chamber. However, the chamber was located in a laboratory environment where the ambient conditions were approximately $22\pm 1^{\circ}\text{C}$ ($72\pm 2^{\circ}\text{F}$), $50\pm 5\%$ rh.

Thermal cycle profiles were determined by the operating characteristics of the thermal cycling apparatus, by the estimated average temperature ramp rates for bonded

components on the C-141, F-22, and HSCT, and by the desire to allow specimens to attain equilibrium at the temperature extremes. The C-141 (Al/FM[®]73M/Al and Al/FM[®]73M/B-Ep), F-22 (Gr-BMI/AF-191/Gr-BMI), and HSCT (Ti/FM[®]x5/Ti) specimens experienced average ramp rates of approximately 12°C (22°F)/min., 6°C (11°F)/min., and 7°C (13°F)/min., respectively. The resulting thermal cycle profiles were relatively asymptotic in shape, reflecting the temperature rise-, hold-, and fall-times of the cycled specimens. (Fig. 15)

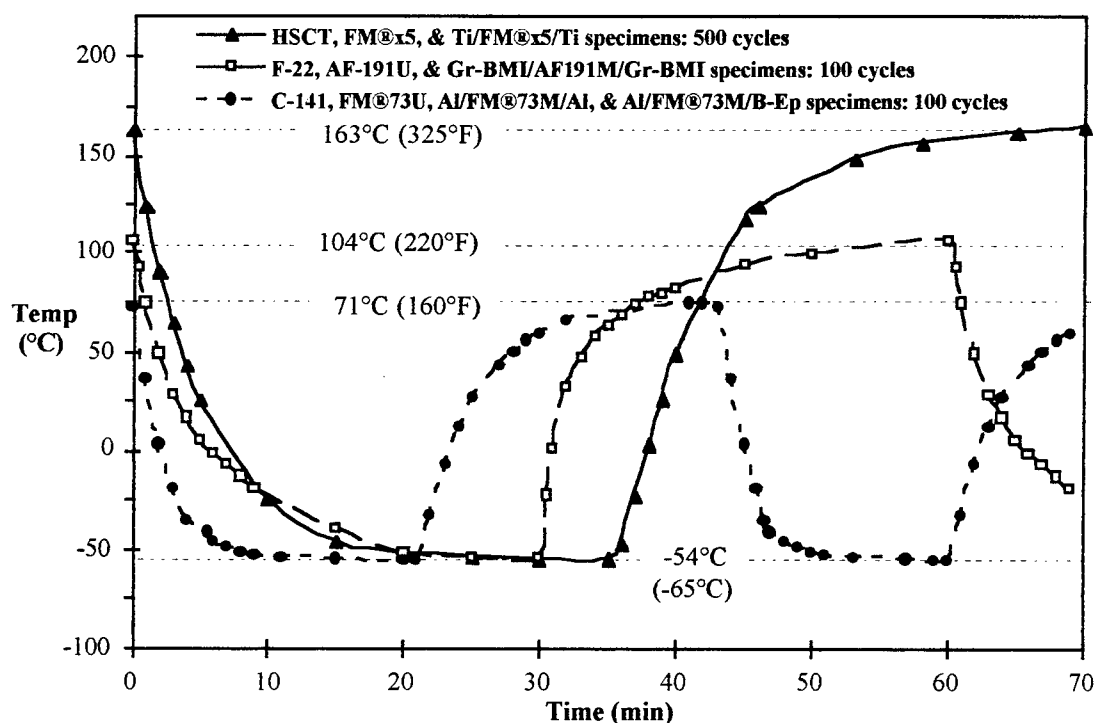


Figure 15. Thermal cycle profiles

4.2.2. Equipment

Thermal cycling was performed using a dual chamber thermal cycling apparatus located at the Warner Robins Air Logistics Center, Robins AFB, GA, manufactured by Russell's Technical Products (Holland, MI). (Fig. 16) The device consisted of two chambers. The upper chamber was maintained at the maximum cycle temperature using electric heating elements while the lower chamber was maintained at the minimum cycle temperature using circulating air cooled with injected liquid nitrogen.



Figure 16. Thermal cycling unit

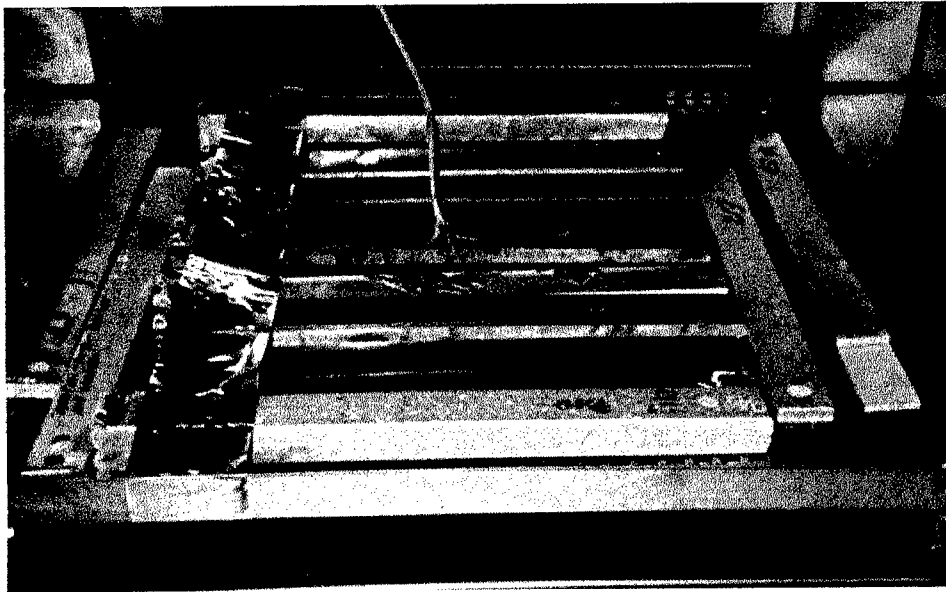


Figure 17. Specimens loaded onto the automatic trolley tray

During thermal cycling, specimens were placed on a tray (Fig. 17), and shuttled between chambers by means of an automatic pneumatic trolley mechanism. The trolley remained in each chamber for a time sufficient to achieve the desired temperature profile. A thermocouple placed between two adherends monitored bond line temperatures.

4.3. Storage

Due to the sensitive nature of adhesives, care was taken to store specimens before testing under conditions that would not destroy the effects of environmental exposure.

4.3.1. Storage Conditions

Three storage conditions were used. The first was a RT/wet condition (22°C [72°F], >90% rh). This was used to store specimens which had been isothermally exposed to hot/wet conditions. The second storage condition, RT/dry (22°C [72°F], <10% rh), was used to store all specimens which had been isothermally exposed to hot/dry conditions and the HSCT-related materials which had been thermally cycled. All other specimens were stored at ambient conditions (22°C [72°F], ~50% rh).

4.3.2. Equipment

The RT/wet storage condition was achieved by storing exposed specimens over a pool of distilled water in a sealed container similar to the humidity chamber described previously in Figure 14. The RT/dry storage condition was achieved by storing exposed specimens over a bed of desiccant in a sealed container. Humidistats were placed in all storage containers to monitor humidity levels.

4.4. Testing

Although most tests were performed under laboratory conditions (22±1°C [72±2°F], 50±5% rh), some were performed at elevated or reduced temperatures simulating actual aircraft service conditions.

4.4.1. Testing Conditions

Selected DCB and CLS bonded joint specimens from the C-141-, F-22-, and HSCT-related groups of specimens were tested at either reduced or elevated temperatures. The test temperature extremes corresponded to the minimum and maximum use temperatures of the bonded applications. Thus, the minimum test temperature common to all bonded material systems was -54°C (-65°F). Some Al/FM[®]73M/Al and Al/FM[®]73M/B-Ep specimens from the C-141 group were tested at 71°C (160°F). Some Gr-BMI/AF-191/Gr-BMI specimens from the F-22 group were tested at 104°C (220°F). Finally, some Ti/FM[®]x5/Ti specimens from the HSCT group were tested at 177°C (350°F).

After being brought to the desired test temperature, specimens were maintained at that temperature for approximately 15-20 minutes before testing was performed. This ensured that the entire specimen, including the interior regions of the bond line, was at the desired temperature.

4.4.2. Equipment

Elevated and reduced test temperatures were achieved using an Model 3610 environmental chamber manufactured by Applied Test Systems (Butler, PA). This test chamber was mounted on a servohydraulic test frame and contained a front and side viewing window through tests could be observed. To achieve elevated temperatures, air, heated by electrical resistance elements, was circulated through the chamber by means of a

small interior fan. Reduced temperatures were achieved by injecting liquid nitrogen through the rear of the chamber. The liquid nitrogen expanded into a gaseous form, was mixed with air inside the chamber, and was circulated by means of the interior fan.

Prior to conducting tests at elevated or reduced temperatures, bonded joint test specimens instrumented with up to ten thermocouples were placed in the chamber and allowed to achieve equilibrium with the various test temperatures to be used. The thermocouples were located along the exterior surfaces of the specimens, between the grips and the specimens, and, when possible, between the specimen adherends. These arrays of thermocouples were used to determine the temperature distribution along the length of the bonded joint specimens. The maximum observed deviation from the intended test temperature was 4°C (7°F). The temperature of each test specimen along its length was typically within 2°C (4°F) of the intended test temperature. The temperature of specimens subjected to testing was monitored with a thermocouple placed on the surface of the specimen near the initial crack tip and another placed within the body of the grip near the attachment point to the specimen.

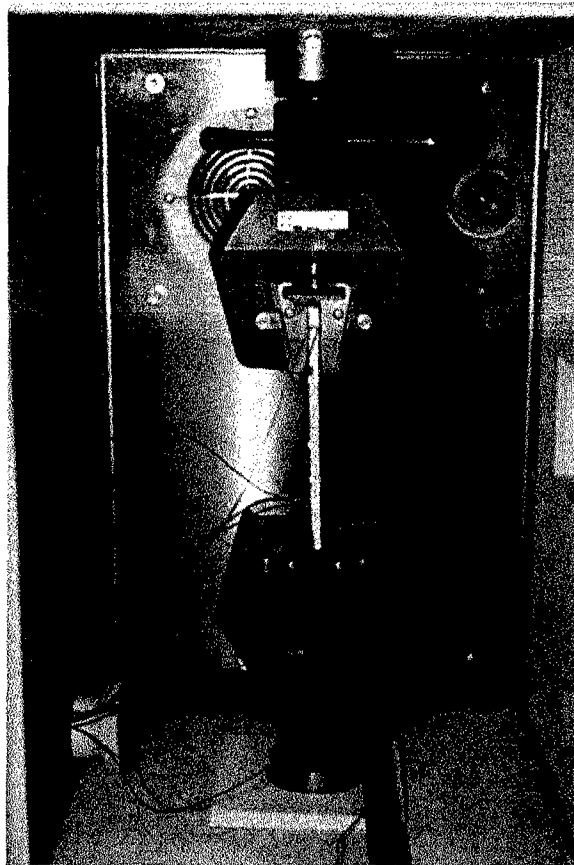


Figure 18. CLS specimen instrumented for temperature validation

CHAPTER V

MECHANICAL TESTING PROCEDURES

This chapter describes the procedures and equipment used for conducting various mechanical tests on adhesive and bonded joint specimens. Tensile and plane stress fracture toughness tests were performed on adhesive specimens. Mode I, Mode II, and mixed Mode I/II monotonic fracture toughness tests and Mode I and mixed Mode I/II fatigue crack growth tests were performed on the bonded joint specimens.

5.1. Mechanical Testing of Adhesive Specimens

Mechanical testing of the adhesive specimens was conducted using a screw driven test frame manufactured by the Instron Corp. (Canton, MA) and modified by MTI Systems (Roswell, GA). (Fig. 19) The test frame was equipped with a 4448 N (1000 lb.) capacity load cell able to resolve loads to within ± 2.2 N (0.5 lb.). Specimens were gripped using flat-faced, pneumatic grips pressurized to 620 kPa (90 psi). To prevent slipping of the high strength FM[®]x5 specimens, abrasive cloth tabs were placed between the faces of the grips and the specimens.

All tests of the adhesive specimens were conducted under displacement control with a crosshead speed of 1 mm (0.04 in) per minute at ambient laboratory conditions ($22\pm 1^{\circ}\text{C}$ [$72\pm 2^{\circ}\text{F}$], $50\pm 5\%$ rh).

A PC-based software program provided test control and continuously acquired load, crosshead displacement, and gage section extension (if available) for each test.

5.1.1. Tensile Testing of Adhesive Specimens

During tensile testing of the adhesive specimens, a non-contact laser extensometer provided gage section extension measurements accurate to ± 0.1 mm (4 mils). The Series 1500 unit was manufactured by Zygo (Middlefield, CT) and used a low-power, helium-neon laser beam. The scanned beam created a vertical line which passed through an aperture created by heavy paper flags affixed to the edges of the gage section on each specimen. (Fig. 20) The laser unit measured the distance between these two flags and, in doing so, provided information about changes in the specimen gage length during testing.

For each tensile test specimen, an engineering stress-strain curve was produced based on specimen dimensions, force readings obtained from the load cell, and displacement values obtained from the laser extensometer.

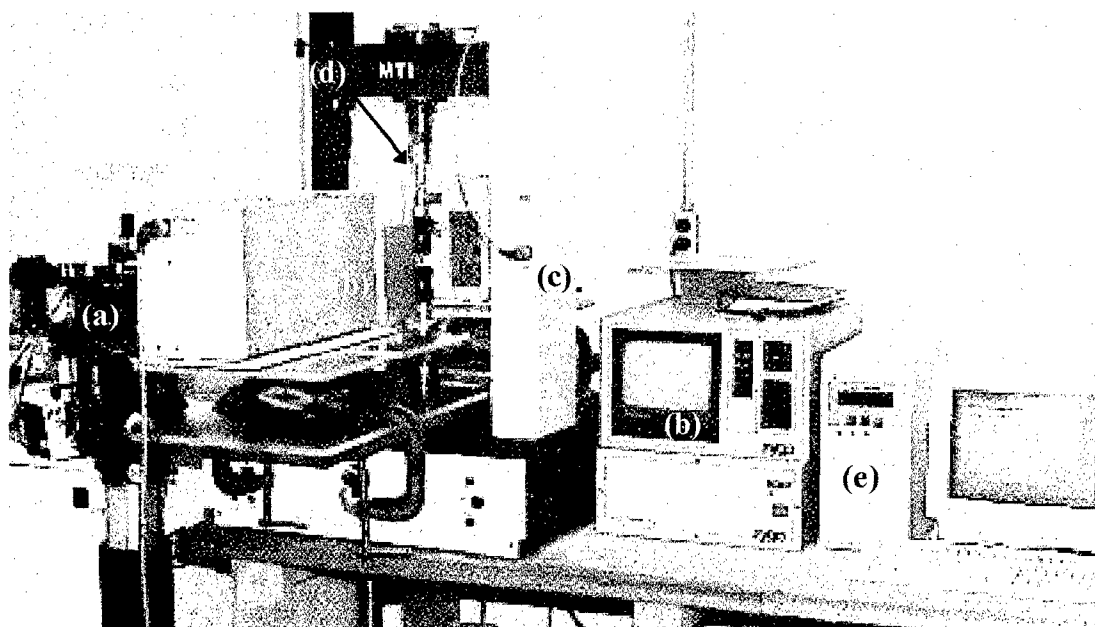


Figure 19. Adhesive film specimen test apparatus showing (a) Questar Microscope (partially hidden behind laser unit), (b) laser extensometer, (c) mechanical test frame, (d) pneumatic grips, and (e) PC for test control and data acquisition

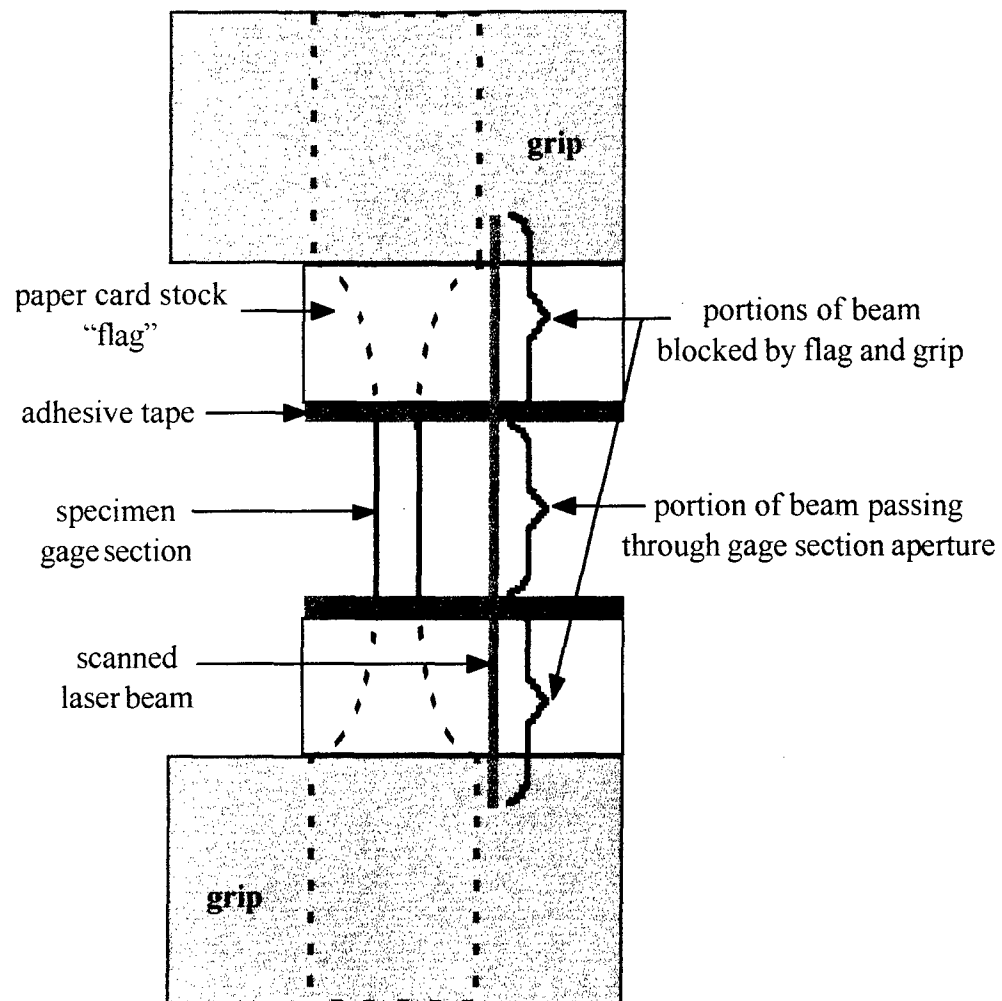


Figure 20. Use of laser extensometer to measure adhesive test specimen gage length

5.1.2. Fracture Toughness Testing of Adhesive Specimens

Toughness testing of the adhesives investigated for this study employed a single-edge notched, straight-sided specimen geometry previously described.

In place of the laser extensometer used for the tensile tests, a long focal length microscope manufactured by Questar (New Hope, PA) was used to monitor crack extension in the fracture toughness tests. This microscope, seen in Figure 19, had an approximate magnification factor of 200X. It was mounted to a movable stage equipped with digital horizontal and vertical position readouts with resolutions to $\pm 10 \mu\text{m}$ (0.4 mils). Images obtained from the microscope were captured by a charge coupled device (CCD) camera. This permitted images to be displayed on a video screen, recorded on tape, and also stored digitally on a computer disk. Use of the microscope and camera was especially valuable in determining the initial crack length and amount of extension which occurred during testing.

Testing to obtain a valid plane-stress fracture toughness was carried out in accordance with procedures developed in previous research by Hinckley, *et al.*,⁹¹ Tsou, *et al.*,⁹² and Klemann & DeVilbiss.⁹³

5.2. Mechanical Testing of Bonded Joint Specimens

Monotonic fracture toughness tests were performed on selected bonded joint specimens with three geometries, double cantilever beam (DCB), end-notched flexure

(ENF), and cracked lap shear (CLS). Fatigue testing was performed on selected DCB and CLS specimens. These tests generated load and displacement data which were used to describe the fracture or fatigue characteristics of the bonded joint specimens in terms of the strain energy release rate (G).

A number of test frames were used for the mechanical testing of the bonded joint specimens. All test frames were outfitted with PC-based test control and data acquisition systems which gathered load, displacement, and strain data (if required). Dedicated hydraulic wedge grips were present on two of the test frames used for this research. Figure 21 shows a typical test frame arrangement.

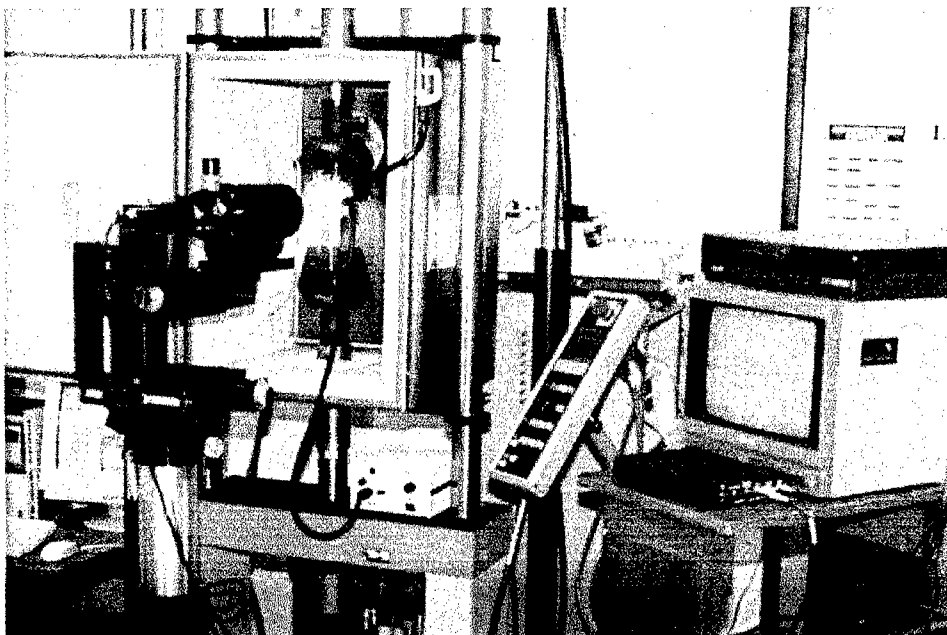


Figure 21. Typical test frame arrangement

The test frames used were as follows:

1. an 89 kN (20 kip) capacity servohydraulic test frame manufactured by Instron Corp. (Canton, MA) equipped with an ATS environmental test chamber (described in the previous chapter) and with the *TestStar* test control and data acquisition system manufactured by MTS, Inc. (Eden Prairie, MN)
2. a 89 kN (20 kip) capacity servohydraulic test frame manufactured by MTS, Inc., equipped with hydraulic wedge grips and with an *UTP-III* test control and data acquisition system manufactured by Interlaken Corp. (Eden Prairie, MN)
3. a 22 kN (5 kip) capacity servohydraulic test frame manufactured by MTS, Inc., equipped with hydraulic wedge grips and with MTS's *TestStar* test control and data acquisition system
4. a 45 kN (10 kip) capacity screw-driven test frame manufactured by Instron Corp., modified by MTI Systems (Roswell, GA), and equipped with MTI's *Phoenix* test control and data acquisition system
5. a 4.5 kN (1 kip) capacity screw-driven test frame manufactured by Instron Corp., modified by MTI Systems and equipped with MTI's *Phoenix* test control and data acquisition system

The choice of a frame to perform a specific test depended upon the required load, upon whether the test was a monotonic or a fatigue test, upon the types of grips available, and upon the presence (if needed) of the environmental test chamber.

The location of the crack tip and the amount of crack extension during a test was determined manually by constant visual monitoring using a Questar (New Hope, PA) long focal length microscope (magnification $\approx 200X$) or a Gaertner (Chicago, IL) traveling microscope (magnification $\approx 20X$). All crack length measurements were made on the edges of the bonded joint test specimens. To further assist in locating the crack tip, one edge of each specimen was lightly sprayed with a thin coat of flat white paint prior to testing. Following painting, the specimens were stamped with a scale having 0.5 mm (0.02 in.) increments. (Fig 22) This graduated scale served as a second means of confirming crack length in addition to microscope readings.

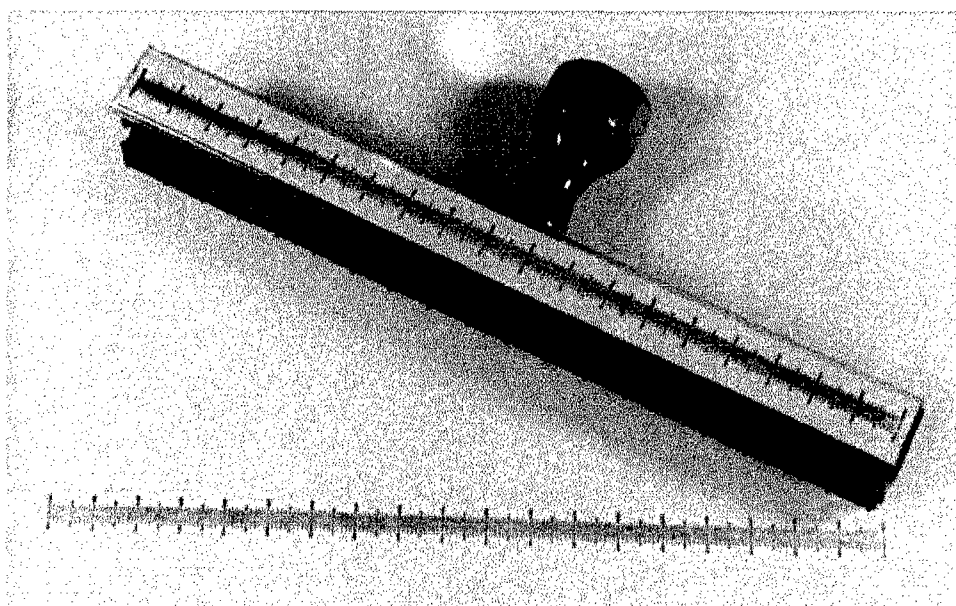


Figure 22. Ink stamp used to apply 0.5 mm graduated scales to specimen edges

The following sections will describe the equipment and procedures used for the various fracture and fatigue tests carried out on bonded joint specimens.

5.2.1. Monotonic Fracture Toughness Testing of Bonded Joint Specimens

Monotonic fracture toughness testing was performed to determine the response of bonded joint specimens to a slowly increasing level of applied load or crack opening displacement.

The geometry of the specimens, capability of the test machines, and the desire to visually observe cracking in the bond line (when possible) determined the rates of loading or crosshead displacement.

Cracks were grown directly from the tip of the Teflon™ or Kapton™ film inserted between the adherends. No pre-fatiguing of the specimens was performed prior to conducting monotonic tests. The decision to forgo pre-fatiguing was based upon 17 tests conducted on two DCB specimens from the Al/FM[®]73M/Al system. One specimen was subjected to fatigue pre-cracking before each monotonic fracture toughness test. The other had several monotonic tests performed on it in succession without periods of fatigue pre-cracking. The average Mode I monotonic fracture toughness from the pre-fatigued specimen was only 2% higher than that from the specimen which was not pre-fatigued. Scatter bands from the two specimens overlapped significantly. Thus, pre-fatiguing of all remaining monotonic fracture toughness tests was not performed.

5.2.1.1. Monotonic Fracture Toughness Testing of DCB Specimens

Monotonic testing of double cantilever beam specimens, using ASTM D3433-75⁹⁴ and D5228-94a⁹⁵ as guidelines, was conducted to obtain a Mode I fracture toughness or critical strain energy release rate (G_{IC}) for all of the bonded systems tested with the exception of the Al/FM[®]73M/B-Ep system. Loads and crosshead displacements (from the test frame LVDT) were collected during testing and were used to calculate G values.

The behavior of the Al/FM[®]73M/B-Ep system was slightly different from that of the other bonded systems. Because of the dissimilar adherends in the Al/FM[®]73M/B-Ep system and the presence of thermal residual stresses within the bond line due to the difference in the coefficient of thermal expansion between the adherends, achieving a state of pure Mode I was impossible. Instead, a mixed Mode I/II state was produced during loading of the DCB specimens of this particular bonded system. Thus, instead of obtaining a critical G_{IC} value, a total strain energy release rate G_{TC} was obtained and subsequently divided into Mode I and Mode II components using finite element analysis.

Load transfer to the specimens was accomplished using one of two methods. Pin joints were bolted to the adherends of the Al/FM[®]73M/Al and Ti/FM[®]x5/Ti specimens and attached to the load train using a pin and clevis arrangement. (Fig. 23) This form of load transfer mechanism was necessary because of the high loads required to produce fracture in the Al/FM[®]73M/Al and Ti/FM[®]x5/Ti DCB specimens. All other DCB

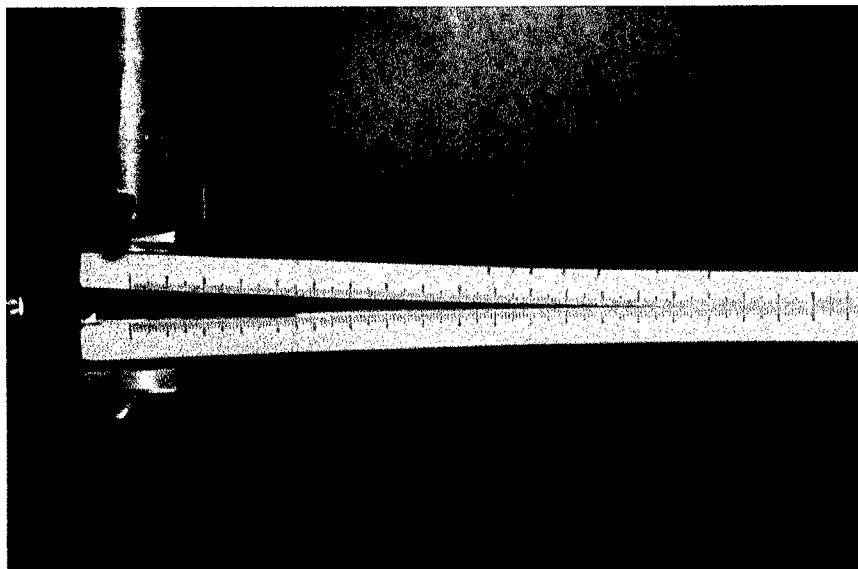


Figure 23. Testing an Al/FM[®]73M/Al DCB specimen using pins-and-clevises

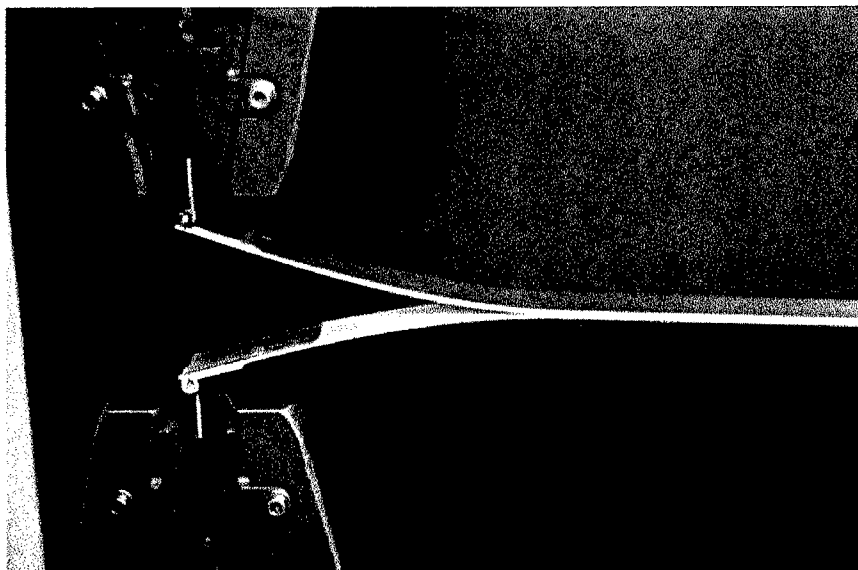


Figure 24. Testing a Gr-BMI/AF-191M/Gr-BMI DCB specimen using hinges

specimens were loaded using hinges clamped into mechanical wedge grips. (Fig. 24) These hinges were bonded to the adherends at the time of manufacture. Initial crack lengths were measured from the intersection of the loading axis and the bond line (i.e. from a point along the mid-line of the specimens and in line with the clevis or hinge pins).

Testing was performed at a constant crosshead displacement rate, equal to a crack mouth opening rate, of 1.0 mm/min. (0.04 in./min.). This testing rate was chosen for many reasons. First, it is consistent with displacement rates used in previous research conducted on the double cantilever beam specimen geometry. These rates ranged from 0.381 mm/min. (0.015 in./min.) used by Liechti & Freda⁹⁶ to 5.1 mm/min. (0.2 in./min.) by Ramkumar & Whitcomb.⁹⁷ A rate of 1 mm/min. was used by Mall & Johnson⁶⁸ and by Rakestraw, *et al.*⁹⁸ Second, preliminary tests were conducted to determine whether testing speed affected strain energy release rate values. Five monotonic toughness tests were performed on a single Al/FM[®]73M/Al double cantilever beam specimen using a crosshead displacement rate of 0.5 mm/min. (0.02 in./min.), and five monotonic toughness tests were conducted on specimen using a crosshead displacement rate of 1.0 mm/min. (0.04 in./min.). No significant difference was found between the two calculated critical strain energy release rates. Finally, a crosshead displacement rate of 1.0 mm/min. (0.04 in./min.) allowed a monotonic double cantilever beam test to be conducted rather quickly over the course of a few hours while loading the specimen at a rate slow enough to permit crack growth to be visually detected.

A deviation from linearity of the load vs. displacement trace indicated the onset of crack growth in the bond line region. This was confirmed by visual observations.

During testing, each DCB specimen was loaded to a point where crack growth began, and the crack was allowed to advance approximately 10 mm (0.4 in.) or more (in the case of rapid growth). The motion of the crosshead was then stopped, crack length measurements were taken, and the crosshead was returned to its starting position. This procedure was repeated multiple times on each specimen resulting in several crack growth runs and permitting the calculation of multiple G_{IC} or G_{TC} values. Figure 25 depicts a typical collection of load vs. displacement data obtained from a single specimen.

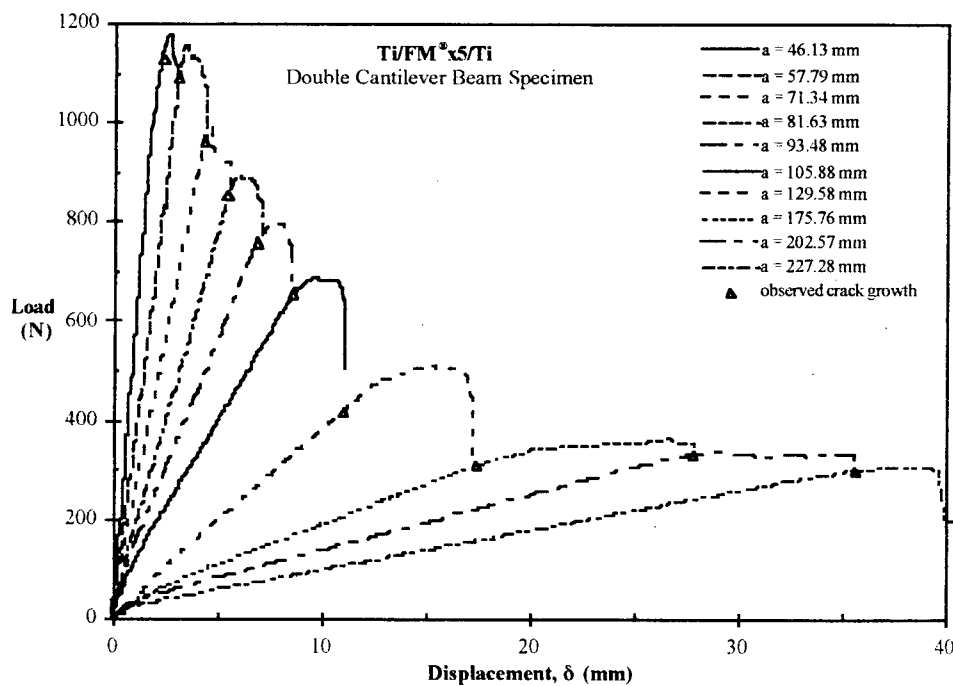


Figure 25. Typical load vs. displacement data from a single DCB specimen

The DCB specimen geometry was, by far, the easiest geometry to test. the opening mode made crack tips distinct. Failure occurred in the bond line before the adherends yielded, fatigued, or failed. The large loads and displacements were easily measured by the test apparatus available. Unfortunately, with the exception of the Al/FM[®]73M/B-Ep system, the DCB test only provided information regarding the Mode I behavior of the adhesives, and good bonded joint designs minimize the amount of Mode I to which adhesives are subjected in service.

5.2.1.2. Monotonic Fracture Toughness Testing of ENF Specimens

Monotonic testing of end-notched flexure specimens was conducted to obtain a Mode II fracture toughness or critical strain energy release rate (G_{IIC}). Although not standardized at this time, the procedures used for the ENF tests conducted for this research followed a protocol developed for round-robin testing (including ASTM participants).⁹⁹

Specimens were loaded using a three-point bending fixture. (Figs. 26 and 27) Loads and center point deflections were collected and were used to calculate G values. Center point deflections were measured using either the test frame LVDT (for specimens experiencing large deflections such as those from the Gr-BMI/AF-191M/Gr-BMI system) or an SLVC (super linear variable capacitor) capacitance gage transducer for specimens experiencing small deflections. The SVLC gage, used for its ability to obtain accurate measurements of small deflections, was manufactured by Automatic Systems

Laboratories, Inc. (New Fairfield, CT), and had a travel length of 5.08 mm (0.20 in.), and a resolution of 2.54 μm (10^{-4} in.).

Cracks were grown from the tip of the Teflon™ or Kapton™ film inserted between adherends. No pre-fatiguing of the specimens was performed prior to conducting the monotonic tests. The initial crack length for testing was always 25.4 mm (1.0 in.). This was accomplished by simply positioning the specimen so that the crack tip was located halfway between an outer and the inner loading pin.

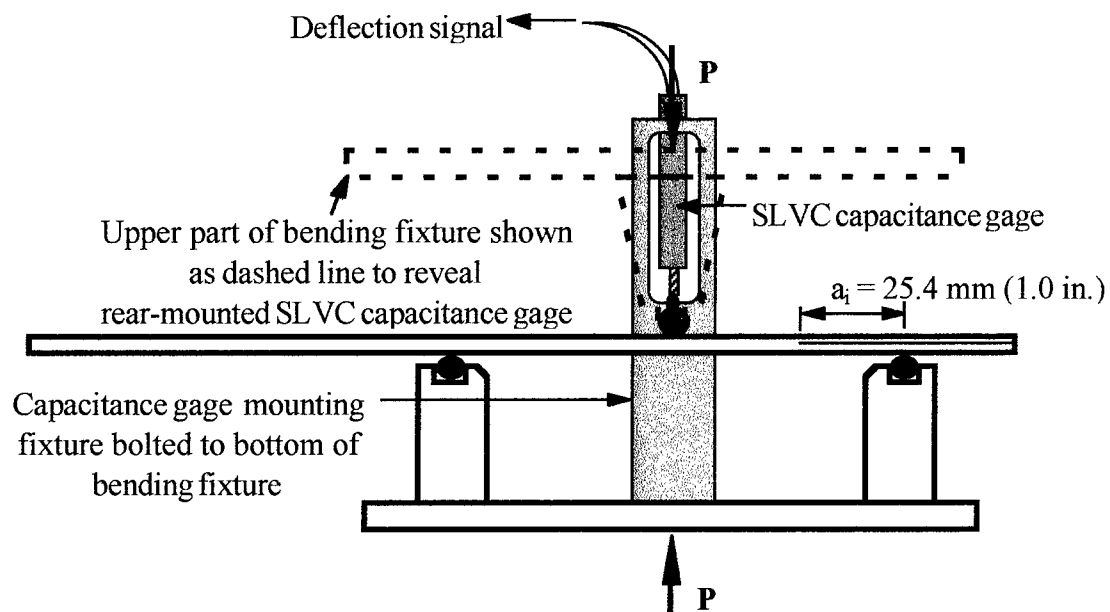


Figure 26. Typical end-notched flexure specimen test set-up

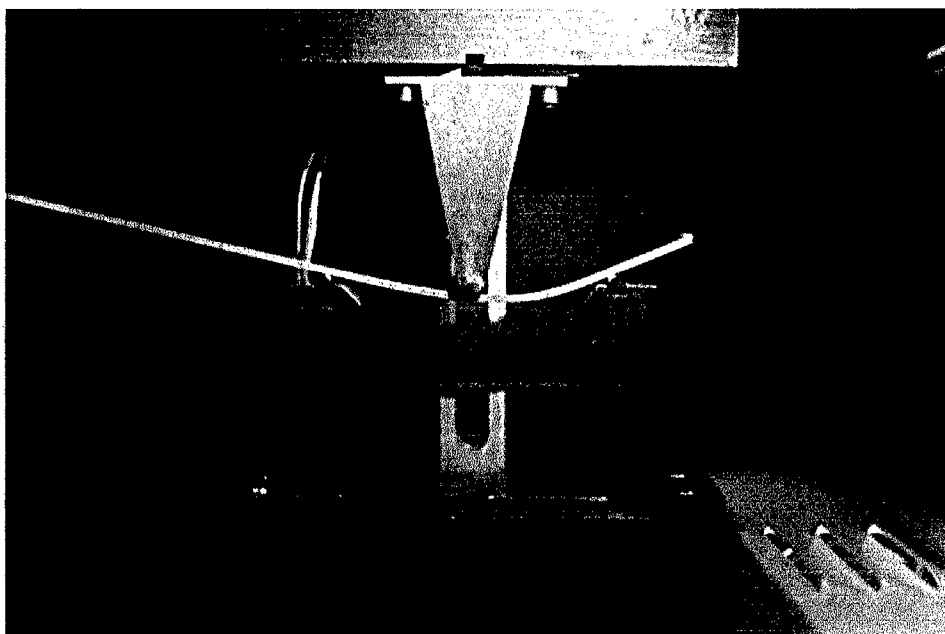


Figure 27. A Gr-BMI/AF-191M/Gr-BMI ENF specimen being tested

Testing of the ENF specimens was performed at a constant crosshead displacement rate of 0.5 mm/min. (0.02 in./min.) in accordance with recommended procedures.⁹⁹

A deviation from linearity of the load vs. displacement trace indicated the onset of crack growth in the bond line region or yielding of the adherends. This was confirmed by visual observations.

The behavior of some specimens permitted multiple tests to be conducted on a single specimen. If multiple tests were possible, the following procedure was used. Following a crack growth test, the length of the crack was measured and the specimen was unloaded. The new crack tip was positioned at a point midway between an outer and the inner loading pins. This effectively reset the crack length to 25.4 mm (1.0 in.). Following this re-positioning, another test was performed.

5.2.1.3. Monotonic Fracture Toughness Testing of CLS Specimens

Monotonic tests of specimens with the cracked lap shear (CLS) geometry were conducted to determine a mixed Mode I/II critical strain energy release rate. This type of testing is currently not covered by an ASTM specification. Thus, test procedures were determined after reviewing previous research which employed the cracked lap shear specimen including studies by Brussat, *et al.*⁶⁴ and Wilkins.¹⁰⁰

Specimen ends were gripped using mechanical or hydraulic wedge grips. To avoid introducing an additional bending moment, a shim, equal in thickness to the lap, was

bonded to the strap prior to testing. This ensured that the axis of the specimen was aligned with the axis of the load train.

Monotonic CLS testing was performed in load control with a rate of 100 N/sec. (22.5 lb./sec.). Though considerably slower than the loading rate used by the developers of the CLS specimen (Brussat, *et al.* used 79 kN/sec [350 kips/sec.]⁶⁴), this loading allowed the crack behavior to be visually observed through one of the microscopes used in this research. Displacement control, as used with the DCB and ENF geometries, was not chosen because of the very small displacements attained during these tests.

CLS specimens were monitored with a 25.4 mm (1.0 in.) gage length extensometer during testing. This device served not to measure the strain in the specimen but, rather, as a sensitive detector of axial displacement. The extensometer was mounted in a position such that its gage length encompassed the point of the initial crack tip as well as a region in which the strap and lap were bonded. (Figs. 28 and 29) Thus, the extensometer's output indicated the onset of crack growth in the same way that the LVDT did for the DCB specimens and that the capacitance gage did for the ENF specimens. A deviation from linearity of the load vs. displacement trace (as determined by the extensometer) often indicated the onset of crack growth. However, visual indications of crack growth proved to be much more reliable.

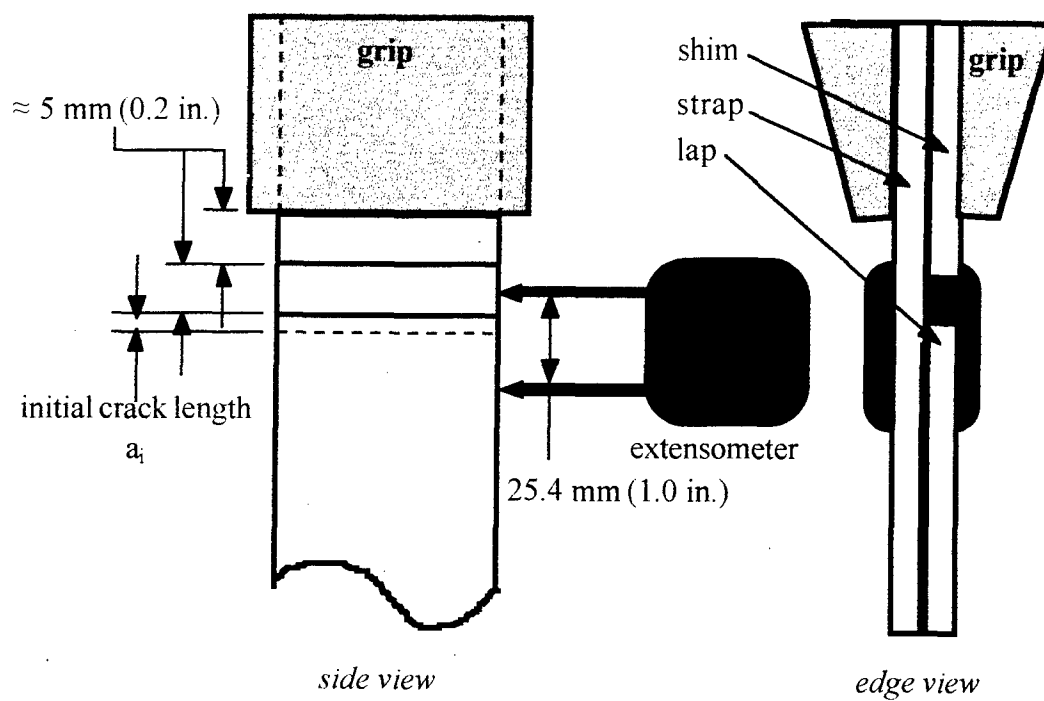


Figure 28. Placement of an extensometer on the cracked lap shear specimens

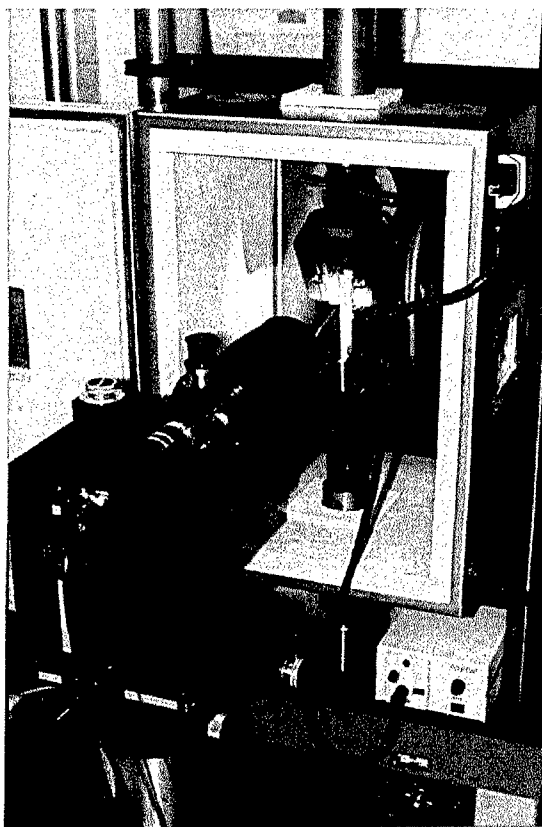


Figure 29. Typical cracked lap shear test set-up

Unlike the DCB and ENF tests, only one crack growth test was performed on each CLS specimen.

5.2.2. Fatigue Testing of Bonded Joint Specimens

Only two specimen geometries, the double cantilever beam and cracked lap shear, were subjected to fatigue testing. Of these, only the DCB specimens were tested extensively. Problems with fatigue failures of the strap adherends limited the fatigue

testing carried out on the CLS specimens. All fatigue tests were conducted on servohydraulic test frames.

5.2.2.1. Fatigue Testing of the DCB Geometry

Fatigue testing of DCB specimens was carried out using the same types of load transfer mechanisms (pin-and-clevis joints or hinges) as used for the monotonic tests.

Fatigue tests were performed under displacement control using a displacement R-ratio ($\delta_{\min}/\delta_{\max}$) of 0.1. This permitted the applied strain energy release rate to be “shed” (i.e. G levels fell during the course of the fatigue tests) so that a threshold crack growth rate could be approached as the crack propagated. The threshold fatigue crack growth rate of 10^{-6} mm/cycle (4×10^{-8} in./cycle) was chosen based upon previous work by Marceau, *et al.*⁸⁰ and Mall, *et al.*¹⁰¹

The identification of this crack growth rate as a “threshold” appears to be somewhat arbitrary. Previous fatigue data showed no evidence of a major reduction in growth rate below this level as is displayed in the sigmoidal shapes of da/dN vs. ΔK (or ΔG) curves from metals. Nor was any evidence of a “tailing off” of the growth rate observed in the fatigue tests conducted for this research. Thus the choice of 10^{-6} mm/cycle (4×10^{-8} in./cycle) as the threshold level was based purely on previous research in the field which has somewhat established this level as a benchmark.

The Al/FM[®]73M/Al and Ti/FM[®]x5/Ti specimens were tested at a frequency of 10 Hz. Due to the flexibility of the composite adherends, large deflections (up to 10 mm

[0.4 in]) were necessary to induce fatigue crack growth in the Al/FM[®]73M/B-Ep and Gr-BMI/AF-191/Gr-BMI specimens. Because of these large deflections, the hydraulic tests system performance limited the test frequencies for these two systems to 1 Hz. For all specimens, periodic cycles conducted at 0.1 Hz captured peak/valley load and displacement values used in compliance calculations and in estimates of crack length and G_I or G_T .

Because the loads obtained during these fatigue tests were relatively low (as low as 25 N (5.5 lb.) for some of the Gr-BMI/AF-191/Gr-BMI specimens), a low-force load cell with a maximum capacity of 1.1 kN (500 lbs.) was used when possible. However, load readings at low loads were very noisy, and this prevented compliance data from being used to infer crack lengths. Thus, optical measurements taken periodically throughout the course of a fatigue test using a traveling microscope were relied upon for crack length measurements.

5.2.2.2. *Fatigue Testing of the CLS Geometry*

Fatigue tests of the CLS specimens were performed under load control using an R-ratio (P_{min}/P_{max}) of 0.1, a load ratio based upon previous research in this area.^{67,68,101} Tests were conducted at a frequency of 10 Hz. Periodic cycles conducted at 0.1 Hz captured peak/valley load and displacement values used in compliance calculations and in estimates of crack length and G_T .

Other procedures used for the fatigue testing of CLS specimens were similar to monotonic testing procedures. Specimens were gripped using hydraulic or mechanical wedge grips. Shims were used to align the longitudinal axis of the specimen with the test frame load train. An extensometer was used to monitor displacement across a 25.4 mm (1.0 in.) region of the specimen that included the initial crack tip. Crack growth was periodically monitored visually using a traveling microscope.

CHAPTER VI

ANALYSIS OF MECHANICAL TESTS

This chapter describes the procedures used for analyzing the tensile and fracture toughness tests conducted using adhesive specimens and for analyzing the double cantilever beam, end-notched flexure, and cracked lap shear bonded joint specimen geometries.

The analysis of the adhesive specimens was relatively straightforward. However, adhesively bonded joints are complex structures which may be analyzed using a variety of techniques to determine the fracture modes present at a crack tip. In many cases, for simple joint geometries and loading paths, closed-form solutions are sufficient. In other cases, such as joints with dissimilar adherends, a finite element model is required. This chapter will include a brief description of the finite element techniques used in work conducted by Valentin⁷² at the Georgia Institute of Technology to analyze the Al/FM[®]73M/B-Ep specimens with dissimilar adherends.

For the fracture analyses, all materials (adherends and adhesives) were assumed to be homogeneous, isotropic, and linearly elastic. Furthermore, their properties were assumed constant regardless of pre-test environmental exposure or test temperature.

6.1. Analysis of the Adhesive Tensile Tests

For each adhesive tensile test specimen, an engineering stress-strain curve was produced based on force and displacement values and specimen dimensions. From this curve, the elastic modulus (E), failure strain (ϵ_f), 2% offset yield strength ($\sigma_{ys(0.2)}$), intercept yield strength (σ_{iys}), and ultimate strength (σ_{uts}), were calculated.

Two approaches were used to determine the yield strength of the adhesive specimens. The first was a traditional 0.2% offset method. The second method involved constructing a line parallel to the elastic modulus (Fig. 30, line a) and a line indicating a secondary modulus corresponding to a linear strain hardening rate (line b). If the stress-strain curve did not contain a secondary modulus or if it peaked before relaxing and leveling-off, line b was drawn horizontally through the point of ultimate stress (as in Fig. 30). A vertical line (c) was then constructed to pass through the intersection of lines (a) and (b). The point where this line (c) intercepted the stress vs. strain curve was identified as the intercept yield strength (σ_{iys}) of the material.

Previous work performed by Krieger^{102,103} used a line (d) which bisected the angle formed by lines a and b. The intersection of line d with the stress-strain data is known as the “knee”. However, the intercept yield strength method is easier to perform and provides a more conservative estimate of the beginning of non-linear tensile behavior.

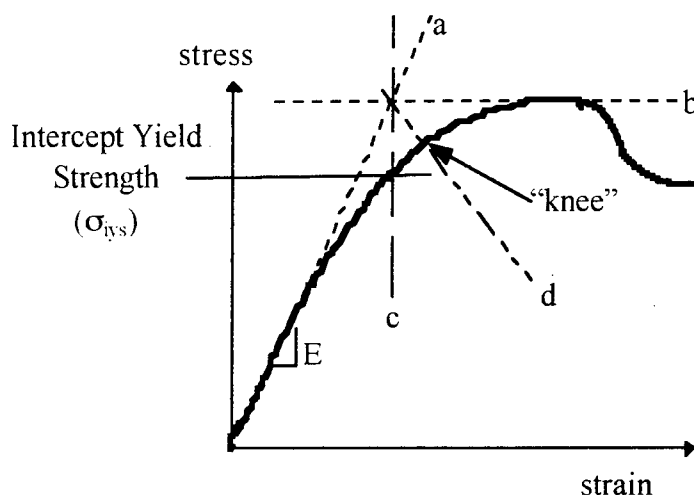


Figure 30. Obtaining the Intercept Yield Strength

The elastic modulus of the adhesive specimens was determined from a least squares fit to a range of points obtained from the initial linear portion of a stress vs. strain curve. The particular range of points used was chosen so as to obtain a minimum coefficient of deviation (R^2 value). For the epoxies (AF-191 and FM[®]73), data between 5 and 25 MPa (0.73 and 3.6 ksi) were used ($0.88 < R^2 < 0.95$). For the FM[®]x5, data between 20 and 100 MPa (2.9 and 14.5 ksi) were used ($0.97 < R^2 < 0.99$).

6.2. Analysis of the Adhesive Fracture Toughness Tests

Due to the thin nature of the adhesive films being tested, plane-strain fracture toughness values were unobtainable. However, testing to obtain a valid plane-stress fracture toughness was carried out in accordance with procedures developed in previous research by Hinckley, *et al.*,⁹¹ Tsou, *et al.*,⁹² and Klemann & DeVilbiss.⁹³ To satisfy the

requirement of plane stress, the adhesive fracture toughness specimens met the following criteria:

$$\sigma_f < \frac{2}{3} \sigma_{ys} \quad (1)$$

$$\frac{a}{W} < \frac{1}{3} \quad (2)$$

where:

σ_f = applied far-field stress at fracture instability

σ_{ys} = yield strength of the material

a = crack length

W = specimen width

The fracture toughness, which can be expressed in terms of a strain energy release rate, G_I , or a stress intensity factor, K_I , (Equation 3), was based on the initial crack length and the stress at fracture instability.

$$K_I = f(a/W) \sigma_f \sqrt{a_0} = \sqrt{G_I E} \quad (3)$$

where:

σ_f = applied far-field stress at fracture instability

a_0 = initial crack length (≈ 3 mm [0.12 in.])

$f(a/W)$ = geometric correction factor for single-edge notched specimens = $1.12\sqrt{\pi}$

Because these tests were conducted in displacement control, a period of steady crack growth occurred prior to unstable, catastrophic failure of the specimens.

To confirm that this method yielded meaningful results, values from the three adhesives investigated were compared with the current literature on the plane stress fracture toughness of polymeric films. Fracture toughness values for all three of these adhesives were similar to those obtained for other polymers such as cellulose acetate,⁹¹ LARC-TPI,⁹² polyamide-imide,⁹² Kapton polyimide,^{92,93} and polystyrene.⁹³

6.3. Analysis of the Double Cantilever Beam Specimens

The analysis of the double cantilever beam (DCB) specimens was carried out in closed-form for specimens with identical adherends. However, for specimens with dissimilar adherends, such as the C-141 Al/FM[®]73M/B-Ep system, a finite element analysis was required to determine what effects thermal residual stresses, specimen

curvature, and differences in the flexural modulus of the adherends had on the fracture modes present at the crack tip.

6.3.1. Closed-Form Solution for the Mode I Strain Energy Release Rate (G_I)

Determination of the applied strain energy release rate, G_I , for DCB specimens with two adherends of the same material may be performed using Equation (4).^{59,104}

$$G_I = \frac{P^2}{2b} \frac{dC}{da} \quad (4)$$

where:

P = load

C = specimen compliance (δ/P)

b = specimen width

a = crack length

δ = crosshead or crack mouth opening displacement

Using beam theory and the assumption that the DCB specimen consists of two cantilever beams with a built-in support on the end opposite the load application point,

(4) reduces to

$$G_I = \frac{3P\delta}{2ba} \quad (5)$$

Equation (5) may be further modified^{105,106} to account for the relationship between specimen compliance and observed crack length using

$$G_I = \frac{3P\delta}{2b(a + |\Delta|)} \quad (6)$$

The value Δ is the intercept of the a-axis obtained from a linear relationship between $C^{1/3}$ and a. (Fig. 31) This term serves as a correction to account for the fact that the uncracked end of the DCB specimen is free rather than built-in.

For the monotonic tests of the adhesives, the fracture toughnesses or critical strain energy release rates (G_{IC}) were obtained using this Modified Beam Theory, Equation (6), the visually observed crack length, and the critical load, P, at which crack growth began. This load corresponded to the load at which the load vs. displacement data deviated from linearity.

Equation (6) was also used to determine the applied strain energy release rates for fatigue tests.

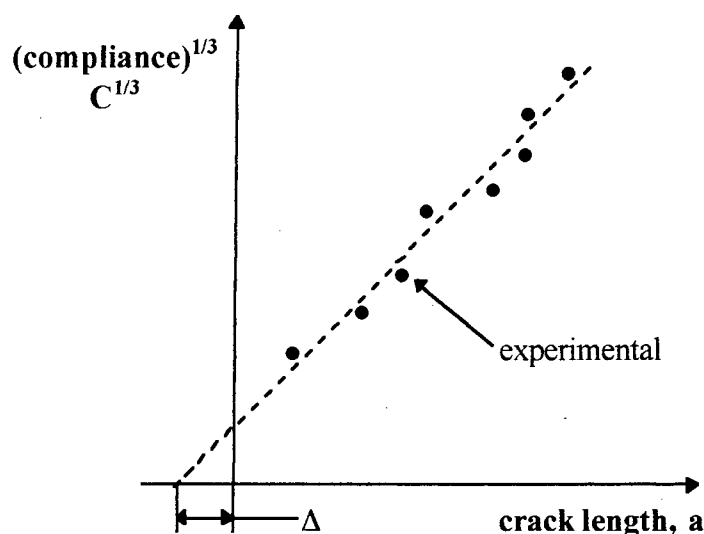


Figure 31. Determination of the end correction term, Δ

6.3.2. Analysis of Double Cantilever Beam Specimens Subjected to Fatigue

Fatigue data are presented in the Results & Discussion chapter in a manner similar to da/dN vs. ΔK curves familiar to those with experience in fatigue analyses of metallic materials. However, instead of using a stress intensity range (ΔK), a strain energy release rate range (ΔG) is used. This was done because the constraint caused by the relatively thick adherends on the thin bond line prevents the formation of a fully developed plastic zone. Complicated stress analyses are required if K solutions are to be used for such a constrained layer of adhesive in a globally inhomogeneous bonded specimen. The energy-

based concept of G , however, does not require modifications based upon such constraints and remains a useful, straightforward way of analyzing a bonded joint.

A link between the crack growth and applied strain energy release rate was proposed by Roderick, *et al.*¹⁰⁷ to follow the classical Paris Law relationship, $da/dN = c(G_T)^n$, where G_T represents the maximum total strain energy release rate applied to a joint or specimen during fatigue testing. Roderick, *et al.* found that this expression correctly represented fatigue test data for double lap joints consisting of aluminum bonded to either graphite-epoxy or S-glass-epoxy. Johnson & Mall⁶⁷ successfully employed this relationship in their work on the fatigue of composite cracked lap shear joints. In subsequent work, Roderick, *et al.*¹⁰⁸ found that a similar relationship of, $da/dN = c(\Delta G_T)^n$, where ΔG_T represents the range of total applied strain energy release rate (i.e., $G_{T,max} - G_{T,min}$), accurately predicted fatigue behavior in joints where cohesive fatigue cracking was observed. Mall *et al.*¹⁰⁹ confirmed this in their work on bonded graphite-epoxy adherends.

For the purposes of this research, fatigue data were expressed in terms of $da/dN = c(\Delta G_T)^n$. Values of ΔG_T were always very close to values of $G_{T,max}$ due to the small displacement R-ratio of 0.1 which was used. Furthermore, with the exception of the Al/FM[®]73M/B-Ep specimens with dissimilar adherends, crack growth was cohesive.

For the case of the DCB specimens with similar adherends, ΔG_I was used. Because of the lack of any Mode II component, ΔG_I in this case is equivalent to ΔG_T , the

total applied strain energy release rate range. For the case of the Al/FM[®]73M/B-Ep specimens with dissimilar adherends, ΔG_T was obtained by a combination of experimental observations and ABAQUS finite element analyses. The use of ΔG_T accounts for the presence of G_{II} in these specimens arising from thermally induced strains during curing and from mismatched flexural stiffness of the adherends. In addition, the use of ΔG_T for the Al/FM[®]73M/B-Ep specimens permits the fatigue crack growth data to be compared to that from the other bonded systems.

6.4. Analysis of the End-Notched Flexure Specimens

Determination of the applied Mode II strain energy release rate, G_{II} , for ENF specimens was carried out using several closed-form solutions discussed in the literature by Russell & Street,⁶² Carlsson, *et al.*,⁶³ O'Brien, *et al.*,¹¹⁰ and covered in a draft ASTM standard⁹⁹ obtained from G.B. Murri at NASA Langley Research Center (Hampton, VA).

The Beam Theory method is presented in Equation (7). The Direct Beam Theory method is presented in Equation (8). The Compliance Calibration method is presented in Equation (9).

$$G_{II} = \frac{9P^2 a^2}{16Eb^2t^3} \quad (7)$$

$$G_{II} = \frac{9Pa^2\delta}{2b(2L^3 + 3a^3)} \quad (8)$$

$$G_{II} = \frac{3mP^2a^2}{2b} \quad (9)$$

where:

P = load a = crack length (= 25.4 [1.0 in.])

E = adherend elastic modulus b = specimen width

t = thickness of one adherend δ = center point deflection

L = distance from center loading point to outer roller (= 50.8 mm [2.0 in.])

m = slope of a line describing the relationship between compliance and crack

length with an equation of $C = C_o + ma^3$

For the monotonic ENF tests of the bonded joints, the fracture toughness or critical strain energy release rate (G_{IIC}) was obtained using these three equations, and observations of critical loads and displacements made during testing. As with the DCB tests, crack growth was observed to begin at or near the onset of nonlinearity in the load vs. displacement data.

ENF results presented later in this thesis are those obtained using the Direct Beam Theory method, Equation (8), or finite element analysis. The Direct Beam Theory method was chosen for several reasons. First, it was computed directly from experimental deflection observations. Inconsistent readings obtained from the Beam Theory method (perhaps because this method employs the tensile modulus rather than a deflection value) and from the Compliance Calibration method (perhaps because this method relies upon a relationship constructed between compliance and crack length). In addition, Direct Beam Theory values typically fell between those obtained from the Beam Theory and Compliance Calibration methods. Finally, Direct Beam Theory values and those obtained using the finite element method generally differed by less than 10%. Therefore, it appeared that the Direct Beam Theory provided the best estimate of the Mode II fracture toughness.

Friction between the adherends was not accounted for in this analysis. In much of the previous literature, friction has also been neglected. (This may have been because of the relatively smooth surfaces of interlaminar cracks in composites for which the test was designed.) However, when multiple tests were conducted on single bonded joint specimen for this research project, the computed strain energy release rate usually increased from test to test. This suggests that friction is, indeed, a factor which merits additional consideration if the ENF specimen is to be used extensively for the analysis of adhesive bonds.

6.5. Analysis of the Cracked Lap Shear Specimens

Analysis of the cracked lap shear specimens was performed using closed-form and finite element methods. This specimen geometry was developed by Brussat, *et al.* and reviewed by Johnson¹¹¹ and Lai,¹¹² among others.

The closed-form solution used for the analysis of the CLS joint specimens is based upon beam theory and is presented in Equation (10)

$$G_r = \frac{P^2}{2b^2} \left[\frac{1}{E_s t_s} - \frac{1}{E_s t_s + E_l t_l} \right] \quad (10)$$

where:

P = load

b = specimen width

E_s = strap elastic modulus

E_l = lap elastic modulus

t_s = strap adherend thickness

t_l = lap adherend thickness

Note that this equation does not provide for the determination of the Mode I and Mode II components present in the cracked lap shear specimen. Research continues on ways to separate these two distinct strain energy release rate modes using closed-form solutions. However, for the purposes of this research, the Mode I and Mode II components were determined using the ABAQUS finite element program. For specimens

with identical adherends, ABAQUS-derived G_T values varied by a maximum of 5% from those obtained using Equation (10). For specimens having dissimilar adherends, closed-form G_T values were approximately 25% lower than ABAQUS values for the Al/FM[®]73M/B-Ep specimens with a B-Ep strap, and 25% higher than ABAQUS values for Al/FM[®]73M/B-Ep specimens with a B-Ep lap.

6.6. Finite Element Analyses

Finite element analyses were required to determine Mode I and Mode II components on the cracked lap shear specimens and were also needed to analyze all specimen geometries for the Al/FM[®]73M/B-Ep system. Due to the dissimilar adherends in the Al/FM[®]73M/B-Ep specimens, they exhibited pronounced curvature following curing (as described previously in this thesis). Thermal residual stresses, the root cause of the exhibited curvature, resulted in a thermally-induced Mode II strain energy release rate (G_{II}) being present at the crack tip with no applied load. Upon loading, the G_I and G_{II} levels could not be determined using closed-form solutions. Thus, a numerical, finite element model was required to determine the amount of mode mixity and to fully understand the behavior of G_I and G_{II} present at the crack tip during specimen loading. Details of this analysis may be found in Valentin's work.⁷² A brief review of these efforts is provided in the following sections.

When it was possible to perform finite element and closed-form analyses, the agreement between the two methods was generally very good. Most differences between

the two methods were less than 10%, with the finite element method generally providing higher values of toughness than the closed-form methods.

6.6.1. Programs

Two software programs were used in this research: the commercially-available ABAQUS and GAMNAS (Geometric And Material Nonlinear Aalysis for Structures), developed at NASA-Langley.^{73,111} ABAQUS, which was used for the majority of the finite element studies performed for this thesis, is a versatile commercial code with extensive analytical capabilities including thermal residual stress calculations. GAMNAS, developed specifically for bonded joints, is incapable of incorporating thermal residual stresses in its present form. However, it was used to verify ABAQUS analyses of specimens with identical adherends which did not contain thermal residual stresses. Both programs are capable of incorporating material and geometric nonlinearity in their analyses, but only geometric nonlinearities were accounted for in this research.

6.6.2. Assumptions and Model Details

Both finite element programs used for this research required the tensile properties of the adherend and adhesive materials. In addition, both programs could account for non-linear material behavior. Tensile data is readily available for the adherend materials used for the bonded joint specimens that were examined. Shear data is also available for the adhesives. However, the tensile properties for the adhesive materials are not as common. (In fact, the tensile and fracture toughness tests of adhesive specimens conducted for this

research were intended to provide some of this information for future finite element model development.) In addition, the temperature-dependent behavior of the adhesives and the tensile properties of these adhesives following environmental exposure have not been extensively investigated. Therefore, materials were assumed to be linearly elastic having constant, room temperature, as-received properties. The main implication of these assumptions is that the finite element models would most likely predict a greater specimen stiffness, and greater toughness, for all tests conducted at room temperature or above. For tests conducted at lower than ambient temperatures, it is unknown exactly how these assumptions will affect the models. However, as will be explained in Section 6.6.4, good agreement was obtained between experimental and calculated load vs. displacement data, suggesting that these assumptions are not unreasonable.

Because the specimen width was much greater than the bond line thickness, plane-strain was also assumed.

Models were developed for each specimen geometry. These models were two dimensional and could be used by both the ABAQUS and GAMNAS programs. Four-noded quadrilaterals were employed as elements. To enhance the performance of these elements under bending conditions, a reduced integration technique was used. Typically, the adhesive layer was modeled using four rows of elements and the adherends were modeled with ten rows for monolithic metal adherends or with one row per ply in the case of composite adherends.

6.6.3. Determination of Strain Energy Release Rate

Strain energy release rates were calculated using a modified crack closure technique.⁷⁴ This technique is incorporated directly in GAMNAS but, when using ABAQUS, it must be performed manually using the nodal forces and displacements computed by the ABAQUS program. Figure 32, shows the modified crack closure technique schematically. The crack tip within a component subject to an opening force, P , is identified by two nodes, A and B. These nodes originally share the same location before crack propagation (Fig. 32b). Upon crack extension under Mode I, these two nodes are released and separate by a distance δ_y . (Fig. 32a) The crack closure technique computes this separation distance and the nodal force, p_n , required to return nodes A and B to their original position. A very stiff spring element located between nodes C and D is used to calculate this force, p_n . The nodal force multiplied by the nodal displacement is the work or energy required to close the crack tip. This quantity is equivalent to the strain energy "released" as the crack tip propagates from nodes AB to nodes CD. The strain energy, $\delta_y p_n$, divided by the amount of new crack area which is formed as the crack propagates, $2\Delta a$, is the Mode I strain energy release rate or G_I . A similar set of arguments for separation of nodes A and B in the x-direction applies to Mode II and the determination of G_{II} . Due to bond line rotation, forces and displacements are transformed to a coordinate system with axes that are parallel and perpendicular to the crack.

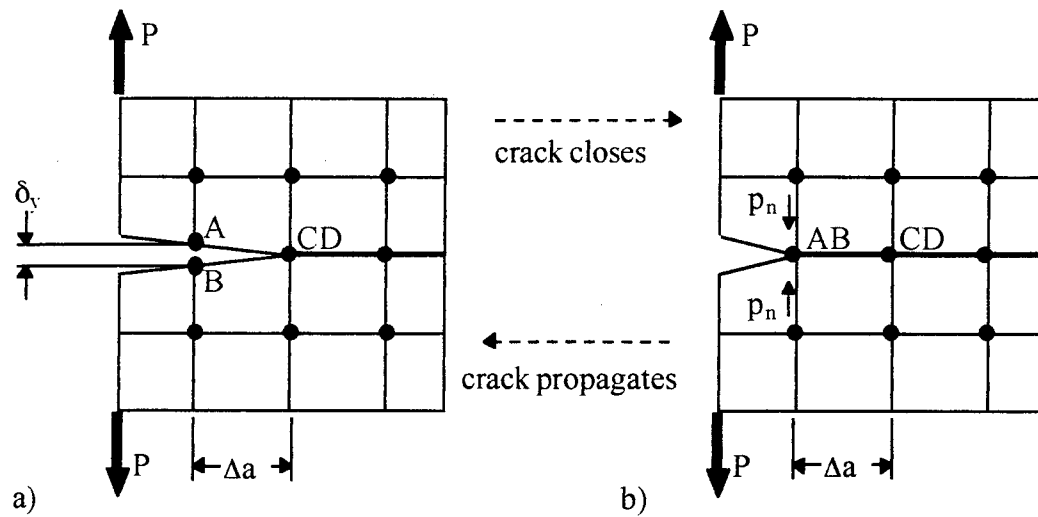


Figure 32. The modified crack closure technique (model is of unit width)

Critical strain energy release rate values were obtained by applying the experimentally-observed critical load at the onset of crack growth to the finite element model

6.6.4. Verification of Analysis

Prior to using the finite element method to analyze the curved Al/FM[®]73M/B-Ep specimens, a verification of the results was sought using analyses performed on Al/FM[®]73M/Al and Ti/FM[®]x5/Ti DCB specimens. These systems were fabricated using a single material for both adherends and, therefore, provided a means to compare the results of the ABAQUS and GAMNAS programs with those obtained from the closed-form solution.

Verification of the analysis was successful. Agreement was obtained between the ABAQUS and GAMNAS programs. In addition, G_{IC} values generated by the finite element analyses were a maximum of 10% lower than those calculated by using a closed-form solution. This small discrepancy may be attributed to scatter in the observed load and displacement data, use of linearly elastic adhesive properties, and the general trend for finite element models to be less compliant (predicting less displacement for a given load) than the component which is being modeled. To illustrate the close agreement between the finite element analysis and test data, Figure 33 shows a comparison between ABAQUS results and experimental load vs. displacement runs from a Ti/FM[®]x5/Ti specimen.

6.6.5. Analysis of the Curved Al/FM[®]73M/B-Ep Specimens

The ABAQUS software was used exclusively for the analysis of the Al/FM[®]73M/B-Ep specimens, in which thermal residual stresses were introduced during the curing process. Initially, the adherends were modeled as straight adherends rather than curved (i.e. in their pre-cured state). Following construction of the finite element mesh, a decrease in temperature of approximately 53°C (95°F) was introduced. This model temperature drop forced the mesh to conform to the curvature observed in the specimens but was less than that experienced by the specimens during cooldown (95°C

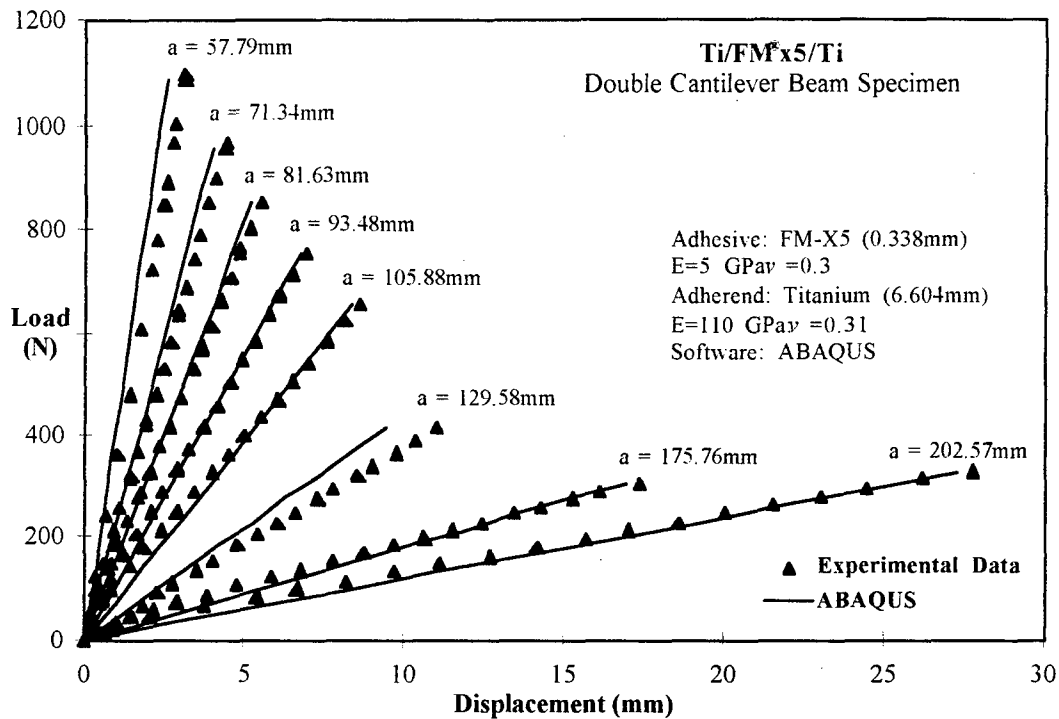


Figure 33. A comparison of load vs. displacement data obtained experimentally and computed using the ABAQUS finite element program

[170°F]). Reasons for this discrepancy include the use of invariant room temperature properties for the laminate and adhesive and the possibility that these published values differ from those displayed by the materials tested. Thus, it is recognized that modeling the adhesive with temperature invariant properties is an undesired, though presently unavoidable, simplification.

To further ensure that the finite element model represented the behavior of actual test specimens, the crack was modeled at the interface between the adhesive and the boron-epoxy adherend.

Mode I, Mode II, and total strain energy release rates were computed using ABAQUS for 5-10 loads for the DCB, CLS, and ENF specimens and also for 5 crack lengths for the DCB specimens. Figure 34 shows a typical G vs. applied load curve for one crack length of a double cantilever beam specimen. A series of these curves were used to determine G_I and G_{II} for the tests of the Al/FM[®]73M/B-Ep DCB specimens.

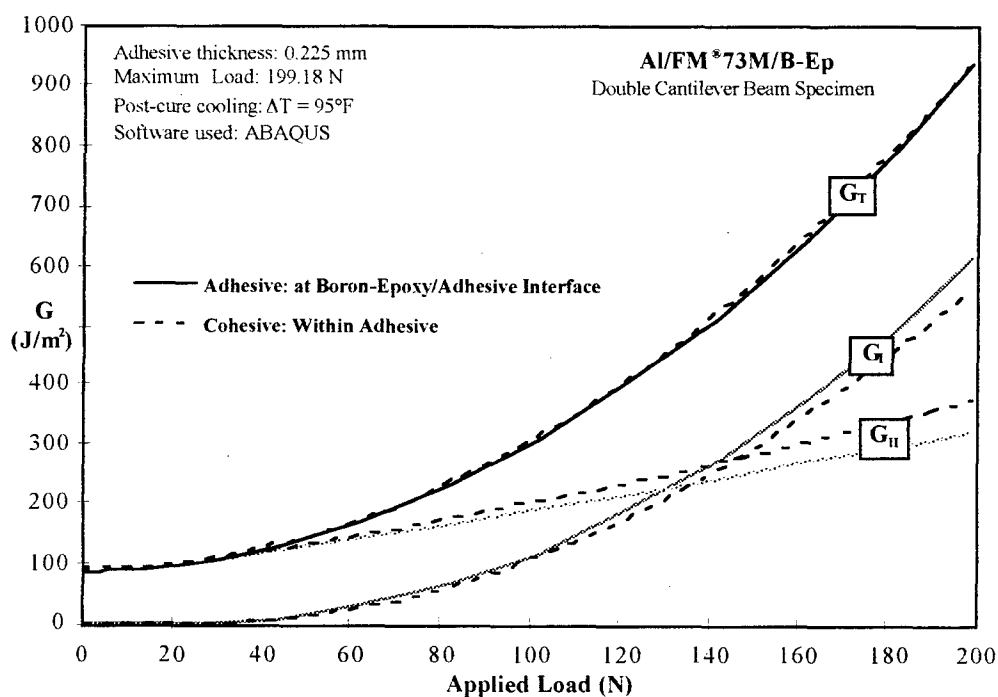


Figure 34. Computed Mode I, Mode II and total applied strain energy release rates for an Al/FM[®]73M/B-Ep DCB specimen as a function of load for a single crack length

Note that Figure 34 also shows the presence of G_{II} even at no applied load. This residual strain energy release rate is directly linked to the residual thermal stresses present in the

bond line due to the difference in the coefficients of thermal expansion between the aluminum and boron-epoxy adherends.

It was found that G vs. applied load data could be fit with a quadratic (parabolic) trendline with R^2 values of 0.99 or greater. This assisted in interpolation of G values for loads not run on ABAQUS. Strain energy release rate values for crack lengths not included in the ABAQUS models of the DCB specimens were determined via linear interpolation between the results for known crack lengths.

6.7. Statistical Analysis of Multiple Data Points

This research program generated a great amount of data. Multiple adhesive film specimens of the same geometry, material, and exposure condition were tested for tensile and fracture toughness data to obtain a better estimate of specific properties. Repeated tests were not normally performed on bonded joint specimens because of their limited supply. However, when possible, several crack growth runs were performed on a single specimen to provide multiple values for a given property.

To best express the implications of having multiple values, the averages, standard deviations, and 95% confidence intervals of data sets having multiple values were computed. Results presented in the following sections will refer to the average and confidence interval if more than one value was obtained for a property from a particular material/exposure/specimen combination.

Based upon the Student t-distribution, the confidence interval is a useful way to compare average values.^{113,114} Given an average value, \bar{x} , a sample size, n , with a standard deviation, s , the confidence interval around the *true* mean of a property, μ , can be estimated with a degree of certainty $(1-\alpha)$ using the following relationship:

$$\bar{x} - t_{\alpha/2} \frac{s}{\sqrt{n}} < \mu < \bar{x} + t_{\alpha/2} \frac{s}{\sqrt{n}} \quad (11)$$

Here, $t_{\alpha/2}$ is obtained from Student t-distribution charts.

For the current project, 95% confidence intervals ($\alpha = 0.05$) were computed and used to compare data. In general, small sample populations (i.e. small numbers of values with which to compute an average) result in large confidence intervals and, therefore, more uncertainty about the true value for a given property.

The significance of the confidence interval may be understood by way of a simple example. Assume that the average Mode I toughness of a particular adhesive in the as-received condition was computed as 1000 J/m² and that the 95% confidence interval was determined to be 200 J/m². According to the experiments, one would expect additional toughness values from adhesive in the same condition to fall between 800 and 1200 J/m²

95% of the time. One could also believe with 95% certainty that the *true* adhesive toughness would fall between 800 and 1200 J/m².

When using confidence intervals for comparisons, a simple rule to follow is that overlapping intervals signal that there is no significant difference between the two average values being compared. Conversely, non-overlapping 95% confidence intervals identify, with 95% certainty, that there is a significant difference between the two properties being compared.

In this thesis, confidence intervals will be shown numerically in tables for the testing conducted on the adhesive film specimens. Appendix B contains a collection of charts which include confidence intervals for the bonded joint specimen data.

The use of the confidence interval concept is intended to be for qualitative purposes only and to provide the reader with a possible method for comparing the average values of properties obtained from a number of similar tests. In some cases the small number of tests conducted have resulted in confidence intervals which are quite large and, for all intents and purposes, of limited value. Therefore, comparisons of average values using confidence intervals should be carried out prudently. It should also be recognized that additional tests would likely reduce the size of the confidence intervals presented in this thesis. This would result in an increase in the number of significant differences observed in the data as sizes of confidence intervals and the probability of interval overlaps decreased.

CHAPTER VII

CHEMICAL AND PHYSICAL TESTING PROCEDURES

Three analytical techniques were used to identify changes in the chemical structure and physical behavior of the adhesives being investigated. These techniques included Fourier transform infrared (FTIR) spectroscopy, differential scanning calorimetry (DSC), and thermogravimetric analysis (TGA). These techniques were performed on adhesive samples in the as-received state and following periods of environmental exposure. The analyses were intended to explore any links which might exist between changes in the mechanical properties of these adhesives due to environmental exposure and changes in their chemical structure and/or physical properties.

7.1. Fourier Transform Infrared Spectroscopy (FTIR)

Fourier transform infrared (FTIR) spectroscopy was conducted to provide information on any changes to the structure of the adhesive polymers which might have been caused by environmental exposure. Changes in the spectrographic signatures of adhesives exposed to various environmental can indicate, in a qualitative way, formation or destruction of specific functional groups within the polymer chains.

The principle of infrared spectroscopy is based upon the ability of individual functional groups (i.e. aromatic rings, hydroxyl groups, nitrile groups, etc.) within a polymer chain to absorb characteristic levels of infrared energy (wavelengths in the 1-50 μm range.¹¹⁵) If incident radiation contains wavelengths (or frequencies) that match the natural rotational/vibrational energy of these functional groups, it is absorbed.^{116,117} Other wavelengths are transmitted (in the case of thin films or suspensions) or reflected (in the case of surfaces).

Since chemical functional groups absorb only specific frequencies of infrared radiation, monitoring the incident spectrum and comparing it with the transmitted or reflected spectrum permits the polymer makeup to be qualitatively analyzed. That is, the presence or absence of certain types of bonding arrangements and substructures may be inferred. Furthermore, the intensity of absorption bands in the transmitted or reflected spectra is proportional to the concentration of particular functional groups within the polymer sample.¹¹⁸

Spectrometers measure the interaction of infrared radiation with experimental samples and record the frequencies which are absorbed. The Fourier transform capability of the spectrometers used for this research allowed all frequencies to be measured simultaneously, resulting in fairly short scan times (several minutes per scan).

The output from these instruments is commonly presented in plots showing the percentage of radiation transmitted or absorbed vs. wavelength expressed in

wavenumbers. (Fig. 35) Wavenumbers have units of reciprocal centimeters. Spectra used for infrared analyses typically have wavenumbers of 4000 to 4000 cm^{-1} or wavelengths between 2 and 16 μm .

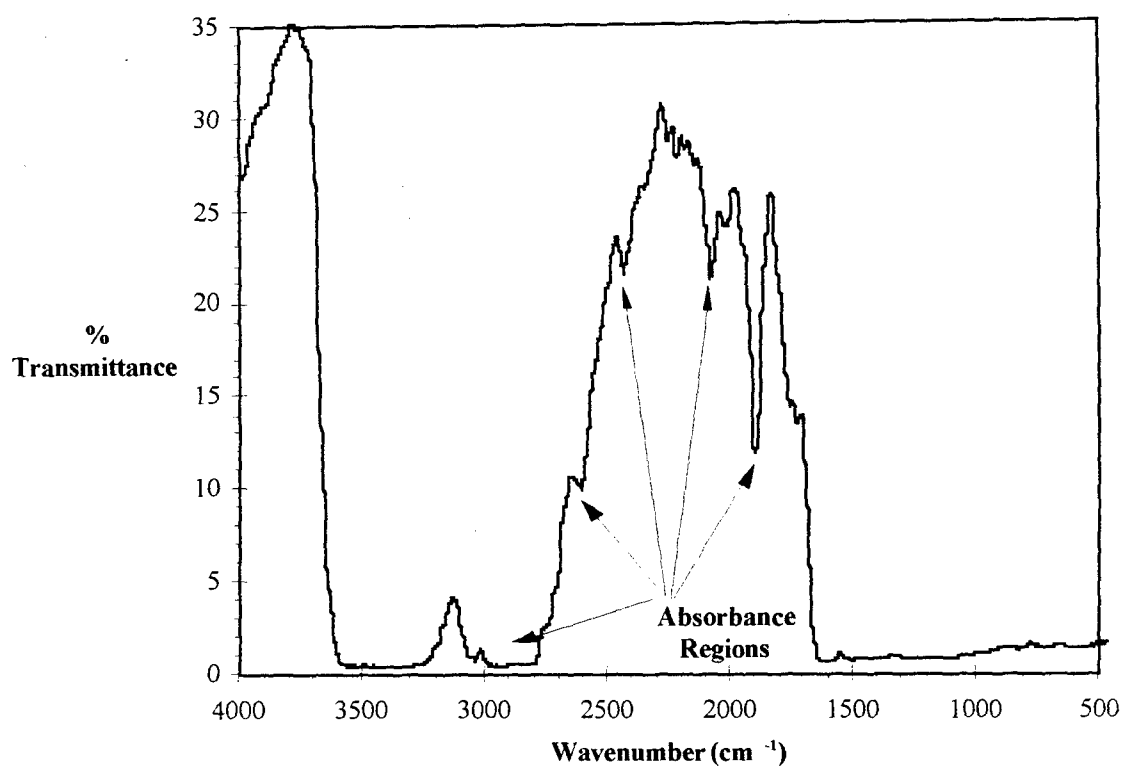


Figure 35. Typical FTIR spectroscopy results

Additional information on the fundamentals and use of infrared spectroscopy may be found in works by Silverstein¹¹⁹ and Brown, *et al.*¹²⁰

FTIR spectroscopy was carried out in two formats, transmittance and reflectance. Transmittance FTIR spectroscopy was performed using a Nicolet Instrument Co. (Madison, WI) model 520 FTIR spectrometer provided by Georgia Tech's School of Chemistry. Transmittance spectra were obtained for the thin adhesive specimens. Attempts were made to use reflectance FTIR spectroscopy to examine the fracture surfaces of bonded joint specimens. This process used a Nicolet Nic-Plan microscope fitted with the spectrometer optics and made available by the Chemistry Department at Clark Atlanta University. Both transmittance and reflectance spectroscopy was performed using Nicolet's OMNIC software for the set-up, control, and analysis of spectroscopic scans.

7.2. Differential Scanning Calorimetry (DSC)

Differential scanning calorimetry (DSC) was used to identify possible changes in the glass transition temperature (T_g) of adhesive specimens exposed to various environments.

Differential scanning calorimetry was performed using a Perkin-Elmer (Norwalk, CT) DSC 7 device provided by Georgia Tech's School of Chemistry. This particular instrument operates using a power compensation technique based upon a "null-balance" principle.^{121,122} This operating principle of the Perkin-Elmer DSC is based on the device's ability to determine the difference in power supplied to two sample holders while raising them to the same temperature at the same rate.

Using dual sample holders, the DSC 7 was programmed to scan a temperature range while monitoring the power necessary to maintain the sample holders at the same desired temperature. One sample holder contained the material of interest, a fully cured sample of adhesive with a weight of approximately 20-25 mg, encased in an aluminum pan. The other sample holder contained an empty aluminum pan serving as a reference. Platinum heaters and thermometers were used in the DSC 7 to provide heat and monitor temperature.

Scans were performed at a linear heating rate of 10°C (18°F) per minute. The range of each temperature scan depended upon the type of adhesive being investigated and previously published T_g values (if available). FM[®]73 samples, with an estimated T_g of 100°C (212°F), were scanned between 50°C (122°F) and 150°C (302°F). AF-191 samples, with an expected T_g of 230°C (446°F), were scanned between 150°C (302°F) and 250°C (482°F). FM[®]x5 samples, with an expected T_g of 250°C (482°F), were scanned between 200°C (392°F) and 300°C (572°F). Three scans were performed for each adhesive following each type of environmental exposure. The last two scans from each group of three were used to calculate the glass transition temperature. Transient effects present during the first scan precluded it from being used for calculations..

During each scan, heater power was automatically adjusted to maintain the adhesive and reference sample holders at the identical temperature. The difference between the power required by the adhesive and that required by the reference was

measured in terms of milliwatts and normalized by the adhesive sample weight. Data was then plotted in terms of watts per gram (W/g) vs. temperature.

When raising the temperature of a polymer through its glass transition temperature region, the free volume of the material increases.¹¹⁵ This change occurs gradually over a range of temperatures¹²³ although only a single temperature is typically identified as “the” glass transition temperature. The increase in free volume is accompanied by physical changes in the structure of the polymer which, in turn, result in changes in properties such as heat capacity.

The DSC technique essentially measures this change in heat capacity while raising the temperature of the polymer (adhesive) sample. To maintain the same temperature ramp rate in a polymer sample as in a reference sample, additional power must be added during its passage through the glass transition region. This additional power requirement was revealed on the DSC plots as a region of inflection. The DSC's computer software analyzed this inflection region to identify a particular point which was labeled as the glass transition temperature (T_g). (Fig. 36) Further information on the fundamentals and use of differential scanning calorimetry may be found in works by Turi¹²⁴ and Wunderlich.¹²⁵

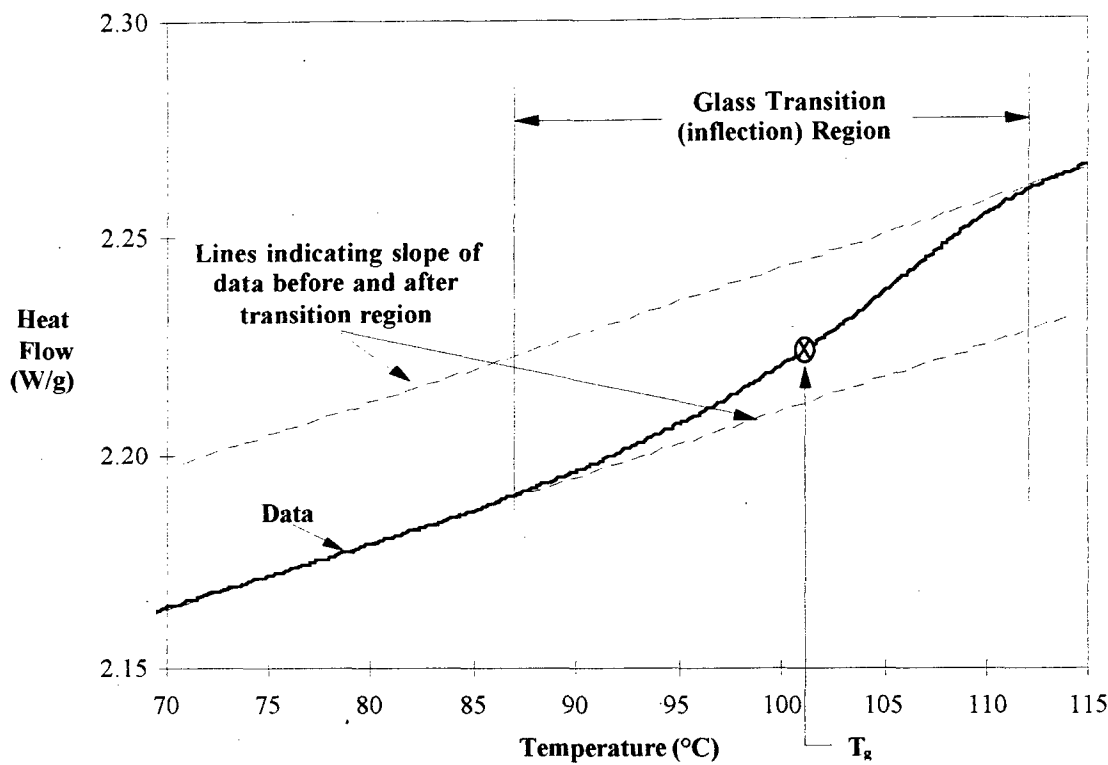


Figure 36. Typical Differential Scanning Calorimetry results

7.3. Thermogravimetric Analysis (TGA)

Thermogravimetric analysis (TGA) was performed to determine whether the various environmental exposure conditions used in this project affected the degradation temperature of the adhesive materials. Originally it was believed that changes in the degradation temperature would identify changes in the degree of crosslinking of the adhesive polymers. However, upon further investigation, this proved not to be the case.

Nevertheless, the TGA process was performed, and the results are presented as another piece of information regarding the adhesives investigated for this research.

Thermogravimetric analysis was performed using a Perkin-Elmer (Norwalk, CT) TGA 7 Thermogravimetric Analyzer provided by Georgia Tech's School of Chemistry. (Fig. 35) This device consists of a vertical tube furnace capable of achieving temperatures of 1000°C (1832°F) and a microbalance capable of detecting changes as small as 0.1 μg .¹²⁶

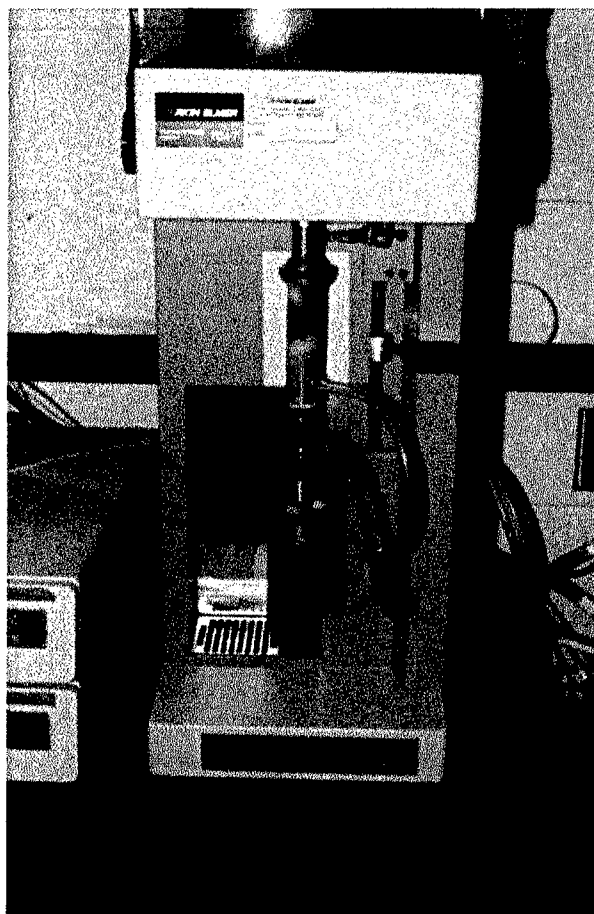


Figure 37. The Perkin Elmer TGA 7 Thermogravimetric Analyzer

The TGA 7 was programmed to follow a linear temperature ramp rate of 20°C/min. (36°F/min.) between 50°C (122°F) and 900°C (1652°F), a temperature sufficient to cause degradation in all adhesives investigated. A fully cured sample of each adhesive weighing approximately 10 mg was placed on a platinum pan connected to the device's microbalance. The sample and pan were then sealed within the TGA 7 furnace while the temperature was increased. During heating, the weight of the sample was continuously monitored.

The microbalance operated on a "null balance" principle in which an servo-motor compensated for weight changes in the sample material and supplied a torque to maintain a constant position of the sample holder during a TGA run. The torque required was directly proportional to the electrical current. The current was monitored to reveal changes in the weight of the sample material.

By accurately weighing a small sample of adhesive while it was slowly heated, the temperature at which it began to oxidize or otherwise degrade was determined. This degradation was depicted graphically by plotting the percentage of the original weight of the sample vs. temperature. (Fig. 36) Computer software associated with the TGA 7 device determined the onset of the major weight loss which accompanied degradation, and also calculated the midpoint temperature of the degradation process.

Further information on the fundamentals and use of thermogravimetric analysis may be found in works by Turi¹²⁴ and Wunderlich.¹²⁵

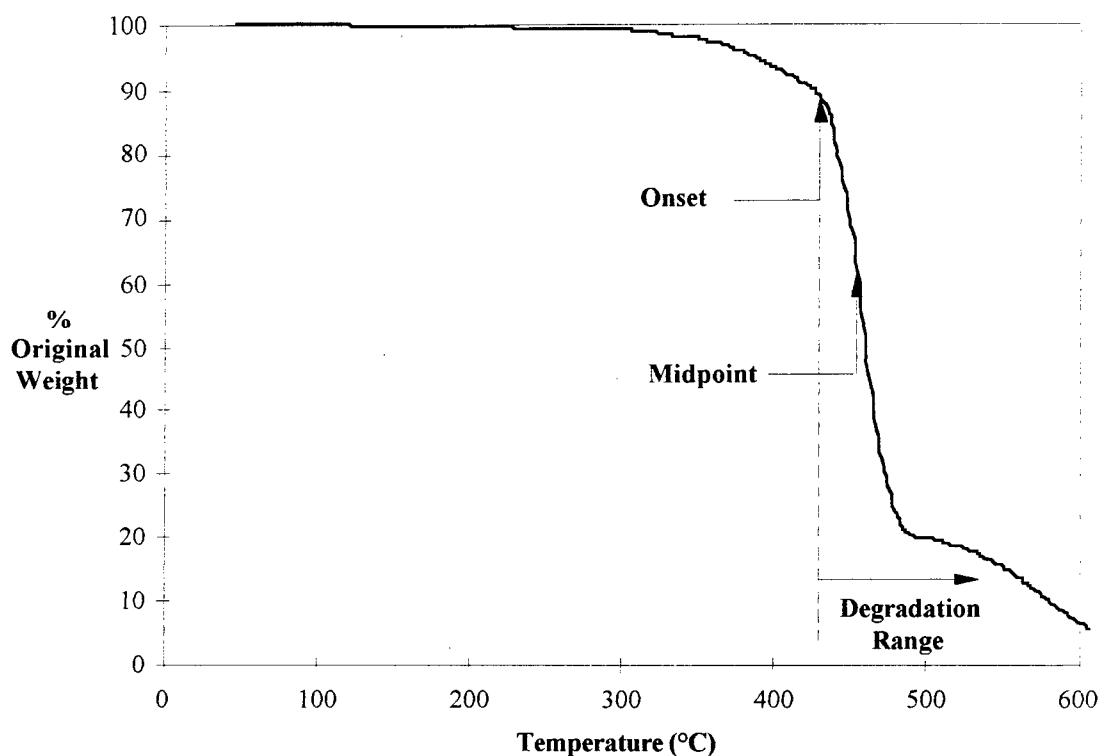


Figure 38. Typical Thermogravimetric Analysis results

For a polymer, an increase or decrease in the degradation temperature signals an increase or decrease in the thermal stability of the polymer structure. Although the temperature at which degradation occurs is important, equally informative is the difference between the onset and midpoint temperatures. A large difference between these two quantities reveals non-uniformity in the structure (molecular weight, degree of polymerization, etc.) of the adhesive or polymer being examined, while a smaller difference indicates that the structure of the polymer or adhesive is more homogeneous.

CHAPTER VIII

RESULTS AND DISCUSSION

Prior to reviewing and discussing test results, summary tables are presented at the beginning of each of the following sections covering the test results for the adhesive specimens and for the bonded joint specimens. These tables are intended to recap the various combinations of materials, pre-test exposure environments, specimen geometries, testing environments, and types of tests which were used in this research program. Due to the great number of possible combinations of these parameters, every possible combination was not examined. However, an effort was made to perform experiments on a wide range of materials and environmental conditions to identify general trends and areas for further research.

8.1. Adhesives

This section presents the results from several tests conducted on the adhesive specimens. These tests include FTIR spectroscopy, differential scanning calorimetry, thermogravimetric analysis, and tensile and fracture toughness tests.

Tensile and fracture toughness tests were performed primarily to examine the effect of the various environmental exposures on the mechanical properties of the

adhesives. In addition, the two epoxy adhesives, FM[®]73 and AF-191, were tested with and without a non-woven scrim cloth to determine the effect of that support material. For the specimens tested that contained a scrim cloth, the effect of the orientation of the cloth was also examined.

Stress-strain curves shown for the adhesive specimens are from individual specimens but are typical of the behavior exhibited by all of the specimens tested in the same condition. Multiple tests permitted results to be statistically analyzed. Significant differences between values of the unsupported and supported epoxies occurred when the mean values differed and when there was no overlap of the confidence intervals. Such significant differences are indicated by highlighted portions of the various tables which summarize tensile and fracture toughness properties.

Table 3. Summary Table for Tests and Analyses of Adhesive Specimens

<i>Test or Analysis¹</i>						
ADHESIVE	EXPOSURE ²	FTIR	DSC	TGA	TENSILE	FRACTURE
FM [®] 73U	As-Received	1	1	1	6	6
	Thermally Cycled ³	1	1	1	4	4
	Hot/Dry ⁴	1	1	1	3	3
	RT/Wet ⁵	1	1	1	3	3
	Hot/Wet ⁶	1	1	1	3	3
FM [®] 73M	As-Received				9	9
AF-191U	As-Received	1	1	1	6	6
	Thermally Cycled ⁷	1	1	1	4	4
	Hot/Dry ⁸	1	1	1	3	3
	Hot/Wet ⁶	1	1	1	3	3
AF-191M	As-Received				11	11
FM [®] x5	As-Received	1	1	1	4	4
	Thermally Cycled ⁹	1	1	1	3	3
	Hot/Dry ¹⁰	1	1	1	2	2
	Hot/Wet ³	1	1	1	3	3

Notes:¹ Table entries indicate number of specimens tested² Isothermal exposure = 5,000 hours³ -54°C (-65°F) to 71°C (160°F), 100 cycles⁴ 71°C (160°F), 0% rh⁵ 22°C (72°F), >90% rh⁶ 71°C (160°F), >90% rh⁷ -54°C (-65°F) to 104°C (220°F), 100 cycles⁸ 104°C (220°F), 0% rh⁹ -54°C (-65°F) to 163°C (325°F), 500 cycles¹⁰ 177°C (350°F), 0% rh**8.1.1. FM[®]73**

Chemical and physical analyses were performed on the unsupported version of the FM[®]73 adhesive (FM[®]73U). Tensile and fracture toughness tests were performed on unsupported and supported (FM[®]73M) versions of the adhesive which contained a scrim cloth.

FM[®]73U specimens subjected to long-term exposure were periodically weighed and observed. Figure 39 shows the weight changes resulting from exposure. As expected, the specimens exposed to a high humidity environment gained weight due to

moisturization while those exposed to a hot/dry environment lost weight due to moisture loss. A higher exposure temperature fostered moisture absorption. No other gross changes (warping, color change, etc.) were observed in the exposed FM[®]73U specimens.

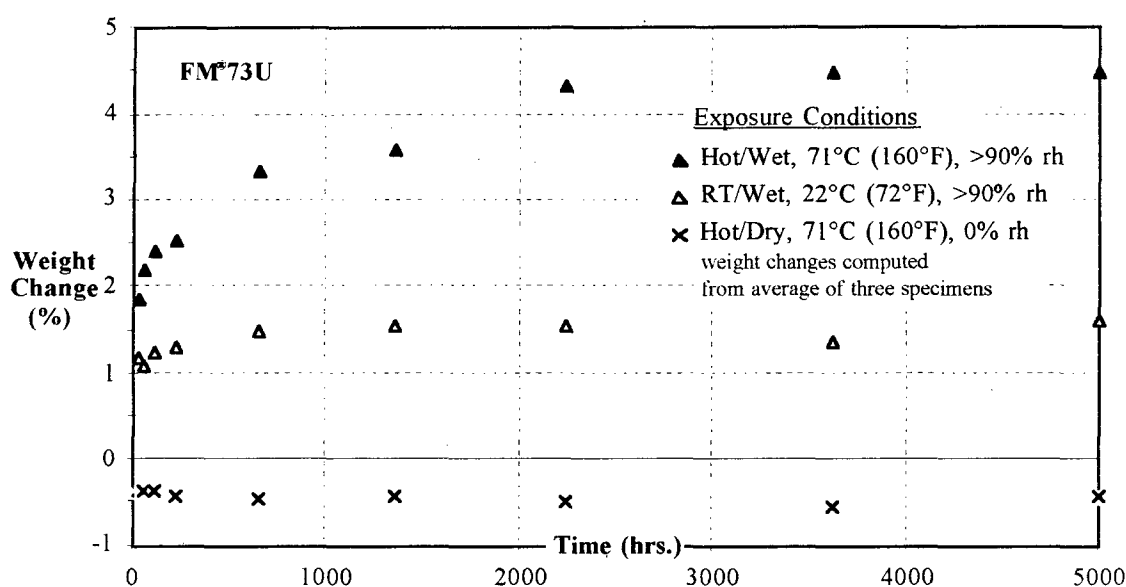


Figure 39. Weight changes in FM[®]73U adhesive due to long-term exposure

8.1.1.1. FTIR Spectroscopy

Transmittance FTIR spectroscopy performed on thin, cured FM[®]73U specimens revealed subtle changes in the spectra among the five environmental conditions to which the specimens were subjected. Figure 40 shows the full range (400-4000 cm⁻¹) of all spectra obtained. Because the transmittance levels of the spectra are very similar, they

have been vertically separated in Figure 41 by adding a fixed percentage of transmittance to each one as indicated. In this manner, important changes in the shapes and relative sizes of specific peaks are more easily seen.

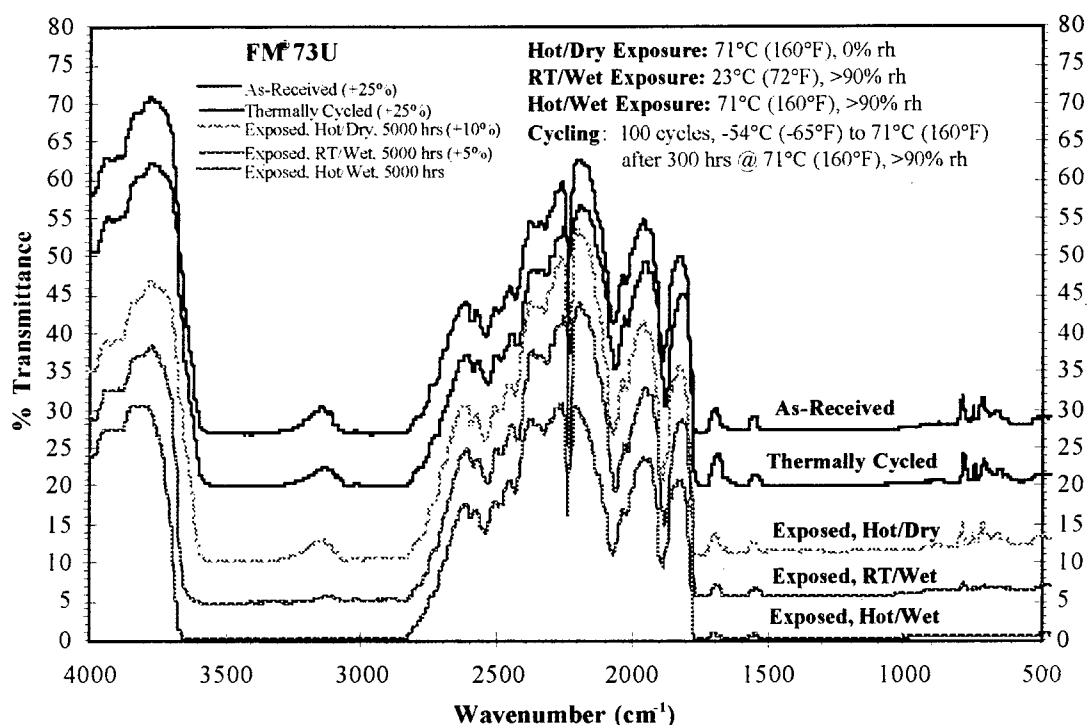


Figure 40. Full FTIR transmittance spectra for FM[®]73U adhesives (spectra shifted by amount indicated in parentheses to provide vertical separation)

Major changes in the FM[®]73U FTIR transmittance spectra occurred between wavenumbers 3200 and 600. This region is expanded in Figure 41, and three specific areas of interest are indicated. Because the exact structure of this epoxy and the

ingredients used to modify it are proprietary, the identification of the specific causes of the changes in these areas is strictly conjecture. However, some possibilities for the spectral changes are suggested in the following paragraphs. Unless otherwise noted, the suggested causes result from a comparison of the FM[®]73U spectra with standard correlation charts in the CRC Handbook of Chemistry and Physics.¹²⁷

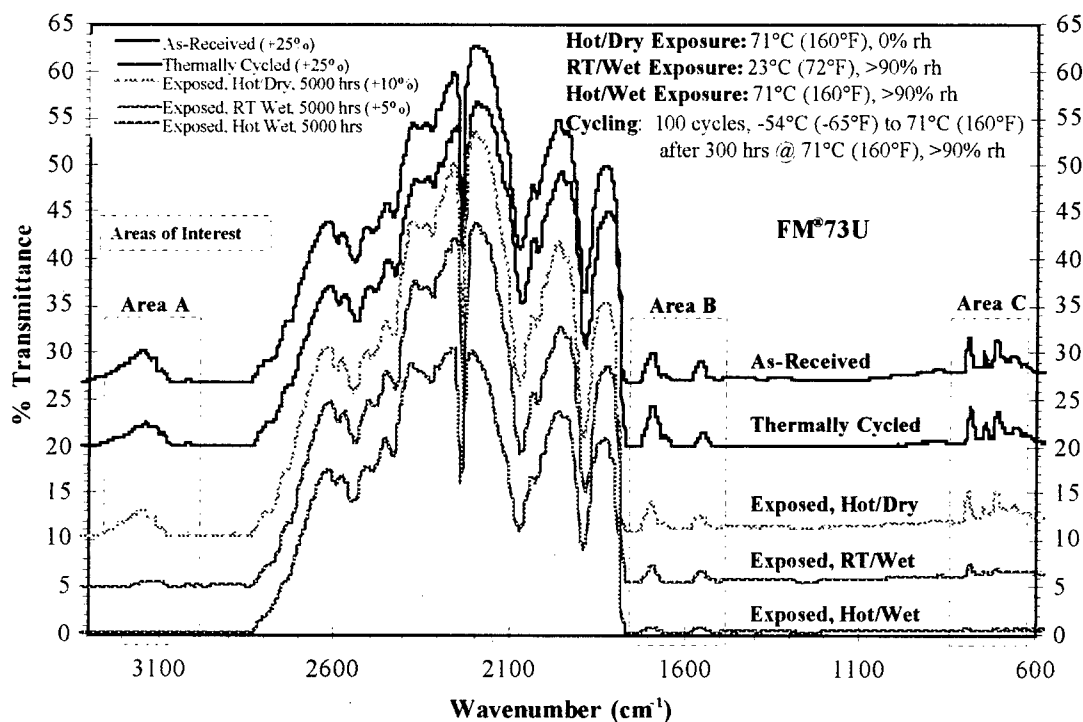


Figure 41. Expanded FTIR transmittance spectra for FM[®]73U adhesives (spectra shifted by amount indicated in parentheses to provide vertical separation)

At this point a brief review of the chemistry of a typical epoxy might be helpful. Figure 42 shows the typical creation of a generic epoxy during the various stages of curing.¹²⁸ The process begins with two compounds, epichlorohydrin and bisphenol A which combine to form diglycidyl ether of bisphenol A (DGEBA). The DGEBA, in turn, reacts with additional bisphenol A to form the epoxy, a compound similar to DGEBA except for the repeated structure in the middle of the polymer and the absence of an "open" epoxy group on one end. During curing, the epoxy chains also crosslink. Often this crosslinking is caused by the introduction of an amine ($R-NH_2$) group as shown.¹²³

Area A in Fig. 41 shows a decrease with exposure in the strength of a peak located near 3050 cm^{-1} . This could indicate that exposure causes an increase in the number of C-H bonds in the polymer structure. This increase may be indicative of continued curing and crosslinking of the adhesive during exposure. However, note that the peak at 3050 cm^{-1} completely disappears after 5,000 hours of exposure to hot/wet conditions. The absorption of water by the adhesive could cause a broad range of reduced transmittance around 3500 cm^{-1} due to an increase in the concentration of O-H bonds. This range of reduced transmittance could be strong enough to mask¹¹⁷ the peak at 3050 cm^{-1} , effectively causing it to "disappear" as the amount of moisture in the adhesive increases.

Area B shows a decrease in intensity of a double peak centered around 1600 cm^{-1} . This may be due to an increase in the amine ($R-NH_2$) concentration which would tend to reduce transmittance in the $1550\text{-}1700\text{ cm}^{-1}$ range. Since an amine is often used to

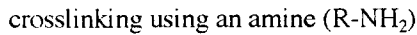


Figure 42. General epoxy curing and crosslinking process

crosslink epoxy chains, an increase in its concentration may imply that the exposure of the FM[®]73U specimens is destroying crosslinks. This might result in the creation of additional amine structures as the nitrogen atoms are lost from the linked epoxy chains. These additional amine groups would, in turn, absorb additional infrared radiation in this range and reduce the observed peaks.

Area C shows a decrease in intensity of several peaks in the 700-800 cm^{-1} range. This range is indicative of substitutions made to aromatic rings. This reduction in transmittance may suggest that additions are being made to the aromatic rings in the epoxy structure.

The general trend in these spectra is the disappearance of transmittance peaks which suggests increased absorption caused by an increase in the concentration of certain bonding arrangements. Further curing of the adhesive during exposure to elevated temperatures could cause such structural changes. However, Haslam & Willis have stated that curing in most epoxies is characterized only by the disappearance of a peak at 917 cm^{-1} associated with the loss of a terminal epoxy group.¹²⁹ This difference was not seen in the spectroscopic analysis of the FM[®]73U. Therefore, it appears unlikely that the observed changes in the spectra are the result of continued curing of the FM[®]73U during exposure. Additional mechanisms which are not fully identified by this spectroscopy are, most probably, the cause of the changes in the FM[®]73U spectra.

8.1.1.2. *Differential Scanning Calorimetry (DSC)*

Results from the DSC analysis of the FM[®]73U adhesive are shown in Figure 43. The heat flow axis was normalized by dividing by the heat flow required to attain the maximum temperature during the DSC runs (115°C [239°F]). This allowed the curves to be more easily compared.

Since differences in T_g values of 5°C or less are not usually considered significant,¹³⁰ only the low T_g value of the specimen exposed to 5,000 hours of isothermal exposure to a hot/wet environment is of interest.

The decrease in T_g from the as-received level signifies an increase in the mobility of the epoxy polymer structure.¹¹⁵ This may be due to a decrease in the number of crosslinks caused by plasticization resulting from the absorption of water during exposure.

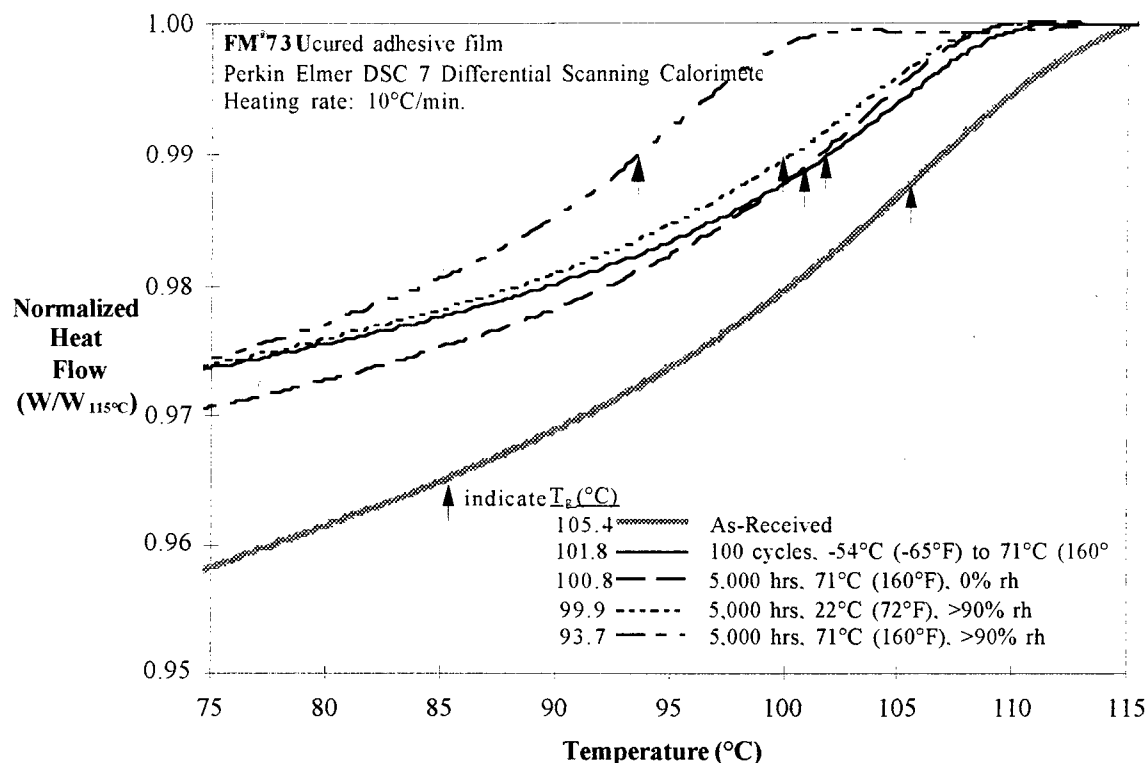


Figure 43. Results from the DSC analysis of the FM[®]73U adhesive

8.1.1.3. Thermogravimetric Analysis (TGA)

Figure 44 shows the results from the thermogravimetric analysis of the FM[®]73U adhesive. The degradation temperature was unaffected by the exposure environment. Furthermore, the onset of degradation occurred in a temperature range far above the maximum recommended use temperature FM[®]73. Therefore, no changes in the mechanical behavior of the adhesive or of bonded joints fabricated with this adhesive should be attributed to large scale degradation of the FM[®]73 polymer. In addition, the

steepness of the transient region indicates that the FM[®]73 polymer structure appears quite uniform since degradation occurs over a relatively small range of temperatures

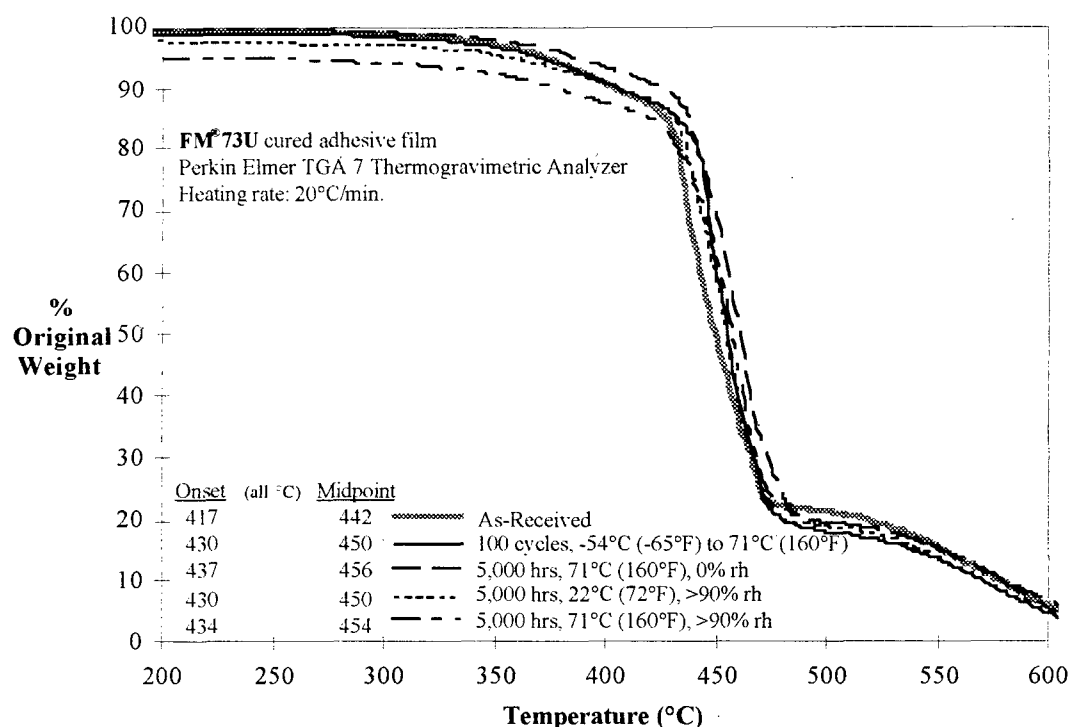


Figure 44. Results from the thermogravimetric analysis of the FM[®]73U adhesive

8.1.1.4 Mechanical Test Results

Figure 45 shows tensile curves for the unsupported and supported (scrim-containing) versions of the FM[®]73 epoxy adhesive. These stress-strain curves are for individual specimens but are typical of the behavior exhibited by the multiple specimens tested. Although the non-woven scrim cloth in this adhesive is described as a “random

mat,” specimens containing the scrim cloth (FM[®]73M) were tested in two orientations based upon the direction in which the uncured adhesive film was rolled upon delivery: longitudinal (with the loading axis parallel to the rolled direction of the uncured film) and transverse (with the loading axis perpendicular to the rolled direction of the uncured film).

Table 4 contains the mean values for the key tensile and fracture properties examined during testing of the supported and unsupported FM[®]73. In general, the presence of the scrim cloth reduced the failure strain, strength, and fracture toughness of the FM[®]73M adhesive with respect to those of its unsupported version (FM[®]73U). No significant differences were noted between the longitudinal and transverse specimen orientations. Thus, the non-woven scrim cloth did not impart in-plane reinforcement and may serve only to improve “handle-ability” and control the bond line thickness when this epoxy adhesive film is used to manufacture bonded components. However, the effect of the scrim cloth on out-of-plane and shear properties of the FM[®]73M adhesive is unknown. Since these properties are important to the performance of bonded joints, this issue is a candidate for future research.

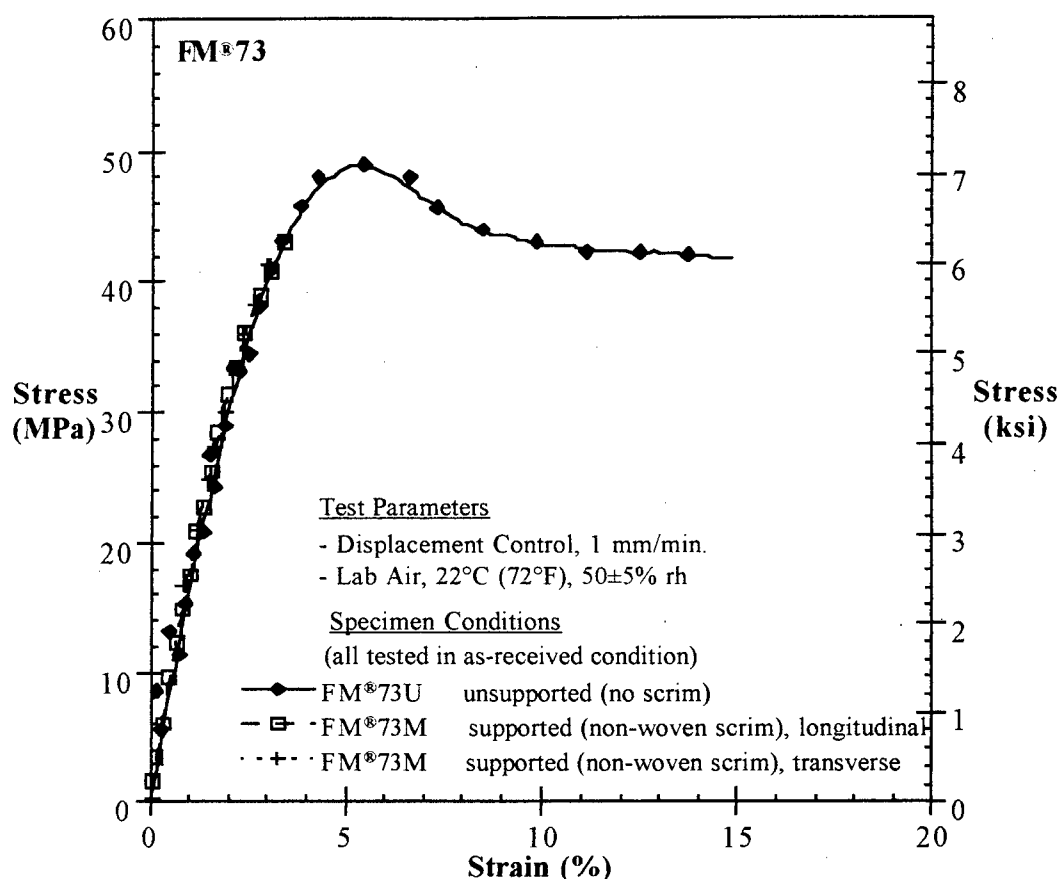


Figure 45. Tensile behavior of the FM®73U and FM®73M adhesives

Table 4. In-Plane Properties of FM®73U (unsupported) and FM®73M (supported)

ADHESIVE Scrim Direction [# tested] ¹	E (MPa)	ε_f (%)	σ_{uts} (MPa)	σ_{ys(0.2)} (MPa)	σ_{lys} (MPa)	G_I (J/m ²)
FM®73U no scrim [6]	1432 ±131	12.2 ±1.0	47 ±2	38 ±2	41 ±3	3168 ±208
FM®73M longitudinal [4]	1778 ±138	3.6 ±0.5 ⁶	44 ±1 ⁶	30 ±1	35 ±0	1134 ±120
FM®73M transverse [5]	1597 ±133	3.3 ±0.4	41 ±2	32 ±1	35 ±1	1485 ±164

Notes: • statistically significant differences from unsupported values are boldfaced
 • 95% confidence intervals shown following ± sign
¹ number of specimens tested in brackets [] unless note appears within table
⁶ 6 specimens tested instead of number listed in brackets []

Figure 46 shows tensile curves for FM[®]73U adhesive specimens subjected to various environmental conditions. These stress-strain curves are for individual specimens but are typical of the behavior exhibited by the multiple specimens tested.

Table 5 contains the mean values for the key tensile and fracture properties examined during testing of the FM[®]73U adhesive exposed to various environments.

In general, FM[®]73 exhibited tensile properties similar to those of AF-191, a fact not unexpected since these adhesives are both epoxies. The modulus (E), ultimate strength (σ_{uts}), and yield strengths ($\sigma_{ys(0.2)}$ and σ_{lys}), of the FM[®]73 were similar to those of the AF-191, but far below those of the FM[®]x5. The failure strain of the FM[®]73U was higher than that of the AF-191U and much higher than that of the FM[®]x5. This was manifested by necking in the gage section of the FM[®]73U. However, inclusion of a scrim cloth reduced the failure strain of the FM[®]73M to levels below that of the supported AF-191M and equal to that of the FM[®]x5.

Although the tensile properties of the two epoxies were quite similar, the fracture toughness of the FM[®]73U was nearly three times that of the AF-191U but closer to the toughness of the FM[®]x5. This was consistent with material behavior observed during preparation of the fracture toughness specimens. While creating a notch in the FM[®]73 was performed relatively easily, doing so for the AF-191 was difficult due to its more brittle behavior. Crack growth in the unsupported FM[®]73U was preceded by a slight

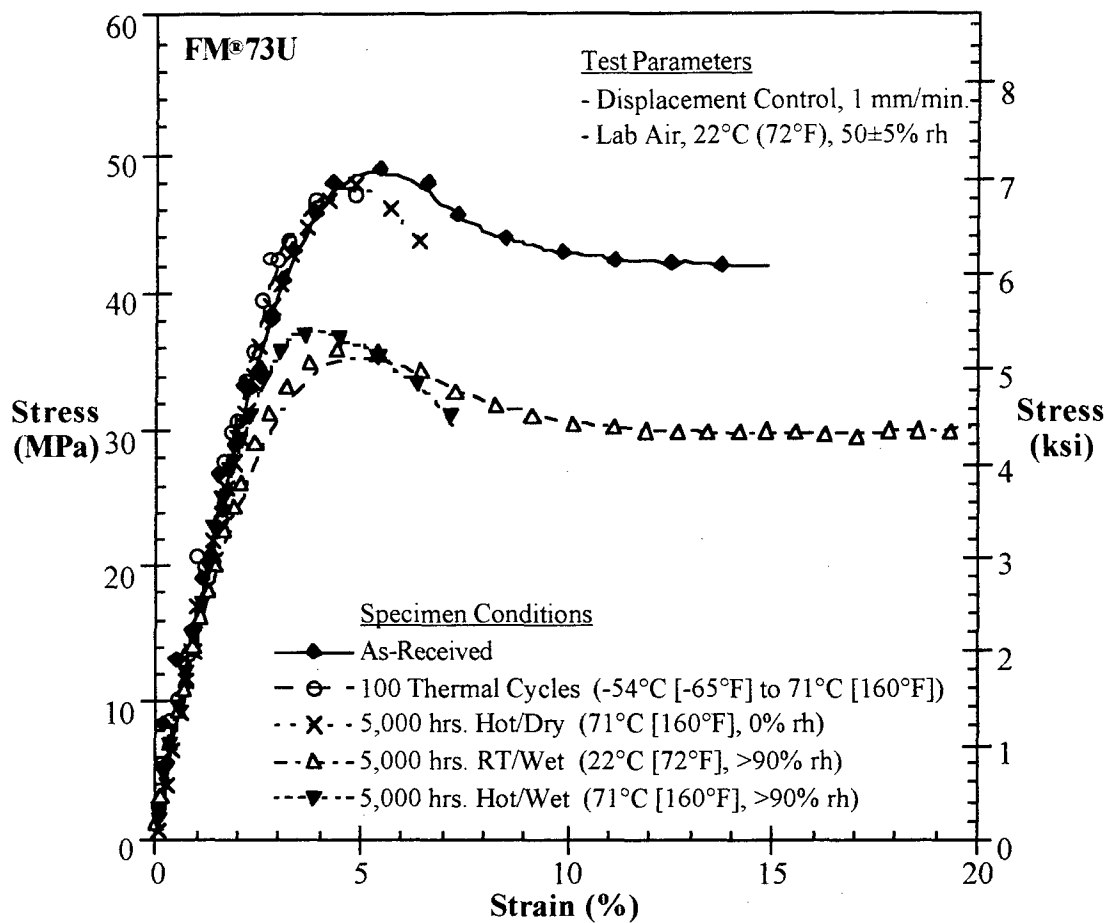


Figure 46. Tensile behavior of FM[®]73U adhesive exposed to various environments

Table 5. Properties of FM[®]73U Following Exposure to Various Environments

ADHESIVE Condition [# tested] ¹	E (MPa)	ϵ_f (%)	σ_{uts} (MPa)	$\sigma_{ys(0.2)}$ (MPa)	σ_{iys} (MPa)	G_I (J/m ²)
FM[®]73U						
As-Received [6]	1432 ±131	12.2 ±1.0	47 ±2	38 ±2	41 ±3	3168 ±208
Thermally Cycled [4]	1340 ±43	5.6 ±1.2	49 ±1	38 ±3	43 ±1	3106 ±152
Hot/Dry [3]	1565 ±78	5.9 ±1.7	46 ±3 ²	37 ±5 ²	40 ±4 ²	2283 ±133
RT/Wet [3]	1386 ±188	21.9 ±3.1	36 ±0	29 ±2	31 ±0	2085 ±98
Hot/Wet [3]	1543 ±217	9.6 ±3.9	37 ±2	28 ±1	31 ±1	2077 ±209

Notes: • statistically significant differences from as-received values are **boldfaced**

• 95% confidence intervals shown following ± sign

¹ number of specimens tested in brackets [] unless note appears within table

² 2 specimens tested instead of number listed in brackets []

blunting of the crack tip and the formation of a whitened, Dugdale-like process zone. (Fig.

47) The crack then propagated evenly for up to approximately 1 mm before growth became unstable. The extent of crack tip blunting and the size of the process were reduced in the scrim-containing FM[®]73M material.

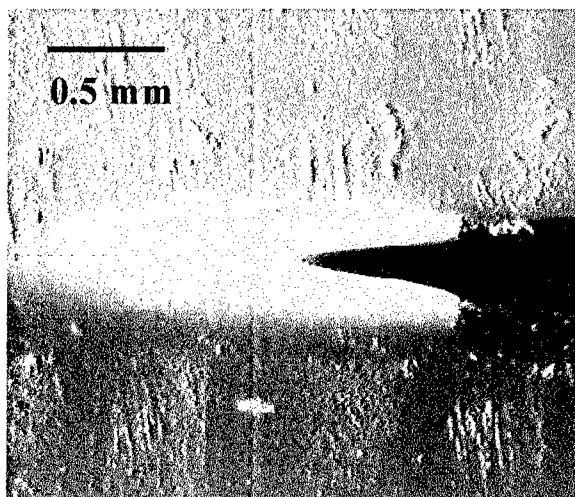


Figure 47. Process zone in FM[®]73U during a plane stress fracture toughness test

Several effects of environmental exposure on the tensile and fracture behavior of the FM[®]73U may be observed in Table 5. Thermal cycling affected FM[®]73U the least, causing a significant decrease only in the failure strain perhaps due to additional crosslinking caused by the time spent at an elevated temperature. Isothermal exposure to a hot/dry (71°C [160°F], 0% rh) environment may have also caused additional crosslinking in the polymer which reduced the failure strain and the fracture toughness, G_I . The most noticeable effects, though, resulted from the exposure of the FM[®]73U specimens to a moist environment. The yield and ultimate strengths and the fracture toughness were all significantly reduced by the high humidity environments. Because decreases in these properties were observed for the RT/wet and hot/wet environments, it

appears that possible moisture-induced plasticization played the dominant role in strength and fracture toughness degradation under these conditions.

8.1.1.5. Summary of Test Results for the FM[®]73 Adhesive

This section presents a brief synopsis of results from tests performed on the FM[®]73U and FM[®]73M adhesives.

- FTIR Spectroscopy:
 - some evidence of moisturization after 5,000 hours of hot/wet and RT/wet exposure
 - no evidence of change in the polymer structure including additional curing or degradation of bonds and functional groups
- Differential Scanning Calorimetry
 - $T_g \downarrow 12^\circ\text{C}$ (22°F) after exposure to hot/wet conditions for 5,000 hours indicating some degree of plasticization
- Thermogravimetric Analysis
 - no change in degradation temperature for any exposure condition indicating no major increases in the degree of crosslinking
- Tensile Tests
 - $\epsilon_f \downarrow \sim 50\%$ after 100 thermal cycles
 - $\epsilon_f \downarrow \sim 50\%$ after 5,000 hours hot/dry exposure

- σ_{ult} and σ_y \downarrow ~ 20% after 5,000 hours RT/wet and hot/wet exposure
- Plane Stress Fracture Toughness Tests
 - G_I \downarrow ~ 28% after 5,000 hours hot/dry exposure
 - G_I \downarrow ~ 34% after 5,000 hours RT/wet and hot/wet exposure

8.1.2. AF-191

Chemical and physical analyses were performed on the unsupported version of the AF-191 adhesive (AF-191U). Tensile and fracture toughness tests were performed on unsupported and supported (AF-191M) versions of the adhesive which contained a scrim cloth.

AF-191U specimens subjected to long-term exposure were periodically weighed and observed. Figure 48 shows the weight changes resulting from exposure. As expected, the specimens exposed to hot/wet conditions gained weight due to moisturization while those exposed to hot/dry conditions lost weight due to moisture loss. Weight gain was slightly lower than in the FM®73U. The AF-191U specimens exposed to the hot/dry environment were observed to gradually darken from pale yellow to dark brown during exposure. This change was first noticed after approximately 215 hours of exposure.

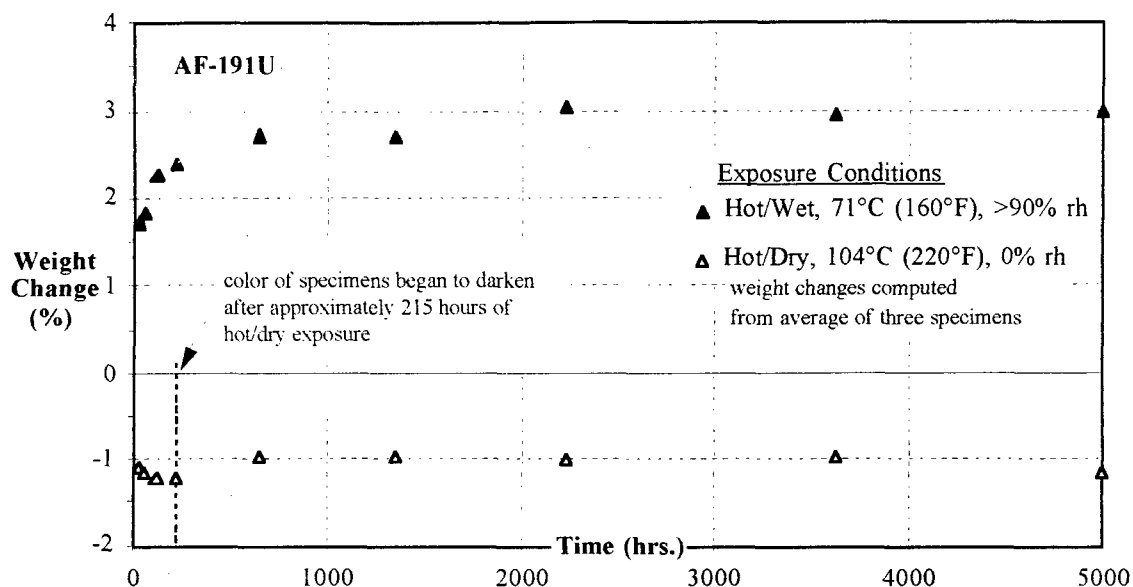


Figure 48. Weight changes in AF-191U adhesive due to long-term exposure

8.1.2.1. FTIR Spectroscopy

Transmittance FTIR spectroscopy was also performed on thin, cured AF-191U specimens. As with the FM[®]73U, this analysis revealed subtle but significant spectral differences among the four environmental conditions to which the specimens were subjected. Figure 49 shows the full range (400-4000 cm⁻¹) of all spectra obtained. Like the FM[®]73U spectra, the AF-191U spectra are very similar, and Figure 47 includes vertical separation.

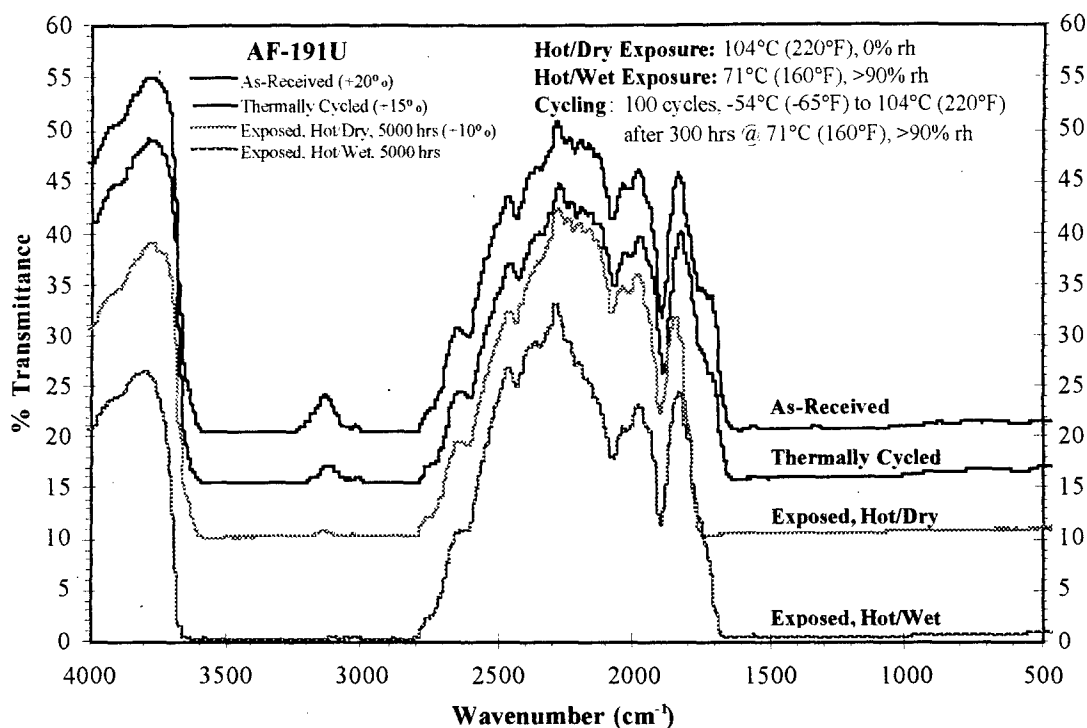


Figure 49. Full FTIR transmittance spectra for AF-191U adhesives
 (spectra shifted by amount indicated in parentheses to provide vertical separation)

Major changes in the AF-191U FTIR transmittance spectra occurred between wavenumbers 3500 and 1500. This region is expanded in Figure 50, and three specific areas of interest are indicated. As with the FM[®]73U epoxy, the exact structure of the AF-191U is proprietary. Thus, the identification of the specific causes of the changes in these areas of interest is strictly conjecture, but some possible explanations for the spectral changes are suggested in the following paragraphs. Unless otherwise noted, the explanations result from a comparison of the AF-191U spectra with standard correlation

charts in the CRC Handbook of Chemistry and Physics.¹²⁷ Please refer to Figure 42 in the previous section for a review of the basic epoxy chemistry.

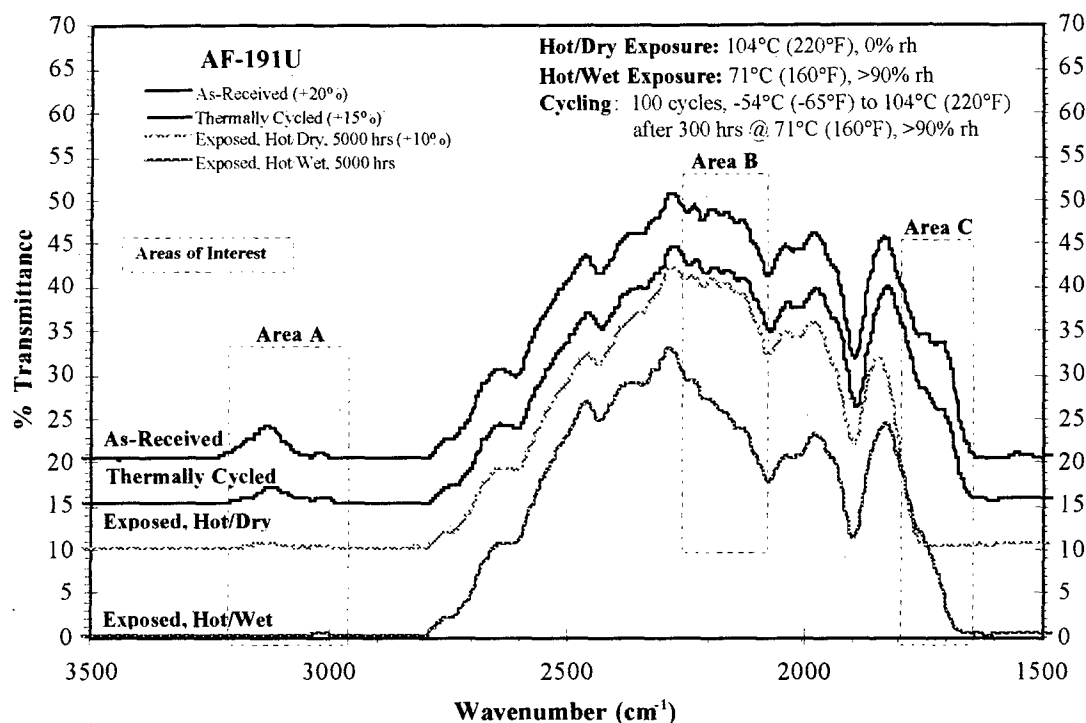


Figure 50. Expanded FTIR transmittance spectra for AF-191U adhesives (spectra shifted by amount indicated in parentheses to provide vertical separation)

Area A in Fig. 47 shows a decrease with exposure in the strength of a peak located near 3100 cm^{-1} . This could be caused by the masking effect of absorbed water mentioned in the section describing the spectroscopic analysis of the FM[®]73U. However, the near absence of the peak in the hot/dry spectrum is not consistent with this explanation.

Other exposure-induced changes in the polymer may be occurring which result in the observed spectral characteristics.

Area B shows a decrease in intensity of a range of peaks in the $2100\text{-}2300\text{ cm}^{-1}$ range due to exposure to hot/wet conditions. Although this range corresponds to that of nitrile compounds (commonly used to impart additional flexibility to epoxy adhesives), it is unknown what this spectral change implies

Area C shows a decrease with exposure in peaks in the $1650\text{-}1800\text{ cm}^{-1}$ range. This change is similar Area B in the FM[®]73U spectra and may be due to an increase in the amine (R-NH_2) concentration. This would suggest a breakdown of the crosslinking of the AF-191U structure resulting in the creation of additional amine structures as the nitrogen atoms are lost from the linked epoxy chains. Additional amine structures would absorb the infrared radiation in this range and reduce the transmittance peaks present in the as-received spectrum.

As with the FM[®]73U spectra, a general trend is the disappearance of transmittance peaks suggesting increased absorption caused by an increase in the concentration of certain bonding arrangements. However, the same reasoning used to evaluate the FM[®]73U spectra may be used for the AF-191U spectra. Thus, it also appears unlikely that the changes in the AF-191U spectra are caused by further curing of the adhesive. The observed changes in the spectra are most probably caused by mechanisms not fully identified by this spectroscopic study.

8.1.2.2. *Differential Scanning Calorimetry (DSC)*

Results from the DSC analysis of the AF-191U adhesive are shown in Figure 51. The heat flow axis was normalized by dividing by the heat flow required to attain the maximum temperature during the DSC runs (250°C [482°F]). This allowed the curves to be more easily compared.

Significant decreases in T_g were observed in the specimens which had been isothermally exposed to hot/wet and hot/dry conditions. As in the case of the FM[®]73U DSC analysis, the decrease in the hot/wet AF-191U specimens may be due to moisture-induced plasticization enhancing the mobility of the polymer structure. The decrease due to hot/dry conditions, however, is more difficult to understand. Perhaps extended time at elevated temperatures results in the scission of some crosslinks or in the severing of branches and side groups on the polymer chains. The loss of such structures would promote chain mobility and, thus, reduce the glass transition temperature.

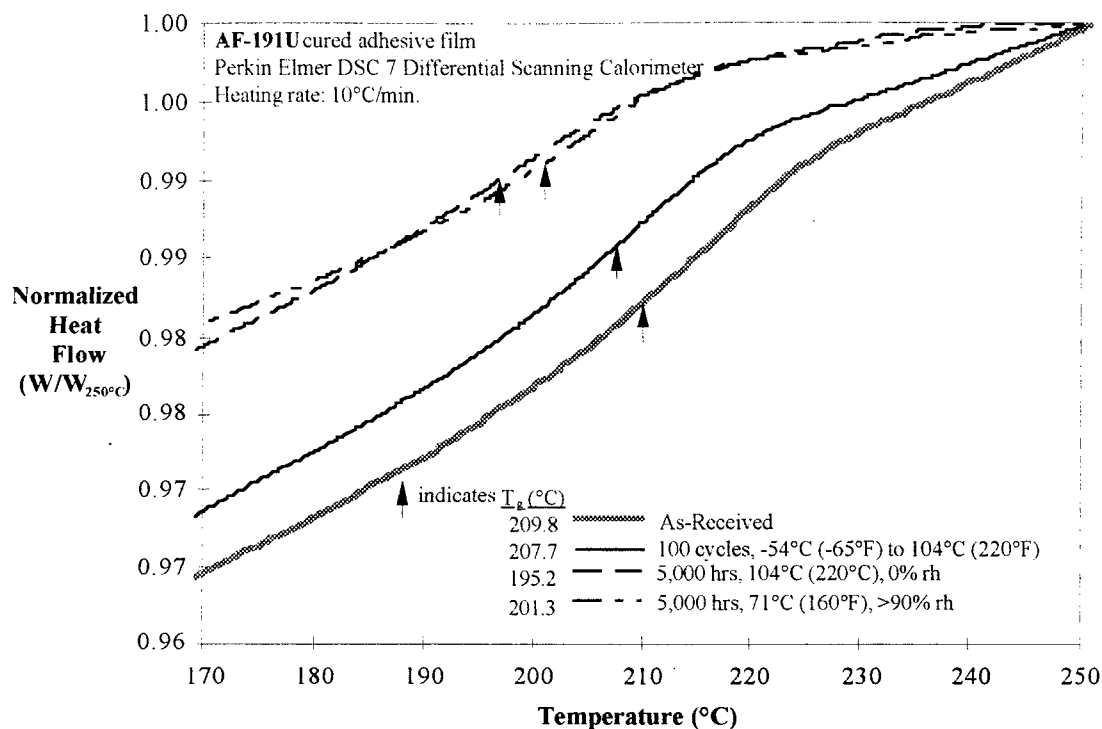


Figure 51. Results from the DSC analysis of the AF-191U adhesive

8.1.2.3. Thermogravimetric Analysis (TGA)

Figure 52 shows the results from the thermogravimetric analysis of the AF-191U adhesive. The degradation temperature was unaffected by the exposure environment. Furthermore, the onset of degradation occurred in a temperature range far above the maximum recommended use temperature AF-191. Therefore, no changes in the mechanical behavior of the adhesive or of bonded joints fabricated with this adhesive should be attributed to large scale degradation of the AF-191U polymer. Additionally, the uniformity of the AF-191 structure appears to be less than that of the FM[®]73. This

is suggested by the relatively large difference between the onset and midpoint degradation temperatures and the resulting gradual slope of the TGA degradation curves.

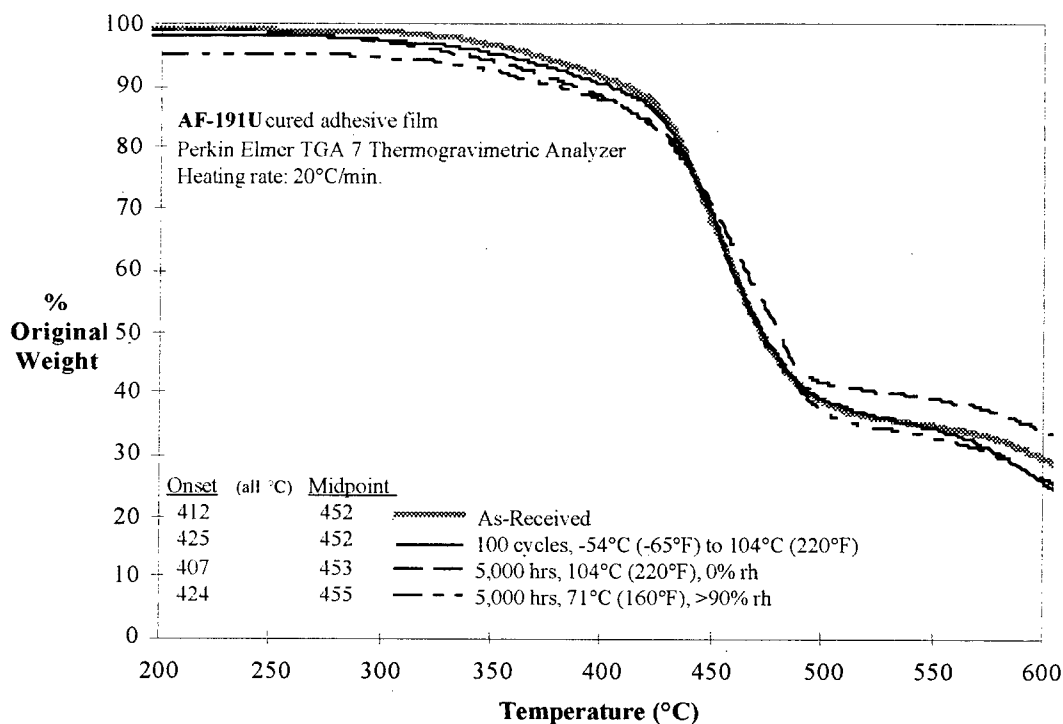


Figure 52. Results from the thermogravimetric analysis of the AF-191U adhesive

8.1.2.4. Mechanical Test Results

Figure 53 shows tensile curves for the unsupported and scrim-containing versions of the AF-191 epoxy adhesive. These stress-strain curves are for individual specimens but are typical of the behavior exhibited by multiple specimens. Although the non-woven scrim cloth in this adhesive is described as a “random mat,” specimens containing the

scrim cloth (AF-191M) were tested in two orientations based upon the direction in which the uncured adhesive film was rolled upon delivery: longitudinal (with the loading axis parallel to the rolled direction of the uncured film) and transverse (with the loading axis perpendicular to the rolled direction of the uncured film).

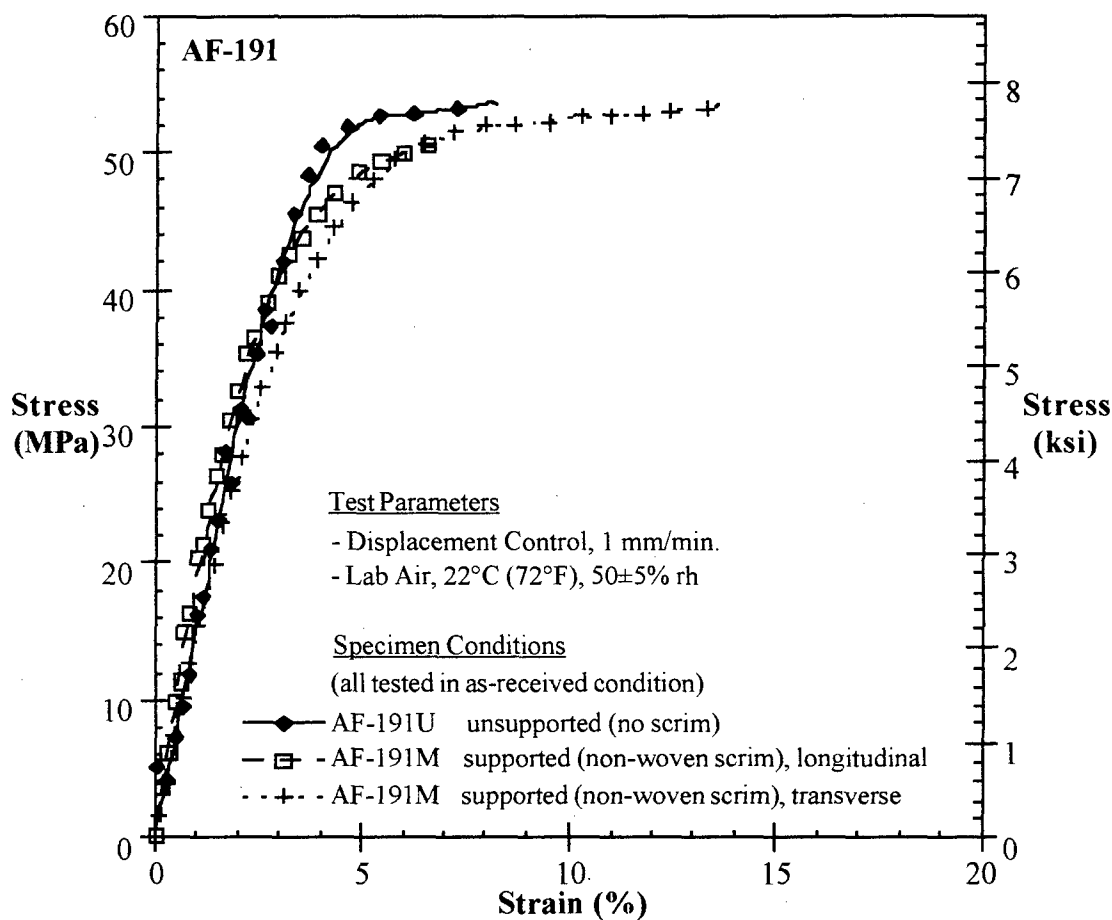


Figure 53. Tensile behavior of the AF-191U and AF-191M adhesives

Table 6 provides numerical values for the key properties examined during the tensile and fracture toughness testing of the supported and unsupported AF-191. The presence of the scrim cloth reduced the yield strength and fracture toughness of the AF-191M adhesive with respect to those of its unsupported version (AF-191U). No significant differences were noted between the longitudinal and transverse specimen orientations. Thus, as with the FM[®]73 adhesive, the non-woven scrim cloth did not impart in-plane reinforcement and may serve only to improve “handle-ability” and control the bond line thickness when this epoxy adhesive film is used to manufacture bonded components. However, the effect of the scrim cloth on out-of-plane and shear properties of the AF-191M adhesive is unknown. Since these properties are important to the performance of bonded joints, this issue is a candidate for future research.

Table 6. In-Plane Properties of AF-191U (unsupported) and AF-191M (supported)

ADHESIVE Scrim Direction [# tested] ¹	E (MPa)	ϵ_f (%)	σ_{uts} (MPa)	$\sigma_{ys(0.2)}$ (MPa)	σ_{fys} (MPa)	G_I (J/m ²)
AF-191U no scrim [6]	1396 ±51	8.7 ±2.3	51 ±2	40 ±2	44 ±1	1084 ±53
AF-191M longitudinal [6]	1611 ±257	7.1 ±3.8	46 ±5	30 ±2	37 ±3	659 ±77
AF-191M transverse [5]	1457 ±263	16.1 ±7.0	51 ±2	29 ±2	37 ±2	815 ±86 ⁶

Notes: • statistically significant differences from unsupported values are boldfaced
 • 95% confidence intervals shown following ± sign
¹ number of specimens tested in brackets [] unless note appears within table
⁶ 6 specimens tested instead of number listed in brackets []

Figure 54 shows tensile curves for AF-191U adhesive specimens subjected to various environmental conditions. These stress-strain curves are for individual specimens but are typical of the behavior exhibited by the multiple specimens tested.

Table 7 contains the mean values for the key tensile and fracture properties examined during testing of the AF-191U adhesive exposed to various environments.

The modulus (E), ultimate strength (σ_{uts}), and yield strengths ($\sigma_{ys(0.2)}$ and σ_{lys}), of the AF-191 were similar to those of the FM[®]73, but far below those of the FM[®]x5. In terms of failure strain, that of the AF-191 was less than that of the FM[®]73, but greater than that of the FM[®]x5.

Despite having tensile properties similar to the FM[®]73, the fracture toughness of the AF-191 was much lower. The fracture toughness of the AF-191 was also far below that of the FM[®]x5. This lower toughness of the AF-191 as compared with that of the FM[®]73 was evident even during fracture toughness specimen preparation. During notching of the less tough AF-191, a longer than desired lead crack often formed ahead of the razor blade tip forcing several specimens to be discarded. As with the FM[®]73, crack growth in the unsupported AF-191U was preceded by a slight blunting of the crack tip and the formation of a whitened, Dugdale-like process zone. (Fig. 55) However, the process zone was smaller and cracks in the AF-191U propagated evenly for only approximately 0.3 mm before becoming unstable. Crack tip blunting and process zone formation were restricted in the scrim-containing AF-191M material

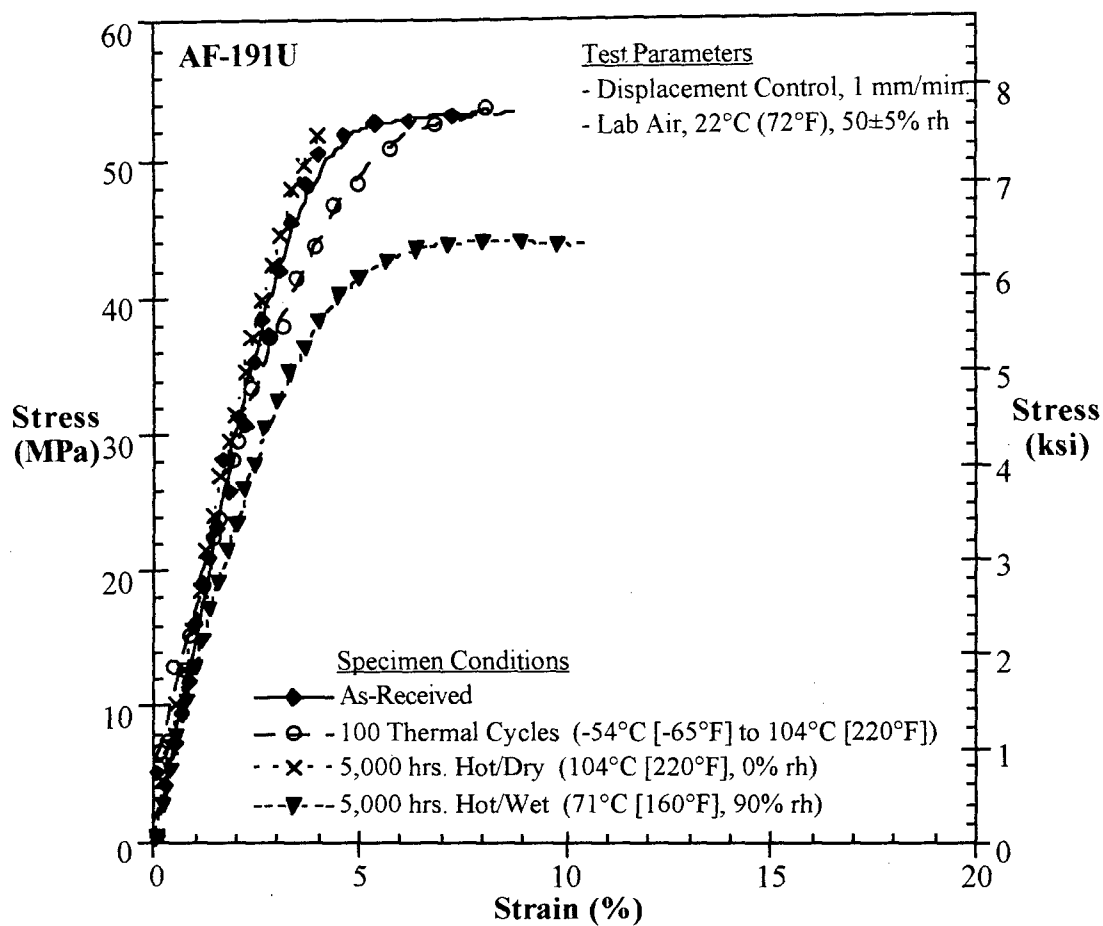


Figure 54. Tensile behavior of AF-191U adhesive exposed to various environments

Table 7. Properties of AF-191U Following Exposure to Various Environments

ADHESIVE Condition [# tested] ¹	E (MPa)	ϵ_f (%)	σ_{uts} (MPa)	$\sigma_{ys(0.2)}$ (MPa)	σ_{iys} (MPa)	G_I (J/m ²)
AF-191U As-Received [6]	1396 ±51	8.7 ±2.3	51 ±2	40 ±2	44 ±1	1084 ±53
Thermally Cycled [4]	1386 ±235	11.1 ±2.7	55 ±2	37 ±3	45 ±2	937 ±74
Hot/Dry [3]	1666 ±92	3.8 ±0.6	52 ±2	41 ±6	46 ±1	836 ±64
Hot/Wet [3]	1210 ±159	9.7 ±3.9	43 ±1	28 ±2	35 ±1	929 ±78

Notes: • statistically significant differences from as-received values are **boldfaced**
• 95% confidence intervals shown following ± sign
¹ number of specimens tested in brackets [] unless note appears within table

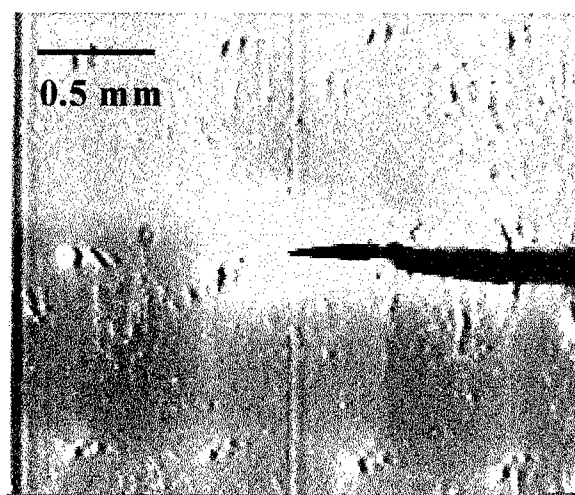


Figure 55. Process zone in AF-191U during a plane stress fracture toughness test

In terms of environmental exposure, the AF-191U adhesive was affected in a similar way as the FM[®]73U. Exposure to a hot/dry (104°C [220°F], 0% rh) environment increased the modulus, but decreased the failure strain making the polymer more rigid. Also similar to the FM[®]73U, the largest effects resulted from the exposure of the AF-191U specimens to a hot/wet environment. The yield and ultimate strengths and the fracture toughness were all significantly reduced by the high humidity environments. As with the other epoxy examined for this research, it appears that the high humidity resulted in moisture-induced plasticization which played the dominant role in strength and fracture toughness degradation.

8.1.2.5. Summary of Test Results for the AF-191 Adhesive

This section presents a brief synopsis of results from tests performed on the AF-191U and AF-191M adhesives.

- FTIR Spectroscopy:
 - some evidence of moisturization after 5,000 hours of hot/wet exposure
 - no evidence of change in the polymer structure including additional curing or degradation of bonds and functional groups
- Differential Scanning Calorimetry
 - $T_g \downarrow \sim 15^\circ\text{C}$ (27°F) after 5,000 hours hot/dry and hot/wet exposure indicating some degree of plasticization

- Thermogravimetric Analysis
 - no change in degradation temperature for any exposure condition indicating no major increases in the degree of crosslinking
- Tensile Tests
 - $\epsilon_f \downarrow \sim 50\%$, $E \uparrow \sim 20\%$ after 5,000 hours hot/dry exposure
 - $\sigma_{ult} \downarrow \sim 15\%$ and $\sigma_y \downarrow \sim 30\%$ after 5,000 hours hot/wet exposure
- Plane Stress Fracture Toughness Tests
 - $G_I \downarrow \sim 12\%$ after 100 thermal cycles
 - $G_I \downarrow \sim 20\%$ after 5,000 hours hot/dry exposure
 - $G_I \downarrow \sim 15\%$ after 5,000 hours hot/wet exposure

8.1.3. FM[®]x5

All chemical, physical, tensile, and fracture tests were performed on FM[®]x5 adhesive which contained a woven glass scrim cloth.

FM[®]x5 specimens subjected to long-term exposure were periodically weighed and observed. Figure 52 shows the weight changes resulting from exposure. As expected, the specimens exposed to a hot/wet condition gained weight due to moisturization while those exposed to a hot/dry environment lost weight due to moisture loss. These weight changes were substantially lower than those experienced by the epoxy adhesives. However, the FM[®]x5's relatively high volume fraction glass scrim cloth probably

absorbed minimal water thereby contributing to the low weight change percentages seen in this adhesive. No other gross changes (warping, color change, etc.) were observed in the exposed FM[®]x5 specimens.

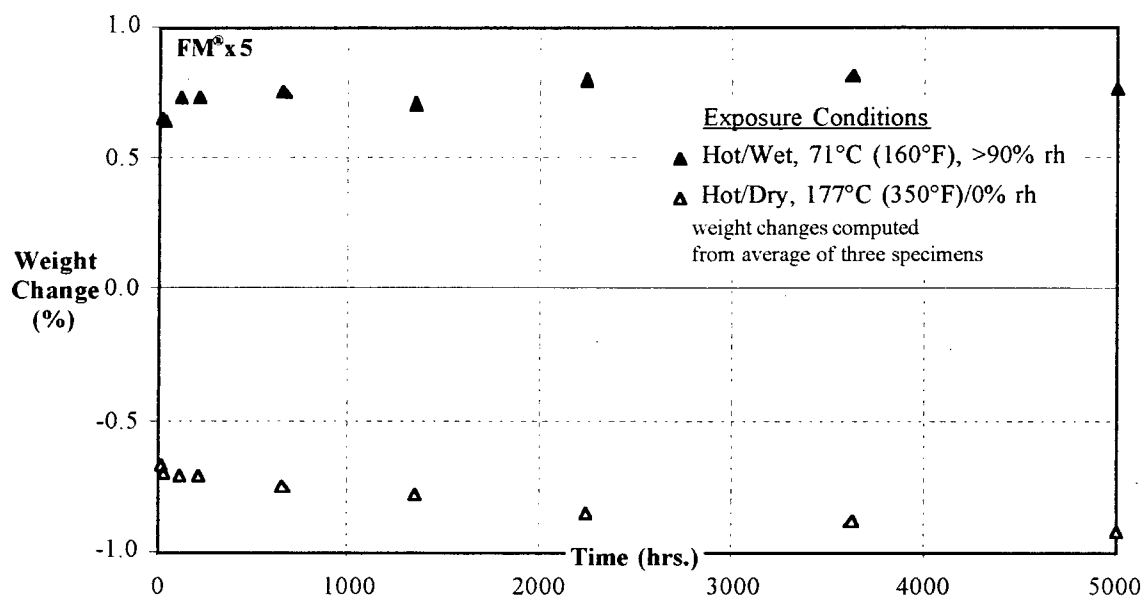


Figure 56. Weight changes in FM[®]x5 adhesive due to long-term exposure

8.1.3.1. FTIR Spectroscopy

Transmittance FTIR spectroscopy was also performed on thin, cured FM[®]x5 specimens. These specimens were relatively thick and opaque compared to the epoxies, but were somewhat transparent to infrared radiation. However, the amount of transmittance obtained was significantly lower than it was for the epoxies. As with the

epoxies this analysis revealed subtle spectral differences among the four environmental conditions to which the specimens were subjected. Figure 57 shows the full range (400-4000 cm^{-1}) of all spectra obtained. These spectra are very similar, and Figure 58 includes a vertical separation of the spectra.

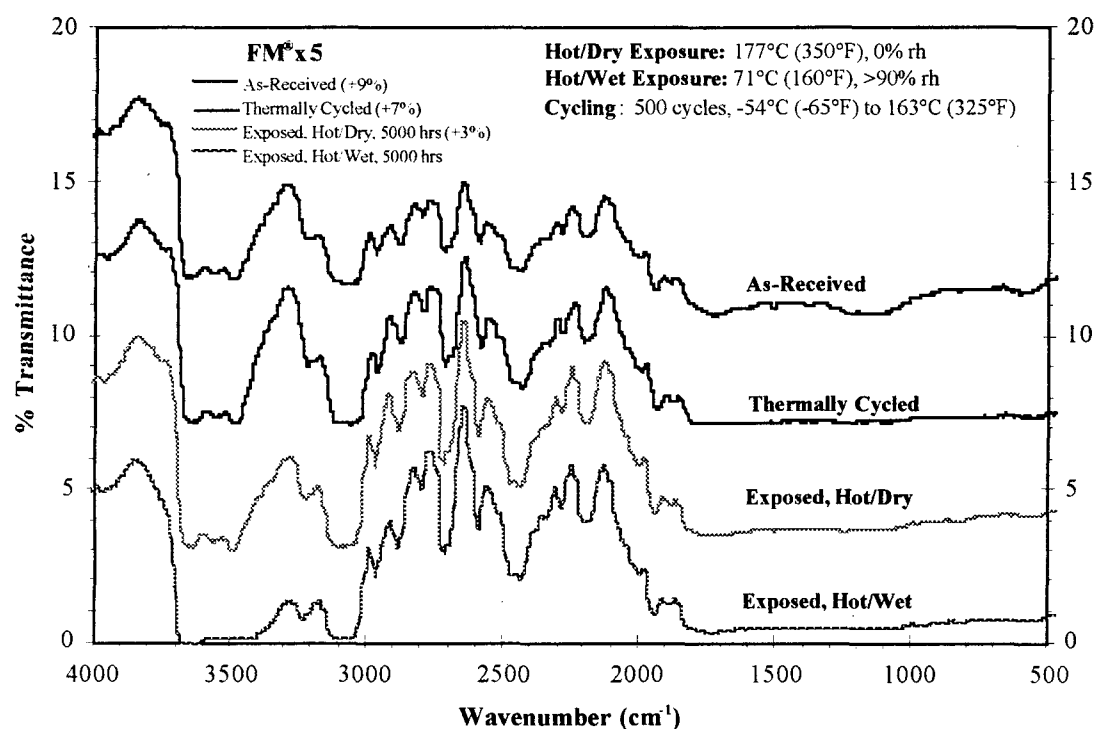


Figure 57. Full FTIR transmittance spectra for FM[®]x5 adhesives (spectra shifted by amount indicated in parentheses to provide vertical separation)

Major changes in the FM[®]x5 FTIR transmittance spectra occurred between wavenumbers 3500 and 1800. This region is expanded in Figure 54, and two specific

areas of interest are indicated. As with the epoxies, the exact structure of the FM[®]x5 is proprietary. Thus, the identification of the specific causes of the changes in these areas of interest is strictly conjecture, but some possible explanations for the spectral changes are suggested in the following paragraphs. Unless otherwise noted, the explanations result from a comparison of the AF-191U spectra with standard correlation charts in the CRC Handbook of Chemistry and Physics.¹³¹ Figure 55 shows a typical polyimide structure.

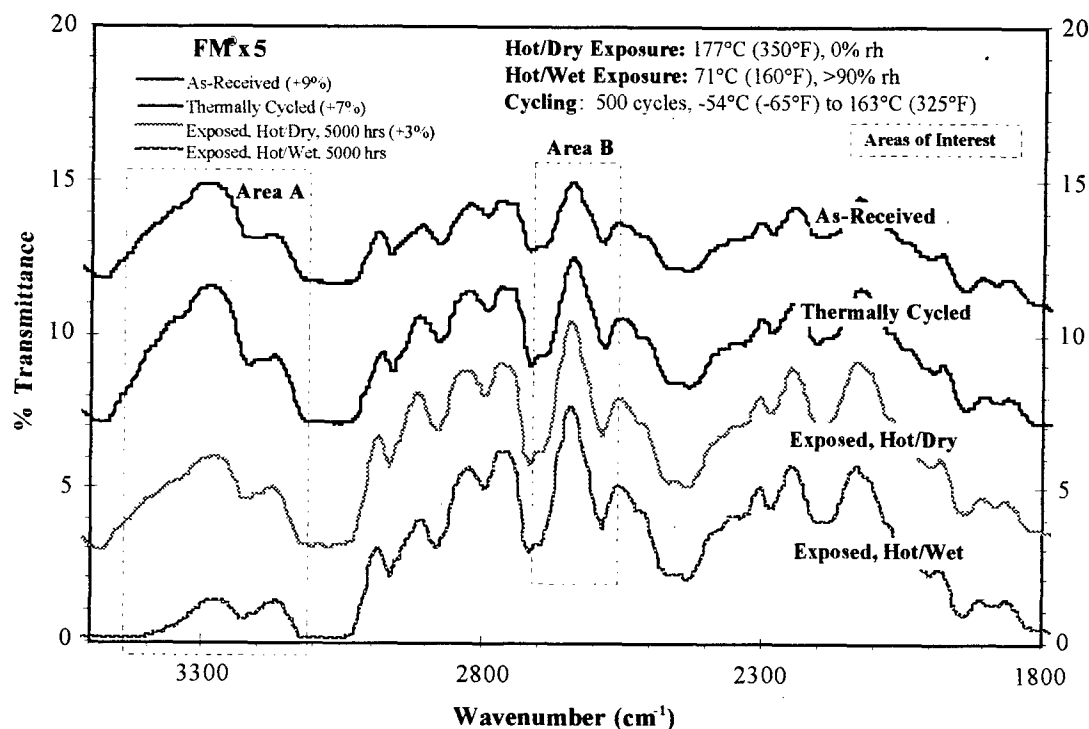


Figure 58. Expanded FTIR transmittance spectra for FM[®]x5 adhesives (spectra shifted by amount indicated in parentheses to provide vertical separation)

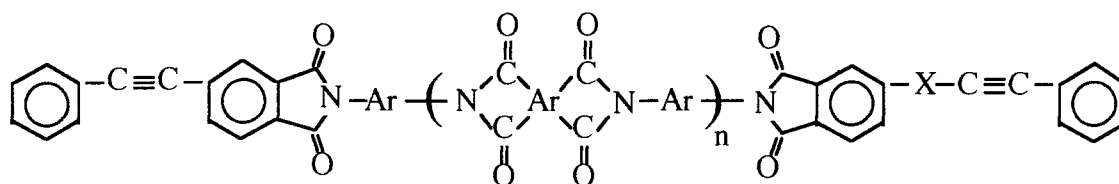


Figure 59. Typical polyimide structure

Area A in Fig. 58 shows a decrease with exposure in the strength of peaks located near 3200 cm^{-1} . This could be caused by the masking effect of absorbed water mentioned in the section describing the spectroscopic analysis of the FM[®]73U.

Area B shows an increase in intensity of a peak at approximately 2650 cm^{-1} due to exposure. This is the only increase observed in the FTIR spectroscopy conducted for this research and suggests a possible degradation of the triple bonds connecting the terminal aromatic groups to the polyimide structure.¹³²

The spectra of the FM[®]x5 appeared to be fairly consistent regardless of the type of environmental exposure to which specimens were subjected. The changes noted were subtle, and their significance is questionable due to the very small spectral differences observed. In general, the spectra of FM[®]x5 polyimide adhesive suggest that it was less affected than the epoxies by the various exposure environments.

8.1.3.2. Differential Scanning Calorimetry (DSC)

Results from the DSC analysis of the FM[®]x5 adhesive are shown in Figure 60. The heat flow axis was normalized by dividing by the heat flow required to attain the maximum temperature during the DSC runs (300°C [572°F]). This allowed the curves to be more easily compared.

Differences in T_g values of 5°C or less are not usually considered significant.¹³⁰ Thus, the closely grouped T_g values indicate that, at least in terms of the glass transition temperature, FM[®]x5 is relatively stable under the conditions examined.

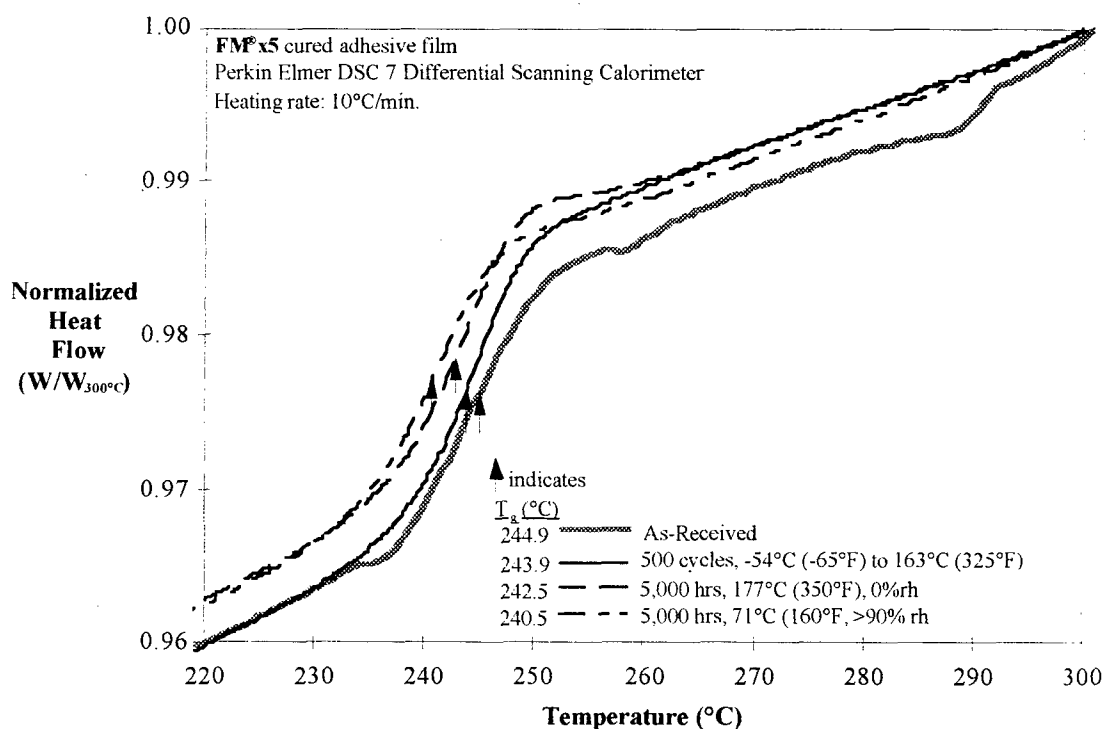


Figure 60. Results from the DSC analysis of the FM[®]x5 adhesive

8.1.3.3. Thermogravimetric Analysis (TGA)

Figure 61 shows the results from the thermogravimetric analysis of the FM[®]x5 adhesive. The degradation behavior and temperature were unaffected by the exposure environment, a finding which is consistent with the lack of environmental effect on the glass transition temperature. Furthermore, the onset of degradation occurred in a temperature range far above the maximum recommended use temperature FM[®]x5. Therefore, no changes in the mechanical behavior of the adhesive or of bonded joints fabricated with this adhesive should be attributed to large scale degradation of the FM[®]x5 polymer. In an unreinforced or unfilled resin, a gradual slope of TGA data such as that displayed by the FM[®]x5 suggests that the polymer structure lacks uniformity and that some constituents begin to degrade at low temperatures while other do not degrade until much higher temperatures are reached. However, the FM[®]x5 contained a relatively large percentage of woven glass scrim cloth, and it is postulated that the presence of this component caused the large differences between the onset and midpoint degradation temperatures.

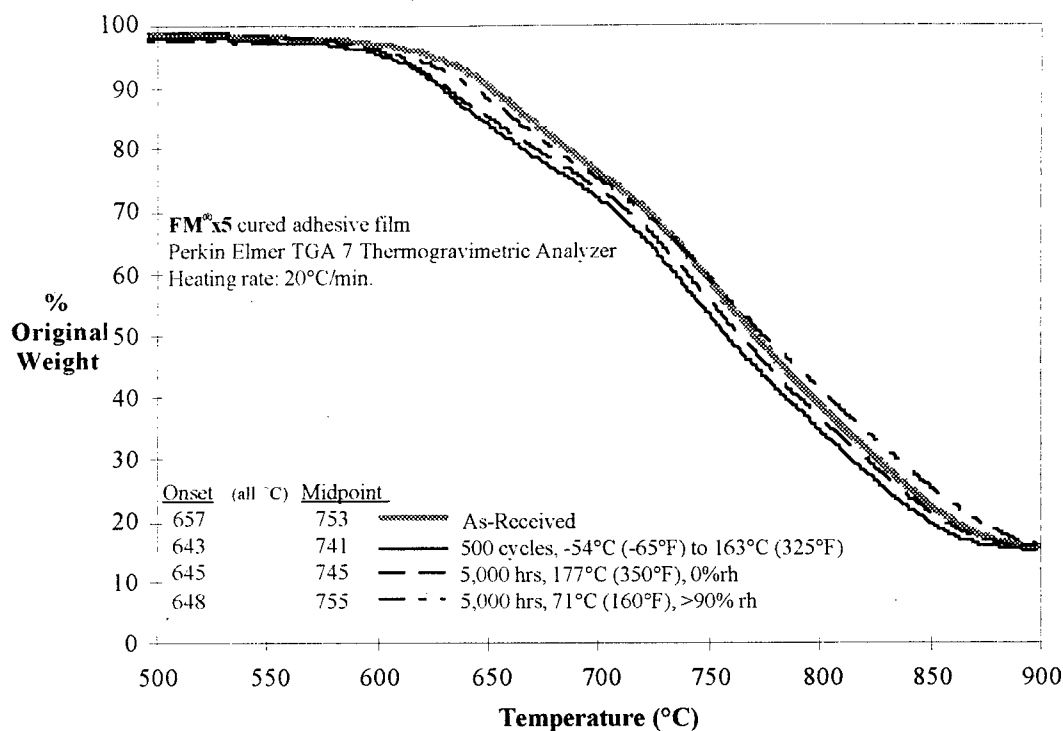


Figure 61. Results from the thermogravimetric analysis of the FM®x5 adhesive

8.1.3.4. Mechanical Test Results

Figure 62 illustrates the tensile behavior of the FM®x5 adhesive in the as-received condition and following various types of environmental exposure. The curves are typical of the behavior exhibited by multiple specimens.

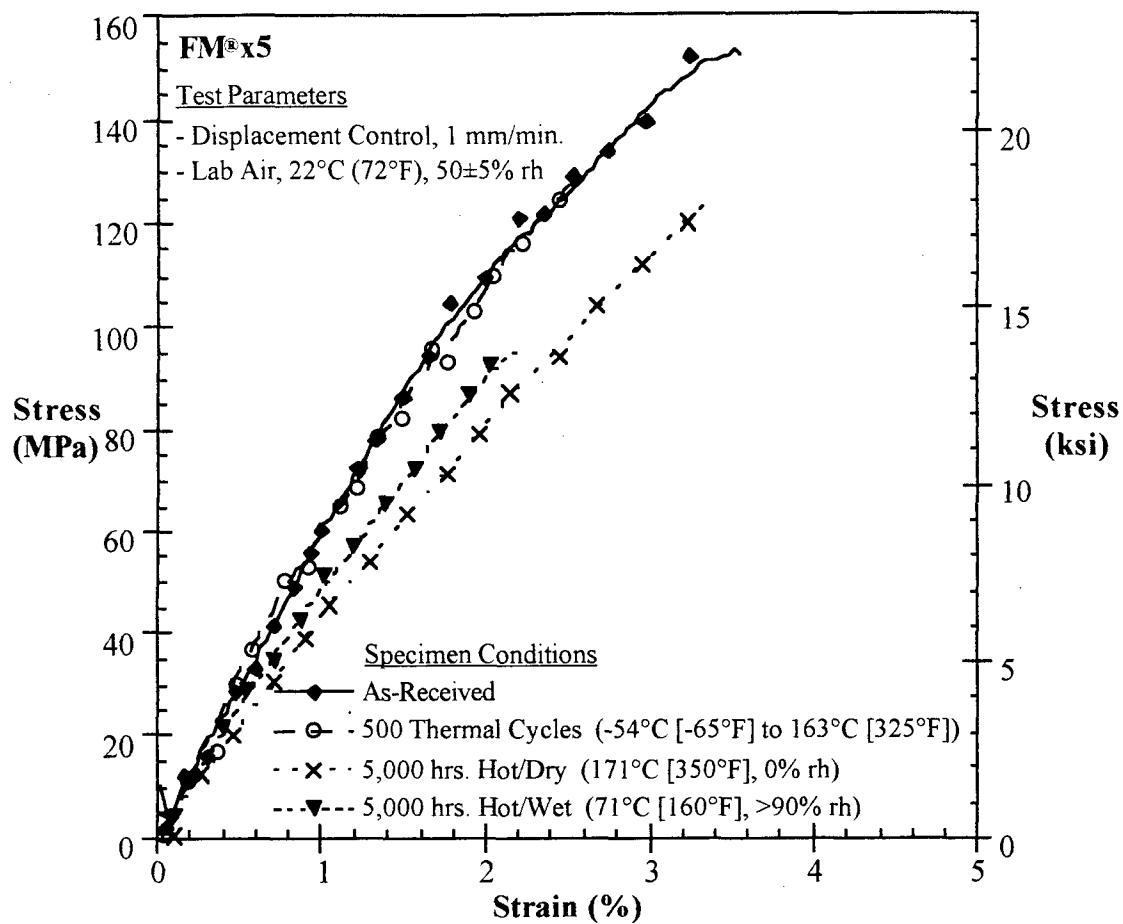


Figure 62. Tensile behavior of FM®x5 adhesive exposed to various environments

Table 8 contains the mean values for the key tensile and fracture properties examined during testing of the FM[®]x5 adhesive exposed to various environments.

Table 8. Properties of FM[®]x5 Following Exposure to Various Environments

ADHESIVE Condition [# tested] ¹	E (MPa)	ϵ_f (%)	σ_{uts} (MPa)	$\sigma_{ys(0.2)}$ (MPa)	σ_{iys} (MPa)	G_I (J/m ²)
FM [®] x5 As-Received [4]	5296 ±763	3.6 ±1.0	160 ±19	133 ±17	140 ±18	4048 ±1329
Thermally Cycled [3]	4827 ±886	3.6 ±1.1	151 ±22	126± 19	136 ±21	3813 ±809
Hot/Dry [2]	4177 ±108	3.3 ±0.3	130 ±4	96 ±1	114 ±3	2800 ±647 ³
Hot/Wet [3]	4778 ±621	2.6 ±0.3	99 ±9	80 ±32	84 ±19	3200 ±483

Notes: • statistically significant differences from as-received values are **boldfaced**
 • 95% confidence intervals shown following ± sign
¹ number of specimens tested in brackets [] unless note appears within table
³ 3 specimens tested instead of number listed in brackets []

With the exception of failure strain, the tensile and fracture toughness properties of the FM[®]x5 adhesive film exceeded those of the epoxy adhesives. In one respect, the lower failure strain was reflected in the nearly linearly elastic behavior of the FM[®]x5. Though it was expected that the strength and toughness of the polyimide FM[®]x5 would exceed those of the epoxies, the differences observed were no doubt magnified by the high volume fraction of woven glass scrim cloth which reinforces the brittle FM[®]x5 polymer.

It should be reiterated here that these tests were conducted in-plane with the scrim cloth whereas bonded joints would result in more shear and out-of-plane loading to the adhesive-scrim system. Nevertheless, the differences between the properties of the polyimide and epoxies are quite notable.

Another noteworthy difference between the behavior of the polyimide and epoxy adhesives is the much larger confidence intervals (i.e. greater degree of scatter) displayed by the FM[®]x5. It is possible that slightly different numbers and orientations of scrim fibers present within the gage sections of the FM[®]x5 specimens increased the observed scatter bands.

In contrast to the fracture behavior of the epoxies, no process zone was observed ahead of the crack tip in the FM[®]x5. In addition, very little, if any, stable crack growth was noted prior to final fracture.

Exposure to various environments had some effect upon the properties of the FM[®]x5, primarily on the ultimate and yield strengths. Exposure to hot/dry (177°C [350°F], 0% rh) and hot/wet (71°C [160°F], >90% rh) environments both significantly reduced strength values. It is uncertain what roles heat and humidity had in producing these changes. In addition, exposure to a hot/dry environment reduced the tensile modulus. The effect of exposure upon the fracture toughness of the FM[®]x5 could not be determined using a confidence interval approach because the large amount of scatter

resulted in very large, overlapping confidence intervals. However, the average toughness values did decrease with exposure.

8.1.3.5. *Summary of Test Results for the FM[®]x5 Adhesive*

This section presents a brief synopsis of results from tests performed on the FM[®]x5 adhesive.

- FTIR Spectroscopy:
 - some evidence of moisturization after 5,000 hours of hot/wet exposure
 - slight evidence of loss of terminal aromatic groups after 5,000 hours of hot/dry and hot/wet exposure
- Differential Scanning Calorimetry
 - no change in T_g for any exposure condition indicating no changes in structure which would promote or reduce chain mobility
- Thermogravimetric Analysis
 - no change in degradation temperature for any exposure condition indicating no major increases in the degree of crosslinking
- Tensile Tests
 - $E \downarrow \sim 20\%$ after 5,000 hours hot/dry exposure
 - σ_{ult} and $\sigma_y \downarrow \sim 25\%$ after 5,000 hours hot/dry exposure
 - σ_{ult} and $\sigma_y \downarrow \sim 45\%$ after 5,000 hours hot/wet exposure

- Plane Stress Fracture Toughness Tests

- no significant differences using a confidence interval approach due to a large amount of scatter, however:
- average $G_I \downarrow \sim 30\%$ after 5,000 hours hot/dry exposure
- average $G_I \downarrow \sim 20\%$ after 5,000 hours hot/wet exposure

8.2. Bonded Joints

Investigations of bonded joint specimens included monotonic and fatigue testing of three basic specimen geometries, four bonded material systems, and a variety of environmental exposure conditions based upon each bonded material system's particular application. Table 9 on the following page summarizes the tests conducted for this portion of the program.

8.2.1. Al/FM[®]73M/Al

This group of specimens was tested to investigate the effect of environmental exposure on the bonded system investigated by the USAF PABST study. It also provided information on the behavior of the same FM[®]73M adhesive used in the Al/FM[®]73M/B-Ep specimens which, because of their dissimilar adherends, were more difficult to test and analyze.

One group of specimens was tested in the as-received state with no pre-test environmental exposure. A second group was subjected to 100 thermal cycles between

-54°C (-65°F) and 71°C (160°F) after being exposed for 300 hours to hot/wet conditions (71°C (160°F), >90% rh) prior to mechanical testing. A third group was subjected to 5,000 hours of hot/dry isothermal exposure at 71°C (160°F), 0% rh, prior to mechanical testing. A fourth group was subjected to 5,000 hours of RT/wet isothermal exposure at 22°C (72°F), >90% rh, prior to mechanical testing. A fifth group was subjected to 5,000 hours of hot/wet isothermal exposure at 71°C (160°F), >90% rh, prior to mechanical testing. A sixth group was subjected to 10,000 hours of hot/wet isothermal exposure at 71°C (160°F), >90% rh, prior to mechanical testing. A seventh group was subjected to 5,000 hours of hot/wet isothermal exposure followed by 5,000 of desiccation at 22°C (72°F), 10% rh, prior to mechanical testing.

Table 9. Summary of Tests Conducted on Bonded Joint Specimens

Table 9. Summary of Tests Conducted on Bonded Joint Specimens

System	Specimen Geometry » Test Type » Test Temperature »	DCB			DCB			ENF			CLS			CLS		
		M	M	RT	M	M	Hot	M	M	RT	M	M	RT	M	M	Hot
C-141 bonded repairs Al/FM [®] 73M/Al	As-Received	3 (27)	1 (3)	1 (6)	1 (54)	1 (2)	2 (2)	1 (1)	1 (1)	1 (1)	4 (27)					
	100 Thermal Cycles	1 (6)			1 (29)	1 (1)	1 (1)									
	5000 hrs, Hot/Dry	1 (5)				1 (1)										
	5000 hrs, RT/Wet	1 (5)				1 (1)										
	5000 hrs, Hot/Wet	1 (10)			1 (28)	1 (1)	1 (1)									
	10000 hrs., Hot/Wet	1 (5)				1 (3)	1 (1)									
	5000 hrs., Desiccated	1 (5)				1 (3)										
F-22 control surfaces Gr-BMI/AF-191M/Gr-BMI (unidirectional) (quasi-isotropic)	As-Received	1 (11)	1 (3)	1 (3)	1 (47)		2 (2)	1 (1)	1 (1)							
	100 Thermal Cycles	1 (6)			1 (26)		1 (1)									
	5000 hrs., Hot/Wet	1 (7)			1 (22)		1 (1)									
	5000 hrs., Desiccated	1 (5)														
	As-Received	2 (19)	1 (3)	1 (4)	1 (12)	1 (5)	2 (2)	1 (1)	1 (1)							
	100 Thermal Cycles	2 (14)			1 (18)	1 (4)	1 (1)									
	5000 hrs., Hot/Dry	1 (7)			1 (24)	1 (5)	1 (1)									
HSCT wing or fuselage components Ti/FM [®] x5/Ti	10000 hrs., Hot/Dry	1 (6)				1 (5)	1 (1)									
	As-Received	1 (9)	1 (2)	1 (3)		1 (1)	2 (2)	1 (1)	1 (1)							
	100 Thermal Cycles	1 (7)					1 (1)									
	As-Received	2 (19)	1 (4)	1 (5)	1 (16)	1 (4)	3 (3)									
	500 Thermal Cycles	1 (6)			1 (25)	1 (2)	1 (1)									
	5000 hrs., Hot/Dry	1 (9)			1 (30)	1 (3)	1 (1)									
	10000 hrs., Hot/Dry	1 (5)			1 (53)	1 (3)	1 (1)									
KEY>>	Hot = 71°C (160°F)															
	Hot = 104°C (220°F)															
	Hot = 177°C (350°F)															
	Thermal Cycles = -54°C (-65°F) to 71°C (160°F)															
	Thermal Cycles = -54°C (-65°F) to 104°C (220°F)															
	Thermal Cycles = -54°C (-65°F) to 163°C (325°F)															
	Thermal Cycles = 71°C (160°F), >90% rh															
	Hot/Wet = 104°C (220°F), 0% rh															
	Hot/Dry = 177°C (350°F), 0% rh															
	Desiccated = 22°C (72°F), 10% rh															
	after 5,000 hrs. Hot/Wet exposure															

M = Monotonic

F = Fatigue

RT = 22°C (72°F)

Cold = -54°C (-65°F)

Hot <see KEY below>

CLS	CLS	CLS	CLS
M	M	M	F
RT	Cold	Hot	RT
B-Ep Strap, Al Lap			
2 (2)	1 (1)	1 (1)	1 (7)
1 (1)			
1 (1)			

#s indicate:
of specimens tested
followed by
(# of values obtained)

Al/FM[®]73M/Al bonded joint specimens subjected to long-term exposure were periodically weighed and observed. Figure 63 shows the weight changes resulting from exposure. As expected, the specimens exposed to hot/wet conditions gained weight due to moisturization while those exposed to hot/dry conditions lost weight due to moisture loss. However, due to the small area of exposed adhesive and the relatively massive adherends, weight change magnitudes were extremely small compare to those of the FM[®]73U adhesive.

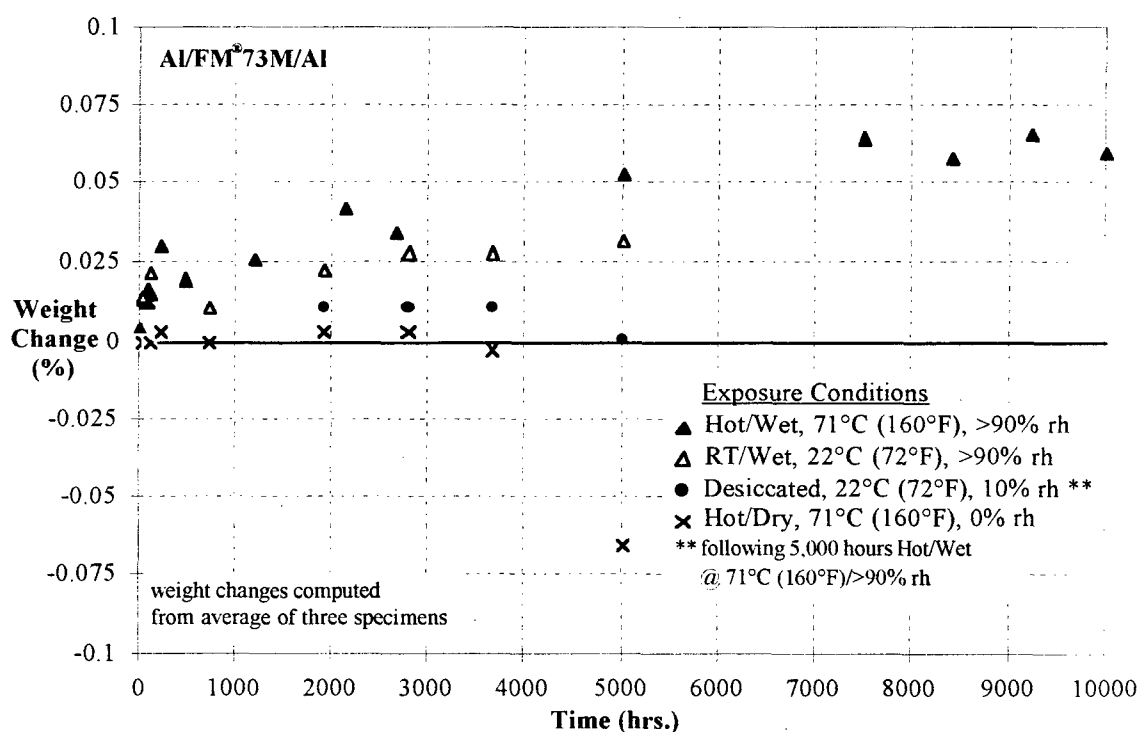


Figure 63. Weight changes in Al/FM[®]73/Al bonded joint specimens due to exposure

It can also be seen that the specimens first exposed to hot/wet conditions for 5,000 hours and then desiccated at 10% rh for 5,000 hours did not experience a complete loss of moisture.

Surface observations did not show any changes in the color of the bond line. However, subsequent fracture testing of specimens exposed to elevated temperature conditions did show some darkening of the normally pale yellow FM[®]73M which extended into the bond line for approximately 1-3 mm (0.04 - 0.12 in.) around the exposed edges.

The most visibly affected parts of the specimens were the aluminum adherends. All exterior aluminum surfaces on the specimens exposed to high humidity conditions were attacked by corrosion with approximately 100 hours. After approximately 1000 hours, corrosion products were heavily deposited on the exposed aluminum surfaces.

8.2.1.1. Mode I (DCB)

Monotonic Mode I testing of the Al/FM[®]73M/Al system revealed a strong dependence of the fracture toughness (G_{IC}) on environmental exposure, especially the moisture content of the exposure atmosphere. The as-received Mode I toughness was approximately 2800 J/m² (16 in.-lb./in.²). This value is in agreement with G_{IC} values obtained for FM[®]73M by Ting & Cottingham¹³³ and Ripling, *et al.*¹³⁴

As shown in Figure 64, thermal cycling following 300 hours of hot/wet exposure significantly reduced G_{IC} by approximately 30%. Specimens subjected to long-term

exposure were more affected by moisture or the combination of moisture and elevated temperature than by elevated temperature alone. The greatest reductions seen in G_{IC} occurred in specimens exposed to hot/wet conditions. This effect did not appear to be recoverable by "drying out" the bonded system in a desiccator at room temperature. Drying at elevated temperatures (71°C [160°F]) may have reversed the effect of absorbed moisture by providing the same amount of thermal driving force required to moisturize the specimens. However, for this research, such a drying method was not used because the effect of additional time at a high temperature was unknown.

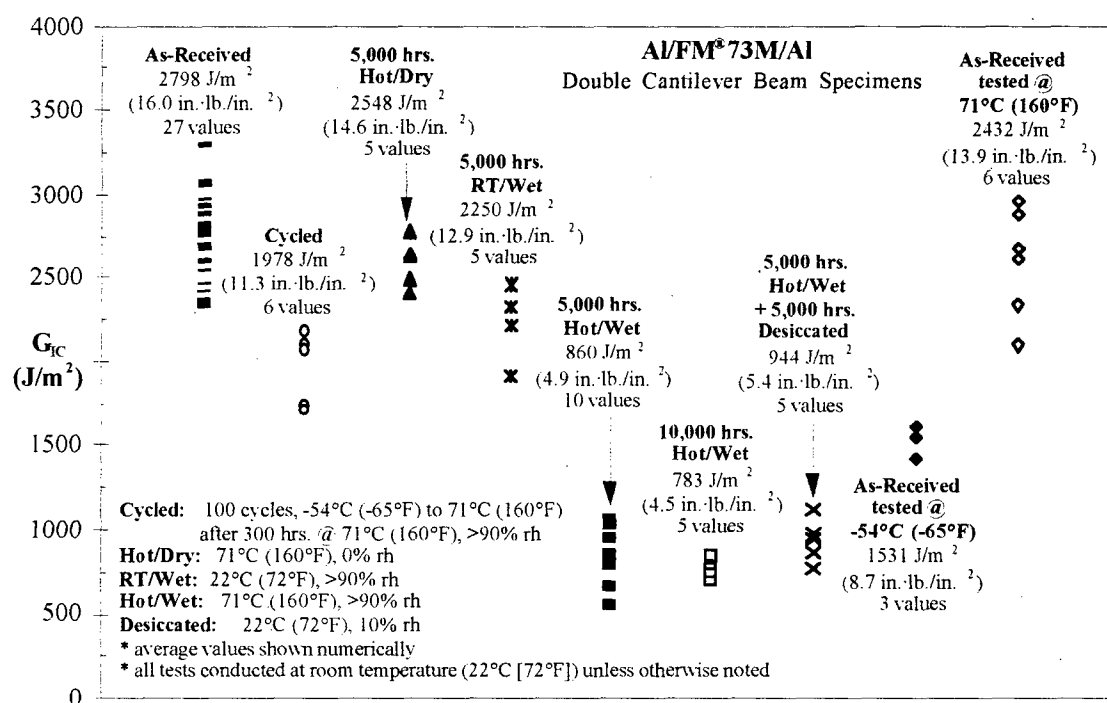


Figure 64. Mode I fracture toughness of the Al/FM[®]73/Al bonded system

Test temperature also had a significant effect on the toughness. Testing at -54°C (-65°F) resulted in a 45% lower G_{IC} . Since this temperature is far below the 100°C (212°F) T_g of the adhesive, the reduction in toughness is most probably caused by embrittlement at the lower temperature.

A version of Figure 64 with confidence intervals can be found in Appendix B.

Crack progression in the fracture toughness specimens was cohesive. The crack propagated through the middle of the adhesive layer, relatively distant from either adhesive-adherend interface, leaving an adhesive layer on both adherends. (Fig. 65) Fracture surfaces showed evidence of some distributed porosity within the bond line consisting mainly of pores with diameters of 1.5 mm (0.06 in) or less. During testing, scrim cloth fibers bridged the open crack mouth for approximately 5 mm (0.20 in) behind the crack tip. The shape of the crack front was slightly curved with the interior advancing 1-2 mm (0.04 - 0.08 in) ahead of the edges.

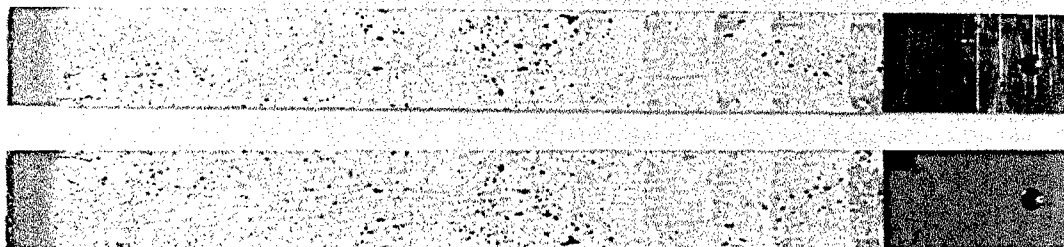


Figure 65. Fracture surfaces of the Al/FM[®]73M/Al bonded system

No significant differences were noted among the fracture surfaces of the monotonic toughness specimens exposed to the various environments. Although some discoloration was discovered around the edges of interior voids, the fracture path was always cohesive. This suggests that the surface preparation for the aluminum was adequate for the environmental conditions examined. In addition, it also implies that the changes in the Mode I fracture toughness are due to changes in the adhesive. Recall that RT/wet and hot/wet exposure also reduced ultimate and yield strength values as well as plane stress fracture toughness values of the FM[®]73M adhesive film specimens. In addition, RT/wet and hot/wet exposure also reduced the glass transition temperature which signals a change in the polymer structure that may be linked to the changes in the toughness.

Mode I fatigue testing of the Al/FM[®]73M/Al specimens showed that the fatigue crack growth behavior of this system was affected by long-term isothermal exposure to a "hot/wet" environment but not (noticeably) by thermal cycling. (Fig. 66) Isothermal exposure shifted the da/dN vs. ΔG_I locus to the left, significantly reducing the threshold level of applied strain energy release rate ($\Delta G_{I,th}$). The threshold level is defined as 10^{-6} mm/cycle. However, the slope of the data was unaffected by the exposure. This slope, a measure of the sensitivity of crack growth rate to changes in the applied load or strain energy release rate, had a value of approximately 4, twice that of aluminum.¹³⁵ This

indicates the high degree of sensitivity displayed by crack growth in the adhesive bond line. Crack growth in the fatigue specimens was also cohesive.

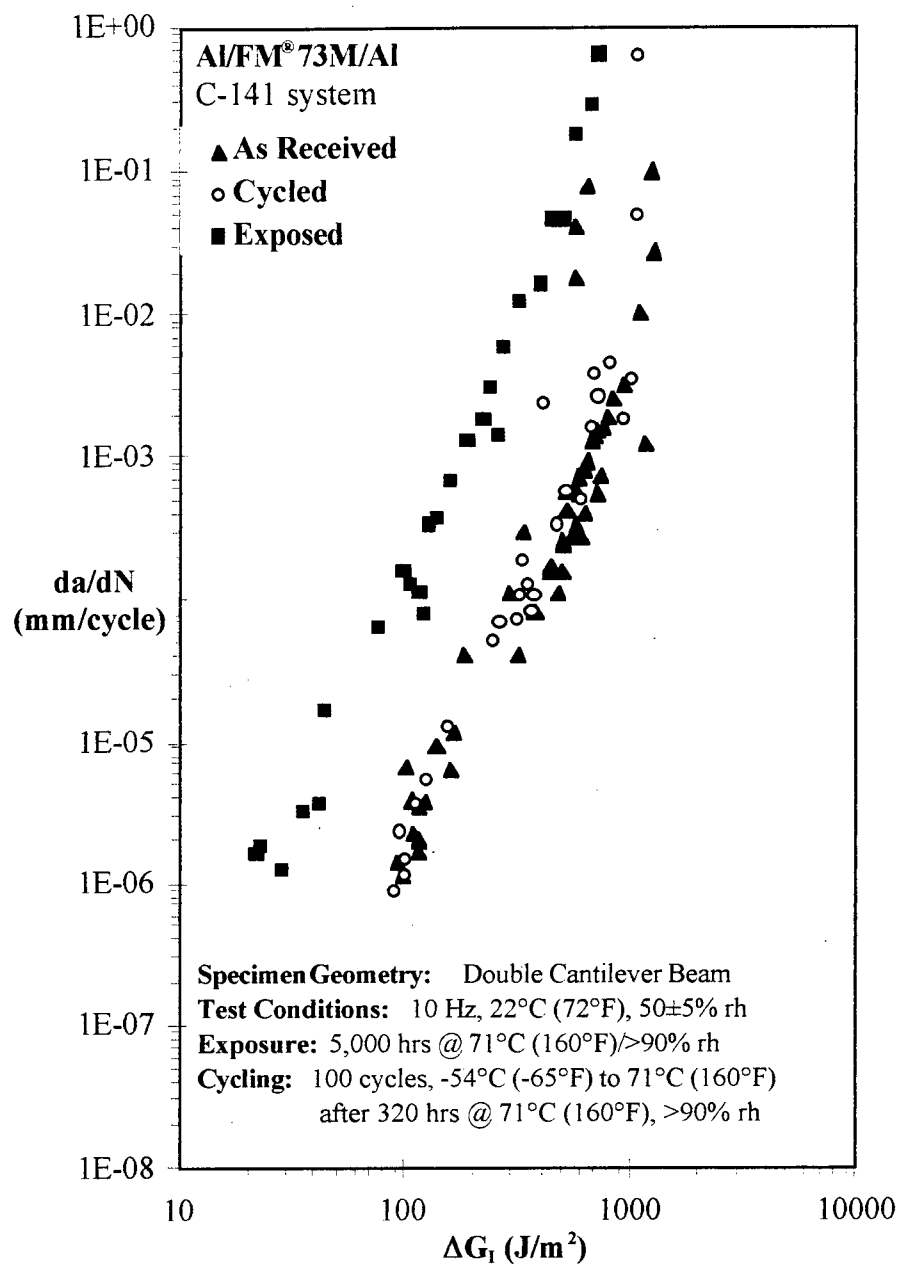


Figure 66. Mode I fatigue behavior of the Al/FM[®]73/Al bonded system.

8.2.1.2. Mode II (ENF)

Attempting to determine the Mode II fracture toughness of the Al/FM[®]73/Al bonded system was challenging. The initial specimen design did not anticipate that the fracture toughness of the adhesive would be as high as it proved to be. Therefore, for the majority of the ENF tests conducted on Al/FM[®]73/Al specimens, yielding in the adherends was observed prior to crack growth. Under these circumstances, only a lower bound of approximately 1000 J/m² (5.7 in.-lb./in.²) could be established. This maximum applied G_{II} level was attained in all specimens with no crack growth except for the specimen subjected to 10,000 hours under hot/wet conditions. Cracking occurred in this specimen at approximately this lower bound value of 1000 J/m². Thus the 10,000 hour exposure condition may be deemed most detrimental, but the severity of the other environments on the Mode II fracture toughness of the Al/FM[®]73/Al system cannot be gauged.

Crack growth in the specimen exposed to 10,000 hours of hot/wet conditioning was cohesive. The fracture surface was very similar to that observed in the double cantilever beam specimens. Two small, 4 mm (0.16 in.) regions in the cracked region revealed exposed and slightly corroded aluminum. One specimen in the as-received condition was tested past yielding to fail the bond line. This fracture path, too, was cohesive. However, due to the large relative motion between the adherends, the fracture surface was macroscopically rough.

No fatigue testing was performed on the ENF specimens.

8.2.1.3. *Mixed Mode (CLS)*

Monotonic testing of CLS specimens from the Al/FM[®]73/Al system was also difficult again due to improper estimation of the toughness of the adhesive during planning stages for this research. A finite element analysis showed that these specimens would yield at loads (approximately 25 kN [5.6 kips]) which produced a total strain energy release rate at the crack tip of only 815 J/m² (4.7 in.·lb./in.²). However, much higher loads were experienced by all specimens prior to observed bond line cracking. Cracking was observed in most specimens only after a load of 50 kN (11.2 kips) or more was reached. Gross yielding of the strap at these loads and a Mode III contribution caused by Poisson's ratio effects undoubtedly fostered crack growth at these high post-yield loads. Such behavior was visually apparent during testing. Thus, specimens in the as-received condition and subject to all forms of exposure exhibited mixed mode monotonic toughness values in excess of 815 J/m² (4.7 in.·lb./in.²).

However, it should be noted that cracking in the monotonic fracture toughness specimens was observed in specimens subjected to 5,000 and 10,000 hours of hot/wet exposure at loads 20% lower than those required to cause cracking in the other specimens. This observation, though based on post-yield behavior, does suggest that the effect of environmental exposure to a high temperature, high humidity atmosphere decreased the

mixed mode fracture toughness of the Al/FM[®]73M/Al system in the same general manner as it affected the Mode I and (possibly) Mode II behavior.

Difficulties were also experienced with the fatigue testing of the Al/FM[®]73/Al CLS specimens. Four specimens were tested at 10 Hz with $R = 0.1$. Because the maximum load which could be applied without yielding the strap was so low, very little crack growth was observed before the straps on the tested specimens failed in fatigue.

In an attempt to prevent fatigue failure of the strap, one specimen was shot-peened prior to testing. Peening was performed by Delta Airlines maintenance personnel at their facility in Atlanta, GA. The process involved 100% coverage of the entire bonded Al/FM[®]73M/Al CLS specimen at a 0.014 Almen A intensity, a standard industrial procedure for aluminum. Unfortunately, shot-peening failed to prevent fatigue failure from occurring in the strap prior to cracking in the bond line.

The limited fatigue data obtained showed crack growth rates on the order of 5×10^{-5} mm/cycle (2×10^{-6} in./cycle) at an applied total strain energy release rate range (ΔG_T) of 500 J/m^2 ($2.9 \text{ in.}\cdot\text{lb./in.}^2$). This crack growth rate is similar, but slightly lower than that displayed by the DCB specimens tested in fatigue at a comparable level of ΔG_I . The small regions of cracking observed appeared to be mainly cohesive, but near the strap/adhesive interface.

8.2.1.4. Summary of Test Results for the Al/FM[®]73M/Al System

This section presents a brief synopsis of results from tests performed on the Al/FM[®]73M/Al bonded system. Figure 67 presents a graphical summary of the toughness data obtained from this bonded joint system and may be compared with Figure 1 and Figure 4a described previously in this report.

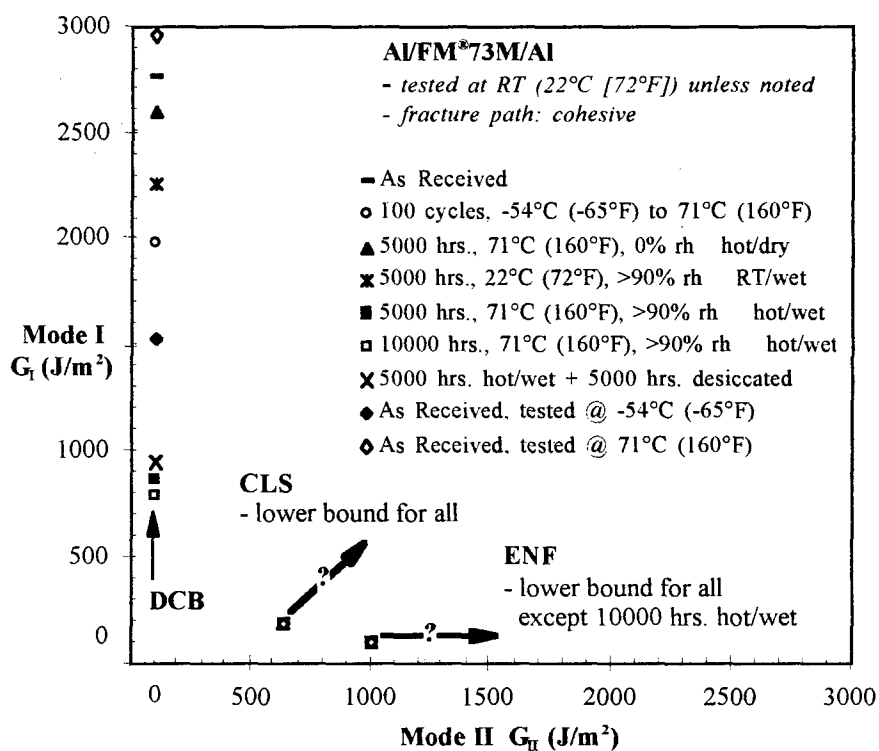


Figure 67. Summary of fracture toughness data for the Al/FM[®]73M/Al bonded system

- Mode I Fracture Toughness (via DCB tests):
 - as-received value: $G_{Ic} \approx 2800 \text{ J/m}^2$ (16.0 in.·lb./in.²)
 - reduced:
 - ~ 20% by 5,000 hours hot/dry exposure
 - ~ 30% by 100 thermal cycles
 - ~ 45% by testing at -54°C (-65°F)
 - ~ 70% by 5,000 and 10,000 hours hot/wet exposure
 - reduction by hot/wet exposure not recovered by desiccation at RT
- Mode I Fatigue Behavior (via DCB tests):
 - as-received & thermal cycled threshold: $\Delta G_I \sim 100 \text{ J/m}^2$ (0.6 in.·lb./in.²)
 - reduced: ~ 60% by 5,000 hours hot/wet exposure
 - high crack growth rate sensitivity ($n \approx 4$) unaffected by exposure
- Mode II Fracture Toughness (via ENF tests):
 - unable to determine due to adherend yielding
 - lower bound established at $G_{IIc} \approx 1000 \text{ J/m}^2$ (5.7 in.·lb./in.²)
 - specimen exposed for 10,000 hours to hot/wet conditions exhibited bond line cracking near yield load indicating that this exposure condition was most severe
- Mixed Mode I/II Fracture Toughness (via CLS tests):
 - unable to determine due to adherend yielding
 - lower bound established at $G_{Tc} \approx 815 \text{ J/m}^2$ (4.7 in.·lb./in.²)

- specimens exposed for 5,000 and 10,000 hours to hot/wet conditions failed at lowest (post-yield) loads indicating that these exposure conditions were most severe
- Mixed Mode I/II Fatigue Behavior (via CLS tests):
 - unable to determine due to fatigue failures in strap
- Fracture Path:
 - cohesive for DCB and ENF specimen geometries
 - appeared cohesive but near strap adhesive interface for CLS geometry
 - surface preparation appeared adequate for environmental conditions examined; no interfacial failures observed

8.2.2. Al/FM[®]73M/B-Ep

The Al/FM[®]73M/B-Ep system was examined because it is the same material system widely used for adhesively bonded aircraft repair. Thus, its durability is paramount for the safe operation of several hundred aging military and civilian aircraft worldwide.

One group of specimens was tested in the as-received state with no pre-test environmental exposure. A second group was subjected to 100 thermal cycles between -54°C (-65°F) and 71°C (160°F) after being exposed for 300 hours to hot/wet conditions 71°C (160°F), >90% rh, prior to mechanical testing. A third group was subjected to 5,000 hours of hot/wet isothermal exposure at 71°C (160°F), >90% rh, prior to

mechanical testing. A fourth group was subjected to 5,000 hours of hot/wet isothermal exposure followed by 5,000 of desiccation at 22°C (72°F), 10% rh, , prior to mechanical testing.

Al/FM[®]73M/B-Ep bonded joint specimens subjected to long-term exposure were periodically weighed and observed. Figure 68 shows the weight changes resulting from exposure. As expected, the specimens exposed to hot/wet conditions gained weight due to moisturization while those exposed to hot/dry conditions lost weight due to moisture loss. These weight changes were nearly an order of magnitude higher than those experienced by the Al/FM[®]73M/Al bonded joint specimens because the boron-epoxy adherends also sustained moisturization. However, as with the Al/FM[®]73M/Al bonded joint specimens, the small area of exposed adhesive and the relatively massive adherends kept weight change magnitudes much lower than those experienced by the FM[®]73U adhesive. Unlike the Al/FM[®]73M/Al specimens, the Al/FM[®]73M/B-Ep specimens desiccated at 10% rh for 5,000 hours following 5,000 hours of exposure to hot/wet conditions did lose most of their weight gained during moisturization..

Surface observations did not show any changes in the color of the bond line nor did subsequent fracture testing reveal any color changes on the fracture surface. However, the mode of fracture was always adhesive (at or near the adhesive/boron-epoxy interface). Therefore, any color changes in the adhesive observed on the cohesive fracture surfaces of the Al/FM[®]73M/Al specimens were undetectable on the Al/FM[®]73M/B-Ep specimens.

Considerable corrosion was also seen on the exterior aluminum surfaces of the Al/FM[®]73M/B-Ep specimens which were exposed to high humidity conditions.

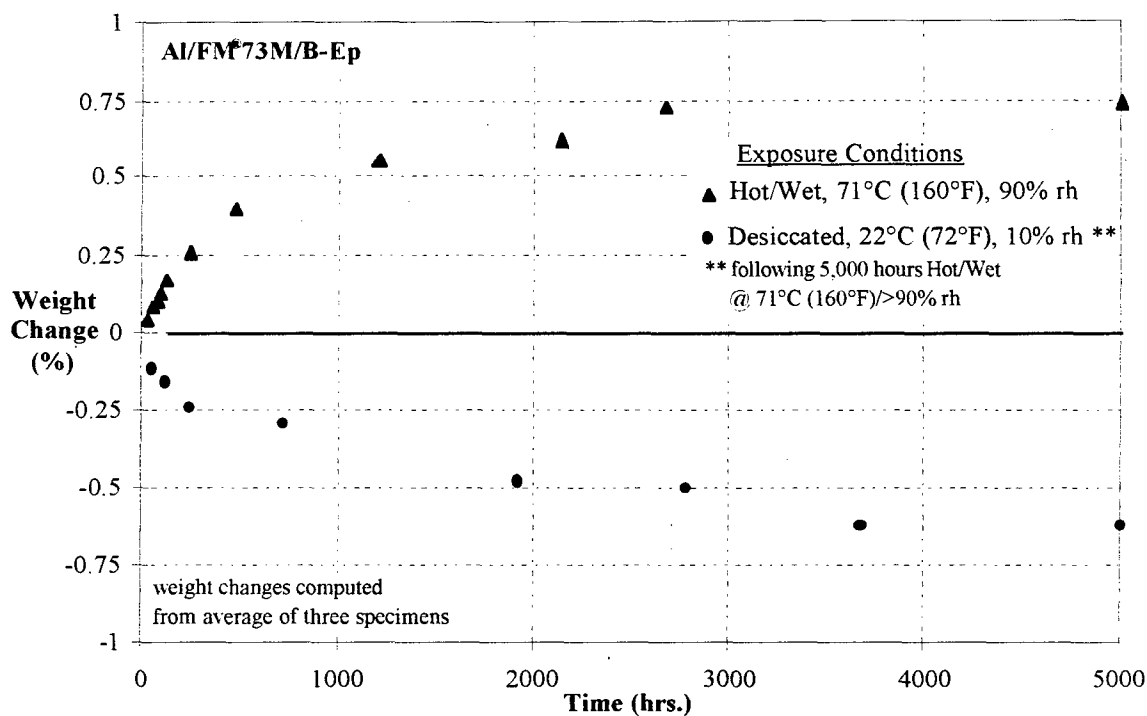


Figure 68. Weight changes in Al/FM[®]73M/B-Ep bonded joint specimens due to exposure

8.2.2.1. Mode I (DCB)

Although it employed the same adhesive, the Al/FM[®]73M/B-Ep system's fracture toughness was significantly less than that of the Al/FM[®]73M/Al system. For specimens similarly exposed and subjected to the same test conditions, the fracture

toughness of the Al/FM[®]73M/B-Ep system was an average of 65% lower than the fracture toughness of the Al/FM[®]73M/Al system.

The as-received fracture toughness of the Al/FM[®]73M/B-Ep system was approximately 840 J/m² (4.8 in.·lb./in.²). As with the Al/FM[®]73M/Al system, the thermally cycled, isothermally exposed, exposed-then-desiccated, and cold tested specimens revealed significant losses in fracture toughness. (Fig. 69) Appendix B contains a version of Figure 69 which displays confidence intervals and identifies the amount of the fracture toughness attributed to Modes I and II.

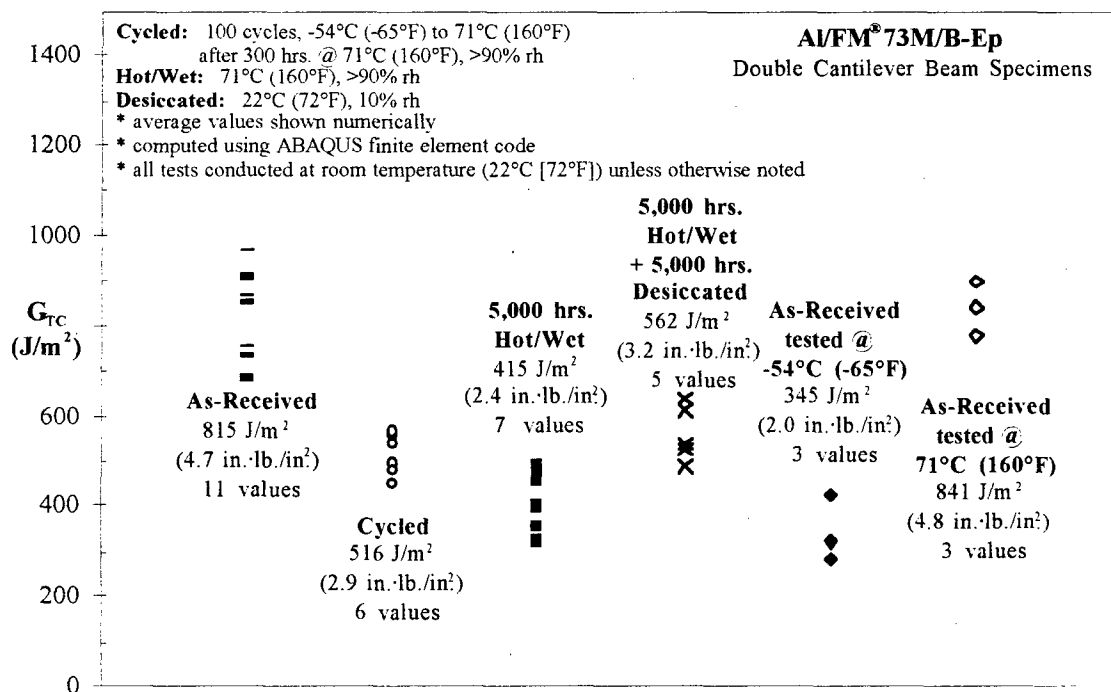


Figure 69. Fracture toughness of the Al/FM[®]73/B-Ep DCB specimens

Note that the fracture toughness of the Al/FM[®]73M/B-Ep system is expressed in terms of G_T to reflect the presence of G_I and G_{II} , whereas the fracture toughness of the Al/FM[®]73M/Al system was expressed in terms of G_I (which is equivalent in the case of similar adherends to G_T .)

Again, as with the Al/FM[®]73M/Al system, no evidence of aluminum surface corrosion within the bonded area was found on these specimens. Thus, the surface preparation of the aluminum was sufficient. The low toughness values of this system, however, can be attributed to the location of the crack path which was adhesive at or near the adhesive/composite interface in all cases. Figure 70 portrays this feature of the Al/FM[®]73M/B-Ep specimens.

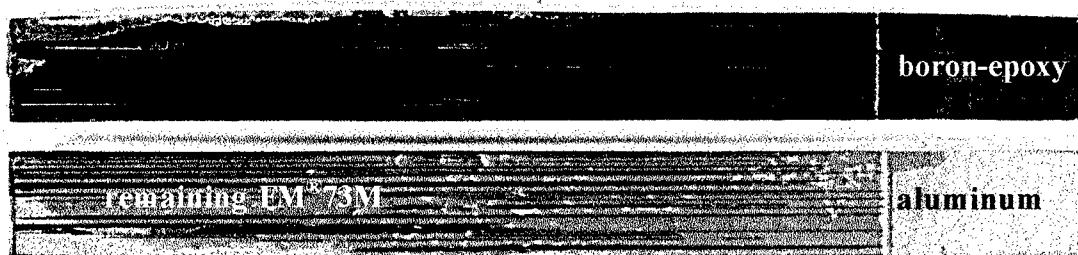


Figure 70. Fracture surfaces of the Al/FM[®]73M/B-Ep bonded system

Visual and reflective FTIR spectroscopic inspection of the fracture surface indicated that the crack path in these specimens was generally in the matrix layer of the composite adherend near the adhesive-composite interface. The exact location with

respect to the interface was undetermined. However, fiber bridging, a lack of adhesive on the fracture surface of the boron-epoxy, regions of the patterned resin-rich layer from the composite found on the fracture surface of the adhesive suggest that cracking occurred in the composite but between the fibers and the FM[®]73M adhesive. This characteristic should support further investigation of improvements to this crucial interfacial region, to composite surface preparation, and to the properties of the boron-epoxy matrix material. Mode I fatigue testing of the Al/FM[®]73M/B-Ep specimens showed similar trends as the Al/FM[®]73M/Al system. Fatigue crack growth behavior was affected by long-term isothermal exposure to a "hot/wet" environment but not (noticeably) by thermal cycling. (Fig. 71) Isothermal exposure shifted the da/dN vs. ΔG_T locus to the left, effectively reducing the threshold level (10^{-6} mm/cycle) of applied strain energy release rate ($\Delta G_{T,th}$) by approximately 50% or more. However, the slope of the data was unaffected by the exposure. Comparison of the fatigue data from the Al/FM[®]73M/Al and Al/FM[®]73M/B-Ep systems reveals that the slope of the Al/FM[®]73M/B-Ep data ($\approx 8-12$) is approximately double that of the Al/FM[®]73M/Al. This suggests an even greater sensitivity of crack growth rate to applied G values and is consistent with the lower fracture toughness of the Al/FM[®]73M/B-Ep system.

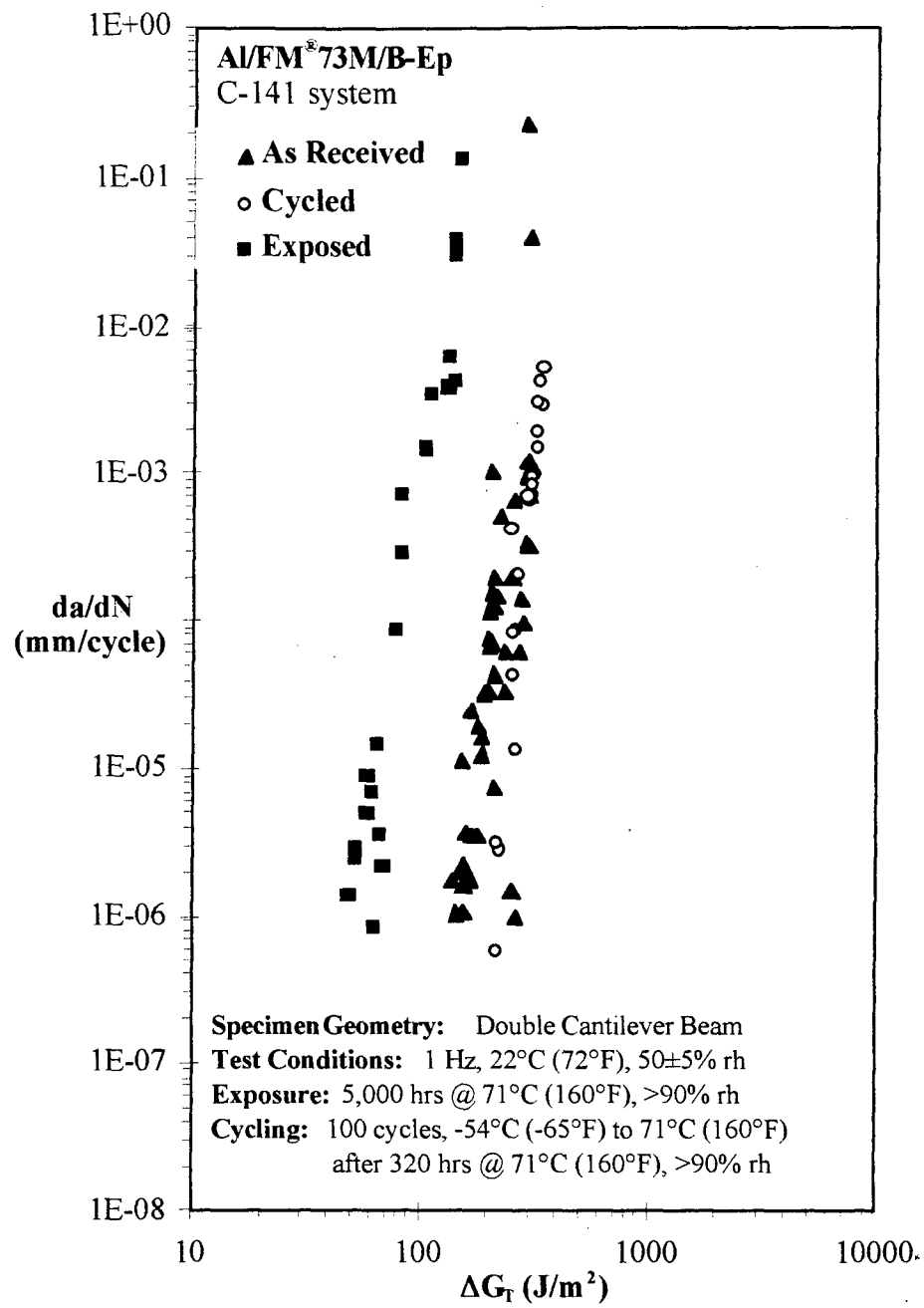


Figure 71. Fatigue behavior of the Al/FM[®]73/B-Ep bonded system

Crack growth in the fatigue specimens, as was the case in the fracture toughness specimens, was in the composite matrix at or near the composite/adhesive interface.

8.2.2.2. *Mixed Mode (CLS)*

Two forms of Al/FM[®]73M/B-Ep CLS specimen were tested. One was fabricated with an aluminum strap and a boron-epoxy lap, and the other used a boron-epoxy strap with an aluminum lap.

Aluminum Strap - These specimens experienced the same problems as did the Al/FM[®]73M/Al CLS specimens. The load required to yield the aluminum strap was much lower than that needed to cause crack growth in most of the specimens. A lower bound of approximately 930 J/m^2 ($5.3 \text{ in.}\cdot\text{lb./in.}^2$) at the yield load was determined using finite element analysis. However, the specimen exposed to hot/wet conditions displayed crack growth at a G_T level of approximately 340 J/m^2 ($1.9 \text{ in.}\cdot\text{lb./in.}^2$), and the specimen tested at 71°C (160°F) displayed crack growth as low as 65 J/m^2 ($0.4 \text{ in.}\cdot\text{lb./in.}^2$). The former result is consistent with an estimated lower toughness in the hot/wet exposed Al/FM[®]73M/Al CLS system. The result from the test conducted at 71°C (160°F) is inconsistent with the DCB tests conducted at the same temperature which exhibited a toughness nearly the same as that obtained from a test conducted at room temperature. However, the reason for this inconsistency is unknown at this time.

Boron-Epoxy Strap - These specimens exhibited vastly different behavior and experienced cracking at relatively low loads. Crack growth occurred in the composite matrix near the adhesive/strap interface and in a slow, controlled manner. Again, the specimen exposed for 5,000 hours to a hot/wet environment exhibited a lower G_{TC} . (Fig. 72) In addition, the specimen tested at -54°C (-65°F) also failed at a much lower level of applied strain energy release rate. These two occurrences fit the pattern of decreasing toughness with bond line moisture content and also with a decrease in the test temperature. However, it should be stressed that these results are single values from single specimens, and, therefore, only suggest possible trends.

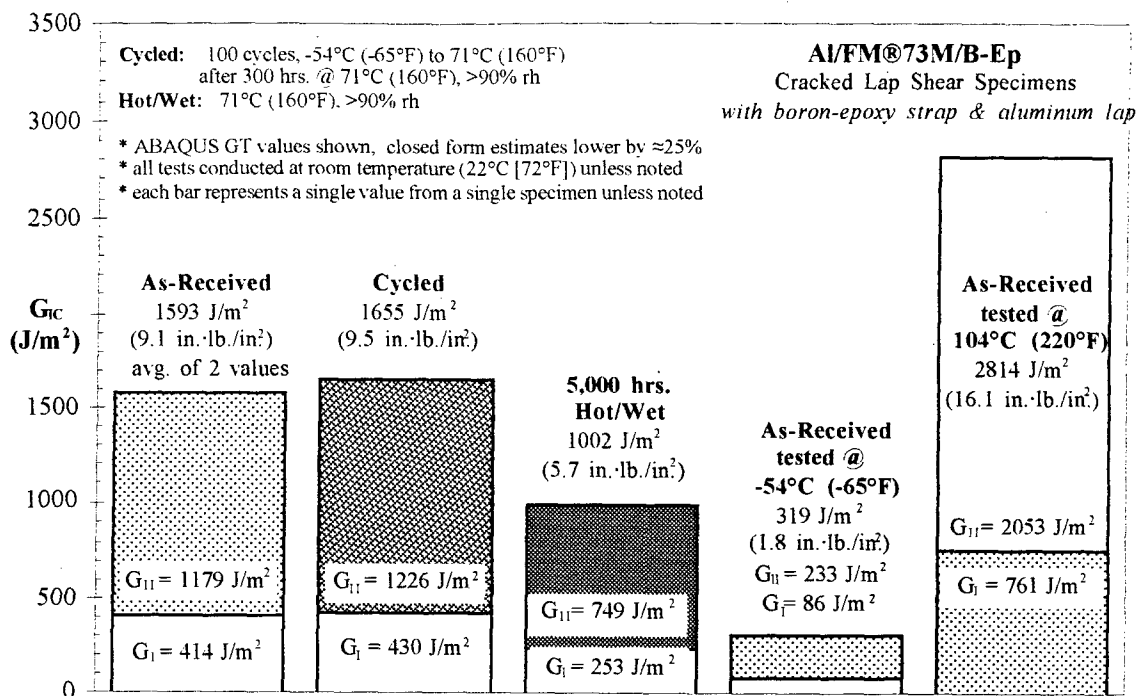


Figure 72. Mixed mode fracture toughness of Al/FM®73M/B-Ep CLS specimens with boron-epoxy straps

- Primarily Mode I Fracture Toughness (via DCB tests):
 - as-received value: $G_{Tc} \approx 815 \text{ J/m}^2$ (4.7 in.·lb./in.²)
 - reduced:
 - ~ 35% by 100 thermal cycles
 - ~ 50% by 5,000 hours hot/wet exposure
 - ~ 55% by testing at -54°C (-65°F)
 - reduction by hot/wet exposure not recovered by desiccation at RT
 - much lower toughness values than Al/FM[®]73M/Al system
- Primarily Mode I Fatigue Behavior (via DCB tests):
 - as-received & thermally cycled threshold: $\Delta G_T \approx 100 \text{ J/m}^2$ (0.6 in.·lb./in.²)
 - reduced: ~ 50% by 5,000 hours hot/wet exposure
 - extremely high crack growth rate sensitivity ($n \approx 10$) unaffected by exposure
- Mixed Mode I/II Fracture Toughness (via CLS tests, Al strap):
 - unable to determine due to adherend yielding
 - lower bound established at $G_{Tc} \approx 930 \text{ J/m}^2$ (5.3 in.·lb./in.²)
- Mixed Mode I/II Fracture Toughness (via CLS tests, B-Ep strap):
 - as-received value: $G_{Tc} \approx 1600 \text{ J/m}^2$ (9.2 in.·lb./in.²)
 - reduced:
 - ~ 35% by 5,000 hours hot/wet exposure
 - ~ 80% by testing at -54°C (-65°F)

- Fracture Path:
 - in matrix of boron-epoxy for all specimen geometries
 - boron-epoxy adherend devoid of F M[®]73M adhesive after fracture
 - some boron fibers embedded in adhesive remaining on aluminum adherend

8.2.3. Gr-BMI/AF-191M/Gr-BMI

Two sets of these specimens using materials from the F-22 fighter aircraft were fabricated and tested. The first set consisted of primarily unidirectional adherends intended simply to represent the graphite-bismaleimide and AF-191 adhesive materials and fabrication process. The second set consisted of quasi-isotropic adherends intended to simulate actual production parts in all aspects including composite ply lay-up.

One group of unidirectional specimens was tested in the as-received state with no pre-test environmental exposure. A second group was subjected to 100 thermal cycles between -54°C (-65°F) and 104°C (220°F) after being exposed for 300 hours to hot/wet conditions 71°C (160°F), >90% rh, of prior to mechanical testing. A third group was subjected to 5,000 hours of hot/dry isothermal exposure at 104°C (220°F), 0% rh, prior to mechanical testing. A fourth group was subjected to 10,000 hours of hot/dry isothermal exposure, prior to mechanical testing.

Because of the limited number of quasi-isotropic specimens available, they tested only in the as-received and thermally cycled states.

Specimens subjected to long-term hot/dry exposure were periodically weighed and observed. Figure 74 shows the weight losses resulting from exposure. As expected, the weight of the specimens decreased as moisture was lost. However, as with the Al/FM[®]73M/Al and Al/FM[®]73M/B-Ep specimens, the small area of exposed adhesive and the relatively massive adherends kept weight change magnitudes much lower than those experienced by the AF-191U adhesive.

Surface observations revealed the same color change as noted with the AF-191U adhesive specimens which were exposed to hot/dry conditions. The normally pale yellow color of the adhesive began to darken after approximately 200 hours of exposure becoming dark brown by 5,000 hours. This color change was noted only on the exposed surfaces of the AF-191M adhesive. Regions in the interior of the bonded specimens retained a pale yellow color even after 10,000 hours of exposure to a hot/dry environment. No other changes were noted in the appearance or physical makeup of the exposed Gr-BMI/AF-191M/Gr-BMI specimens.

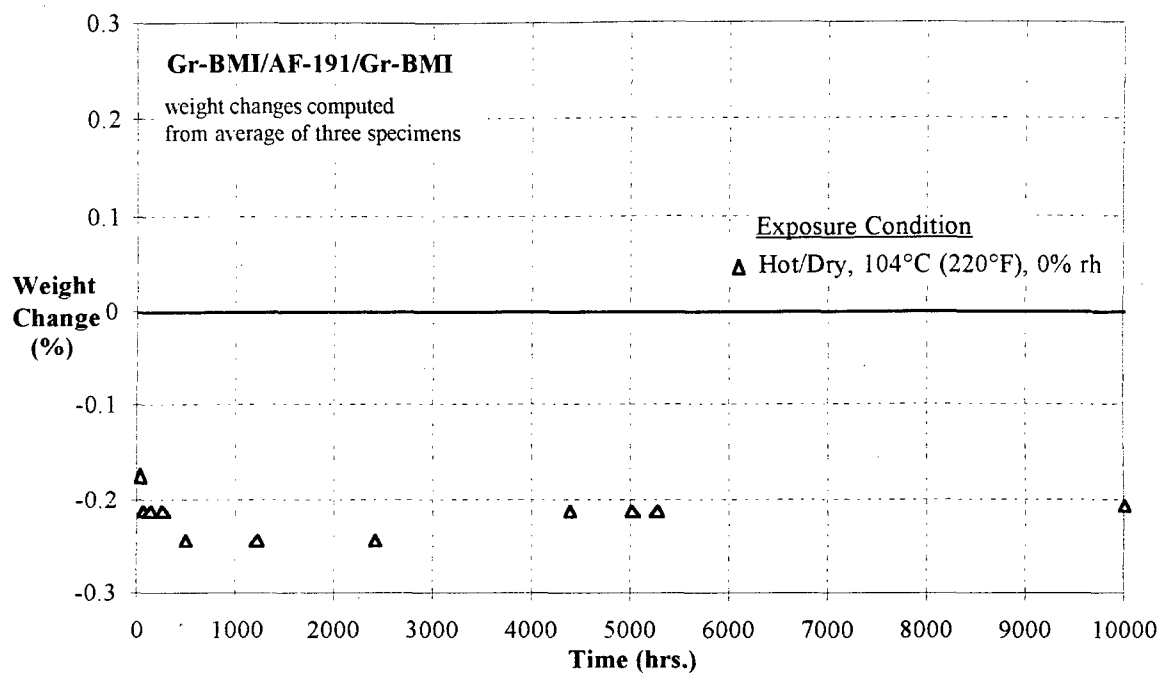


Figure 74. Weight changes in Gr-BMI/AF-191M/Gr-BMI bonded joint specimens due to exposure

8.2.3.1. Mode I (DCB)

The Mode I fracture toughnesses of the Gr-BMI/AF-191/Gr-BMI specimens subjected to various environments are shown in Figures 75-76. (Versions of these figures with estimated confidence intervals may be found in Appendix B.) Significant differences appear only between as-received and exposed values for the unidirectional adherend specimens and between the specimens with quasi-isotropic adherends and their unidirectional counterparts. The former difference, a drop of approximately 20% for the

exposed specimens, is consistent with an observed reduction in the failure strain of the AF-191 adhesive film with exposure.

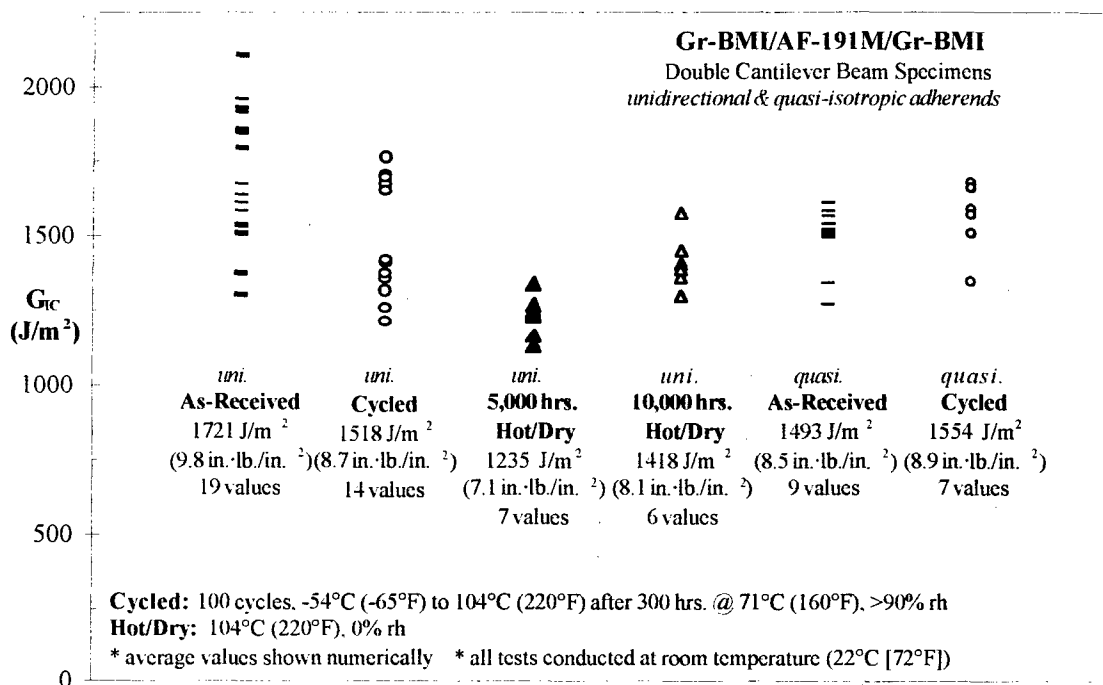


Figure 75. Effect of environmental exposure on the Mode I fracture toughness of the Gr-BMI/AF-191/Gr-BMI bonded system

The difference between specimens with unidirectional and quasi-isotropic adherends was also evident in the results of tests conducted at reduced and elevated temperatures. (Figs. 75 and 76) In these tests, G_{IC} for the specimens with unidirectional adherends was most reduced at 104°C (220°F) while the toughness of the specimens with quasi-isotropic adherends was reduced most by specimens tested at -54°C (-65°F).

These differences due to adherend lay-up appear to be due chiefly to the fracture path observed during testing.

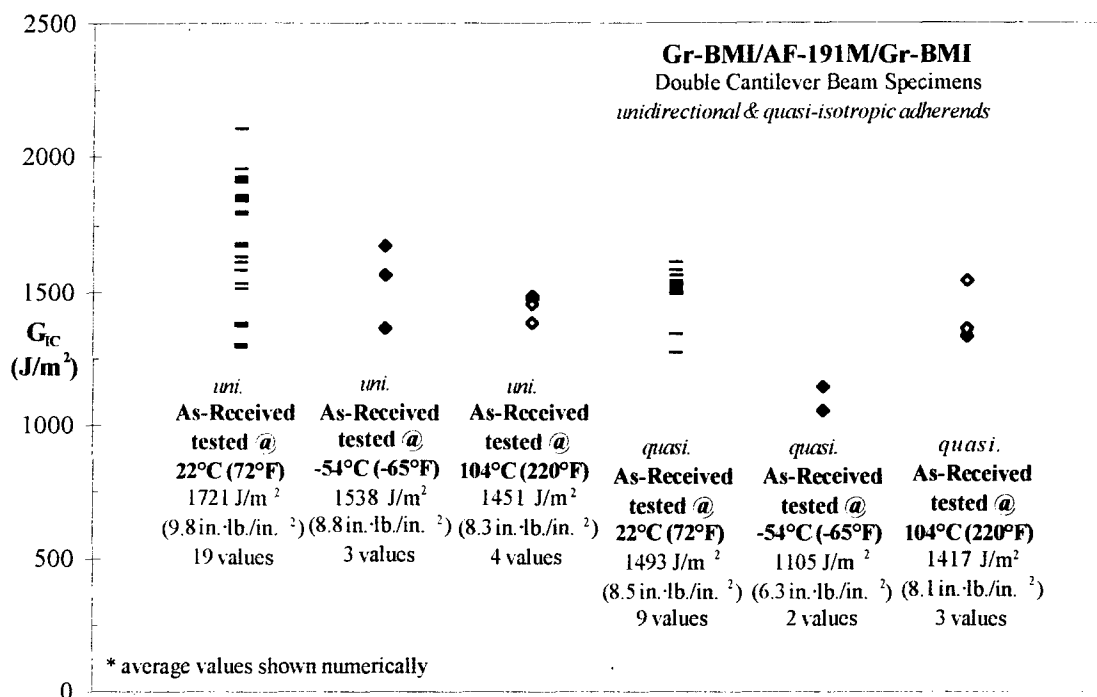


Figure 76. Effect of test temperature on the Mode I fracture toughness of the Gr-BMI/AF-191/Gr-BMI bonded system

The crack path for the Gr-BMI/AF-191/Gr-BMI with unidirectional adherends was, in general, cohesive. However, because the scrim cloth within the AF-191 was located closer to one face of the adhesive film, the crack path was offset towards one adherend and followed the plane of the scrim cloth. The crack front was nearly straight

across the adherends with little evidence of “tunneling” in which the interior portion of the crack grows more rapidly than that located near the edge.

In specimens containing quasi-isotropic adherends, the crack often departed from the adhesive layer and caused interlaminar cracking within the $\pm 45^\circ$ plies. These plies were located at the bond line, and their cracking indicates the importance of placing a 0° ply at the adhesive-adherend interface to prevent cracks from growing into composite adherends. (Fig. 77)

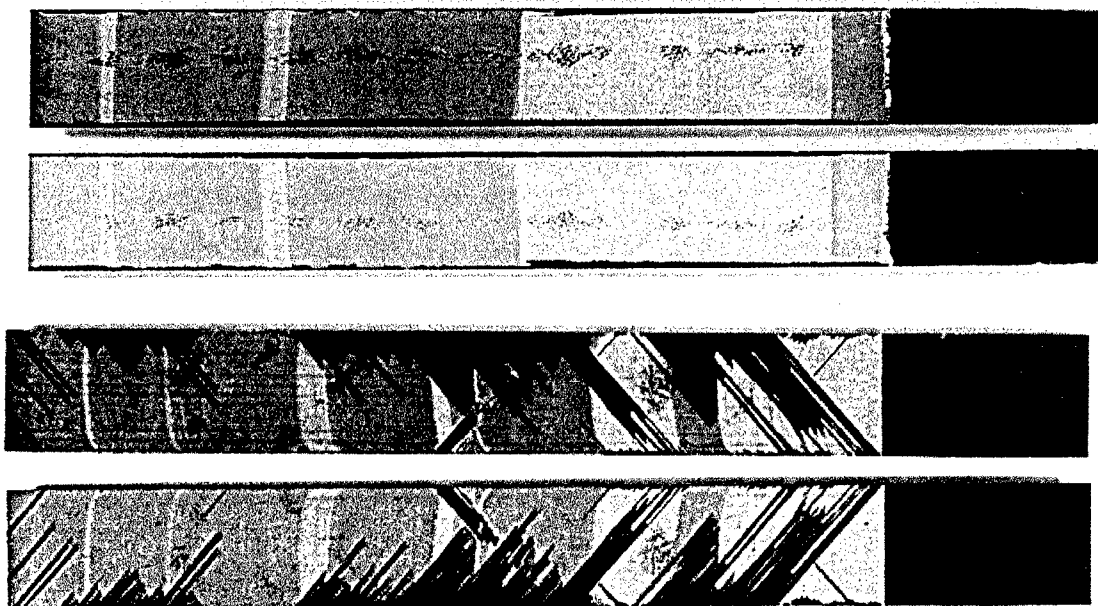


Figure 77. Fracture surfaces of the Gr-BMI/AF-191/Gr-BMI bonded systems
upper pair: unidirectional adherends, lower pair: quasi-isotropic adherends
scrim cloth was located closest to surface of top adherend of each pair

The lower G_{IC} values for the quasi-isotropic adherends may depend upon the observed difference in crack path. Cracking within the $\pm 45^\circ$ plies of the quasi-isotropic specimens occurred because the Mode I delamination strength of the graphite-bismaleimide was lower than that of the AF-191M adhesive. Wilkins¹⁰⁰ also noticed the same trend in crack location depending on ply orientation at the bond line. He found that the Mode I fracture toughness of a Gr-BMI system (T-300/V37A) varied between 137 J/m² (0.78 in. \cdot lb./in.²) at -54°C (-65°F) to 149 J/m² (0.85 in. \cdot lb./in.²) at 22°C (72°F) to 144 J/m² (0.82 in. \cdot lb./in.²) at 149°C (300°F). Though these values are low compared to the toughness exhibited by the quasi-isotropic specimens, fiber bridging observed during testing of the DCB specimens may have contributed to the overall toughness of the specimens. The path of the crack through the near-bond line plies in the quasi-isotropic system rather than through the adhesive layer resulted in the fracture toughness of the quasi-isotropic system being lower than its unidirectional counterpart.

Limited fatigue data from this system suggest a trend exhibited by the Al/FM[®]73M/Al and Al/FM[®]73M/B-Ep systems: no discernible difference in crack growth behavior between the as-received and thermally cycled specimens. (Fig. 78) The slope of the crack growth data is approximately 6, again indicating a relatively high degree of sensitivity to small changes in the applied load or strain energy release rate. Cracking was cohesive and exhibited the same characteristics as described for the monotonic tests.

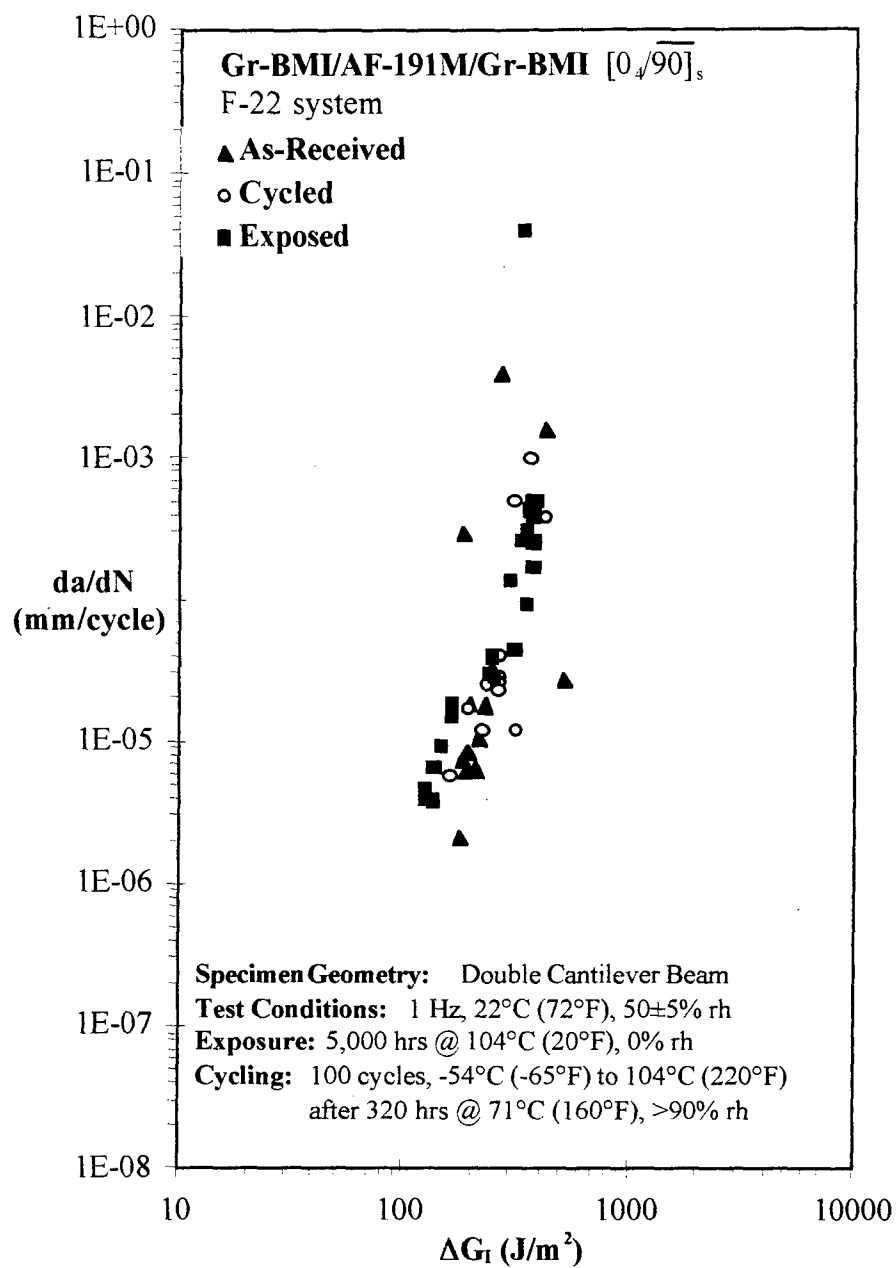


Figure 78. Mode I fatigue behavior of the Gr-BMI/AF-191M/Gr-BMI bonded system

8.2.3.2. Mode II (ENF)

Mode II fracture toughness testing of the Gr-BMI/AF-191M/Gr-BMI revealed no significant differences in G_{IIC} among the specimens subjected to various exposure conditions. (Fig. 79; a version of this figure displaying estimated confidence intervals may be found in Appendix B). The mode II toughness of the unidirectional system was approximately 3000 J/m^2 ($17.1 \text{ in.}\cdot\text{lb./in.}^2$) or nearly twice that of the Mode I fracture toughness. No significant effects of exposure were observed.

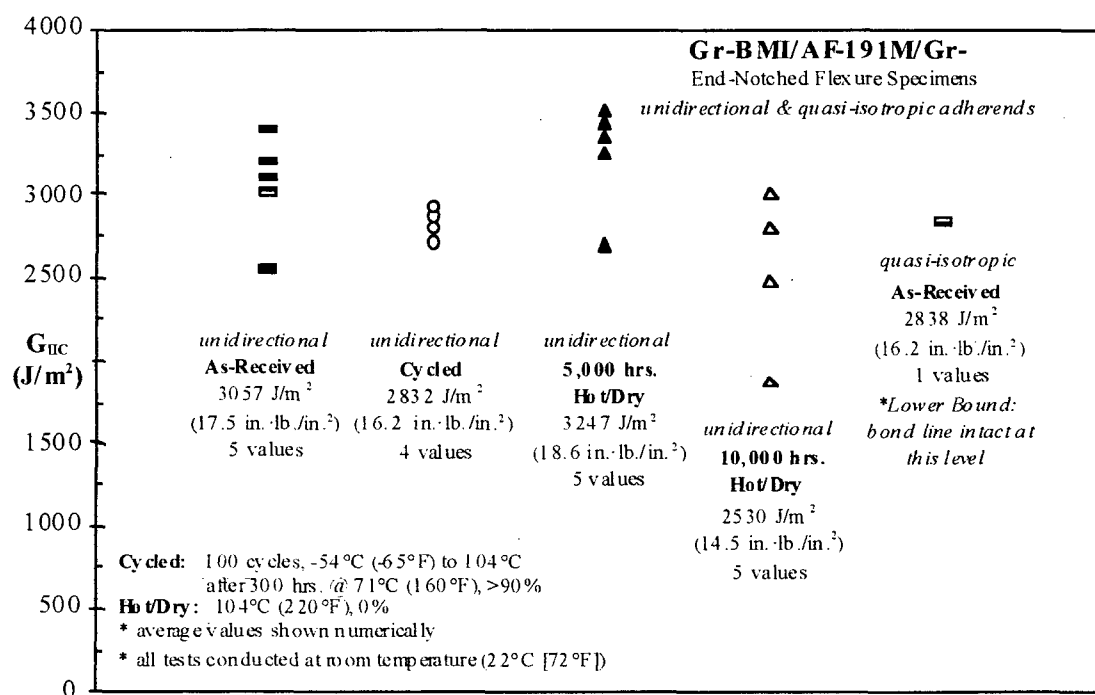


Figure 79. Mode II fracture toughness of the Gr-BMI/AF-191/Gr-BMI bonded system

Testing of the quasi-isotropic Gr-BMI/AF-191M/Gr-BMI system revealed a similar lower bound for the fracture toughness. However, testing was curtailed prior to the formation of a crack because the adherends failed in compression at the loading points.

8.2.3.3. *Mixed Mode (CLS)*

Figure 80 shows the results of tests conducted on cracked lap shear specimens from the unidirectional Gr-BMI/AF-191/Gr-BMI bonded systems. Crack growth in all specimens was catastrophic and appeared to occur in the matrix layer of the composite strap nearest to the adhesive/strap interface. This resulted in no adhesive remaining on the strap and a small number of fibers embedded in the adhesive remaining on the lap. One exception to this was the specimen tested at 104°C (220°F) which experienced tensile failure of the strap before crack growth occurred. Because of the nature of the crack growth, only one value was obtained for each sample. However, it does appear that the mixed mode fracture toughness was adversely affected by testing at -54°C (-65°F), the typical high altitude subsonic cruise condition.

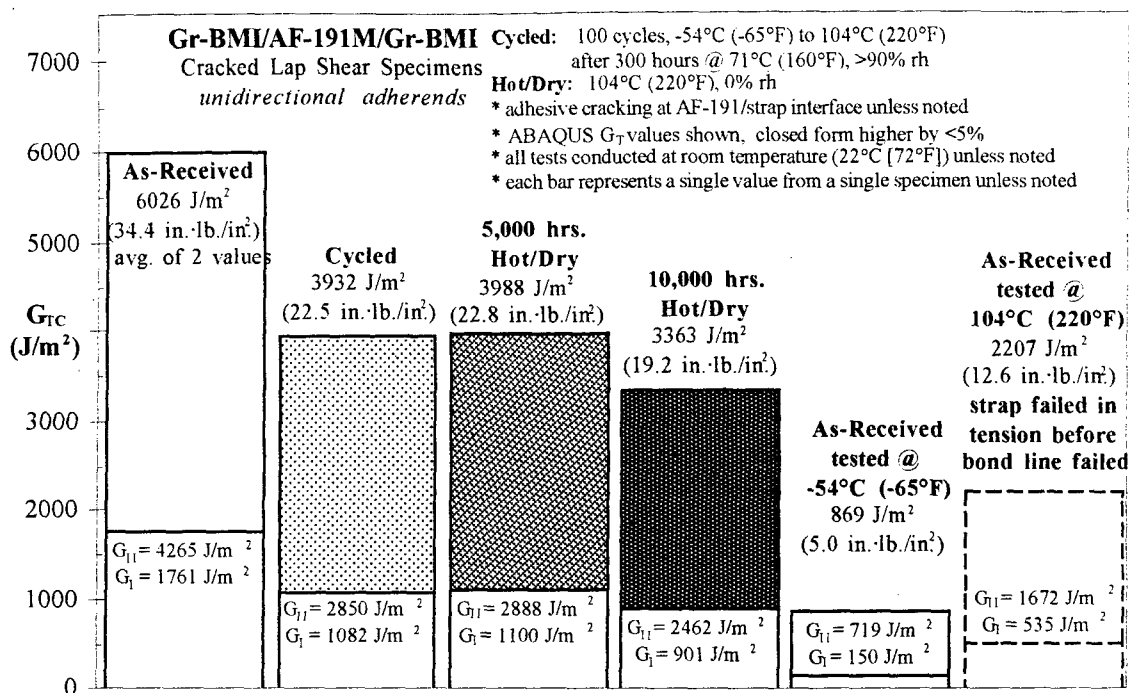


Figure 80. Mixed Mode fracture toughness of the Gr-BMI/AF-191/Gr-BMI bonded system with unidirectional adherends

A similar projection of reduced toughness at reduced temperatures may be made for the toughness of the quasi-isotropic Gr-BMI/AF-191/Gr-BMI system. (Fig. 81) Crack growth in these specimens was also catastrophic and, as in the DCB specimens, it proceeded through the $\pm 45^\circ$ plies located next to the adhesive bond line. This may account for the lower fracture toughness observed.

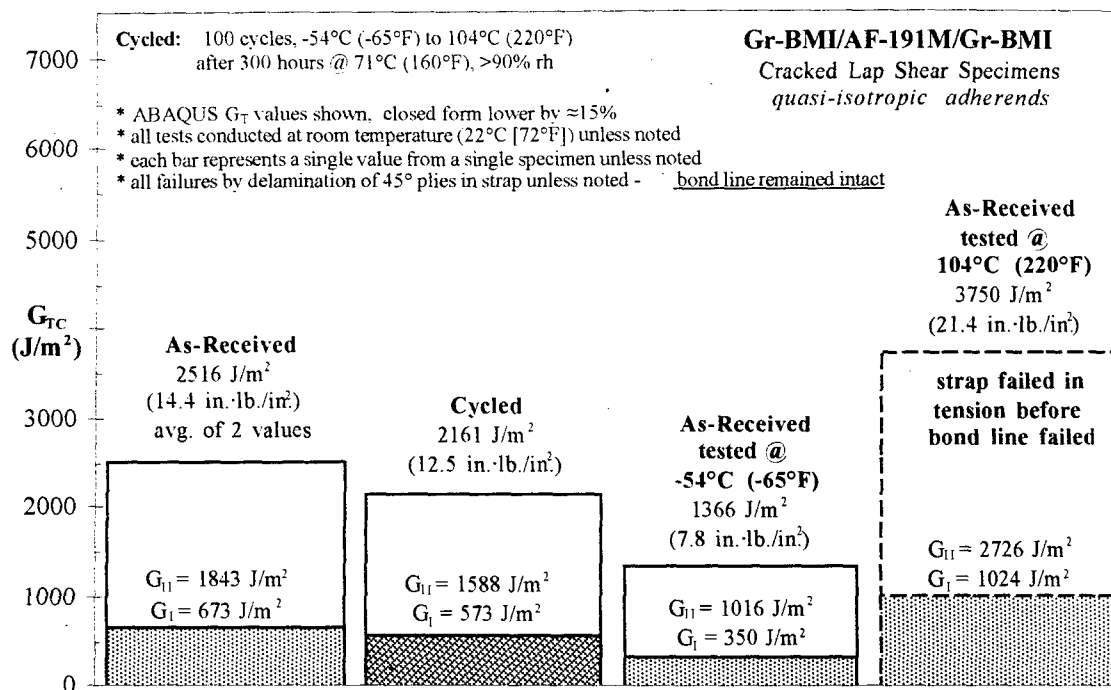


Figure 81. Mixed mode fracture toughness of the Gr-BMI/AF-191/Gr-BMI bonded system with quasi-isotropic adherends

8.2.3.4. Summary of Test Results for the Gr-BMI/AF-191M/Gr-BMI System

This section presents a brief synopsis of results from tests performed on the Gr-BMI/AF-191M/Gr-BMI bonded systems manufactured with primarily unidirectional [uni] and quasi-isotropic [quasi] adherends. Figures 82 and 83 present graphical summaries of the toughness data obtained from these bonded joint systems and may be compared with Figure 1 and Figure 4a described previously in this report.

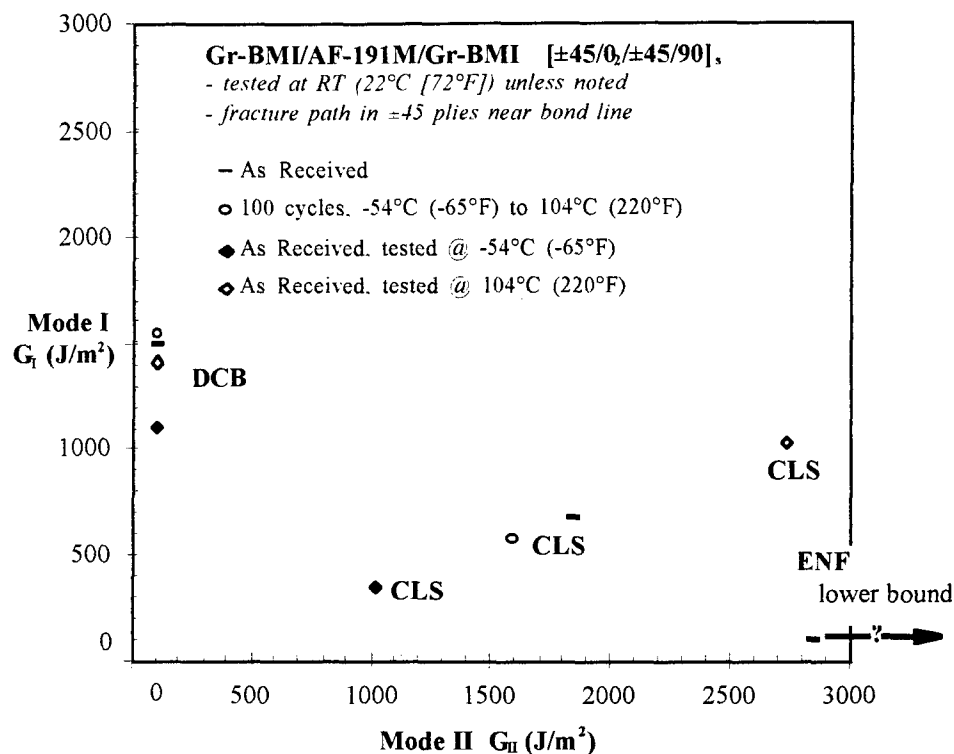


Figure 83. Summary of fracture toughness data for the Gr-BMI/AF-191M/Gr-BMI bonded system with quasi-isotropic adherends

- Mode I Fracture Toughness (via DCB tests):

- as-received values: $G_{Ic} \approx 1720 \text{ J/m}^2$ (9.8 in.·lb./in.²) [uni]

- $G_{Ic} \approx 1490 \text{ J/m}^2$ (8.5 in.·lb./in.²) [quasi]

- reduced: ~ 10% by 100 thermal cycles [uni]

- ~ 10% by testing at -54°C (-65°F) [uni]

- ~ 20 - 30% by 5,000 - 10,000 hours hot/dry exposure [uni]

- Mode I Fatigue Behavior (via DCB tests, unidirectional adherends):

- threshold: $\Delta G_I \sim 100 \text{ J/m}^2$ ($0.6 \text{ in.}\cdot\text{lb./in.}^2$) unaffected by exposure
- high crack growth rate sensitivity ($n \approx 6$) unaffected by exposure
- fairly large amount of scatter
- Mode II Fracture Toughness (via ENF tests):
 - as-received values: $G_{IIc} \approx 3060 \text{ J/m}^2$ ($17.5 \text{ in.}\cdot\text{lb./in.}^2$) [uni]
 - apparent reduction for exposed specimens (with unidirectional adherends) may be factor of large amount of scatter
 - lower bound established at $G_{IIc} \approx 2840 \text{ J/m}^2$ ($16.2 \text{ in.}\cdot\text{lb./in.}^2$) for system with quasi-isotropic adherends due to adherend crushing
- Mixed Mode I/II Fracture Toughness (via CLS tests):
 - as-received values: $G_{Tc} \approx 6030 \text{ J/m}^2$ ($34.4 \text{ in.}\cdot\text{lb./in.}^2$) [uni]

$$G_{Tc} \approx 2520 \text{ J/m}^2$$
 ($14.4 \text{ in.}\cdot\text{lb./in.}^2$) [quasi]
 - reduced:
 - $\sim 35\%$ by 100 thermal cycles [uni]
 - $\sim 35\text{-}45\%$ by 5,000 - 10,000 hours hot/dry exposure [uni]
 - $\sim 85\%$ by testing at -54°C (-65°F) [uni]
 - $\sim 15\%$ by 100 thermal cycles [quasi]
 - $\sim 45\%$ by testing at -54°C (-65°F) [quasi]
- Fracture Path:
 - cohesive for DCB and ENF specimen geometries [uni]
 - in matrix layer of strap near bond line interface for CLS geometry [uni]

- interlaminarily in $\pm 45^\circ$ plies next to bond line [quasi]

8.2.4. Ti/FM[®]x5/Ti

The Ti/FM[®]x5/Ti specimens were fabricated from materials to be used on the future HSCT aerospace vehicle. One group of specimens was tested in the as-received state with no pre-test environmental exposure. A second group was subjected to 5,000 hours of "hot" isothermal exposure at 177°C (350°F), 0% rh, prior to mechanical testing. A third group was subjected to 5,000 hours of "hot/wet" isothermal exposure at 71°C (160°F), 94±3% rh, prior to mechanical testing. A fourth group was subjected to 500 thermal cycles between -54°C (-65°F) and 163°C (325°F) prior to mechanical testing.

Ti/FM[®]x5/Ti bonded joint specimens subjected to long-term exposure were periodically weighed and observed. Figure 84 shows the weight changes resulting from exposure. As expected, the specimens exposed to hot/wet conditions gained weight due to moisturization while those exposed to hot/dry conditions lost weight due to moisture loss. However, these changes were extremely small in comparison to those observed in the epoxy-based bonded joint specimens and less than half of the weight changes seen in the FM[®]x5 adhesive specimens exposed to the same environments. These differences are most probably due to a combination of a small amount of exposed adhesive area, large adherends, and the relatively nonabsorbent nature of the FM[®]x5 polyimide.

Only one other general change occurred during the long-term exposure of the Ti/FM[®]x5/Ti specimens. The normally bluish tint left on the titanium adherends from

the chromic acid surface preparation was slightly bleached out during prolonged exposure to hot/dry conditions.

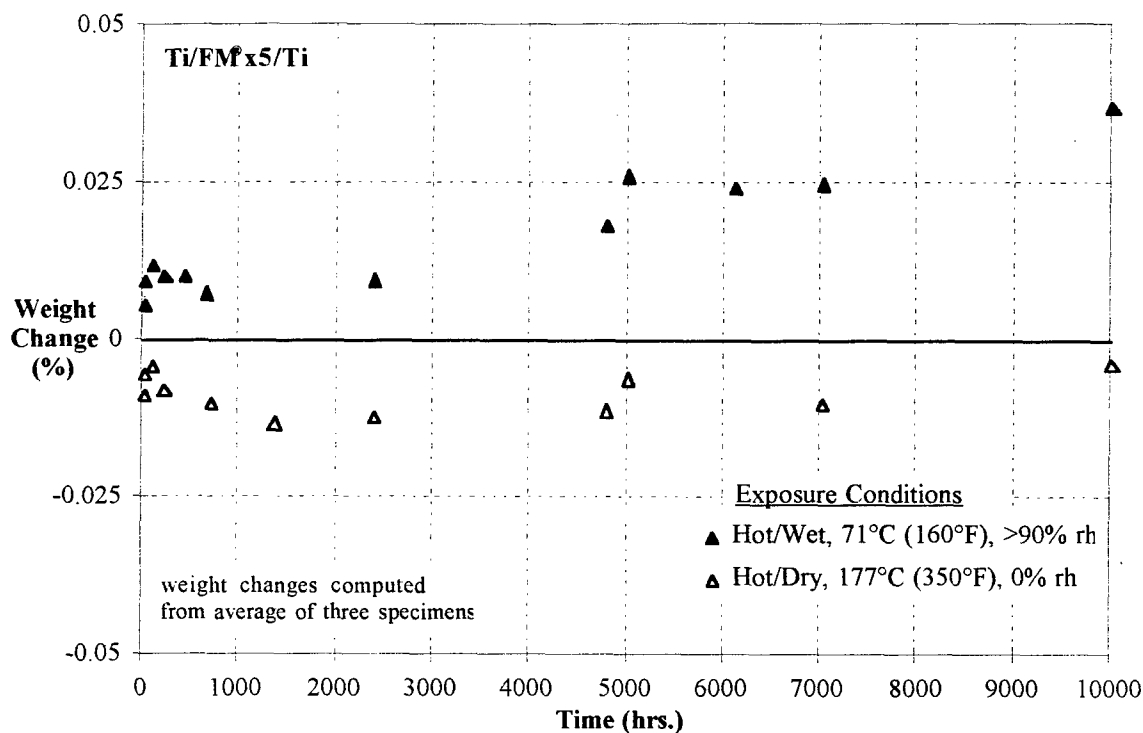


Figure 84. Weight changes in Ti/FM^{x5}/Ti bonded joint specimens due to exposure

8.2.4.1. Mode I (DCB)

Figure 85 shows the results of the monotonic fracture toughness tests on the Ti/FM^{x5}/Ti system. The Mode I toughness of approximately 2500 J/m² (14.3 in.·lb./in.²) is in agreement with values obtained by Parvatareddy, *et al.*¹³⁶

Thermal cycling and 5,000 hours of exposure to a hot/wet atmosphere did not appear to affect the toughness of this system. However, long-term exposure to hot/dry conditions significantly reduced G_{IC} by approximately 30%. Recall that reductions in the strength of the FM[®]x5 adhesive film were also observed following exposure to hot/dry conditions. This is a significant finding in light of the intended long-term operation of the HSCT at high Mach numbers and elevated temperatures. Interestingly, the toughness of adhesive system appeared to increase when tested under hot conditions.

Also somewhat suspect is the level of G_{IC} following 5,000 hours of exposure to a hot/wet condition. Exposure of the adhesive film to these same conditions resulted in a loss of modulus and strength, yet such degradation is only evident in the bonded joint specimens subjected for 10,000 hours to hot/wet conditions. Perhaps this delay in the loss of properties is due to the diffusion of moisture through the adhesive, a process which proceeds more slowly in bonded joints than in adhesive film specimens.

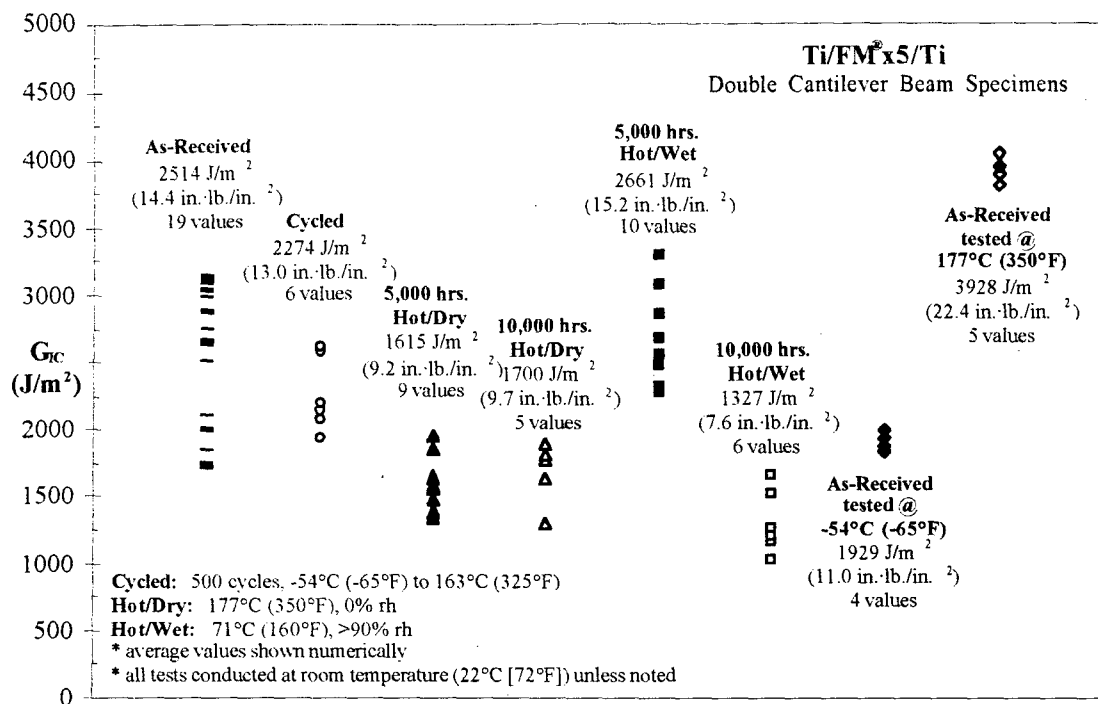


Figure 85. Mode I fracture toughness of the Ti/FM[®]x5/Ti bonded system

Mode I crack growth was generally cohesive in this system. The crack propagated mainly along the plane of the scrim cloth. (Fig. 86) However, the fracture surfaces of the specimen subjected to long-term isothermal exposure at 177°C (350°F) exhibited a greater degree of cracking in resin-rich regions between the scrim cloth and adherends suggesting a possible change in the properties of the polyimide material. The shape of the crack front was indistinct on the fracture surfaces perhaps due to the presence of the relatively bulky scrim cloth.

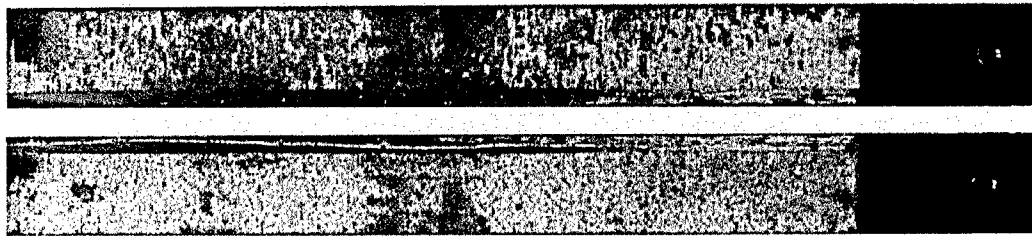


Figure 86. Fracture surfaces of the Ti/FM[®]x5/Ti bonded system

Fatigue crack growth in the Ti/FM[®]x5/Ti system exhibited significant scatter among the specimens subjected to various environmental exposures. (Fig. 87) Given the apparent insensitivity of G_{IC} to the environmental exposures examined by way of fatigue testing, such a trend is to be expected. Threshold crack growth (10^{-6} mm/cycle [4×10^{-8} in./cycle]) occurred at applied strain energy release rate ranges near 100 J/m^2 ($0.57 \text{ in.}\cdot\text{lb./in.}^2$). The slope of the data, a measure of the sensitivity of crack growth to changes in the applied ΔG_I , was approximately 3 to 4, twice that of monolithic titanium.¹³⁴ This indicates the high degree of sensitivity displayed by crack growth in the adhesive bond line and is consistent with the high growth rate sensitivity displayed by the Al/FM[®]73M/Al bonded system.

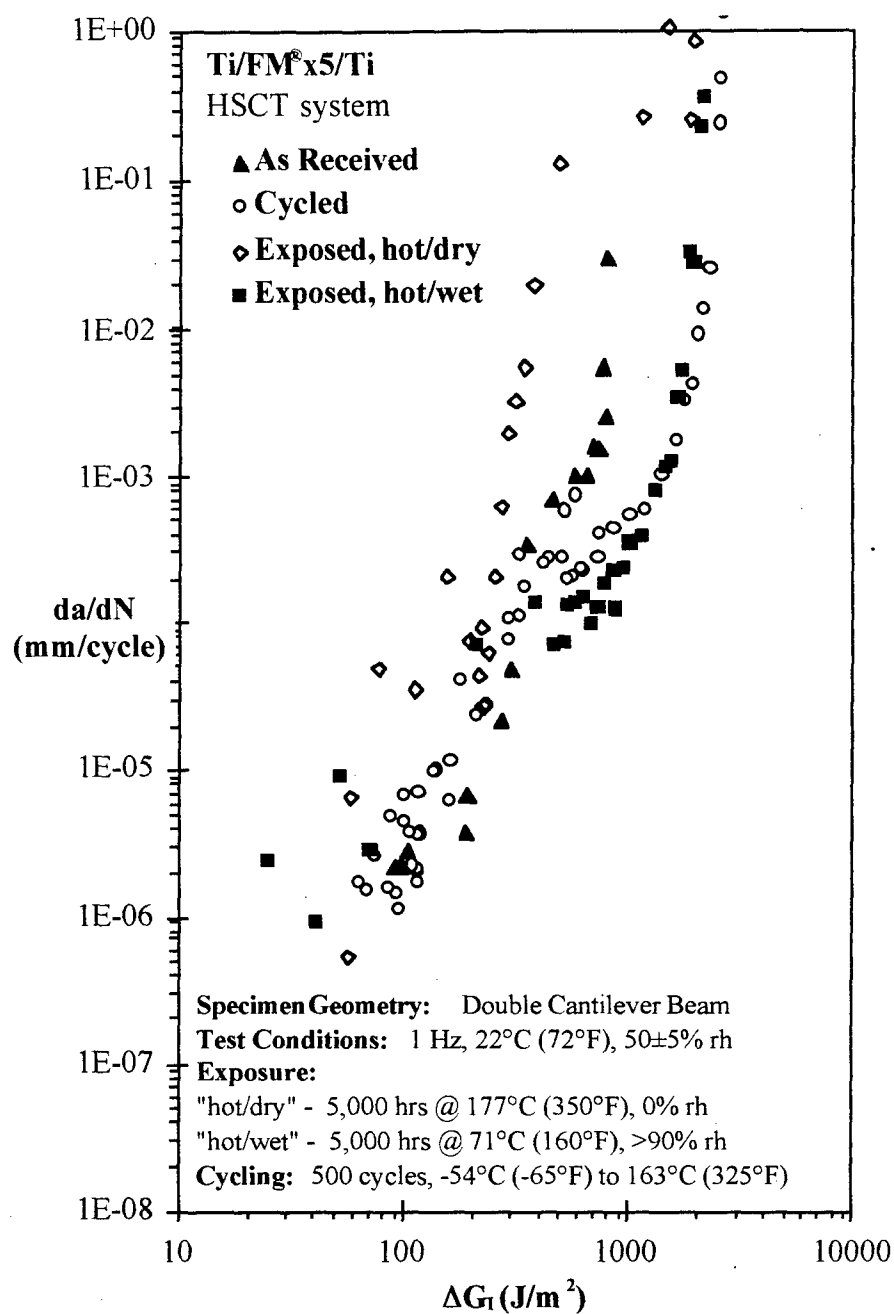


Figure 87. Mode I fatigue behavior of the Ti/FM[®]x5/Ti bonded system

8.2.4.2. Mode II (ENF)

Mode II fracture toughness testing of Ti/FM[®]x5/Ti ENF specimens was attempted, but results were inconsistent and a great deal of scatter was present in multiple G_{IIC} values computed for single specimens (Fig. 88). No trend is evident in the test data except for the apparent Mode II fracture toughness lower bound of approximately 3500 J/m² (20.0 in.·lb./in.²).

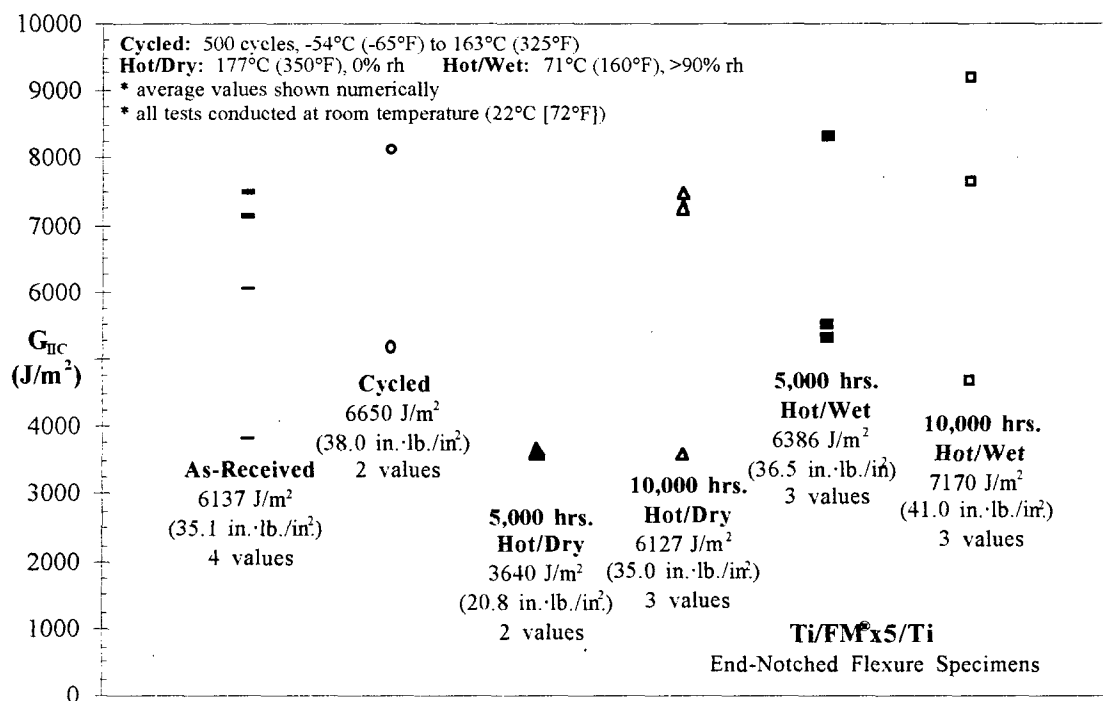


Figure 88. Mode II fracture toughness of the Ti/FM[®]x5/Ti bonded system

Crack growth in these specimens was generally interfacial, but the crack meandered from one interface to the other with no distinct pattern. Crack growth was a mixture of slow extension and sharp, rapid runs of the crack tip. Cracking often initiated several millimeters away from the Kapton™ crack starter strip, even occurring on the opposite side of the central loading pin. Second and third crack growth runs in single specimens resulted in G_{IIC} rates higher than the initial value obtained from the start of a crack at the tip of the starter strip. This suggests that a region of higher stress concentration existed at the initiation point provided by the Kapton™ film than was subsequently present at the natural crack tip. It also suggests that friction due to relative motion between the two adherends in the cracked region of a specimen may play a significant role in the determination of Mode II toughness values for this bonded system using the ENF geometry. Given the tortuous crack path, relatively thick bond line, and bulky woven glass scrim cloth, friction is a non-negligible factor.

The presence of the relatively thick scrim cloth in the FM®x5 adhesive may be the main reason behind the somewhat inconsistent data obtained from the ENF test on this system. The scrim contributes substantially to the formation of a very rough fracture surface, thereby enhancing friction. On a local scale, the scrim may also promote or prohibit crack growth, depending upon where the crack tip is located with respect to the weave of the scrim.

8.2.4.3. Mixed Mode (CLS)

Rapid crack growth in the Ti/FM[®]x5/Ti CLS specimens permitted only a single mixed mode fracture toughness value to be obtained for each specimen. Three specimens in the as-received conditions were tested. The results are shown in Figure 89.

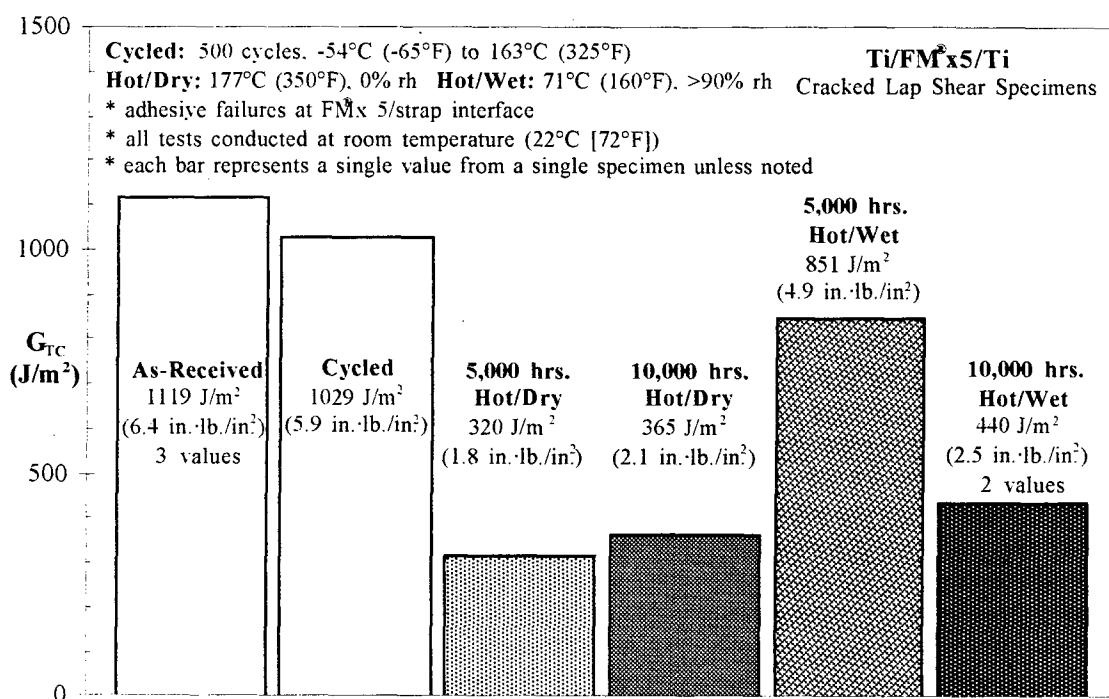


Figure 89. Mixed mode fracture toughness of the Ti/FM[®]x5/Ti bonded system

The mixed mode fracture toughness of the as-received Ti/FM[®]x5/Ti system of approximately 1100 J/m² (6.28 in·lb./in.²) is less than its Mode I or Mode II fracture toughness. This may be due to the nature of crack growth which was almost totally

adhesive at the strap/adhesive interface. This interfacial failure was free of the tortuosity displayed by the fracture surfaces of the ENF specimens and resulted in a clean, adhesive-free, bond surface on the strap adherend.

Interpretation of the single G_{IIC} data points for given environmental conditions is difficult. However, it is notable that the pattern of decreased mixed mode fracture toughness with respect to environmental exposure mirrors that displayed by the Mode I fracture toughness for this system. Comparing Figure 89 to Figure 87 suggests that perhaps the relatively few mixed mode fracture toughness values obtained are consistent with other data on this system.

8.2.4.4. Summary of Test Results for the Ti/FM[®]x5/Ti System

This section presents a brief synopsis of results from tests performed on Ti/FM[®]x5/Ti bonded system. Figure 90 presents a graphical summary of the toughness data obtained from this bonded joint system and may be compared with Figure 1 and Figure 4a described previously in this report.

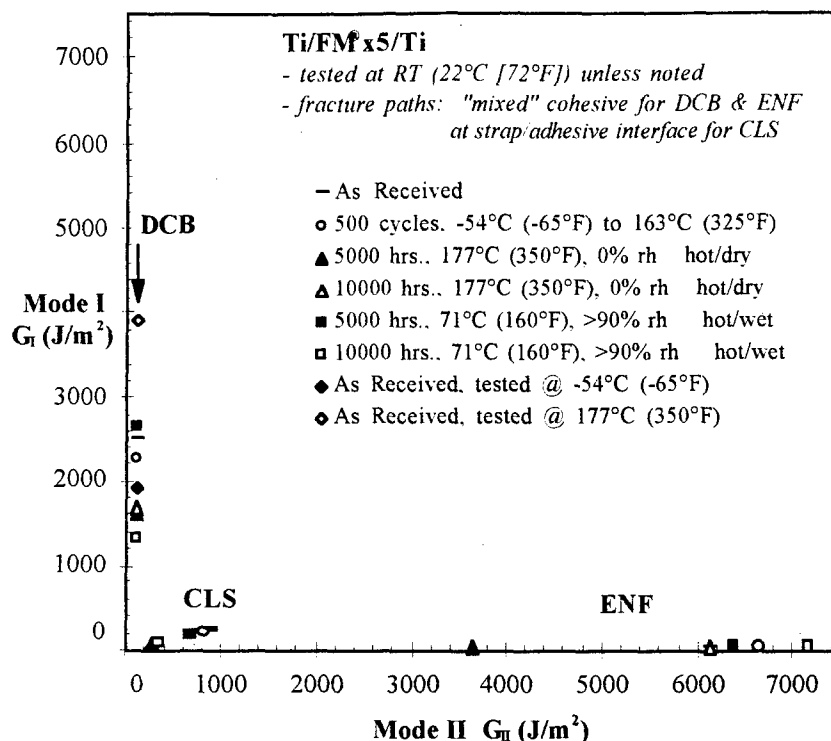


Figure 90. Summary of fracture toughness data for the Ti/FM[®]x5/Ti bonded system

- Mode I Fracture Toughness (via DCB tests):

- as-received value: $G_{Ic} \approx 2500 \text{ J/m}^2$ (14.4 in.·lb./in.²)

- reduced: ~ 20% by testing at -54°C (-65°F)

- ~ 35% by 5,000 - 10,000 hours hot/dry exposure

- ~ 45% by 10,000 hours hot/wet exposure

- Mode I Fatigue Behavior (via DCB tests, unidirectional adherends):

- threshold: $\Delta G_I \sim 100 \text{ J/m}^2$ (0.6 in.·lb./in.²) unaffected by exposure

- high crack growth rate sensitivity ($n \approx 4$) unaffected by exposure

- large amount of scatter
- Mode II Fracture Toughness (via ENF tests):
 - as-received values: $G_{IIc} \approx 6140 \text{ J/m}^2$ (35.1 in.·lb./in.²)
 - great amount of scatter due to inconsistent crack growth pattern
- Mixed Mode I/II Fracture Toughness (via CLS tests):
 - as-received values: $G_{Tc} \approx 1120 \text{ J/m}^2$ (6.4 in.·lb./in.²)
 - reduced: ~ 25-60% by 5,000 - 10,000 hours hot/wet exposure
 ~ 70% by 5,000 - 10,000 hours hot/dry exposure
- Fracture Path:
 - “mixed” cohesive for DCB and ENF specimen geometries
 - adhesive at strap/adhesive interface for CLS geometry

8.3. Discussion of Results

8.3.1. Exposure and Test Environments

In comparing the exposure environments, it is evident that the hot/wet (71°C [160°F], >90% rh) condition was certainly the most aggressive. Exposure to this conditions caused significant decreases in the tensile and fracture toughness properties of the adhesive films and in most of the fracture toughness properties of the bonded systems containing FM[®]73M. This environment was also the only one to cause a reduction in the fatigue threshold. With respect to the bonded joint systems, it appears that any gains in

toughness due to increased plasticization of the adhesive were offset by other effects (possibly chemical or physical) within the bond line. Metal surface preparation for all specimens appeared able to protect the joints from the harmful effects of the hot/wet exposure, at least for the times tested for this research. Yet, clearly, exposure to a hot/wet environment is severe and provides a challenge to the durability of bonded joints.

Some may argue that such an exposure environment is too severe, that it does not duplicate actual service conditions, or that it is arbitrary. However, the hot/wet condition used for this research was based upon years of evaluating various worldwide operating environments and is, thus, not arbitrary. As for being too, severe, its aggressiveness may actually be beneficial by way of serving as an environmental safety factor. Because the subtleties of time, temperature, and humidity interactions are not yet fully understood, ensuring the durability of bonded joints in an aggressive hot/wet environment provides a measure of insurance against the unknown effects of the environment.

Attempts to reverse the effects of hot/wet exposure by placing specimens in a room temperature, desiccating environment proved unsuccessful. Although the weight of the desiccated specimens approached its as-received level, a similar restoration of toughness values was not observed. Perhaps the temperature-related driving force which moisturized the bond lines during hot/wet exposure is also required during desiccation to completely draw out the absorbed moisture.

However, such long-term exposure to a hot/dry environment can also take its toll on the properties of adhesives and bonded systems. The Ti/FM[®]x5/Ti and Gr-BMI/AF-191M/Gr-BMI systems both exhibited reductions in toughness after such long term exposures to hot/dry conditions.

A form of environmental exposure initially expected to cause reductions in fracture properties, thermal cycling, proved to be rather benign. However, this should not be surprising considering the fact that the specimens were not loaded or restrained during cycling (as actual aircraft components are) and, therefore, were not subjected to any thermally induced stresses and strains that could have affected the adhesive.

This can be said for all of the environmental exposures. In no cases were the specimens constrained. Thus, it is expected that the environmentally-induced changes presented in this thesis represent lower bounds or "best case" estimates of the effect of operating conditions on bonded joints in service.

Finally, the role of the test environment should be addressed. Fracture toughness levels in nearly specimen tested at -54°C (-65°F) were lower than room temperature values by an average of 50%. Although such low temperature embrittlement is not surprising, it is significant that it was evident under several different modes of loading and also because this temperature cannot be avoided for many aircraft operations. Furthermore, the reduced low temperature performance of the adhesives investigated

must be considered by designers in conjunction with environmental exposure which was also shown to be detrimental.

8.3.2. Chemical and Physical Analysis Methods

Although considerable effort was put into analyzing the possible chemical and physical changes of the neat adhesive materials, the results were inconclusive and few were directly related to changes seen in the tensile, fracture, and fatigue properties of adhesive films and bonded joints. The sensitivity and accuracy of the chemical and physical analysis instruments used for these analyses are very high. Thus, the lack of correlation between "global" properties such as fracture toughness and "local" properties such as the glass transition temperature suggests that other, as yet unidentified, mechanisms are responsible for the changes seen in the properties of the bonded joints.

8.3.3. Material Properties

It is useful to briefly discuss and contrast the performance of the bonded material systems investigated for this research.

To choose the "toughest" system would be difficult since the bonded material combinations ranked differently in terms of Mode I, Mode II, and mixed mode fracture toughness. However, in general, the Al/FM[®]73M/B-Ep system exhibited the lowest fracture toughness properties. This was due to the dissimilar adherends imparting a thermally induced strain energy release rate to the adhesive bond line and also to the

apparent low adhesive strength of the composite matrix through which the fractures appeared to grow.

The FM[®]x5 adhesive and bonded system, on the other hand, performed remarkably well in light of the fact that much higher temperatures and many more thermal cycles were used during exposure of this system than were used for the epoxy adhesive systems.

The importance of considering the types of adherends in a bonded system was also evident in the Gr-BMI/AF-191M/Gr-BMI system. With this type of bonded composite, unidirectional adherends promoted cracking in the adhesive layer while quasi-isotropic adherends exhibited cracking in the $\pm 45^\circ$ plies near the bond line. The type of failure displayed by the quasi-isotropic adherends resulted in lower fracture toughness values than exhibited by the unidirectional system.

The relationship between Mode I, Mode II, and mixed mode fracture toughness was inconsistent among the systems tested. Difficulties in testing the FM[®]73M systems prevented some forms of fracture toughness values from being obtained. For the AF-191M systems, $G_I < G_{II} < G_{\text{mixed}}$, but for the FM[®]x5 system, $G_I < G_{II} > G_{\text{mixed}}$. The difference in these relationships may be due to the different fracture paths exhibited by the bonded systems. But the trend for the mixed mode fracture toughness to exceed the single mode fracture toughnesses is contrary to the observations of Johnson & Mangalgiri (Fig. 1) and should be investigated further.

In terms of fatigue, the adhesively bonded systems share two common features. The first is an extremely high crack growth rate sensitivity. If the fatigue data were to be described using a Paris-type relationship ($da/dN = C[\Delta G]^n$), the slope of the crack growth data in the bonded systems ($4 \leq n \leq 10$) is very steep compared to crack growth data for Ti-6Al-4V and 7075-T6 Al ($n \approx 2$). This suggests that crack growth in bonded joints is much more sensitive to changes in applied loads or strain energy release rates than in monolithic metals. This high level of sensitivity appeared to be relatively unaffected by the form of environmental exposure. The second feature is the relatively low level of strain energy release rate necessary to cause threshold crack growth rates (10^{-6} mm/cycle [4×10^{-8} in./cycle]). The value for $\Delta G_{T,th}$ was approximately 100 J/m^2 for all systems tested except for when exposure to a hot/wet environment reduced this value for the Al/FM[®]73M/B-Ep and Al/FM[®]73M/Al system. The significance of this value lies not with the fact that it is similar for all the tested adhesives, but that it is low in comparison to their monotonic fracture toughness.

Though not specifically addressed as part of this experimental effort, the effect of environmental exposure on the performance of composite adherends must also not be ignored. Considerable losses in adherend strength and stiffness due to high temperatures and/or high humidity levels may also reduce the durability of bonded composite joints. To accurately understand the durability of bonded composites, it is necessary to have

knowledge of the effect of exposure on the individual materials and on the entire adherend-adhesive-interphase system.

CHAPTER IX

CASE STUDIES

This chapter explores how the experimental data presented in the previous chapter may be utilized to analyze other forms of adhesively bonded structures. The focus of this chapter is on the Al/FM[®]73M/B-Ep bonded repair system. Two studies were conducted to examine how fracture mechanics concepts and the experimental data generated in this project could be used. The first study compared the experimental data from this research with an independent assessment of the fatigue durability of an adhesively bonded patch. The second study attempted to relate the current research to the expected flight loads on fuel transfer hole ("weep-hole") patches bonded to the C-141 aircraft.

9.1. Case Study 1: The Boeing/Textron Bonded Doubler Program

Results from fatigue tests conducted on the Al/FM[®]73M/B-Ep system as part of the research reported in this thesis were compared with those from a second, independent project conducted by the Boeing Airplane Company and Textron Specialty Materials, Inc.^{40,137} The Boeing/Textron effort consisted of extensive fatigue testing of cracked aluminum panels patched with boron-epoxy laminates ("doubblers") and focused on the

ability of a bonded patch to retard or eliminate crack growth in the underlying aluminum substrate. Although the Boeing/Textron study focused on the behavior of a crack in the patched aluminum structure, results also showed that no debonding of the doubler occurred after 300,000 cycles at typical commercial aircraft fuselage stress levels.

It was the observation of no debonding that could best be analyzed in a fashion similar to the approach used for the research performed for this thesis. Furthermore, fracture mechanics analyses are typically not performed to evaluate the integrity of the bond line for these types of repairs. Therefore, an objective of this small study was to determine how and if results from the Georgia Tech research could be applied to the Boeing/Textron project. Finite element analyses of the specimens tested at Georgia Tech determined the levels of strain energy release rate in the bond line and checked if the lack of debonding in the Boeing/Textron specimens was consistent with experimental results from the Georgia Tech program.

9.1.1. Materials and Specimens

The Boeing/Textron program used the same materials as used for the research contained in this thesis: bare 7075 aluminum, Textron's F4/5521 boron-epoxy composite material, and FM[®]73M adhesive.

Patched aluminum panels used in the Boeing/Textron program (Fig. 91) were 1.6 mm (0.063 in) thick, 100 mm (4 in) wide, and 406 mm (16 in) long. Each panel contained a 13 mm (0.5 in) long by 0.8 mm (0.03 in) wide sawcut simulating a crack initiating at the

specimen edge. Several different configurations of the boron-epoxy doubler were investigated. However, the most common consisted of a 6-ply unidirectional lay-up with a 25:1 ply drop-off ratio (taper) used at the edges of the doubler. The cross-sectional stiffness ratio between the doubler and the aluminum was 1.4:1. Figure 91 shows the most common geometry used in the Boeing/Textron study and that which has been analyzed for this thesis.

Because of the coefficient of thermal expansion mismatch between the aluminum ($\alpha_{Al} = 22.1 \times 10^{-6}/^{\circ}\text{C}$ [$12.3 \times 10^{-6}/^{\circ}\text{F}$]) and the boron-epoxy ($\alpha_{B-Ep} = 4.5 \times 10^{-6}/^{\circ}\text{C}$ [$2.5 \times 10^{-6}/^{\circ}\text{F}$]), all cured specimens were distinctly curved as shown.

Residual curvature of the Boeing/Textron specimens was eliminated by the application of a 21 MPa (3 ksi) tensile stress to the aluminum.

Although bonded repairs to aircraft do not result in such gross deformations of the underlying structure, residual stress states are always present in the adhesive bond line due to the CTE mismatch. It was imperative, to understand the consequences of the curvature using finite element analyses and experimental test results.

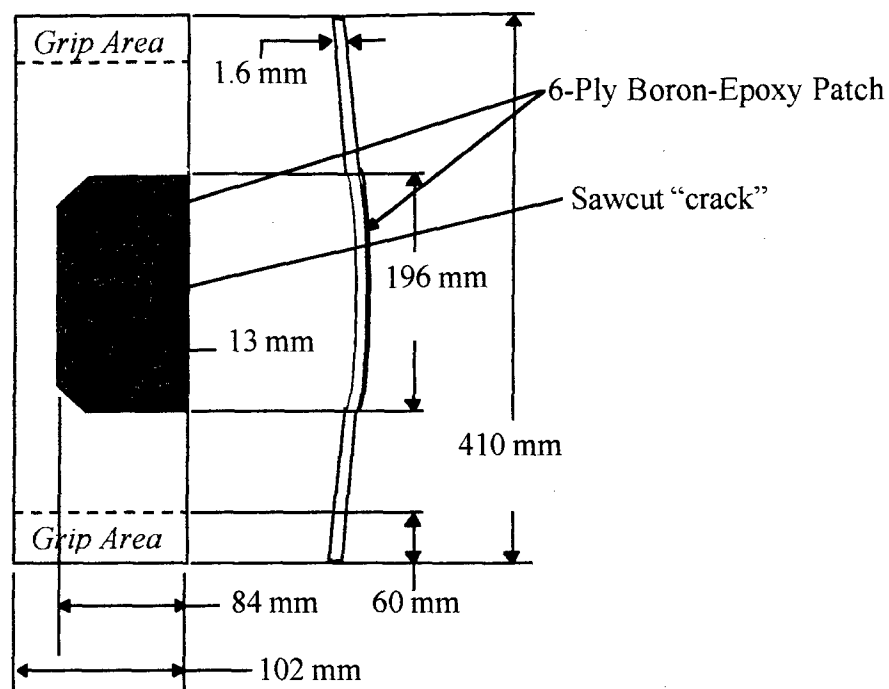


Figure 91. Geometry of the Boeing/Textron patched panel

9.1.2. Boeing/Textron Testing Procedures

For the Boeing/Textron program, fatigue tests, using ASTM D3479¹³⁸ and E647¹³⁹ as guidelines, were conducted under constant amplitude at 5 Hz, $R=0.15$, and stress levels of 21 to 138 MPa (3 to 20 ksi). The lower stress level was chosen to eliminate the residual curvature in the specimens. The upper stress limit corresponded to the sum of the maximum stress level experienced by B737 and B747 commercial aircraft fuselage skins (≈ 118 MPa [17 ksi]) and the 21 MPa (3 ksi) offset required to eliminate specimen curvature. Runout was set at 300,000 cycles. Loads were applied to the specimens using

hydraulic grips “fixed” directly to the test frame (i.e. without a universal joint).^{140,141}

Subsequent finite element modeling accounted for these grip conditions.

9.1.3. Finite Element Analysis

ABAQUS was used for the finite element studies performed for this thesis because of its extensive analytical capabilities including thermal residual stress calculations.⁷² The analysis accounted for geometric non-linearities introduced by large deformations and specimen curvature.

All materials were assumed to be linearly elastic and to have invariant, room temperature properties (Table 10). Because of the large width of the specimens compared to the bond line thickness, plane-strain was assumed. The adhesive layer was modeled using four rows of two-dimensional, four-noded quadrilateral elements, the aluminum using ten rows, and the boron-epoxy using one row per ply.

Table 10. Material Properties Used for the Model of the Boeing/Textron Specimen

Material	E_{11} (GPa)	E_{22} (GPa)	E_{33} (GPa)	ν_{12}	α_{12} ($\times 10^6/^{\circ}\text{F}$)	α_{23} ($\times 10^6/^{\circ}\text{F}$)	α_{13} ($\times 10^6/^{\circ}\text{F}$)
7075-T6 Aluminum	70.8	70.8	70.8	0.33	13	13	13
FM [®] 73M	2.07	2.07	2.07	0.34	40	40	40
Boron- Epoxy	207	17.2	17.2	0.21	2.5	13.1	13.1

Strain energy release rates were calculated using a modified crack closure technique⁷⁴ which determined nodal forces and displacements required to close a crack to its original position

A reduced integration technique was used to enhance the performance of the elements under the bending conditions present during testing.

Since the Boeing/Textron patched panel was generally symmetric about the horizontal axis, only half of the patch was modeled. (Fig. 92)

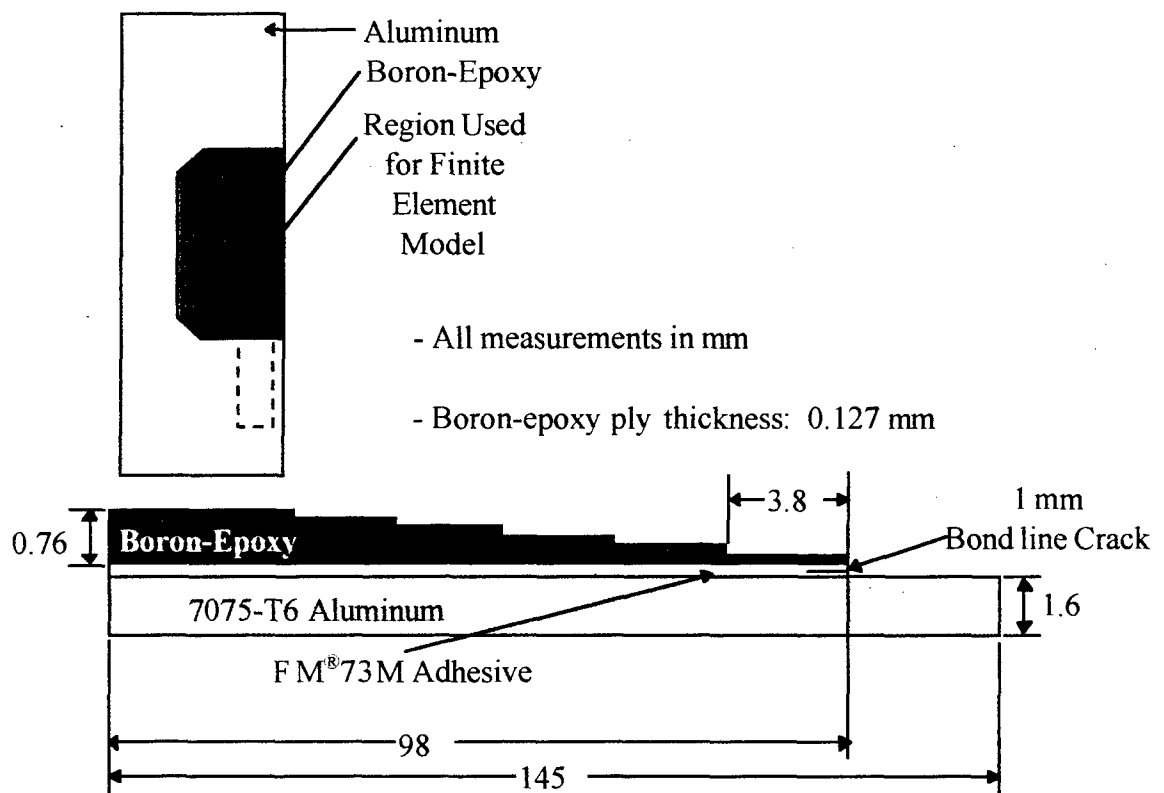


Figure 92. Model of the Boeing/Textron patched panel fatigue test specimen

The model employed 3827 nodes and 3560 "incompatible mode" elements designed specifically to accommodate bending.

Although no known crack or debond was present in the bond line of the Boeing/Textron specimens, the finite element model contained one to provide a location at which to calculate G . In the model, a 1 mm (0.04 in) debond was introduced at the mid-plane of the adhesive. The size of the debond was based upon that of small voids observed in the bond lines of the DCB specimens tested at Georgia Tech and is indicative of a flaw which may go undetected using current nondestructive inspection techniques. The choice of this crack location was based upon the assumption that a bond line defect might be more common than an interlaminar defect between the boron-epoxy plies. Thus, patch failure due to interlaminar cracking was not explored. However, given the results of the testing conducted on the Al/FM[®]73M/B-Ep system for this thesis, failure of the patch due to cracking in the boron-epoxy laminate is a distinct possibility. Additional studies could employ a similar finite element model with cracks in various locations to identify the most critical location.

The temperature drop applied to the model of the patched panel specimen to simulate post-cure cool-down was governed by observations from the Boeing/Textron project showing that curvature was eliminated with the application of a 21 MPa (3 ksi) stress. Because of this linkage of curvature and applied load, the magnitude of the temperature drop depended upon the grip conditions used in the finite element modeling.

A 14°C (25°F) temperature drop was necessary. The temperature drop used in the finite element analyses was considerably less than that experienced by the specimens during the post-cure cool-down (61°C [110°F]). Reasons for this discrepancy include the use of invariant room temperature properties for the laminate and adhesive and the possibility that published properties differ from those displayed by the materials tested.

9.1.4. Comparison of the Experimental Data and Finite Element Analysis

As described earlier in this thesis, threshold crack growth rates (10^{-6} mm/cycle [4×10^{-9} in./cycle]) appeared to occur at a ΔG_T value of approximately 100 J/m^2 ($0.57 \text{ in.}\cdot\text{lb./in.}^2$) in the Al/FM[®]73M/B-Ep system.

Mode II was dominant in the bond line of the Boeing/Textron specimen under applied stress, and comprised the majority of G_T . An estimated G_{II} level of 0.85 J/m^2 ($4.9 \times 10^{-3} \text{ in.}\cdot\text{lb./in.}^2$) existed in the specimens at zero load following fabrication. Installing the specimen in the grips of the test machine produced some deflection and increased the Mode II component to approximately 2.77 J/m^2 ($1.6 \times 10^{-2} \text{ in.}\cdot\text{lb./in.}^2$) immediately prior to loading. Overall, the strain energy release rates at the minimum fatigue stress of 21 MPa (3 ksi) were negligible. During fatigue testing, G_I varied between zero and approximately 8 J/m^2 ($4.6 \times 10^{-2} \text{ in.}\cdot\text{lb./in.}^2$) and G_{II} varied between approximately 0.4 J/m^2 ($2.3 \times 10^{-3} \text{ in.}\cdot\text{lb./in.}^2$) and approximately 33 J/m^2 ($0.19 \text{ in.}\cdot\text{lb./in.}^2$).

at the debond tip. Thus, G_T varied between approximately 0.4 and 41 J/m² ($\Delta G_T \approx 40$ J/m² [0.23 in.·lb./in.²]).

A comparison of the results of the fatigue tests conducted on the DCB specimens in the Georgia Tech program and the patched panel specimens in the Boeing/Textron program yields a useful result. Given a fatigue threshold level of $\Delta G_T \approx 100$ J/m² (0.51 in.·lb./in.²) established by experiments on DCB specimens and $\Delta G_T \approx 40$ J/m² (0.23 in.·lb./in.²) for the Boeing/Textron specimen, it is not surprising that no debonding was observed in the Boeing/Textron program after 300,000 cycles. Furthermore, no significant pre-existing bond line flaws were known to be present in the patched panel specimens. Thus, the absence of debonding in the adhesive layer of the Boeing/Textron specimens is consistent with the experimental results obtained at Georgia Tech. However, these values could change significantly for specimens which are pre-conditioned in a hostile environment or for operations at reduced temperatures.

This project demonstrated the viability of fracture mechanics concepts in the analysis of bonded repairs. Experimental data from a relatively simple specimen geometry were analyzed and, with the help of finite element analyses, compared to data from tests conducted on more realistic specimens.

9.2. Case Study 2: Bonded Patches on C-141 Transport Aircraft

The importance and applicability of the results of this research to actual applications depends upon typical stress levels encountered during operations. Estimated flight loads were obtained for structures repaired using bonded patches on the C-141 transport. These loads were converted to stresses and applied to the adherends of an appropriate specimen geometry to simulate flight conditions. Using finite element results and observations from fracture toughness and fatigue testing, these loads were converted to bond line strain energy release rates and compared to critical values obtained during testing. The following short analyses are, admittedly, crude in their approximations of aircraft structure by laboratory specimens. However, they do provide an opportunity to relate test data to operational applications.

Currently, the most common area to use bonded repairs on the C-141 is the lower wing skin. Here patches have been applied using FM[®]73M (and similar adhesives) to alleviate the problem of "weep-hole" cracking mentioned previously in this thesis. The thickness of the aluminum skin in these areas is approximately 4.83 mm (0.19 in.), and the design limit stress is 221-234 MPa (32-34 ksi).¹⁴²

This configuration may be modeled as the cracked lap shear specimen having an aluminum strap (representing the aircraft structure) and a boron-epoxy lap (representing the bonded patch). If the minimum applied strain energy release rate were zero, application of the stated design limit stress to the appropriate Al/FM[®]73M/B-Ep CLS

specimen would result in maximum ΔG_T values in the bond line of 131-166 J/m² (0.75-0.95 in.·lb./in.²). Though higher than observed $\Delta G_{T,th}$ values of 100 J/m² (0.57 in.·lb./in.²), these estimated values occur only when the structure experiences limit loads.

Bonded repairs have also been considered for the fuselage where the typical in-flight pressure of 59.5 kPa (8.6 psi), fuselage radius of 2.18 m (85 in.) and skin thickness of 15 mm (0.6 in.) combine to produce an average skin stress of 82.7 MPa (12 ksi).¹⁴²

Again the configuration may be modeled using an Al/FM[®]73M/B-Ep CLS specimen with an aluminum strap and a boron-epoxy lap. The average skin stress in this case results in a maximum strain energy release rate of approximately 21 J/m² (0.12 in.·lb./in.²). If the minimum applied strain energy release rate were zero This level is well below the observed fatigue threshold G level for the Al/FM[®]73M/B-Ep system.

Given the many assumptions made in this analysis, determining the level of conservatism present in the current repair designs would be risky. However, this small and, admittedly, simplified approach demonstrates the value in using experimental fatigue and fracture data for bonded joints coupled with a firm understanding of the bond line strain energy release rate due to flight loads.

CHAPTER X

SUMMARY AND CONCLUSIONS

A broad experimental and analytical effort was conducted to investigate, quantify, and improve the understanding of how environmental exposure affects the fracture and fatigue behavior of bonded joints. Three aerospace adhesives and four bonded joint systems indicative of present or future bonded aircraft materials were examined. Fracture mechanics was used as the prime analytical tool to quantify environmentally-induced degradation in Mode I, Mode II, and mixed mode fracture and fatigue properties of bonded joints. Changes in these properties due to isothermal exposure, thermal cycling, and test temperature were noted. In parallel efforts, tensile and fracture toughness testing was performed on neat adhesive specimens subjected to the same exposure conditions. These adhesives were also subject to a battery of chemical and physical analytical techniques intended to identify exposure-related changes in the structures of the adhesives. Finally, the utility of fracture mechanics techniques and of the experimental results from this research was demonstrated in two small case studies.

The chemical and physical analyses proved to be less useful than originally anticipated. Interpretation of the FTIR spectroscopy revealed only very slight differences in the spectra from adhesive exposed to various environments. Most of these

changes appeared to have been caused by moisturization of the adhesives exposed to high humidity environments. DSC analysis revealed that exposure to a hot/wet environment produced slight decreases in the T_g of the epoxy adhesives. The degradation temperature, as identified by TGA analysis, remained constant for all adhesives under all conditions. In short, the results obtained from these tests indicated, at best, subtle changes in the chemical and physical characteristics of adhesives exposed to various environments. These changes did not correlate well with shifts in the mechanical behavior of the adhesive film specimens or in the fracture and fatigue behavior of the bonded joint specimens.

The correlation between tensile and plane stress fracture properties of the adhesive films and the bonded joint specimens was considerably better. Reductions in the yield and ultimate stresses of the adhesive films were often caused by the same exposure conditions that reduced the fracture toughness of bonded joint specimens. In addition, the plane stress fracture toughness values obtained from the adhesive film specimens exhibited the same general trend of environmental degradation as did the Mode I fracture toughness values obtained from bonded joint specimen exhibiting cohesive fracture paths. Numerically, the plane stress fracture toughness values were close to the plane strain toughness values obtained from the bonded joints. The differences observed in these two forms of fracture toughness likely stem from the presence or absence of and the orientation of the scrim cloth relative to the loading direction.

Monotonic fracture toughness values obtained from bonded joint tests generally followed a trend of increased degradation with environmental exposure. Although the Mode I, Mode II, and mixed mode toughnesses were affected to different degrees, none of the environments investigated greatly improved the properties of the adhesives or bonded joints - changes were almost always detrimental. Considering all the environments to which the various specimens were subjected, the most detrimental, by far, was hot/wet exposure. 5,000 hours (or more) of exposure to hot/wet conditions generally reduced tensile properties of all adhesive film specimens and severely degraded the performance of the Al/FM[®]73M/Al and Al/FM[®]73M/B-Ep systems. A curious exception to this trend was the toughness of the Ti/FM[®]x5/Ti system which was slightly tougher after 5,000 hours of exposure to a hot/wet environment suggesting, perhaps, that the adhesive was plasticized and, therefore, possessed a higher toughness. Testing at -54°C (-65°F) was also quite detrimental causing large reductions in the fracture toughness of nearly every specimen tested under these cold conditions. Given that this low temperature is unavoidable during high altitude sub sonic flight, these results are especially significant.

During the monotonic tests, crack growth was indicated by a deviation from linearity of the load-displacement data. In many cases, the fracture path was cohesive suggesting that surface preparations were adequate to protect against the environmental conditions investigated. However, there were exceptions to this observation of cohesive crack growth.

In the Al/FM[®]73M/B-Ep system, the crack path was always located in the matrix of the composite adherend near the adhesive/composite interface. Residual thermal stresses due to the dissimilar adherends, differing flexural moduli, and, a composite matrix which, evidently, was less tough than the epoxy adhesive drove the crack tip to follow this "near interfacial" path. Fracture away from the bondline also occurred in the Gr-BMI/AF-191M/Gr-BMI system with quasi-isotropic adherends. In these specimens, the $\pm 45^\circ$ plies nearest the bond line failed interlaminarly showing that the toughness of the adhesive exceeded the toughness of the BMI matrix. The behavior of these two bonded systems highlights the need to examine bonded joints as material systems. The performance of two joints having the same adhesive but different adherends cannot be assumed to be identical. Finally, cracking in the CLS specimens occurred at or near the adhesive/strap interface in all specimens with the exception of the quasi-isotropic Gr-BMI/AF-191M/Gr-BMI system (where cracking was interlaminar as previously described). Maximum G_I occurred at the adhesive/strap interface, so this observation indicates that Mode I dominates the location of the crack and is consistent with adhesives exhibiting lower Mode I toughness than Mode II toughness.

Attempts at constructing a mixed mode failure diagram such as that shown in Figures 1 and 4a were of limited success. When sufficient data on a bonded system was available, it appeared that the $G_{Ic} < G_{IIc}$, and that G_{Ic} and G_{IIc} were affected similarly by environmental exposure. Mixed mode toughness values also appeared to follow this trend

of degradation. However, the mixed mode CLS tests did not yield results which confirmed the linear relationship between G_{Ic} and G_{IIc} that was previously proposed.^{1,66} Additional work is needed to explain the mixed mode behavior of the systems investigated for this research.

In terms of the fatigue behavior of the bonded systems, their characteristics are similar to those exhibited by metals in that da/dN and ΔG values can be related using a power law (Paris Law) relationship. However, the similarity ends here. Crack growth rates in the bonded joints were 2-6 times more sensitive to changes in ΔG_T than those of aluminum and titanium (as measured by the slope of da/dN vs. ΔG_T data). However, these growth rate sensitivities appeared to be unaffected by environmental exposure. In contrast, the threshold ΔG_T level in the Al/FM[®]73M/Al and Al/FM[®]73M/B-Ep systems was significantly degraded by exposure to a hot/wet environment. In the design and use of bonded joints, continued operation below identified threshold conditions (i.e. a safe-life approach) appears most conservative and, perhaps, imperative.

Despite their degradation in the presence of service environments, the adhesively bonded systems investigated for this research exhibited relatively high toughness values. Of particular note are the FM[®]x5 adhesives and Ti/FM[®]x5/Ti bonded joints. This high temperature system performed remarkably well in light of the fact that it was exposed to much higher temperatures and thermally cycled for many more cycles than were the epoxy adhesive systems.

From the standpoint of conducting the fracture and fatigue tests, the success of the experimental program was mixed. The bonded joint specimens exhibited higher toughness values than originally expected, so the testing of several joint geometries proved to be impossible due to premature adherend yielding or fatigue failures.

Application of the test results to two scenarios revealed how the fracture mechanics approach may be employed in the analysis and design of bonded joints. Though rough and approximate, these small studies illustrated how the data generated for and the analytical methods used in this thesis may be applied to analyze specific bonded components.

From a design viewpoint, analysis of the results of this research leads to several broad conclusions:

- exposure to aircraft service environments can be detrimental to bonded joint performance
- the extent and characteristics of environmental degradation in bonded joints cannot be generalized - they depend upon the specific bonded material system of interest
- similarly, the fracture path in bonded joints is dependent upon the adherend materials

- environmentally-induced trends in the fracture or fatigue properties of bonded joints may not always be revealed by chemical or physical analyses of the adhesives
- when surface preparation of the adherends is adequate, environmentally-induced trends in the fracture or fatigue properties of bonded joints may be revealed by changes in mechanical or fracture properties of the adhesives
- a safe life approach to fatigue design appears best in light of the extremely high crack growth rate sensitivities displayed by bonded joints

Stress-based analyses of adhesive joints have proven valuable in the past for the design of bonded aircraft structures using static strength considerations. However, to better comprehend damage tolerance in the presence of bond line flaws and durability under cyclic loading and environmental exposure, fracture mechanics offers an equally viable and more quantitative method for appropriate cases. The long-term integrity of bonds in repairs to aging aircraft and the full realization of the efficiencies possible with adhesively bonded composite joints for primary structures depends on a thorough understanding of their behavior which fatigue and fracture studies can provide.

Admittedly, the results discussed in this paper are specific to the materials, loading modes, and environments examined. However, these results serve as a valuable foundation for a database which is necessary for the continued and expanded use of bonded joints in the aerospace arena. In addition, regardless of the nature of the adherends, the adhesive, or the particular conditions of environmental exposure, the trend of degraded bonded joint performance should encourage designers and engineers to carefully consider environmental factors in determining the intended lifetimes of bonded structures.

An extension of the fracture mechanics approach to bonded joint assessment will add to current stress-based analyses and lead to a greater understanding of adhesive bond line durability in the presence of flaws, fatigue loads, and environmental factors.

CHAPTER XI

LESSONS LEARNED AND RECOMMENDATIONS

11.1. Lessons Learned

Successes and failures in any task contribute to the learning process, and this research program was no exception. The following sections describe some of the areas which may be improved upon in subsequent investigations of adhesively bonded joints.

11.1.1. Specimen Design

Unexpected problems occurred in the form of premature adherend yielding or fatigue failure in some of the bonded joint specimens. These cause of these problems was an underestimation of the toughness of the adhesives being tested. In retrospect, some preliminary tests should have been conducted to estimate the fracture toughness of the adhesive and to evaluate "candidate" geometries before finalizing specimen design.

11.1.2. Specimen Fabrication

The cooperation received from Lockheed Martin and Boeing in the form of specimen fabrication was outstanding. However, additional information should have been provided to these suppliers regarding some manufacturing details. In particular, the

surface finish of the specimen edges and a dimensional tolerance for specimen width should have been specified. Considerable time and effort was expended in improving "rough cut" surface finishes in the edges of the specimens. In addition, post test analysis of results would have been simplified had all the specimens been fabricated to higher tolerances in the width dimension. Specimen widths varied by approximately ± 4 mm (0.16 in.) from specimen to specimen, and keeping track of these variations was challenging in light of the number of specimens investigated for this program.

11.1.3. Crack Length Determination

Use of the traveling microscope and Questar long focal length microscope aided the determination of crack length during the experiments. However, crack length measurements still comprised the most tedious portion of the laboratory work. This was particularly true for fatigue tests which required monitoring of the specimens during long periods of time. The tasks of locating the crack tip and determining the crack length could be made less labor intensive if some of the capabilities of the Questar system could have been used more effectively. These capabilities specifically include the motorized travel available on one of the Questar models and the video recording equipment connected to both Questar systems in Georgia Tech's MPRL laboratory. In addition, a slight reduction of the magnification of the Questar system would have provided a larger focal area, reducing the need to traverse the microscope while providing adequate magnification to view the crack tip and observe crack growth.

11.2. Recommendations for Future Work

Based upon the experience gained during this research program, there are many issues contained within the general topic of bond durability and the more specific subject of the fracture and fatigue behavior of bonded aerospace joints which deserve further study. A listing at this point of every possibility for additional research would be inappropriate, lengthy, and, undoubtedly, incomplete. The following passages attempt to highlight some of what appear to be the most important topics for additional investigations.

11.2.1. Materials and Environments

Without stating the obvious (that all new adhesives be tested following exposure to all possible environmental conditions), some additional work on the performance of the three adhesives investigated for this project is warranted. Three important issues are the surface preparation of the adherends, the chemical and physical properties of the adhesives, and the determination and use of a realistic service environment.

11.2.1.1. Evaluate Other Surface Preparations

The surface preparations used for the research documented here represent "industry standards." These preparations have evolved over a number of years as methods of promoting adhesion and preserving the environmental durability of the critical interphase region between the adhesive and adherends. However, environmental standards may force the abandonment of some of these preparations, such as the sodium

dichromate based FPL etch used for aluminum and the chromic acid etch used for titanium. Other treatments such as the “scuff and rinse” methods used on composite adherends for this study appear quite arbitrary in light of the complex surface chemistry involved with metal adherends and also considering the interfacial, adhesive failure exhibited by the Al/FM[®]73M/B-Ep specimens. Given these issues, it may be necessary to re-evaluate the environmental durability of the AF-191, FM[®]73, and FM[®]x5 adhesives using alternative surface preparations. These techniques may include the silane process for metal adherends and surface preparations which better address the interaction between the adhesive and polymer-matrix composite adherends.

11.2.1.2. Conduct Additional Chemical and Physical Analyses of Adhesives

The investigations of the glass transition temperature (using DSC), degradation temperature (using TGA), and polymer structure (using FTIR spectroscopy) conducted for this research should be considered preliminary. The proprietary nature of the adhesive formulations prevents many of these test results from being fully understood. The relatively few tests which were conducted do not provide adequate information with which to determine what changes in the observed results may be considered significant. Therefore, a need exists to conduct additional testing on the chemical and physical changes which occur in the adhesives following environmental exposure. These evaluations would mesh neatly with investigations of alternative surface preparations by providing information about the durability of two main components of a bonded joint, the

adhesive and the interphase region. One additional technique which should be added to the current battery of chemical and physical analyses is dynamic mechanical analysis (DMA). This technique detects minute changes in the mechanical behavior of polymers subject to varying temperatures. Because of its ability to link temperature and mechanical properties, DMA may prove to be a technique that provides a valuable connection between chemical/physical changes in the adhesive polymer and changes observed in the mechanical behavior of bonded joints.

11.2.1.3. Investigate "True" Service Environments

The environments used for the exposure of the specimens tested for this research were based upon aircraft service environments (actual and projected) and typical industry test conditions. However, in retrospect, some of the conditions used, particularly the hot/wet condition, may have been too severe. Others, such as the 163°C (325°F) thermal cycling limit for the HSCT joints appeared to be arbitrary. Naturally, environmental conditioning must be conservative, but the environments examined for this research may have raised unfounded concerns regarding adhesive durability. Therefore, before conducting additional experiments, it would be prudent to establish limits on the severity of exposure environments. This may be accomplished through a survey of actual service conditions for a particular bonded component or through the exposure of specimens to atmospheric conditions (i.e. "rooftop" exposure). The latter approach would avoid concerns about misunderstanding the synergistic effects present in accelerated aging. A

small number of Al/FM[®]73M/B-Ep specimens are currently undergoing “rooftop” exposure at Georgia Tech.

In addition, the drastic toughness losses in specimens tested at -54°C (-65°F) for this research should encourage continued investigations of the low temperature behavior of bonded joints. These tests should be conducted on exposed specimens to determine to what extent the effects of low test temperature and environmental exposure are additive.

11.2.2. Test Procedures

The test procedures used to evaluate bonded joints for the current research were based upon methods developed during the last three decades. Modifications to these test methods are continuing. Such modifications may permit a variety of Mode I/II ratios to be produced in pursuit of tests that will more closely duplicate actual operating loads.

11.2.2.1. Conduct Additional Tests at Various Mode I/II Ratios

The DCB and ENF specimen geometries used for this research provided information on the Mode I and Mode II fracture and fatigue behavior of a number of bonded systems. The cracked lap shear geometry was also used to provide information on mixed Mode I/II behavior. Although the CLS geometry is regarded as most closely representing the loads placed on joints in service, it only produces a relatively narrow mode ratio (approximately 20-30% of G_I). In addition, although the DCB geometry was

the easiest to test, the information which it provides is for Mode I, a mode of loading which is uncommon in adhesively bonded joints designed for aircraft use.

Therefore, to more accurately determine a failure envelope for adhesives (such as that suggested by Johnson & Mangalgiri⁶⁶), and to more accurately simulate operational loading modes, additional tests should be conducted at various mode ratios. These could be accomplished using a number of methods including the specialized test fixtures developed by Reeder & Crews⁶⁵ and Fernlund & Spelt.¹⁴³

11.2.2.2. Duplicate Loading Conditions for Specific Applications

In addition to developing failure envelopes for adhesives, mixed mode testing at various mode ratios would also allow adhesives to be evaluated under loading conditions indicative of those on specific bonded components. The test fixtures mentioned in the previous paragraph would allow service conditions to be duplicated in the laboratory environment. The challenge, however, will be expressing joint loads in terms of applied strain energy release rates. Current industry practice describes running loads in terms of force or stress. Prior to attempting to duplicate service conditions with mixed mode fracture and fatigue tests, methods will have to be developed to express these conditions in terms of Mode I, II, and III applied strain energy release rates.

Another way in which actual loading conditions could be further investigated is through a study of R ratio effects. An R of 0.1 was used for the research reviewed in this thesis based upon previous work in the field. However, service applications may

experience much higher R ratio levels, and the effect of these on the fatigue behavior of bonded joints should be examined.

11.2.3. Analysis

Advances in closed-form solutions and finite element methods make the analysis of bonded joints a continually changing research arena. The following sections suggest topics for additional work in this area.

11.2.3.1. Improve Current Models of the Adhesive Layer

The research conducted for this project assumed that the adhesive bond line was homogeneous and linearly elastic. However, all of the adhesives contained some form of scrim cloth, and testing of the adhesive specimens revealed that some display significant plasticity prior to failure. The effects of these details on the performance of analytical models need to be determined. Thus some degree of future work should focus on investigating the viscoelastic behavior of the adhesives and incorporating this information along with the inherent nonlinear behavior of the adhesives into finite element models. This was begun, to a degree, with the use of experimentally-obtained modulus values in the finite element work performed by Valentin for this research. However, the material nonlinearity was not incorporated into his models and merits additional examination.

11.2.3.2. Conduct Parametric Studies on Bonded Joint Applications

To complement future experimental efforts aimed at reproducing the loading conditions of bonded components in laboratory specimens, some analytical work may also be required. Existing methods and codes may be modified or new ones developed to predict the strain energy release rate values present in bonded joints during operation. The results of these analytical studies of bonded joints would prove invaluable in planning and conducting experimental tests designed to duplicate service conditions.

11.2.3.3. Expand Current Finite Element Models

The modeling effort performed for this research using GAMNAS and ABAQUS was aimed at understanding the behavior of experimental test specimens. Some efforts have been made to extend the use of these finite element techniques to address the behavior of bonded applications. However, these efforts have been based upon the models of test specimens and upon a number of assumptions. The finite element programs currently available are capable of much more complex analyses, and these capabilities should be used to develop more realistic models of bonded joints and repairs. The same basic techniques for finding the bond line strain energy release rates should apply. However, this additional work will help to better understand the effect of mixed mode loading in three dimensions.

11.2.4. Additional Topics for Further Research

The environmental durability of bonded joints is a broad area of research. The previous sections covered only some of the opportunities for additional work in this area, but many other topics also need to be addressed. The following suggestions for future work are provided without discussion to add to the list of research issues already included in this chapter.

- perform nondestructive investigation to determine shape and extent of the crack front in the interior of joints and specimens
- evaluate other fracture mechanics parameters such as the J-integral, C^* , etc.
- develop ASTM standardized tests tailored for use with bonded joints for the ENF, CLS, and other specimen geometries if appropriate
- conduct parallel design exercises using stress-based and fracture mechanics approaches on a common bonded component
- investigate the role of Mode III, especially at the edges of specimens and joints
- determine the moisture content of the bond line *in situ* to better understand the effects of environmental exposure
- conduct additional fatigue tests to determine whether a threshold exists for bonded joints and to evaluate the utility of the current threshold of 10^{-6} mm/cycle (4×10^{-8} in./cycle)

- more closely examine the role of scrim cloth and attempt to understand the differences between its in-plane behavior during tensile tests of adhesive film specimens and its out-of-plane behavior in bonded joints

APPENDIX A

SPECIMEN FABRICATION PROCEDURES

This appendix is intended to provide detailed information regarding the fabrication and curing of adhesive and bonded joint specimens. This information is in addition to that contained in Chapter 3 - Materials and Specimens. Specimen dimensions may be found in Chapter 3.

A.1. Adhesive Sheets Used for Tensile and Fracture Toughness Tests

Adhesive test specimens were cut from cured adhesive sheets. These sheets were cured either at the Georgia Institute of Technology or at the adhesive manufacturer depending upon the material.

A.1.2. Curing of FM[®]73 and AF-191 Sheets

FM[®]73 and AF-191 adhesive sheets used for tensile and fracture toughness tests were cured at the Georgia Institute of Technology on a porous Teflon[™]-covered aluminum plate in a Precision "Thelco" circulating air oven. The sheets should be cured without pressure using a single layer of the adhesive film. Use of a vacuum bag or autoclave and attempts at curing multiple film layers resulted in cured sheets with

unacceptably high levels of voids. Curing of these adhesive sheets was performed using the following procedures.

- I. Remove adhesive film from refrigerated storage and keep in sealed bag until adhesive has reached room temperature
- II. Cut adhesive film to desired size (approximately 250 mm × 250 mm [10 in. × 10 in.])
- III. Remove backing sheets and place on Teflon™-covered aluminum plate
- IV. Permit uncured adhesive to be exposed to a laboratory environment (22°C [72°F], 50% rh) for at least two hours. This was found to significantly reduce the amount of voids in the cured materials presumably by allowing volatiles to escape before being entrapped during the curing process.
- V. Place in oven and ramp to 177°C (350°F) [for the AF-191] or 115°C (240°F) [for the FM[®]73] at 4-6°C (8-10°F) per minute
- VI. Hold at temperature for 60 min. [for the AF-191] or 150 min. [for the FM[®]73]
- VII. Remove from oven, air cool

A.1.2. Curing of FM[®]x5 Sheets

FM[®]x5 sheets (approximately 150 mm × 150 mm [6 in. × 6 in.]) were provided by CYTEC Engineered Materials, Inc., and were cured in an autoclave using the following procedure.^{87,144}

- I. Apply full vacuum
- II. Ramp to 250°C (482°F) at 3-4°C (5-7°F) per minute
- III. Hold at 250°C (482°F) for 60 minutes
- IV. Add 0.34 MPa (50 psi) and vent the vacuum
- V. Ramp to 350°C (662°F) at 2-3°C (3-4°F) per minute
- VI. Hold at 350°C (662°F) for 60 minutes
- VII. Cool to 38°C (100°F) at 3-4°C (5-7°F) per minute

A.2. Aluminum/FM[®]73M/Aluminum (Al/FM[®]73M/Al) Specimens

Al/FM[®]73M/Al specimens were fabricated by Lockheed Martin Aeronautical Systems Company (Marietta, GA) according to their standard practice for adhesive bonding.¹⁴⁵ Large plates of 7075-T651 bare Al were bonded together, and individual specimens were subsequently cut from the large bonded panels. Double cantilever beam (DCB) specimens used 9.53 mm (0.375 in.) thick plates. End-notched flexure (ENF) and cracked lap shear (CLS) specimens used 4.06 mm (0.16 in.) thick plates. The following sections provide the manufacturing process details.

A.2.1. Surface Preparation of 7075-T651 Bare Aluminum Plates

- I. Degrease with a methylethylketone (MEK) wipe
- II. Grit blast with 150 grit aluminum oxide (Al₂O₃)
- III. Wipe with methanol

- IV. Scrub with *Alconox* (alkaline soap) cleaner
- V. Rinse thoroughly with water
- VI. Etch using Forest Products Lab "FPL" sodium dichromate paste for 20 minutes
- VII. Rinse thoroughly with water
- VIII. Brush on CYTEC BR[®]127 primer
- IX. Cure primed plates in oven at 113°C (235°F) for 240 minutes

A.2.2 Assembly of Al/FM[®]73M/Al Panels

- I. Determine amount of panel edge to remain unbonded
 - A. DCB specimens: ~ 57 mm (2.25 in.)
 - B. ENF and CLS specimens: ~ 6.4 mm (0.25 in.)
- II. Cut to size CYTEC FM[®]73M adhesive film (300 g/m² [0.06 lb./ft.²]) containing a non-woven polyester scrim cloth
- III. Cut to size Wrightlon[™] 4500 halohydrocarbon release film (51 µm [2 mils] thick, folded for a total thickness of (102 µm [4 mils]))
- IV. Place adhesive and folded release films on one primed panel in a manner such that the desired edges of the final panel assembly remains unbonded due to the presence of the release film
- V. Place second panel on top of adhesive and release films
- VI. Drill corners of panels and install alignment pins

A.2.3 Bonding of Al/FM[®]73M/Al Panels

- I. Place assembled panel on top of tool
- II. Cover panel with the following sequence of materials:
 - A. *Armalon* film
 - B. Release film
 - C. Breather cloth
 - D. Vacuum bag
- III. Pull vacuum (735 Torr [29 in. of Hg])
- IV. Cure assembled panel in oven at 116°C (240°F) for 150 minutes

A.2.4 Cutting of Al/FM[®]73M/Al Panels to Form Individual Specimens

1. Perform with a conventional abrasive wheel on a table saw
2. Lightly grind edges using a water-cooled abrasive belt sander (240 grit)

A.3. Aluminum/FM[®]73M/Boron-Epoxy (Al/FM[®]73M/B-Ep) Specimens

Al/FM[®]73M/B-Ep specimens were fabricated by Lockheed Martin Aeronautical Systems Company (Marietta, GA) according to their standard practice for adhesive bonding.³ Large plates of 7075-T651 bare Al were bonded to pre-cured laminates of Textron Specialty Materials F4/5521 boron-epoxy composite material. Individual specimens were subsequently cut from the large bonded panels. The following sections provide the manufacturing process details.

A.3.1. Aluminum/Boron-Epoxy Combinations for Various Specimen Geometries

Aluminum thicknesses and composite lay-ups for the three specimen geometries examined were as follows:

- I. Double cantilever beam (DCB) specimens
 - A. Al: 9.53 mm (0.375 in.) thick
 - B. B-Ep: $[0_4/90/0_3/90/0]_s$ 20 plies
- II. End-notched flexure (ENF) specimens
 - A. Al: 4.06 mm (0.16 in.) thick
 - B. B-Ep: $[0_4/90/0_3/90/0_3/90/0]_s$ 28 plies
- III. Cracked Lap Shear (CLS) specimens
 - A. Al: 4.06 mm (0.16 in.) thick
 - B. Specimens with B-Ep strap: $[0_6/\bar{0}]_s$ 13 plies
 - C. Specimens with B-Ep lap: $[0_2/90/0_2/90/0_2/90/\bar{0}]_s$ 19 plies

A.3.2. Curing of Boron-Epoxy Laminates

- I. Cover tool with release film
- II. Place desired lay-up of pre-preg on covered tool
- III. Cover lay-up with the following sequence of materials:
 - A. Armalon film
 - B. Breather cloth (thin)

- C. Release film
 - D. Breather cloth
 - E. Vacuum bag
- IV. Cure in autoclave for 75 minutes at:
- A. Temperature: 121°C (250°F)
 - B. Pressure: 585 kPa (85 psi)
 - C. Full Vacuum

A.3.3. Surface Preparation of Cured Boron-Epoxy Laminates

- I. Dry panels at 66°C (150°F) for 180 minutes
- II. Sand with 280 grit abrasive paper
- III. Clean with a methanol wipe

A.3.4. Assembly and Curing of Al/FM[®]73M/B-Ep Panels

Assembly of the panels and subsequent curing of the Al/FM[®]73M/B-Ep panels was performed using the same procedures as outlined for the Al/FM[®]73M/Al specimens.

A.3.5. Bonding of Hinges to Double Cantilever Beam Specimen Panels

- I. Cut hinges to match length of panel edge
- II. Prepare surfaces of panel and hinges using sodium dichromate etch described above
- III. Bag panels as described above

IV. Cure in oven at 110°C (230°F), 735 Torr (29 in. of Hg) for 150 minutes

A.3.6. Cutting of Al/FM[®]73M/B-Ep Panels to Form Individual Specimens

Because of the dissimilar adherends in these specimens (relatively soft aluminum and hard, brittle boron fibers), cutting was a challenge. The thinner panels were cut into individual CLS and ENF specimens using a Marvel saw equipped with a carbide blade. The thick panels were cut into individual DCB specimens in two stages. The first stage used a power hacksaw to cut most of the way through the aluminum. A diamond blade was then used to cut through the boron-epoxy. The edges of all specimens were "cleaned up" using a water cooled belt sander and 240 grit abrasive cloth.

A.4. Graphite-Bismaleimide/AF-191M (Gr-BMI/AF-191M/Gr-BMI) Specimens

Gr-BMI/AF-191M/Gr-BMI specimens were fabricated by Lockheed Martin Aeronautical Systems Company (Marietta, GA) according to their standard practice for adhesive bonding.¹⁴⁶ Large pre-cured laminates of BASF IM7/5250-4 graphite-reinforced bismaleimide composites were secondarily bonded to form large bonded panels. Individual specimens were subsequently cut from the large bonded panels. The following sections provide the manufacturing process details.

A.4.1. Gr-BMI Composite Adherend Lay-Ups

Specimens were fabricated using two varieties of composite laminate lay-up.

- I. "Unidirectional" Lay-up, $[0_4/\overline{90}]_s$ 9 Plies
- II. "Quasi-Isotropic" Lay-up, $[+45/-45/0_2/+45/-45/90]_s$ 14 Plies

A.4.2. Curing of Gr-BMI Laminates

- I. Cover tool with Teflon™ release film
- II. Place desired lay-up of pre-preg on covered tool
- III. Cover lay-up with the following sequence of materials:
 - A. 120 glass cloth peel ply
 - B. Teflon™ release film
 - C. 120 glass cloth
 - D. Breather cloth
 - E. Vacuum bag
- IV. Cure in autoclave
 - A. Temperature: 191°C (375°F)
 - B. Pressure: 620 kPa (90 lb./in.²) minimum
 - C. Full Vacuum

A.4.3. Surface Preparation of Cured Gr-BMI Laminates

- I. Dry panels at 121°C (250°F) for 240 minutes and 177°C (350°F) for 120 minutes
- II. Remove peel ply
- III. Sand with 180 grit abrasive paper

- IV. Wipe with dry cloth
- V. Clean with a methanol wipe
- VI. Perform water break test
- VII. Air dry

A.4.4. Assembly of Gr/BMI/AF-191M/Gr-BMI Panels

- I. Determine amount of panel edge to remain unbonded
 - A. DCB specimens: ~ 57 mm (2.25 in.)
 - B. ENF and CLS specimens: ~ 6.4 mm (0.25 in.)
- II. Cut to size 3M AF-191M adhesive film (300 g/m^2 [0.06 lb./ft.^2]) containing a non-woven nylon scrim cloth on one face
- III. Cut to size Wrightlon™ 4500 halohydrocarbon release film ($51 \text{ } \mu\text{m}$ [2 mils] thick, folded for a total thickness of ($102 \text{ } \mu\text{m}$ [4 mils])
- IV. Place adhesive and folded release films on one primed panel in a manner such that the desired edges of the final panel assembly remains unbonded due to the presence of the release film
- V. Place second panel on top of adhesive and release films
- VI. Drill corners of panels and install alignment pins

A.4.5. Bonding of Gr-BMI/AF-191M/Gr-BMI Panels

- I. Cover tool with release film

- II. Place desired lay-up of pre-preg on covered tool
- III. Cover panel with the following sequence of materials:
 - A. Armalon film
 - B. Release film
 - C. Breather cloth
 - D. Vacuum bag
- IV. Pull vacuum (735 Torr [29 in. of Hg])
- V. Cure assembled panel in oven at 177°C (350°F) for 60 minutes

A.4.6. Bonding of Hinges to Double Cantilever Beam Specimen Panels

- I. Cut hinges to match length of panel edge
- II. Prepare surface of hinges
 - A. Wipe with methanol
 - B. Grit blast with 150 grit aluminum oxide (Al_2O_3)
 - C. Wipe with methanol
 - D. Scrub with Alconox (alkaline soap) cleaner, rinse and dry
 - E. Brush on CYTEC BR[®]127 primer
- III. Prepare surface of cured Gr-BMI panels
 - A. Grit blast with 150 grit aluminum oxide (Al_2O_3)
 - B. Wipe with methanol

- IV. Apply CYTEC FM[®]73M adhesive film (300 g/m^2 [0.06 lb./ft.^2]) containing a non-woven polyester scrim cloth
- V. Place hinges on panels, and place assembly on tool
- VI. Cover assembly with the following sequence of materials:
 - A. Armalon film
 - B. Release film
 - C. Breather cloth
 - D. Vacuum bag
- VII. Cure in oven at 121°C (250°F), 735 Torr (29 in. of Hg) for 60 minutes

A.4.7. Cutting Gr-BMI/AF-191M/Gr-BMI Panels to Form Individual Specimens

Panels used for the CLS and ENF specimens were cut using a diamond wheel. Panels used for the DCB specimens were cut using a diamond-impregnated bandsaw due to the presence of dissimilar materials (aluminum hinges, composite adherends).

A.5. Titanium/FM[®]x5/Titanium (Ti/FM[®]x5/Ti) Specimens

Ti/FM[®]x5/Ti specimens were fabricated by the Boeing Defense & Space Group (Seattle, WA) according to their standard practice for adhesive bonding.¹⁴⁷ Large plates of 6.604 mm (0.26 in.) thick Ti-6Al-4V titanium were bonded to form large panels. Individual specimens were subsequently cut from the large bonded panels. The following sections provide the manufacturing process details.

A.5.1. Surface Preparation of Ti-6Al-4V Titanium Plates

Surface preparation for the titanium adherends followed Boeing's standard chromic acid anodizing procedure, BAC5890,¹⁴⁸ which is comprised of the following steps:

- I. Emulsion degrease IAW BAC5763 or solvent clean IAW BAC5750
- II. Alkaline clean IAW BAC5749
- III. Rinse with hot water (43°C [110°F] minimum) for 5 minutes
- IV. Etch in nitric-hydrofluoric acid solution IAW BAC5753, method II, for 30-90 seconds
- V. Rinse in cold water for 5 minutes
- VI. Anodize in chromic acid solution, continuous agitation, 9-10 volts for 20-22 minutes
- VII. Rinse in cold water for 10-15 minutes
- VIII. Dry at 71°C (160°F) maximum

A.5.2. Assembly of Ti/FM[®]x5/Ti Panels

- I. Determine amount of panel edge to remain unbonded
 - A. DCB specimens: ~ 57 mm (2.25 in.)
 - B. ENF and CLS specimens: ~ 6.4 mm (0.25 in.)
- II. Cut to size CYTEC FM[®]x5 adhesive film containing a woven glass scrim cloth
- III. Cut to size Kapton[™] release film (140 µm [5.5 mil]) thick, folded for a total thickness of (280 µm [11 mils])

- IV. Place adhesive and folded release films on one primed panel in a manner such that the desired edges of the final panel assembly remains unbonded due to the presence of the release film
- V. Place second panel on top of adhesive and release films

A.5.3. Bonding of Ti/FM[®]x5/Ti Panels

- I. Prepare assembled panel for autoclave curing using appropriate bagging materials
- II. Apply full vacuum and apply 69 kPa (10 psi) to autoclave
- III. Heat to 288°C (550°F) at 2°C (4°F) per minute
- IV. Hold at 288°C (550°F) for 30 minutes
- V. Increase autoclave pressure to 345 kPa (50 psi)
- VI. Heat to 350°C (662°F) at 2°C (4°F) per minute
- VII. Hold at 350°C (662°F) for 90 minutes
- VIII. Cool to room temperature at 2°C (4°F) per minute
- IX. Release vacuum and pressure when temperature reaches 93°C (200°F)

A.5.4. Cutting Ti/FM[®]x5/Ti Panels to Form Individual Specimens

Ti/FM[®]x5/Ti panels were cut into individual specimens using a power bandsaw. because this method resulted in a very poor surface finish on the edges of the specimens, subsequent grinding of the edges was performed by the Base Machine Shop, Wright-Patterson AFB, OH.

APPENDIX B

CONFIDENCE INTERVAL ANALYSIS OF SELECTED BONDED SYSTEMS

Some of the testing conducted for this research resulted in a number of fracture toughness values being generated for specific combinations of materials and specimen geometries. These multiple values were analyzed using the confidence interval concept discussed in section 6.7. The results from this effort are presented here. Recall that overlapping confidence intervals signal that the averages of the two data sets being compared cannot be held to be significantly different. Also recall that the confidence intervals in some cases are quite large due to a small number of values from which the average values were computed.

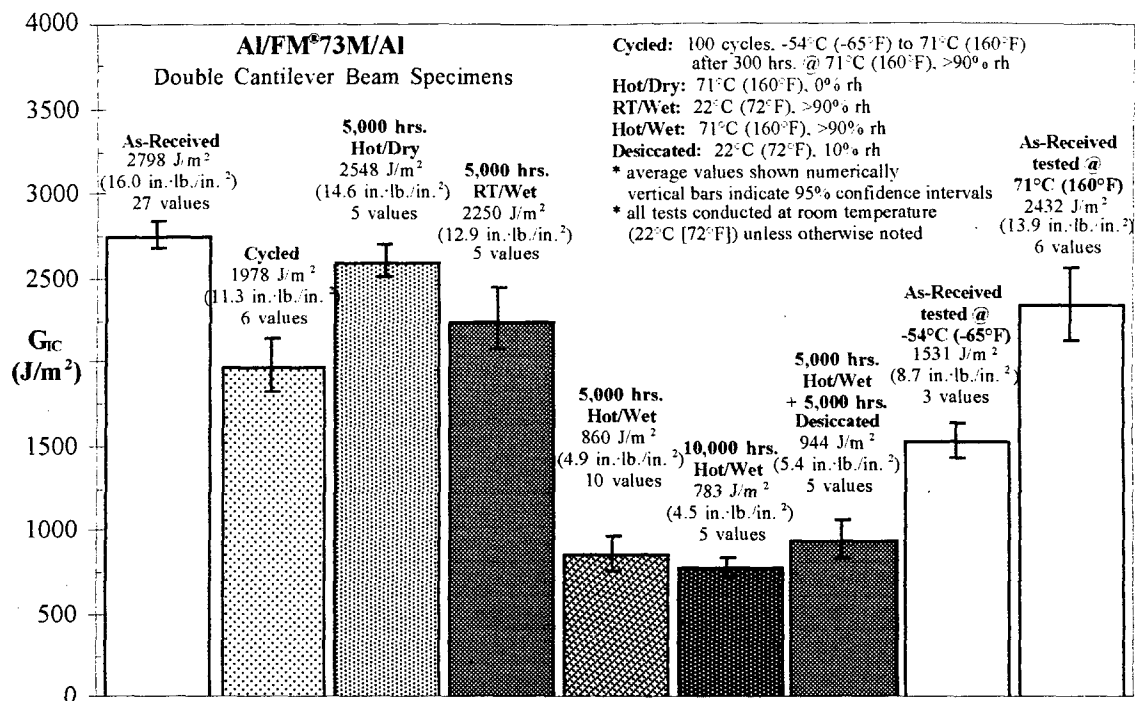


Figure 93. Mode I fracture toughness of the Al/FM[®]73/Al bonded system (with estimated confidence intervals)

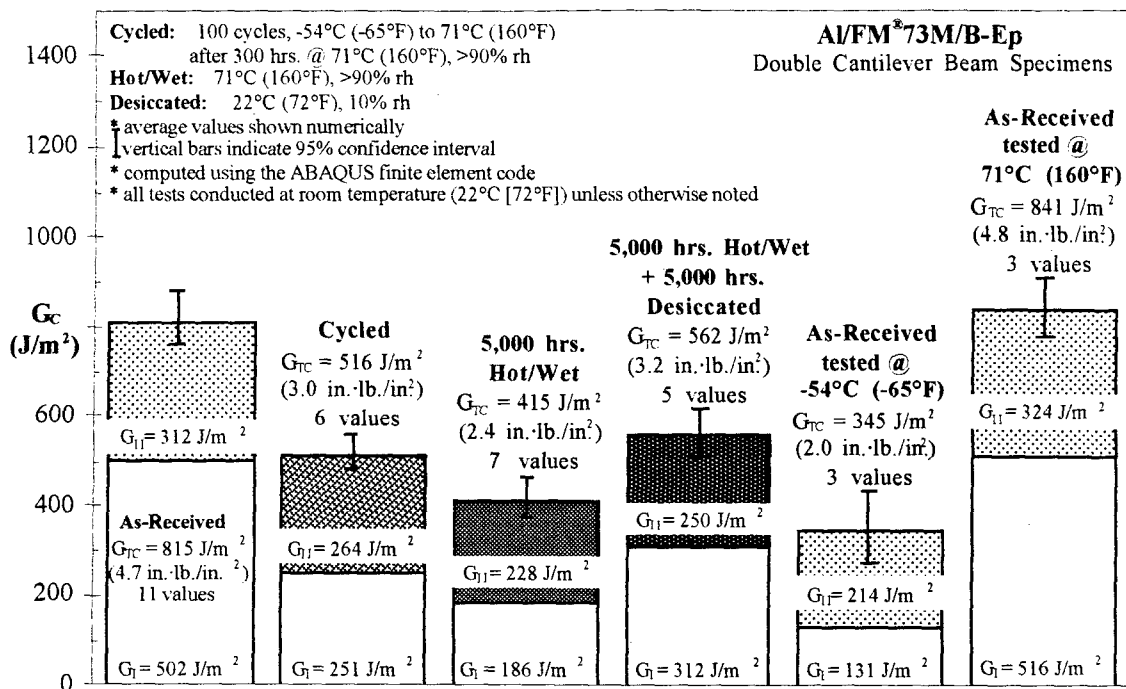


Figure 94. Fracture toughness of the Al/FM[®]73/B-Ep DCB specimens (with estimated confidence intervals)

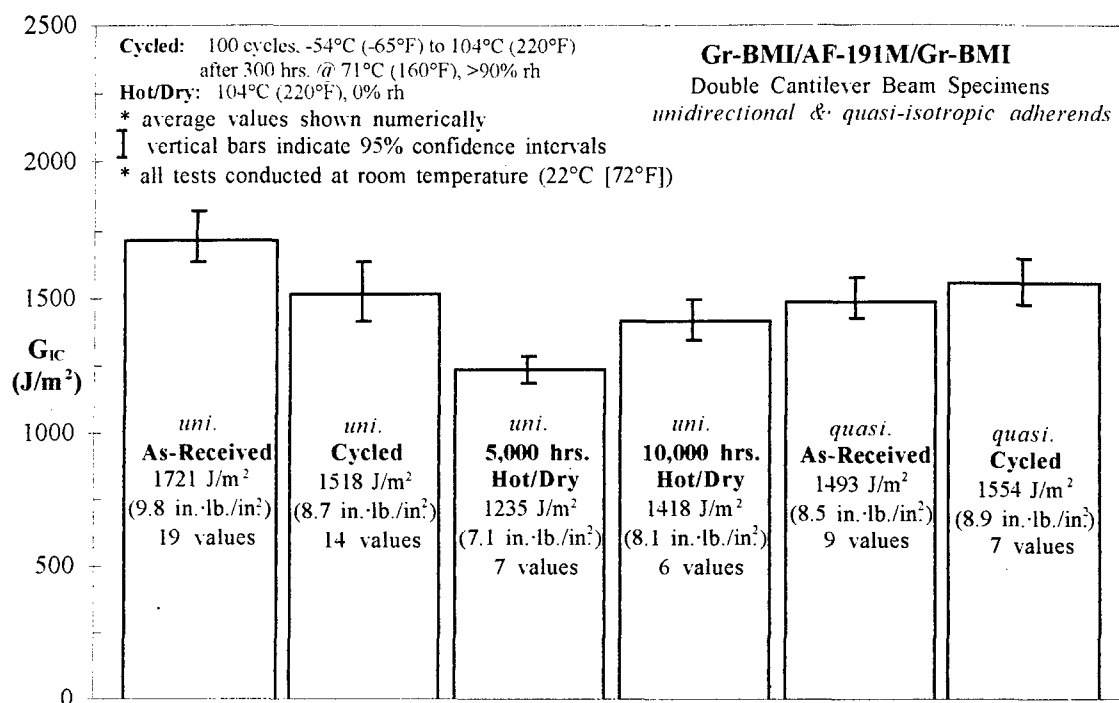


Figure 95. Effect of environmental exposure on the Mode I fracture toughness of the Gr-BMI/AF-191/Gr-BMI bonded system (with estimated confidence intervals)

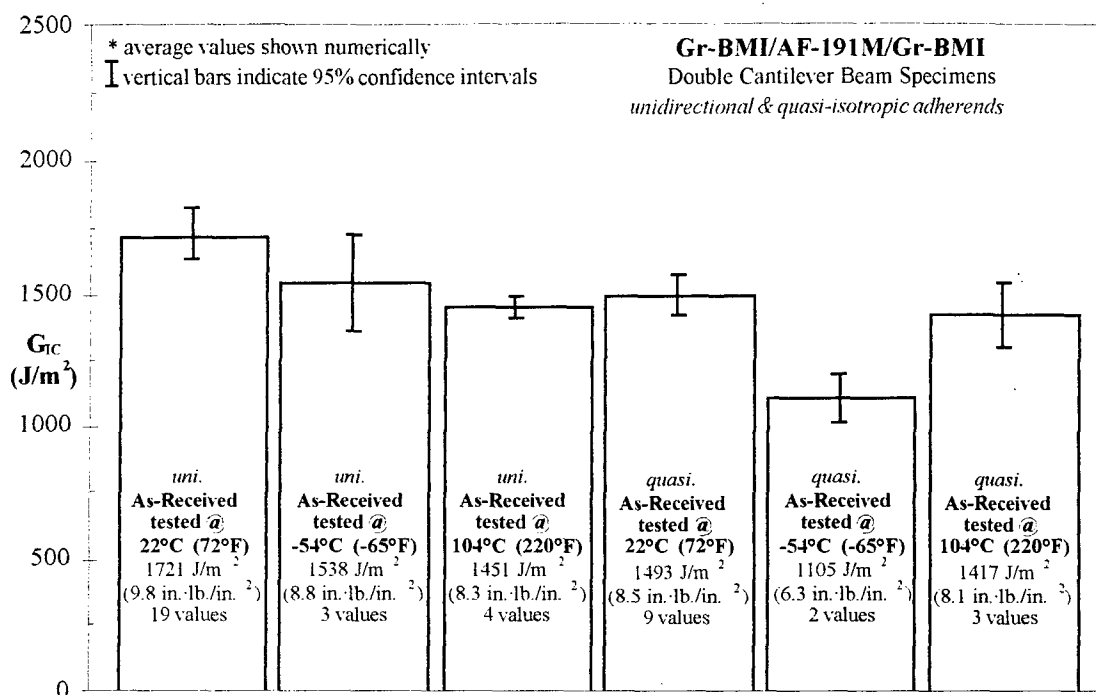


Figure 96. Effect of test temperature on the Mode I fracture toughness of the Gr-BMI/AF-191/Gr-BMI bonded system
 (with estimated confidence intervals)

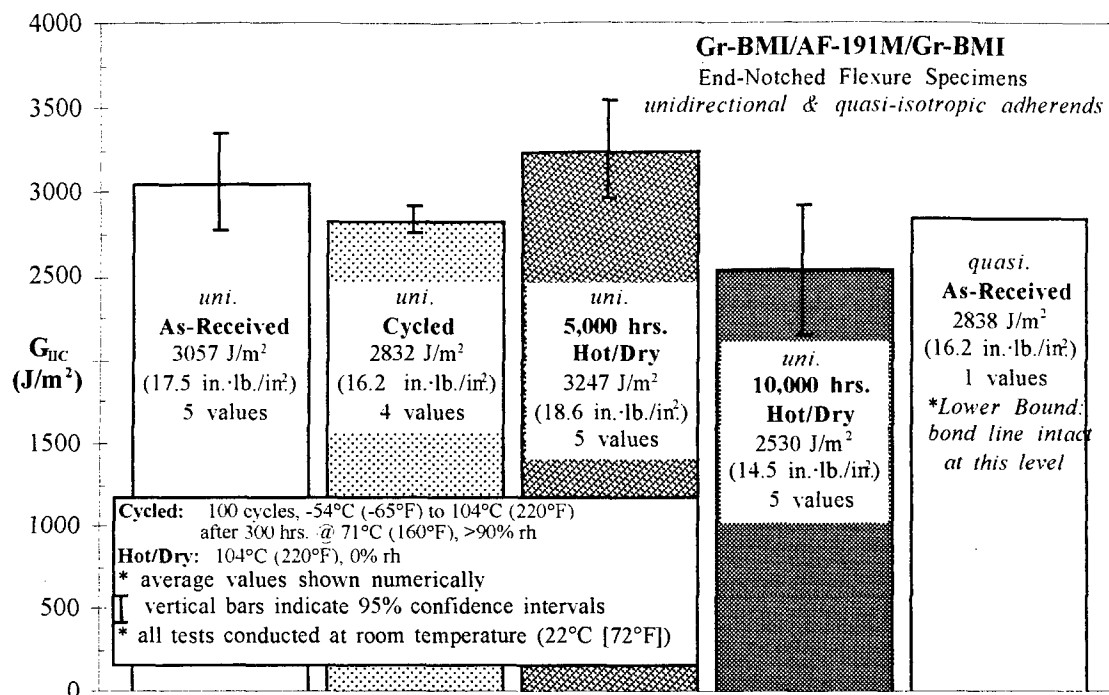


Figure 97. Mode II fracture toughness of the Gr-BMI/AF-191/Gr-BMI bonded system
(with estimated confidence intervals)

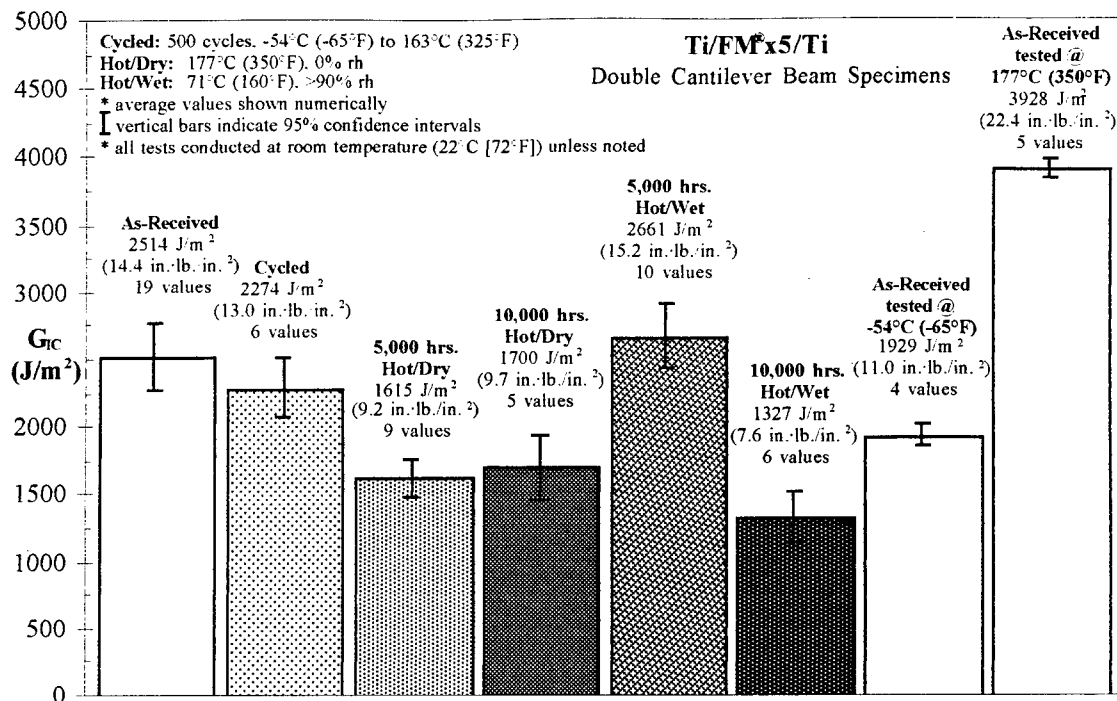


Figure 98. Mode I fracture toughness of the Ti/FM[®]x5/Ti bonded system (with estimated confidence intervals)

ENDNOTES

- ¹ Johnson, W.S. and Butkus, L.M., "Considering Environmental Conditions in the Design of Bonded Structures: A Fracture Mechanics Approach," *International Journal of Fatigue and Fracture of Engineering Materials and Structures*, accepted: July 1997.
- ² Butkus, L.M., Mathern, P.D., and Johnson, W.S., "Tensile Properties and Plane-Stress Fracture Toughness of Thin Film Aerospace Adhesives," *The Journal of Adhesion*, submitted: June 1997.
- ³ Valentin, R.V., Butkus, L.M., and Johnson, W.S., "A Finite Element and Experimental Evaluation of Boron-Epoxy Doublers Bonded to an Aluminum Substrate," *Journal of Composites Technology & Research*, submitted: Apr. 1997.
- ⁴ Ellis, J.R., Bailey, G.L. and Kuhn, G.E., *Laminated Hybrid Wing Box Structure, Part I - Preliminary Design*, Vought Corporation, Dallas, TX, for the USAF Flight Dynamics Laboratory, AFFDL-TR-78-28, Mar 1978.
- ⁵ McClaren, S.W., Maris, J.L. and Ely, R.A., *Advanced Wing Box Evaluations*, AFWAL-TR-80-3033, Vought Corporation, Dallas TX, for the USAF Flight Dynamics Laboratory, Apr. 1980.
- ⁶ Poole, P., Young, A. and Ball, A.S., "Adhesively Bonded Composite Patch Repair of Cracked Aluminum Alloy Structures," in Composite Repair of Military Aircraft Structures: Proceedings of the 79th Meeting of the AGARD (Advisory Group for Aerospace Research & Development) Structures and Materials Panel, Seville, Spain, 1994, pp. 3-1 to 3-12.
- ⁷ Fredell, R.S., Damage Tolerant Repair Techniques for Pressurized Aircraft Fuselages, Technical University of Delft, Delft, the Netherlands, 1994.
- ⁸ Baker, A.A., "Bonded Composite Repair of Metallic Aircraft Structures," in Composite Repair of Military Aircraft Structures: Proceedings of the 79th Meeting of the AGARD (Advisory Group for Aerospace Research & Development) Structures and Materials Panel, Seville, Spain, 1994, pp. 1-1 to 1-14.

- ⁹ Hart-Smith, L.J., "Adhesive Bonding of Aircraft Primary Structures," in High Performance Adhesive Bonding, G. DeFrayne, ed., Society of Manufacturing Engineers, Dearborn, MI, 1983, pp. 99-113.
- ¹⁰ Blomquist, R.F., "Adhesives - Past, Present, and Future," in Adhesion, ASTM STP 360, American Society for Testing and Materials, Philadelphia, PA, 1963, pp. 179-212.
- ¹¹ Kutscha, D., and Hofer, K.E., Jr., *Feasibility of Joining Aerospace Composite Flight Vehicles*, USAF Materials Laboratory, Wright-Patterson AFB, OH, AFML-TR-68-391, Jan. 1969.
- ¹² Committee on Reliability of Adhesive Bonds in Severe Environments, "Reliability of Adhesive Bonds in Severe Environments," National Materials Advisory Board, Washington, D.C., 1984.
- ¹³ Schliekelmann, R.J., "Past, Presence, and Future of Structural Adhesive Bonding in Aero-Space Applications," *Transactions of the Japanese Society of Composite Materials*, Vol. 5, No. 1/2, Dec. 1979, pp. 1-12.
- ¹⁴ "Structural Adhesive Bonding in Fokker-VFW Aircraft," *Ciba-Geigy Technical Notes*, 3/1977, Ciba-Geigy Plastics and Additives, Co., Cambridge, UK, 1977.
- ¹⁵ Irving, R.R., "A Tale of Adhesively-Bonded Aircraft," *Iron Age*, May 4 1981, pp. 87-88.
- ¹⁶ Potter, D.L., *Primarily Adhesive Bonded Structure Technology (PABST), Design Handbook for Adhesive Bonding*, Douglas Aircraft Co., Long Beach, CA, for the USAF Flight Dynamics Laboratory, AFFDL-TR-79-3129, Jan 1979.
- ¹⁷ Vinson, J.R., "On the State of Technology in Adhesively Bonded Joints in Composite Material Structures," in Emerging Technologies in Aerospace Structures, Design, Structural Dynamics, and Materials, J.R. Vinson, ed., American Society of Mechanical Engineers, New York, NY, 1980, pp. 67-85.
- ¹⁸ Jeans, L.L., Grimes, G.C., and Kan, H.P., *Fatigue Spectrum Sensitivity Study for Advanced Composite Materials: Volume 1: Technical Summary*, Northrop Corp., Hawthorne, CA, for USAF Flight Dynamics Laboratory, AFWAL-TR-80-1130, Dec. 1980.

- ¹⁹ Reeve, S., Personal Communications, Lockheed Martin Aeronautical Systems, Co., Marietta, GA, 1995-6.
- ²⁰ Newman, R.J., "Where's the Target?," *U.S. News & World Report*, 7 Oct. 96, pp. 46-48.
- ²¹ Skanchy, T.C., "The F-22 is Too Costly: Scrub It," *Air Force Times*, Feb. 3, 1997, pg. 29.
- ²² Mitchell, S., Personal Communication, The Boeing Company, Seattle, WA, 1 Aug. 1997.
- ²³ Gregg, P.S., Personal Communication, The Boeing Company, Seattle, WA, 5 Aug. 1997.
- ²⁴ Quist, W.E., "The High Speed Civil Transport (HSCT)," Meeting of the Atlanta Chapter of ASM International, 27 May 1997.
- ²⁵ Mehuron, T.A., ed., "USAF Almanac 1995," *Air Force*, **78**, No. 5, Air Force Association, Alexandria, VA, May 1995, pp. 35-125.
- ²⁶ Tirpak, J.A., "The Aging of the Fleet," *Air Force Magazine*, June 1996, pp. 14-17.
- ²⁷ Committee on Aging of U.S. Air Force Aircraft, "Aging of U.S. Air Force Aircraft: Interim Report," National Academy of Sciences, National Materials Advisory Board, Washington, D.C., Mar. 1997.
- ²⁸ Adams, F., "The Life Enhancement Core Area," *Structures Division Current Awareness Bulletin*, Aerospace Structures Information and Analysis Center, Wright-Patterson AFB, OH, Fall/Winter 1996.
- ²⁹ Donohue, G., NASA Assoc. Administrator for Research and Acquisition, "Keynote Address," FAA/NASA Symposium on Continued Airworthiness of Aircraft Structures, Atlanta, GA, Aug. 1996.
- ³⁰ Sandow, F.A., and Cannon, R.K., *Composite Repair of Cracked Aluminum Alloy Aircraft Structure*, USAF Flight Dynamics Laboratory, AFWAL-TR-87-3072, Sept. 1987.

- ³¹ Baker, A.A., Callinan, R.J., Davis, M.J., Jones, R., and Williams, J.G., "Repair of Mirage III Aircraft Using the BFRP Crack-Patching Technique," *Theoretical and Applied Fracture Mechanics*, Elsevier Science Publishers, Holland, Vol. 2, 1984. pp. 1-15.
- ³² Pipkins, D.S. and Atluri, S.N., "A FEAM-Based Methodology for Analyzing Composite Patch Repairs of Metallic Structures," in Composite Repair of Military Aircraft Structures: Proceedings of the 79th Meeting of the AGARD (Advisory Group for Aerospace Research & Development) Structures and Materials Panel, Seville, Spain, 1994, pp. 7-1 to 7-16.
- ³³ Ruschau, J.J. and Coate, J.E., "The Effectiveness of an Adhesively Bonded Composite Patch Repair as Applied to a Transport Aircraft Lower Wing Skin," Proceedings of the 41st International SAMPE Symposium, Society for the Advancement of Material and Process Engineering, Covina, CA, 1996.
- ³⁴ Rutherford, P. and Berg, S., "Evaluation of Bonded Boron/Epoxy Doublers for Reinforcement of Commercial Aircraft Metallic Structures," Boeing Document D658-10401-1, Boeing Aircraft Co., Seattle, WA, 1996.
- ³⁵ Elliott, W.R., "WR-ALC Aging Aircraft - Structures and Corrosion Programs," Proceedings of the 2nd Annual Air Force Aging Aircraft Conference, Air Force Office of Scientific Research, Washington, D.C., May 1994.
- ³⁶ Roach, D., "Performance Analysis of Bonded Composite Doublers on Aircraft Structures," Proceedings of the Composite Repair of Aircraft Structures Conference, Aug. 1995.
- ³⁷ Shah, S. and Roach, D., *Composite Reinforcement of Upper Forward Corner of P3 Passenger Door - Model L1011 Aircraft - Door Surround Structure test Plan and Results*, Lockheed Martin Aeronautical Systems, Company Report LG96ER0006, Marietta, GA, Jan. 1996.
- ³⁸ "Aircraft Fuselage Patch Receives FAA Approval," *Journal of Materials*, **49**, No. 6, June 1997, pg. 9.
- ³⁹ "First In-Service Inspection of Composite Doubler Installation on Delta L-1011 Aircraft," *NAARP News*, Federal Aviation Administration, Apr.-June 1997, pg. 2.

- ⁴⁰ Belason, E.B., "Fatigue and Static Ultimate Tests of Boron/Epoxy Doublers Bonded to 7075-T6 Aluminum with a Simulated Crack," in Proceedings of the 18th Symposium of the International Conference on Aeronautical Fatigue, Melbourne, Australia, May 1995.
- ⁴¹ Elkins, C.A., "Use of Composite Materials to Repair Metal Structures," Proceedings of the 14th Symposium of the International Committee on Aeronautical Fatigue, Ottawa, 8-12 June 1987.
- ⁴² Christian, T.F., Cochran, J.B., and Hammond, D.A., "Composite Material Repairs to Metallic Airframe Components," Proceedings of the 30th Structural Dynamics and Materials Conference - Part 4, AIAA/ASME/ASCE, Mobile, AL, Apr. 1989, pp. 2172-2179.
- ⁴³ Fredell, R., Van Barneveld, W., and Vogelesange, L.B., "Design and Testing of Bonded GLARE™ Patches in the Repair of Fuselage Cracks in Large Transport Aircraft," Proceedings of the 39th International SAMPE Symposium, Society for the Advancement of Material and Process Engineering, Covina, CA, 1994.
- ⁴⁴ McConnell, V.P., "Patches Push the Envelope," *High Performance Composites*, May/June 96, pp24-28.
- ⁴⁵ Belason, E.B., "Status of Bonded Boron/Epoxy Doublers for Military and Commercial Aircraft Structures," in Composite Repair of Military Aircraft Structures: Proceedings of the 79th Meeting of the AGARD (Advisory Group for Aerospace Research & Development) Structures and Materials Panel, Seville, Spain, 1994, pp. 2-1 to 2-12.
- ⁴⁶ Goland, M. and Reissner, E., "The Stresses in Cemented Joints," *Journal of Applied Mechanics*, American Society of Mechanical Engineers, New York, NY, Vol. 11, Mar. 1944.
- ⁴⁷ Harrison, N.L. and Harrison, W.J., "The Stresses in an Adhesive Layer," *Journal of Adhesion*, Vol. 3, 1972, pp. 195-212.
- ⁴⁸ Carpenter, W.C. and Patton, G.C., "Comparison of the Maximum Stress and the Stress Intensity Approaches in the Analysis of Bonded Joints," in Advances in Adhesive Bonded Joints, S. Mall, K.M. Liechti and J.R. Vinson, eds., American Society of Mechanical Engineers, New York, NY, 1988, pp. 23-31.

- ⁴⁹ ASTM D 1002-72, "Standard Test Method for Strength Properties of Adhesives in Shear by Tension Loading (Metal-to-Metal)," Annual Book of ASTM Standards, American Society for Testing and Materials, Philadelphia, PA, 1994.
- ⁵⁰ Guess, T.R., Allred, R.E. and Gerstle, F.P. Jr., "Comparison of Lap Shear Test Specimens," *Journal of Testing and Evaluation*, **5**, No. 3, Mar 1977, pp. 84-93.
- ⁵¹ Adams, R.D., "Testing of Adhesives - Useful or Not? " in Adhesion 15: Proceedings of the 28th Annual Conference on Adhesion and Adhesives, K.W. Allen, ed., Elsevier Applied Science Publishers, London, UK, 1991.
- ⁵² Hart-Smith, L.J., *Adhesive-Bonded Single-Lap Joints*, Douglas Aircraft Co., Long Beach, CA, for NASA Langley Research Center, NASA CR-112236, Jan. 1973.
- ⁵³ Hart-Smith, L.J., *Adhesive-Bonded Double-Lap Joints*, Douglas Aircraft Co., Long Beach, CA, for NASA Langley Research Center, NASA CR-112235, Jan. 1973.
- ⁵⁴ Hart-Smith, L.J., *Adhesive-Bonded Scarf and Stepped-Lap Joints*, Douglas Aircraft Co., Long Beach, CA, for NASA Langley Research Center, NASA CR-112237, Jan. 1973.
- ⁵⁵ Hart-Smith, L.J., *Non-Classical Adhesive-Bonded Joints in Practical Aerospace Construction*, Douglas Aircraft Co., Long Beach, CA, for NASA Langley Research Center, NASA CR-112238, Jan. 1973.
- ⁵⁶ Hart-Smith, L.J., "Designing to Minimize Peel Stresses in Adhesive Joints," in Delamination and Debonding of Materials, ASTM STP 876, W.S. Johnson, ed., American Society for Testing and Materials, Philadelphia, PA, 1985, pp. 238-266.
- ⁵⁷ Hart-Smith, L.J. and Thrall, E.W., "Structural Analysis of Adhesive-Bonded Joints." in Adhesive Bonding of Aluminum Alloys, E.W. Thrall and R.W. Shannon, eds., Marcel Dekker, Inc., New York, NY, 1985.
- ⁵⁸ Ripling, E.J., Mostovoy, S., and Patrick, R.L., "Application of Fracture Mechanics to Adhesive Joints." in Adhesion, ASTM STP 360, American Society for Testing and Materials, Philadelphia, PA, 1963.
- ⁵⁹ Ripling, E.J., Mostovoy, S. and Patrick, R.L., "Measuring Fracture Toughness of Adhesive Joints," *Materials Research and Standards*, American Society for Testing and Materials, Philadelphia, PA, Mar. 1964, pp. 129-134.

- ⁶⁰ Shaw, S.J., "Adhesive Joint Failure - A Fracture Mechanics Approach," in Adhesion 7: Proceedings of the 20th Annual Conference on Adhesion and Adhesives. K.W. Allen, ed., Elsevier Applied Science Publishers, London, UK, 1983.
- ⁶¹ Williams, J.G., "Fracture Mechanics of Polymers and Adhesives," in Fracture of Non-Metallic Materials, K.P. Herrmann and L.H. Larsson, eds., ECSC, EEC, EAEC, Brussels, 1987, pp. 227-255.
- ⁶² Russell, A.J. and Street, K.N., "Moisture and Temperature Effects on the Mixed-Mode Delamination Fracture of Unidirectional Graphite/Epoxy," in Composite Materials: Testing and Design (Seventh Conference), ASTM STP 893, J.M. Whitney, ed., American Society for Testing and Materials, Philadelphia, PA, 1986, pp. 349-370.
- ⁶³ Carlsson, L.A., Gillespie, J.W., and Pipes, R.B., "On The Analysis and Design of the End Notched Flexure (ENF) Specimen for Mode II Testing," *Journal of Composite Materials*, Vol. 20, Nov. 1986, pp. 594-605.
- ⁶⁴ Brussat, T.R., Chiu, S.T., and Mostovoy, S., *Fracture Mechanics for Structural Adhesive Bonds - Final Report*, Lockheed Co., Burbank, CA, for the USAF Materials Laboratory, AFML-TR-77-163, July 1987.
- ⁶⁵ Reeder, J.R. and Crews, J.H., Jr., "Mixed-Mode Bending Method for Delamination Testing," *AIAA Journal*, Vol. 8, No. 7, American Institute of Aeronautics and Astronautics, New York, NY, 1988.
- ⁶⁶ Johnson, W.S. and Mangalgiri, P.D., "Influence of the Resin on Interlaminar Mixed-Mode Fracture," Toughened Composites, ASTM STP 937, N.J. Johnston, ed., American Society for Testing and Materials, Philadelphia, PA, 1987.
- ⁶⁷ Johnson, W.S. and Mall, S., "A Fracture Mechanics Approach for Designing Adhesively Bonded Joints," in Delamination and Debonding of Materials, ASTM STP 876, W.S. Johnson, ed., American Society for Testing and Materials, Philadelphia, PA, 1985.
- ⁶⁸ Mall, S. and Johnson, W.S., "Characterization of Mode I and Mixed-Mode Failure of Adhesive Bonds Between Composite Adherends," in Composite Materials: Testing and Design (Seventh Conference), ASTM STP 893, J.M. Whitney, ed., American Society for Testing and Materials, Philadelphia, PA, 1986.

- ⁶⁹ Johnson, W.S. and Mall, S., "Bonded Joint Strength: Static Versus Fatigue," in Proceedings of the 5th International Congress on Experimental Mechanics. Society for Experimental Stress Analysis, Montreal, 1984.
- ⁷⁰ DeVries, K.L., Williams, M.L. and Chang, M.D., "Adhesive Fracture of a Lap Joint," *Experimental Mechanics*, Vol. 14, No. 3, Society for Experimental Mechanics, Bethel, CT, Mar 1974, pp. 89-97.
- ⁷¹ Oplinger, D., *TJOINTL and TJOINTNL Bond Analysis Programs*, Federal Aviation Administration, Atlantic City Int'l Airport, NJ.
- ⁷² Valentin, R.V., *Finite Element Analysis of Adhesively Bonded Joints*, Masters Thesis, Georgia Institute of Technology, Atlanta, GA, July 1997.
- ⁷³ Dattaguru, B., Everett, R.A., Jr., Whitcomb, J.D. and Johnson, W.S., "Geometrically Nonlinear Analysis of Adhesively Bonded Joints, *Journal of Engineering Materials and Technology*, American Society of Mechanical Engineers, New York, NY, Mar 1984, pp. 59-65.
- ⁷⁴ Rybicki, E. F., and Kanninen, M. F., "A Finite Element Calculation Of Stress Intensity Factor by a Modified Crack Closure Integral," *Engineering Fracture Mechanics*, Vol. 9, 1977, pp. 931-938.
- ⁷⁵ CALCUREP, R. Fredell, USAF Academy, CO, 1995.
- ⁷⁶ PCRep, Pipkins, D.S. and Atluri, S., Knowledge Systems, Inc., Forsyth, GA, 1997.
- ⁷⁷ Walton, T.R. and Nash, H.C., *Adhesive Bond Failure in Aircraft Honeycomb-Sandwich Composites*, NRL Memorandum Report 2213, Chemistry Division, Naval Research Laboratory, Washington, D.C., Feb. 1971.
- ⁷⁸ Brockmann, W., "The Environmental Resistance of Metal Bonds," *Adhesives Age*, March 1976, pp. 33-38.
- ⁷⁹ DeLollis, N.J., "Durability of Structural Adhesive Bonds: A Review," *Adhesives Age*, Sept. 1977, pp. 41-48.
- ⁸⁰ Marceau, J.A., McMillan, J.C. and Scardino, W.M., "Cyclic Stress Testing of Adhesive Bonds," *Adhesives Age*, Apr. 1978, pp. 37-49.

- ⁸¹ Hufferd, W.L., Lemini, D.G., Briggs, W.E., Thompson, R.E., and Francis, E.C., *Time Dependent Fracture in Adhesive Bonded Joints*, United Technologies - Chemical Systems Division, San Jose, CA, for the USAF Materials Laboratory, AFWAL-TR-84-4150, Dec. 1984.
- ⁸² Kinloch, A.J., "Interfacial Fracture Mechanical Aspects of Adhesive Bonded Joints - A Review," *Journal of Adhesion*, Vol. 10, 1979, pp. 193-219.
- ⁸³ Brewis, D.W., Comyn, J., Raval, A.K. and Kinloch, A.J., "The Effect of Humidity on the Durability of Aluminum-Epoxy Joints," *Int'l Journal of Adhesion and Adhesives*, Butterworth-Heinemann, Ltd, Vol. 10, No. 4, Oct. 1990, pp. 247 - 253.
- ⁸⁴ Askins, R.D. and Konopinski, A., *The Effect of Environmental Aging and Rapid Heating (Thermal Spikes) on the Behavior of Adhesively Bonded Honeycomb Sandwich*, University of Dayton Research Institute for the USAF Materials Laboratory, WRDC-TR-90-4056, Aug. 1990.
- ⁸⁵ "FM[®]73 Film Adhesive", CYTEC Engineered Materials, Inc., Havre de Grace, MD, 1994.
- ⁸⁶ "AF191 Structural Adhesive Film - Aerospace Technical Data", Aerospace Materials Department, 3M Corporation, St. Paul, MN, 1987.
- ⁸⁷ Mayhew, R.T. and Kohli, D.K., "Development of High Temperature Service Polyimide Based Adhesives for Titanium and Composite Bonding Applications," Proceedings of the 41st International SAMPE Symposium, Society for the Advancement of Material and Process Engineering, Covina, CA, 1996.
- ⁸⁸ Bryant, R.G., Jensen, B.J., and Hergenrother, P.M., "Chemistry and Properties of a Phenylethynyl-Terminated Polyimide," *Journal of Applied Polymer Science*, Vol. 59, 1996, 1249-1254.
- ⁸⁹ Mayhew, R., CYTEC Engineered Materials, Inc., personal communication, 11 Oct 1995.
- ⁹⁰ ASTM D 638M-94b, "Standard Test Method for Tensile Properties of Plastics," Annual Book of ASTM Standards, American Society for Testing and Materials, Philadelphia, PA, 1994.

- ⁹¹ Hinckley, J.A. and Mings, S.L., "Fracture Toughness of Polyimide Films," *Polymer*, Vol. 31, Jan 1990, pp. 75-77.
- ⁹² Tsou, A.H., Hord, J.S., Smith, G.D., and Schrader, R.W., "Strength Analysis of Polymeric Films," *Polymer*, Vol. 33, No. 14, 1992, pp. 2970-2974.
- ⁹³ Klemann, B.M. and DeVilbiss, T., "The Fracture Toughness of Thin Polymeric Films," *Polymer Engineering and Science*, Vol. 36, No. 1, Jan 1996, 126-134.
- ⁹⁴ ASTM D3433-75, "Standard Practice for Fracture Strength in Cleavage of Adhesives in Bonded Joints." Annual Book of ASTM Standards, American Society for Testing and Materials, Philadelphia, PA; 1994.
- ⁹⁵ ASTM D5528-94a, "Standard Test Method for Mode I Interlaminar Fracture Toughness of Unidirectional Fiber-Reinforced Polymer Matrix Composites." Annual Book of ASTM Standards, American Society for Testing and Materials, Philadelphia, PA, 1994.
- ⁹⁶ Liechti, K.M. and Freda, T., "On the Use of Laminated Beams for the Determination of Pure and Mixed-Mode Fracture Properties of Structural Adhesives," in Advances in Adhesive Bonded Joints, S. Mall, K.M. Liechti and J.R. Vinson, eds., American Society of Mechanical Engineers, New York, NY, 1988, pp. 65 -77.
- ⁹⁷ Ramkumar, R.L. and Whitcomb, J.D., "Characterization of Mode I and Mixed-Mode Delamination Growth in T300/5208 Graphite/Epoxy," in Composite Materials: Testing and Design (Seventh Conference), ASTM STP 893, J.M. Whitney, ed., American Society for Testing and Materials, Philadelphia, PA, 1986, pp. 315-335.
- ⁹⁸ Rakestraw, M.D., Taylor, M.W. and Dillard, D.A., "Time Dependent Crack Growth and Loading Rate Effects on Interfacial and Cohesive Fracture of Adhesive Joints," *Journal of Adhesion*, 1995.
- ⁹⁹ "Protocol for Interlaminar Fracture Testing - End-Notched Flexure," provided by G. Murri, NASA-Langley Research Center, Oct. 1994.
- ¹⁰⁰ Wilkins, D.J., *A Comparison of the Delamination and Environmental Resistance of a Graphite-Epoxy and a Graphite-Bismaleimide*, General Dynamics, Fort Worth, TX, for Naval Air Systems Command, NAV-GD-0037, Aug. 1981.

- ¹⁰¹ Mall, S., Johnson, W.S. and Everett, R.A., Jr., "Cyclic Debonding of Adhesively Bonded Composites," in Adhesive Joints: Formation, Characteristics and Testing, K.L. Mittal, ed., Plenum Press, New York, NY, 1982, pp. 639-656.
- ¹⁰² Krieger, R.B. Jr., "Shear Stress-Strain Properties of Structural Adhesives in Hostile Environments," in Durability of Adhesive Bonded Structures, *Journal of Applied Polymer Science - Applied Polymer Symposium* 32, Bodnar, M.J., ed., John Wiley & Sons, Inc., New York, NY, 1977, pp. 321-340.
- ¹⁰³ Krieger, R.B. Jr., "Stress Analysis Concepts for Adhesive Bonding of Aircraft Primary Structure," in Adhesively Bonded Joints: Testing, Analysis, and Design, ASTM STP 981, W.S. Johnson, ed., American Society for Testing and Materials, Philadelphia, PA, 1988, pp. 264-275.
- ¹⁰⁴ Irwin, G.R. and Kies, J.A., "Critical Energy Rate Analysis of Fracture Strength," *Welding Journal Research Supplement*, Apr. 1954, pp. 193S-198S.
- ¹⁰⁵ Hashemi, S., Kinloch, A.J., and Williams, J.G., "Corrections Needed in Double-Cantilever Beam Tests for Assessing the Interlaminar Failure of Fibre-Composites," *Journal of Materials Science Letters*, Vol. 8, 1989.
- ¹⁰⁶ O'Brien, T.K. and Martin, R.H., "Round Robin Testing for Mode I Interlaminar Fracture Toughness of Composite Materials," *Journal of Composites Technology and Research*, Vol. 15, No. 4, Winter 1993.
- ¹⁰⁷ Roderick, G.L., Everett, R.A., and Crews, J.H., Jr., *Debond Propagation in Composite Reinforced Metals*, U.S. Army Air Mobility Research and Development Laboratory, NASA TM X-71948, NASA Langley Research Center, Hampton, VA, Feb. 1974.
- ¹⁰⁸ Roderick, G.L., Everett, R.A., and Crews, J.H., Jr., "Cyclic Debonding of Unidirectional Composites Bonded to Aluminum Sheet For Constant Amplitude Loading," Fatigue of Composite Materials, ASTM STP 569, American Society for Testing and Materials, Philadelphia, PA, 1975, pp. 295-306.
- ¹⁰⁹ Mall, S., Ramamurthy, G., and Rezaizadeh, M.A., "Stress Ratio Effect on Cyclic Debonding in Adhesively Bonded Composite Joints," *Composite Structures*, Vol. 8, Elsevier Applied Science Publishers, Ltd., London, 1987, pp. 31-45.

- ¹¹⁰ O'Brien, T.K., Murri, G.B., and Salpekar, S.A., *Interlaminar Shear Fracture Toughness and Fatigue thresholds for Composite Materials*, NASA Technical Memorandum TM-89157, NASA Langley Research Center, Hampton, VA, Aug. 1987.
- ¹¹¹ Johnson, W.S., "Stress Analysis of the Cracked Lap-Shear Specimen: An ASTM Round Robin," *Journal of Testing and Evaluation*, Vol. 15, No. 6, American Society for Testing and Materials, Philadelphia, PA, Nov 1987, pp. 303-324.
- ¹¹² Lai, Y.H., Rakestraw, M.D. and Dillard, D.A., "The Cracked Lap Shear Specimen Revisited - A Closed-form Solution," *International Journal of Solids and Structures*, Vol. 33, No. 12, 1996, pp. 1725-1743.
- ¹¹³ Hines, W.H. and Montgomery, D.C., Probability & Statistics in Engineering and Management Science, John Wiley & Sons, New York, NY, 1990, pp.255-280.
- ¹¹⁴ Box, G.P., Hunter, W.G., and Hunter, J.S., Statistics for Experimenters, John Wiley & Sons, New York, NY, 1978, pp. 107-115.
- ¹¹⁵ Young, R.J., Introduction to Polymers, Chapman & Hall, London, 1983, pg. 138.
- ¹¹⁶ Tadokoro, H. and Kobayashi, M., "Vibrational Spectroscopy," in Polymer Spectroscopy, D. Hummel, ed., Verlag Chemie GmbH, Düsseldorf, 1974, pg. 138.
- ¹¹⁷ Hendra, P., Jones, C., and Warnes, G., Fourier Transform Raman Spectroscopy: Instrumentation and Chemical Applications, Ellis Horwood, Ltd., 1991, pp. 21-23.
- ¹¹⁸ Maddams, W.F., "Infrared and Raman Spectroscopy," Analysis of Polymer Systems, L.S. Bark and N.S. Allen, eds., Applied Science Publishers, Ltd., London, 1982, pg. 51.
- ¹¹⁹ Silverstein, R.M., Spectrometric Identification of organic Compounds, John Wiley & Sons, Inc., New York, NY, 1963.
- ¹²⁰ Brown, D.W., Floyd, A.J., and Sainsbury, M., Organic Spectroscopy, John Wiley & Sons, Inc., Chichester, England, 1988.
- ¹²¹ *DSC 7 Differential Scanning Calorimeter User's Manual*, Perkin-Elmer Corp., Norwalk, CT, 1994, pg. 1-1.
- ¹²² Wendlandt, W.W. and Gallagher, P.K., "Instrumentation," in Thermal Characterization of Polymeric Materials, E.A. Turi, ed., Academic Press, Inc., Orlando, FL, 1991.

- ¹²³ Hall, C., Polymer Materials, John Wiley & Sons, New York, 1981, pg. 35.
- ¹²⁴ Turi, E.A., ed., Thermal Characterization of Polymeric Materials, Academic Press, Inc., Orlando, FL, 1981.
- ¹²⁵ Wunderlich, B., Thermal Analysis, Academic Press, Inc., Boston, MA, 1990.
- ¹²⁶ *TGA 7 Thermogravimetric Analyzer User's Manual*, Perkin-Elmer Corp., Norwalk, CT, 1994.
- ¹²⁷ CRC Handbook of Chemistry and Physics, R.C. Weast, ed., CRC Press, Inc., Boca Raton, FL, 1981, pp. F249-F267.
- ¹²⁸ Behm, D.T. and Gannon, J., "Epoxyes," in Engineered Materials Handbook, Volume 3: Adhesives and Sealants, H. Brinson, ed., ASM International, Metals Park, OH, 1990, pp. 94-95.
- ¹²⁹ Haslam, J., and Willis, H.A., Identification and Analysis of Plastics, Van Nordstrom Co., Inc., Princeton, NJ, 1965, pg. 249.
- ¹³⁰ Collard, D., Georgia Institute of Technology, School of Chemistry, Personal Communication, 11 June 1997.
- ¹³¹ CRC Handbook of Chemistry and Physics, R.C. Weast, ed., CRC Press, Inc., Boca Raton, FL, 1981, pp. F249-F267.
- ¹³² Colthup, N.B., Daly, L.H., and Wiberley, S.E., Introduction to Infrared Spectroscopy, Academic Press, New York, NY, 1975, pg. 366.
- ¹³³ Ting, R.Y. and Cottingham, R.L., "Fracture Evaluation of High-performance Polymers," *Adhesives Age*, June 1981, pp. 35-39.
- ¹³⁴ Ripling, E.J., Crosley, P.B., and Johnson, W.S., "A Comparison of Pure Mode I and Mixed Mode I-III Cracking of an Adhesive Containing an Open Knit Cloth Carrier," Adhesively Bonded Joints: Testing, Analysis, and Design, ASTM STP 981, W.S. Johnson, ed., American Society for testing and Materials, Philadelphia, PA, 1988, pp. 163-182.
- ¹³⁵ Skinn, D.A., Gallagher, J.P., Berens, A.P., Huber, P.D., and Smith, J., Damage Tolerant Design Handbook, Purdue Research Foundation, West Lafayette, IN 1994.

- ¹³⁶ Parvatareddy, H., Pasricha, A., Dillard, D.A., Holmes, B. and Dillard, J.G., "High Temperature and Environmental Effects on the Durability of Ti-6Al-4V/LaRC PETI-5 Adhesive Bonded System" "Second Symposium on High Temperature and Environmental Effects on Polymeric Composites", Nov. 1995.
- ¹³⁷ Klemczyk, M. and Belason, E.B., "Analysis of Stresses Near the Edge of a Boron/Epoxy Doubler Bonded to Aluminum," Textron Specialty Materials, Lowell, MA, Apr. 1995.
- ¹³⁸ ASTM D3479-76, "Standard Test Methods for Tension-Tension Fatigue of Oriented Fiber, Resin Matrix Composites." Annual Book of ASTM Standards, American Society for Testing and Materials, Philadelphia, PA, 1994.
- ¹³⁹ ASTM E647, "Standard Test Method for Measurement of Fatigue Crack Growth Rates." Annual Book of ASTM Standards, American Society for Testing and Materials, Philadelphia, PA, 1994.
- ¹⁴⁰ P. Rutherford, personal correspondence, The Boeing, Seattle, WA, 25 Mar. 1997.
- ¹⁴¹ S.Raj, personal communication, InTech, Bothell, WA, 27 Mar. 1997.
- ¹⁴² Burke, C., personal communication, Lockheed Martin Aeronautical Systems Co., 8-10 July 1997.
- ¹⁴³ Fernlund, G. and Spelt, J.K., "Mixed-Mode Fracture Characterization of Adhesive Joints," *Composites Science and Technology*, Vol. 50, Elsevier Applied Science Publishers Ltd., London, England, 1994, pp. 441-449.
- ¹⁴⁴ Mayhew, R.T., Personal Communication, CYTEC Engineered Materials, Inc., Havre de Grace, MD, 4 Oct. 1996.
- ¹⁴⁵ Schneider, D., "Laboratory Data Record," Lockheed Martin Aeronautical Systems Company, Marietta, GA, Aug. 1995.
- ¹⁴⁶ Schneider, D., "Laboratory Data Record," Lockheed Martin Aeronautical Systems Company, Marietta, GA, May 1996.
- ¹⁴⁷ Cao, T., Personal Communication, Boeing Defense & Space Group, Seattle, WA, 1 Oct. 1996.

¹⁴⁸ "Anodizing of Titanium for Adhesive Bonding," Boeing Process Specification BAC5890, Boeing Defense and Space Group, Seattle, WA, 30 Sep. 1994.

VITA

The author [REDACTED]
[REDACTED]

graduated from Waukegan West High School in 1981.

Enrolling at the Massachusetts Institute of Technology on an Air Force ROTC scholarship, the author pursued undergraduate studies in mechanical engineering and received his Bachelor of Science degree in 1985. He performed his thesis work on the shear behavior of aluminum under Prof. L. Anand. He also investigated the adhesion of Space Shuttle coatings through M.I.T.'s Undergraduate Research Opportunities program.

Following graduation, the author was commissioned as a second lieutenant in the U.S. Air Force. He was assigned to the Materials Directorate, Wright Laboratory, Wright-Patterson AFB, Ohio, until 1990. Here he worked on several projects related to the mechanical properties and durability of organic- and ceramic-matrix composites, supporting several aircraft and aerospace programs. During this period, he also earned a Master of Arts in International Affairs degree from the University of Dayton.

In September 1990, he began graduate studies in mechanical engineering at the University of Michigan. Under the direction of Prof. J.W. Holmes, the author investigated the thermomechanical behavior of ceramic composites in support of the Air

Force's Integrated High Performance Turbine Engine Technology program. He received his Master of Science degree in December of 1991.

The author assumed teaching duties in the Department of Engineering Mechanics, U.S. Air Force Academy, Colorado, in January 1992. During his tenure at this institution, he served as an instructor for several mechanics, materials, and design courses and also as the department's executive officer.

Beginning in September of 1994, the author has followed a course of study in the George W. Woodruff School of Mechanical Engineering at the Georgia Institute of Technology. He has been guided through his Ph.D. studies of the durability of adhesively bonded aircraft joints by Prof. W. Steven Johnson. The author will finish his program in September 1997 and graduate in December of the same year. He will be reassigned in October to Wright-Patterson AFB, Ohio, where he will serve in the Flight Systems Branch, Engineering Directorate, Aeronautical Systems Center (ASC/ENFS).

The author is a registered professional engineer in the State of Colorado and certified in the Air Force Acquisition Professional Development Program. He is a graduate of the USAF's Squadron Officer's School and Land & Water Survival schools. The author currently holds the rank of major and is the recipient of the Air Force's Meritorious Service, Commendation, and Achievement Medals. He is a member of the American Society of Mechanical Engineers, ASM International, the American Society of Engineering Education, Tau Beta Pi, and the Air Force Association.

[REDACTED]

The author's list of significant publications include:

Johnson, W.S. and Butkus, L.M., "Considering Environmental Conditions in the Design of Bonded Structures: A Fracture Mechanics Approach," *International Journal of Fatigue and Fracture of Engineering Materials and Structures*, accepted: July 1997.

Butkus, L.M., Mathern, P.D., and Johnson, W.S., "Tensile Properties and Plane-Stress Fracture Toughness of Thin Film Aerospace Adhesives," *The Journal of Adhesion*, submitted: June 1997.

Valentin, R.V., Butkus, L.M., and Johnson, W.S., "A Finite Element and Experimental Evaluation of Boron-Epoxy Doublers Bonded to an Aluminum Substrate," *Journal of Composites Technology & Research*, submitted: April 1997.

Butkus, L.M. and Johnson, W.S., "Durability of Adhesively Bonded Joints," Proceedings of the 4th Annual USAF Aging Aircraft Conference, USAF Academy, CO, 1996.

Johnson, W.S. and Butkus, L.M. and Valentin, R., "Designing for Durability of Bonded Structures" Proceedings of the FAA-NASA Symposium on Continued Airworthiness of Aircraft Structures, Atlanta, GA, 1996.

Butkus, L.M. and Johnson, W.S., "Environmental Effects on the Opening Mode Fracture Behavior of Boron-Epoxy/Aluminum Joints," Proceedings of the 11th Technical Conference of the American Society of Composites, Atlanta, GA, 1996.

Butkus, L.M., "Assessing Structural Integrity of Bonded Joints Using Fracture Mechanics," Proceedings of the 1995 Aircraft Structural Integrity Program (ASIP) Conference, San Antonio, TX, 1995.

Bridge, J.W. and Butkus, L.M., "Hands-On Laboratory Projects that Enhance Learning in Materials Engineering," Proceedings of the 1994 Annual Conference of the American Society of Engineering Education, Edmonton, Alberta, Canada, 1994,, pp. 938 - 943.

Fredell, R., Müller, R., Borsboom, C., and Butkus, L., "Bonded Repair of Multiple Site Damage with GLARE™ Fiber Metal Laminate Patches," Proceedings of the 1994 Aircraft Structural Integrity Program (ASIP) Conference, San Antonio, TX, 1994.

Zawada, L.P., Pernot, J.J. and Butkus, L.M., "The Fatigue Behavior of Several Ceramic Matrix Composites," Proceedings of Fatigue '93, The 5th International Conference on Fatigue and Fatigue Thresholds, J.P. Bailon and J.I. Dickson, eds., Chameleon Press, Ltd., London, 1993, pp. 1307-12.

Butkus, L.M. and Holmes, J.W. and Nicholas, T. , "Thermomechanical Fatigue of a Silicon Carbide Fiber-Reinforced Calcium Aluminosilicate Composite," *Journal of the American Ceramic Society*, Vol. 76, No. 11, 1993, pp. 2817-2825.

Butkus, L.M., Zawada, L.P., and Hartman, G.A., "Fatigue Test Methodology and Results for Ceramic Matrix Composites at Room and Elevated Temperatures," in Cyclic Deformation, Fracture, and Nondestructive Evaluation of Advanced Materials: ASTM STP 1157, M.R. Mitchel and O. Buck, eds., American Society for Testing and Materials, Philadelphia, PA, 1992, pp. 52-68.

Butkus, L.M., "Thermomechanical Fatigue Behavior of a Silicon Carbide Fiber-Reinforced Calcium Aluminosilicate Glass-Ceramic Matrix Composite," WL-TR-92-4071, Wright Laboratories, Wright-Patterson AFB, OH, 1992.

Butkus, L.M., and Holmes, J.W., "Thermomechanical Fatigue of a Nicalon-Reinforced Calcium Aluminosilicate Glass-Ceramic," Ceramic Engineering and Science Proceedings, American Ceramic Society, Westerville, OH, Vol 12, No. 13, 1992, pp. 7-10.

Zawada, L. P., Butkus, L.M., and Hartman, G.A., "Room Temperature Tensile and Fatigue Properties of Silicon Carbide Fiber-Reinforced Aluminosilicate Glass," *Journal of the American Ceramic Society*, Vol. 74, No. 11, 1991, pp. 2851-8.

Butkus, L.M., "An Evaluation of the Effects of 'Hand' Sanding and Plastic Media Blasting (PMB) on Graphite/Epoxy Composite Materials," WRDC-TR-90-4006, Wright Research and Development Center, Wright-Patterson AFB, OH, 1990.

Butkus, L.M., Meuer, G.D. and Behme, A.K., Jr., "Plastic Media Blast (PMB) Paint Removal from Composites", in Advanced Materials: The Challenge for the Next Decade, Proceedings of the 35th International SAMPE Symposium and Exhibition, G. Janicki, V. Bailey, and H Schjeldrup, eds., Society for the Advancement of Material and Process Engineering, Covina, CA, pp. 1385 - 1397, 1990.